

**Palmitoylation In Neurodegeneration:
Analysis Of
Cysteine-String Protein Mutants
Linked with
Neuronal Ceroid Lipofuscinosis**

A thesis presented by

Cinta Diez-Ardanuy

In fulfilment of the requirement for the degree of

Doctor of Philosophy

2017

University of Strathclyde

Strathclyde Institute of Pharmacy and Biomedical Sciences

Declaration of Authenticity and Author's Rights:

This thesis is the result of the author's original research. It has been composed by the author and has not been previously submitted for examination which has led to the award of a degree.

The copyright of this thesis belongs to the author under the terms of the United Kingdom Copyright Acts as qualified by University of Strathclyde Regulation 3.50. Due acknowledgement must always be made of the use of any material contained in, or derived from, this thesis.

Signed:

Date: 03/03/17

A handwritten signature in black ink, appearing to be 'A. J. J.', written in a cursive style.

Acknowledgements

First and foremost, I would like to express my sincere gratitude to my supervisor Prof. Luke H. Chamberlain. I am truly grateful for his continuous support, patience and encouragement. I could not have imagined having a better supervisor and mentor for my PhD studies. Thank you Luke, for this opportunity and for letting me be part of such an amazing project and group, I think you left the bar very, very high!

I could have not gone through this project without the help, knowledge and patience (a lot!) of the whole Chamberlain group: Dr Jennifer Greaves, Dr. Kimon Lemonidis, Dr. Christine Salaun and Marianna Kouskou. Thank you for so many good questions and answers, for the inspiration and the nice chats. I will miss them!

During my time in Glasgow I was lucky enough to encounter beautiful friends: Joana, basically for being my twin; and Ina, for creating a nice and friendly atmosphere to come home to; Josie and Scott, for the endless chats and hashtags that always make me laugh; and Mireia and Anna for the hundred weekend plans. Also, thank you to my friends in Barcelona, especially Tamara, Mon, Míriam and Núria, for always being there despite the distance. Coming home always gave me the much needed energy to finish this thesis.

Finally, I would like to thank Michael for his patience, love, care and curious questions about “proteins and aggregation” that always challenge me. And Mamá, Papá, this is truly all thanks to you and your endless love.

Publications

Lemonidis, K., Werno, M.W., Greaves, J., Diez-Ardanuy, C., Sanchez-Perez, M.C., Salaun, C., Thomson, D.M. and Chamberlain, L.H. (2015) 'The zDHHC family of S-acyltransferases', *Biochemical Society Transactions*, 43(2), pp. 217–221. doi: 10.1042/bst20140270.

Diez-Ardanuy, C., Greaves, J., Munro, K.R., Tomkinson, N.C.O, Chamberlain, L.H. (2017). 'A cluster of palmitoylated cysteines are essential for aggregation of cysteine-string protein mutants that cause neuronal ceroid lipofuscinosis'. *Scientific Reports*, 7(1). doi: 10.1038/s41598-017-00036-8.

Poster communications

Diez-Ardanuy, C., Greaves, J., Chamberlain, L.H. (2014) S-Acylation in Neurodegeneration. Unpublished poster presentation at: FEBS EMBO 2014 Conference, 30th August to 4th September; Paris, France. Appendix I.

Diez-Ardanuy, C., Greaves, J., Chamberlain, L.H. (2014) S-Acylation in Neurodegeneration. Unpublished poster presentation at: Protein Acylation: from Mechanism to Drug Discovery, 10-12th September; Edinburgh, UK. Appendix I.

Diez-Ardanuy, C., Greaves, J., Chamberlain, L.H. (2015). Molecular and cellular analysis of Cysteine-String Protein mutants that cause Neuronal Ceroid Lipofuscinosis. Unpublished poster presentation at: FASEB Science Research Conference: Protein Lipidation, Signaling, and Membrane Domains, 19th-24th July, Saxtons River, VT, USA. Appendix II.

Diez-Ardanuy, C., Greaves, J., Chamberlain, L.H. (2016). Palmitoylation in Neurodegeneration. Unpublished poster presentation at: Protein S-palmitoylation: from Mechanism to Application, 21st-23rd September, Oxford, UK. Appendix III.

Diez-Ardanuy, C., Greaves, J., Chamberlain, L.H. (2016). Palmitoylation in Neurodegeneration. Unpublished poster presentation at: Society for Neuroscience Annual Meeting 2016, 12th-16th November, San Diego, USA. Appendix IV

Table of contents

Acknowledgements	II
Publications	III
Poster communications	IV
Table of contents	VI
List of Figures	XI
List of Tables	XIV
List of Abbreviations	XV
Abstract	XXI
Chapter 1: Introduction	1
1.1 <i>Lipid modifications</i>	1
1.2 <i>Palmitoylation</i>	3
1.2.1 Regulation of palmitoylation.....	4
1.2.2 Functions of palmitoylation.....	7
1.2.3 Palmitoylation in neurological disorders.....	9
1.3 <i>Palmitoylation in synaptic function</i>	15
1.3.1 Synaptic vesicle exocytosis.....	15
1.3.2 SNARE proteins and membrane fusion	17
1.3.3 SNARE regulators and chaperones	23
1.4 <i>Cysteine-string protein alpha (CSPα)</i>	29
1.4.1 Discovery of CSP and isoforms	29
1.4.2 CSP α domains.....	31
1.4.3 Palmitoylation and membrane interactions of CSP α	32
1.4.4 Cellular functions of CSP α	33

1.4.5	Role of CSP α in neurodegeneration	36
1.5	<i>Neuronal Ceroid Lipofuscinoses</i>	38
1.5.1	Diagnosis and classification of NCL.....	41
1.5.2	Adult Neuronal Ceroid Lipofuscinosis (ANCL).....	43
1.5.3	Animal models of NCLs and current therapeutic strategies.....	44
1.6	<i>Aims of this study</i>	46
Chapter 2: Materials and methods		49
2.1	<i>Materials and suppliers</i>	49
2.1.1	Chemicals.....	49
2.1.2	Molecular biology and biochemical reagents.....	49
2.1.3	Electrophoresis and immunoblot equipment	50
2.1.4	Cell culture media and plasticware	50
2.1.5	Mammalian cell lines.....	50
2.1.6	Human Brains	51
2.1.7	Primers	51
2.1.8	Plasmids.....	56
2.1.9	Antibodies	56
2.2	<i>Mammalian cell culture</i>	59
2.2.1	Culturing PC12 cells	59
2.2.2	Culturing HEK293T cells.....	59
2.2.3	Transient transfection of plasmid DNA into mammalian cells	60
2.2.4	Harvesting transfected cells for SDS-PAGE.....	60
2.3	<i>Analysis of human brain tissue</i>	61
2.3.1	Preparation of human brain lysates	61
2.3.2	Quantification of total protein by Bicinchoninic acid (BCA) Protein Assay	61
2.4	<i>Molecular Biology</i>	62
2.4.1	Standard molecular biology protocols	62
2.4.2	DNA amplification by Polymerase Chain Reaction (PCR)	62
2.4.3	Site-Directed Mutagenesis (SDM)	63
2.4.4	Gateway Cloning System	64
2.4.5	Agarose gel electrophoresis	65
2.4.6	DNA purification from agarose gels	66
2.4.7	Restriction endonuclease digestion of DNA	66

2.4.8	DNA dephosphorylation and ligation of DNA inserts with plasmid vectors	67
2.4.9	Transformation of expression plasmid DNA into One Shot®TOP10 cells	67
2.4.10	Small-scale plasmid purification (mini-prep)	68
2.4.11	Large-scale plasmid purification (midi-prep)	68
2.4.12	Spectrophotometric quantification of DNA	69
2.4.13	DNA sequencing	70
2.4.14	Glycerol stock preparation	70
2.5	<i>Generation of mutant constructs</i>	70
2.5.1	Generation of human CSP α constructs by SDM	70
2.5.2	Subcloning of CSP α 14KR into pEGFP-C2 expression vector	71
2.5.3	Generation of 14KR ANCL mutants using SDM	72
2.5.4	Generation of untagged and HA-tagged mutants through the Gateway Cloning system	72
2.5.5	Replacing lysine codons with arginine codons in CSP α	75
2.5.6	Introducing cysteine to alanine/leucine mutations in EGFP-CSP and untagged CSP α plasmids using SDM	75
2.5.7	Generation of CSD mutants using SDM	76
2.5.8	Generation of CSP α -PEST mutants using SDM	76
2.6	<i>Protein biochemistry</i>	77
2.6.1	Cycloheximide treatment	77
2.6.2	Hydroxylamine treatment	77
2.6.3	Brefeldin A treatment	78
2.6.4	Treatment with proteasome and lysosome inhibitors	78
2.6.5	Palmostatin B treatment	79
2.6.6	Metabolic labelling of proteins and turnover detection using “click chemistry”	79
2.6.7	Sodium dodecyl sulfate polyacrylamide gel electrophoresis (SDS-PAGE)	82
2.6.8	Blue Native polyacrylamide gel electrophoresis (BN-PAGE)	84
2.6.9	Immunoprecipitation	87
2.7	<i>Data analysis</i>	88
Chapter 3: Analysis of the aggregation of CSPα mutants		89
3.1	<i>Introduction</i>	89
3.2	<i>Results</i>	91
3.2.1	Comparison of the migration profile of wild-type CSP α and ANCL mutants	91
3.2.2	Characterisation of the oligomeric properties of the ANCL mutants	94

3.2.3	Importance of the C-terminus and the cysteine-string domain of CSP α for aggregation of ANCL mutant proteins	95
3.2.4	Analysis of the effects of cysteine mutations on aggregation and palmitoylation of the L115R and Δ L116 CSP α mutants.....	98
3.3	<i>Analysis of the effects of zDHHC enzyme co-expression on aggregation of ANCL mutant CSPα</i>	108
3.4	<i>Further analysis of the Cys(4-7) region of the CSD</i>	111
3.5	<i>Comparison of palmitoylation dynamics of wild-type and ANCL mutant CSPα</i>	114
3.6	<i>Discussion.....</i>	118
Chapter 4:	Analysis of molecular changes in ANCL brains	127
4.1	<i>Introduction.....</i>	127
4.2	<i>CSPα expression and aggregation in normal and disease human brain</i>	129
4.3	<i>Expression of SNARE proteins in ANCL and HD human brains</i>	131
4.4	<i>Expression levels of other synaptic and palmitoylated proteins in ANCL and HD brains</i>	136
4.5	<i>ANCL patient brains show a dramatic increase in PPT1 expression</i>	142
4.6	<i>Effects of ANCL mutant CSPα on PPT1 expression in cell culture</i>	143
4.7	<i>Discussion.....</i>	145
Chapter 5:	The degradation mechanism of CSPα.....	153
5.1	<i>Introduction.....</i>	153
5.2	<i>Effect of proteasomal and lysosomal inhibitors on CSPα expression levels</i>	154
5.3	<i>CSPα ANCL mutants are degraded via proteasome</i>	157
5.4	<i>Analysis of the role of lysine residues in CSPα proteasomal degradation.....</i>	159
5.5	<i>Analysis of the mechanisms whereby proteasomal inhibition leads to a selective increase of non-palmitoylated CSPα</i>	164
5.6	<i>Analysis of the importance of specific domains in CSPα for targeting to the proteasome ..</i>	167
5.7	<i>Analysis of the effects of mutations in the cysteine-string domain on CSPα proteasomal degradation</i>	171
5.8	<i>PEST sequences are not responsible for CSPα degradation</i>	175

5.9	<i>Unusual ubiquitination profile of CSPα</i>	177
5.10	<i>ANCL mutants also undergo ubiquitination</i>	181
5.11	<i>Discussion</i>	182
Chapter 6:	General discussion	191
Chapter 7:	References	200
Appendix I	250
Appendix II	252
Appendix III	253
Appendix IV	253
Appendix V	255
Appendix VI	256
Appendix VII	257
Appendix VIII	258

List of Figures

Chapter 1

Figure 1.1. . Synaptic vesicle exocytosis	17
Figure 1.2. CSP α KO mice exhibit an age-dependent progressive neurodegeneration.....	38
Figure 1.3. Effects of ANCL mutations	47

Chapter 1

Figure 2.1. Figure 2.1. Outline of the click-chemistry method to detect attachment of azide-conjugated palmitic acid onto cysteine residues of proteins.....	80
--	----

Chapter 3

Figure 3.1. Migration profile of wild-type and mutant CSP α	93
Figure 3.2. The formation of mutant CSP α aggregates is time-dependent.....	95
Figure 3.3. Effect of C-terminal truncation on aggregation of ANCL mutants.....	97
Figure 3.4. Cysteine substitutions on the cysteine-string domain.	99
Figure 3.5. Effect of the C(1-3)A substitutions on aggregation of CSP α	100
Figure 3.6. Effect of C(11-14)A substitutions on the aggregation of CSP α	102
Figure 3.7. Effect of C(8-10)A mutations on the aggregation of CSP α	103
Figure 3.8. C(4-7)A substitutions abolish aggregation of the ANCL mutants.	105
Figure 3.9 C(4-7)L substitutions block aggregation of the ANCL mutants.	107
Figure 3.10. Effect of palmitoylation on aggregation of ANCL mutants.....	109
Figure 3.11. Palmitoylation of C(4-7)L constructs does not lead to aggregation.	110

Figure 3.12. Effect of the C(4-5)L substitutions on the aggregation of wild-type and ANCL mutant CSP α	112
Figure 3.13. Effect of C(6-7)L substitutions on the aggregation of wild-type and ANCL mutant CSP α	113
Figure 3.14. Analysis of CSP α palmitoylation turnover by click chemistry.....	115
Figure 3.15. Palmitoylated monomers of ANCL CSP α mutants are more short-lived than wild-type protein.....	116
Figure 3.16. Effect of palmitoylation inhibition on turnover of palmitoylation on ANCL mutant CSP α	117

Chapter 4

Figure 4.1. CSP α expression in ANCL and HD brain	130
Figure 4.2. Effects of hydroxylamine treatment of brain lysates from control and ANCL patients on CSP α migration profile.....	131
Figure 4.3. Expression levels of SNARE proteins in ANCL and HD brain.....	133
Figure 4.4. Detection of syntaxin 1, SNAP25, VAMP2 and assembled SNARE-complex in non-boiled ANCL and HD brain lysates.	135
Figure 4.5. Expression of α -synuclein in ANCL and HD brain.....	137
Figure 4.6. Expression of PSD95 in ANCL and HD brain.....	138
Figure 4.7. Synaptophysin expression in ANCL and HD brain.....	139
Figure 4.8. Expression of flotillin-1 and flotillin-2 in ANCL and HD brain	141
Figure 4.9. Aberrant expression profile of PPT1 in human brains carrying the <i>DNAJC5</i> mutation	142
Figure 4.10. Co-expression of HA-PPT1 and EGFP-tagged wild-type/ Δ L116/L115R CSP α	143
Figure 4.11. Effect of PPT1 on relative aggregation of ANCL mutants	144

Chapter 5

Figure 5.1. CSP α expression levels are increased by incubation of PC12 cells with MG-132.....	156
Figure 5.2. Expression of ANCL CSP α mutants is increased by incubation of PC12 cells with MG-132.....	157
Figure 5.3. Effect of different proteasomal inhibitors on the expression of wild-type and ANCL mutant CSP α	158
Figure 5.4. Analysis of the effect of 14KR mutations on the migration profile of wild-type and ANCL mutant CSP α on SDS gels.....	160
Figure 5.5. Effect of MG-132 on CSP α -14KR expression.....	161
Figure 5.6. Effect of proteasome and lysosome inhibitors on untagged CSP α constructs.....	163
Figure 5.7. Palmostatin B does not affect the accumulation of non-palmitoylated CSP α induced by proteasomal inhibitors.	165
Figure 5.8. Effect of cycloheximide (CHX) and MG-132 on CSP α expression.	166
Figure 5.9. Prediction of CSP α disordered regions.	168
Figure 5.10. EGFP-tagged C-terminal and N-terminal truncated CSP α mutants are degraded <i>via</i> the proteasome.	169
Figure 5.11. Untagged truncated CSP α mutants are degraded <i>via</i> the proteasome.	170
Figure 5.12. Effect of cysteine mutations in the CSD on degradation of CSP α <i>via</i> proteasome. ...	173
Figure 5.13. Effect of substitution of non-cysteine residues within the CSD on CSP α degradation.	174
Figure 5.14. Identification of potential PEST sequences in CSP α	175
Figure 5.15. PEST sequences do not drive proteasomal degradation on CSP α	176
Figure 5.16. Ubiquitination of EGFP-tagged CSP α constructs.	179
Figure 5.17. Evidence that CSP α is ubiquitinated in absence of lysines.	180
Figure 5.18. Ubiquitination of the ANCL CSP α mutants.	182

List of Tables

Chapter 1

Table 1.1. Involvement of zDHHs and acyl thioesterases in human disease.....	11
Table 1.2. Classification and characteristics of human NCLs.....	42

Chapter 2

Table 2.1. Oligonucleotide primers (5'>3') used to "humanise" bovine CSP α constructs by mutating the coding sequence of isoleucine (bovine) into the coding sequence for valine (human).....	52
Table 2.2. Oligonucleotide primers (5'>3') used to introduce the ANCL mutations into the 14KR mutant.....	52
Table 2.3. Oligonucleotide primers (5'>3') used to mutate the coding sequence for specific cysteine residues within the cysteine-string domain (CSD) to alanines.....	53
Table 2.4. Oligonucleotide primers (5'>3') used to mutate the coding sequence for specific cysteine residues within the CSD to leucines.....	53
Table 2.5. Oligonucleotide primers (5'>3') used to mutate the coding sequence for specific non-cysteine residues within the CSD to alanine.....	54
Table 2.6. Oligonucleotide primers (5'>3') used to mutate the coding sequence for PEST regions [regions rich in proline (P), glutamic acid (E), serine (S) and threonine (T)] within the C-terminal domain of CSP α	55
Table 2.7. Oligonucleotide primer (5'>3') used to mutate the coding sequence for lysines in the linker region of GW-pEF-BOS-HA to arginines.....	55
Table 2.8. Oligonucleotide primers (5'>3') used to introduce attB1/attB2 sequences, and START and STOP codons into CSP truncation mutants.....	56

List of Abbreviations

ABE	Acyl Biotin Exchange
AD	Alzheimer's disease
ALP	Autophagy-lysosome pathway
ALS	Amyotrophic lateral sclerosis
AMPA	α -amino-3-hydroxy-5-methyl-4-isoxazolepropionic acid receptor
ANCL	Adult-onset neuronal ceroid lipofuscinosis
ANOVA	Analysis of variance
APH-1	Anterior pharynx-defective 1
APP	Amyloid precursor protein
APS	Ammonium persulfate
APT1	Acyl protein thioesterase
APT1L	APT1-like
ATR	Anthrax-toxin receptor
AU	Arbitrary units
BACE1	β -site amyloid precursor protein-cleaving enzyme 1
BCA	Bicinchoninic acid
BF	Bafilomycin A1
BFA	Brefeldin A
BK	Calcium-activated potassium channels
BME	β -mercaptoethanol
BN-PAGE	Blue Native polyacrylamide gel electrophoresis
BSA	Bovine serum albumin
CATCHR	Complex associated with tethering containing helical rods
CFTR	Cystic fibrosis transmembrane conductance regulator

CHIP	C-terminus of Hsp70-interacting protein
CHX	Cycloheximide
CLN	Ceroid-lipofuscinosis neuronal gene
CMG2	Capillary morphogenesis gene 2
Cpx1	Complexin-1
Cpx2	Complexin-2
CR	Cysteine-rich
CSD	Cysteine-string domain
CSP α	Cysteine-string protein alpha
CTAF	Conotruncal Anomaly Face Syndrome
CTSD	Cathepsin D
DDM	n-dodecyl- β -D-maltoside
DEPC	Diethylpyrocarbonate
DMEM	Dulbecco's modified eagle medium
DNA	Deoxyribonucleic acid
dNTP	Deoxynucleotide
DTT	Dithiothreitol
ECL	Electrochemiluminescence
EDTA	Ethylenediaminetetraacetic acid
EF	Edema factor
EGFP	Enhanced green fluorescent protein
eNOS	Endothelial nitric oxide synthase
ER	Endoplasmatic reticulum
EtNP	Ethanolamine phosphate
FBS	Foetal bovine serum

FCS	Fluorescence correlation spectroscopy
Ftase	Farnesyl transferase
GAP43	Growth-association protein 43
GCF	Glycine–cysteine–phenylalanine
GDP	Guanosine-5'-diphosphate
GGTase I	Geranylgeranyl transferase I
GPCRs	G-protein-coupled receptors
GPI	glycosylphosphatidylinositol
GTP	Guanosine-5'-triphosphate
HA	Hydroxylamine
HD	Huntington's disease
HEK293T	Human embryonic kidneys 293T
HEPES	4-(2-hydroxyethyl)-1-piperazineethanesulfonic acid
Hh	Hedgehog proteins
HIP14	Huntingtin-interacting protein 14
HIP14L	HIP14-like
HPD	Histidine, proline, and aspartic acid
HRP	Horseradish peroxidase
Hsc70	70-kDa heat shock cognate protein
Hsp70	70-kDa heat shock protein
<i>HTT</i>	Huntingtin (gene)
Htt	Huntingtin (protein)
ID	Intellectual disability
INCL	Infantile neuronal ceroid lipofuscinosis
KO	Knock-out

LB	Lysogeny Broth
LC	Lactacystin
LC/ESI-MS/MS	liquid chromatography/electrospray ionization tandem mass spectrometry
LC-MS/MS	Liquid chromatography–mass spectrometry
LF	Lethal factor
LFB	Luxol fast blue
LFQ	Label free quantification
LP	Leupeptin hemisulfate
LSD	Lysosomal storage disorder
LYPLA1	Lysophospholipase
MAGUK	Membrane-associated guanylate kinase
MAPK	Mitogen-activated protein kinase
MG	MG-132
MS	Mass spectrometry
mSH	Metabolic serine hydrolase family
Munc	Mammalian uncoordinated, mammalian homologue of the <i>C. elegans unc</i> gene
MUN	Mammalian homologue of the <i>C. elegans unc</i> gene
NCL	Neuronal ceroid lipofuscinosis
NCT	Nicestrin
NMDA	N-methyl-D-aspartate receptor
NMT	N-myristoyl transferases
NP	Non-palmitoylated
NSF	N-ethylmaleimide-sensitive

P	Palmitoylated
p38	Synaptophysin
PA	Protective antigen
PalmB	Palmostatin B
PAS	Periodic acid-Schiff
PAT(s)	Protein acyltransferases
PBS	Phosphate-buffered saline
PBS-T	Phosphate-buffered saline-tween
PDZ domain	PSD95 – Drosophila disks large tumor suppressor (Dlg1) – zonula occludens-1 protein (zo-1)
PC12	Pheochromocytoma cell line 12
PCR	Polymerase chain reaction
PD	Parkinson's disease
PEN2/PSENEN	Presenilin Enhancer Gamma Secretase Subunit 2
PEST	Proline (P), glutamic acid (E), serine (S), and threonine (T)
PM	Plasma membrane
PPT1	Palmitoyl-protein thioesterase 1
PrDOS	Protein disorder prediction server
PS1	Presenilin -1
PSD	Post-synaptic density
PSD95	Postsynaptic density protein of 95 kDa
PTM	Post-translational modification
PVDF	Polyvinylidene difluoride
RIM	Rab3-interacting molecules
REAM	Reduced expression associated with metastasis

SDM	Site-directed mutagenesis
SDS	Sodium dodecyl sulfate
SDS-PAGE	Sodium dodecyl sulfate polyacrylamide gel electrophoresis
SEM	Standard Error of the Mean
SGT	Small glutamine-rich tetratricopeptide repeat-containing protein
SM proteins	Sec1/Munc18-like proteins
SNAP25	Synaptosome-associated protein of 25 kDa
SNARE	Soluble NSF attachment protein receptor
SNP	Single nucleotide polymorphism
SOC	Super optimal broth
SYP	Synaptophysin
Syt1	Synaptotagmin 1
TEM8	Tumour endothelial marker 8
TEMED	N,N,N',N'-tetramethyl-ethane-1,2-diamine
TFA	Trifluoroacetic acid
TMD	Transmembrane domains
TPP1	Tripeptidyl peptidase 1
Ub	Ubiquitin
UPS	Ubiquitin-proteasome systems
UV	Ultraviolet
VAMP2	Vesicle-associated protein 2/synaptobrevin
VCFS	Velo-Cardio Facial Syndrome
vGLUT	vesicular glutamate transporter
WT	Wild-type
XLMR	X-linked mental retardation

Abstract

Neuronal Ceroid Lipofuscinoses (NCLs) are neurodegenerative lysosomal-storage disorders characterized by intracellular accumulation of autofluorescent material. Mutations in the *DNAJC5* gene encoding Cysteine-String Protein alpha (CSP α) cause autosomal-dominant adult-onset NCL (ANCL). The disease-causing mutations occur within the cysteine-string domain (CSD), a region of the protein that is extensively palmitoylated.

It has been shown that the ANCL CSP α mutants form aggregates and that this is dependent on palmitoylation. As aggregation is a common feature of neurodegenerative disorders, aggregates formed in ANCL are likely to contribute, together with loss-of-function effects, to disease pathology. The aims of this project were to: (i) investigate features of CSP α that are important for aggregate formation; (ii) identify molecular changes that occur in ANCL; and (iii) identify mechanisms regulating CSP α turnover to provide insight into pathways that might be perturbed in ANCL.

A cluster of palmitoylated cysteines in the CSD were identified as essential for aggregation of the ANCL CSP α mutants, further supporting an association between palmitoylation and aggregation. Analysis of the expression levels of different proteins in post-mortem brain revealed a massive increase in expression of the palmitoyl thioesterase enzyme PPT1 in ANCL samples, which is intriguing as PPT1 functions to depalmitoylate proteins during their degradation and mutations in the *PPT1* gene cause infantile NCL. Further analysis identified several other proteins that had altered expression levels including α -synuclein. Degradation of both wild-type and mutant CSP α proteins was mediated by the proteasome but was independent of lysine ubiquitination. This pathway mediated rapid degradation of non-palmitoylated protein, and blocking proteasome activity enhanced the formation of mutant

aggregates. It will be important in future work to determine how mutations in CSP α affect protein degradation pathways to cause the characteristic NCL lysosomal morphology, and whether there is a role for the lysosome in degradation of palmitoylated or aggregated CSP α .

Chapter 1: Introduction

1.1 Lipid modifications

Proteins are chemically modified in many different ways, which has a major impact on their localisation and functional output. In particular, a wide array of cellular proteins are modified by the covalent binding of lipid groups, including fatty acids, sterols, isoprenoids, phospholipids and glycosylphosphatidylinositol (GPI) (Resh 2013); the covalent attachment of lipid groups to a peptide chain is generally known as lipidation. Due to their hydrophobicity, lipid modifications often enable soluble proteins to become membrane-associated. However, this is not the only role of lipid modifications, which can also modulate protein localisation, stability and function *via* many distinct mechanisms. Lipid modifications can be divided into two sub-groups based on the location where the modification occurs (Nadolski and Linder 2007): cytoplasmic lipidation events include N-myristoylation, S-acylation and prenylation, whereas the attachment of GPI anchors and sterols occurs in the lumen of the secretory pathway.

Prenylation is a post-translational process involving the attachment of farnesyl (C15) or geranylgeranyl (C20) isoprenoids to a C-terminal cysteine *via* an irreversible thioether linkage (Zhang and Casey 1996). The attachment of isoprenoids occurs at a defined CAAX consensus sequence, where A is an aliphatic residue and X is any amino acid. The specific residue present at the X position plays a major role in determining whether the prenylated protein is modified by a farnesyl transferase (FTase) or a geranylgeranyl transferase I (GGTase I). Geranylgeranyl transferase II (GGTase II) recognises a different consensus

sequence (either CXC or CC) and is responsible for the modification of Rab proteins (Resh 2013; Chamberlain and Shipston 2015).

N-myristoylation involves the covalent co-translational addition of myristic acid (C₁₄) to an N-terminal glycine residue *via* an amide bond following the cleavage of the adjacent initiating methionine (Nadolski and Linder 2007; Salaun et al. 2010). N-myristoyltransferases (NMT1 and NMT2) catalyse the covalent attachment of myristic acid to proteins containing the N-terminal consensus sequence Met-Gly-X-X-X-Ser/Thr. Although N-myristoylation generally occurs co-translationally, facilitated by binding of NMTs to ribosomes, and is irreversible, the reaction can also occur post-translationally during apoptosis as a result of exposure of N-terminal glycines following caspase cleavage (Resh 2013).

Glypiation involves the attachment of a phosphatidylinositol group to proteins *via* a carbohydrate-containing linker and *via* an ethanolamine phosphate (EtNP) which is linked to the C-terminal region of the protein. Following addition of the GPI anchor in the endoplasmic reticulum (ER), the modified protein travels through the secretory pathway and becomes attached to the extracellular face of the plasma membrane (Nadolski and Linder 2007; Resh 2013; Englund 1993).

In contrast to the lipid modifications described above, S-acylation is a reversible lipid modification (Nadolski and Linder 2007; Salaun, Greaves, and Chamberlain 2010; Triola, Waldmann, and Hedberg 2012; Chamberlain and Shipston 2015) and is the general term used to designate the addition of fatty acids to cysteine residues through a labile thioester bond. Palmitate (C₁₆) is the most common fatty acid attached to cysteines, explaining why this process is frequently referred to as “palmitoylation” (and will be for the remainder of this thesis). However it should be noted that other acyl groups with different chain length

and degree of unsaturation can also modify proteins in a similar manner, such as stearate (C18:0) and oleate (C18:1) (Salaun, Greaves, and Chamberlain 2010; Greaves and Chamberlain 2011b; Chamberlain and Shipston 2015).

1.2 Palmitoylation

It is over 35 years since protein palmitoylation was first identified (Schmidt and Schlesinger 1979); despite this, research on this process has lagged far behind some other post-translational modifications such as phosphorylation and ubiquitination.

S-Palmitoylation refers to the reversible thioester linkage between the sulfur on the cysteine residue to the electron-rich oxygen of the palmitate. By contrast, N-palmitoylation differs from S-palmitoylation by the fact that the cysteine being modified is always located at the N-terminal of the protein. Moreover, in N-palmitoylation the palmitate temporarily bonds with the sulfur, like in S-palmitoylation, and then quickly binds to the amine of the cysteine for stability. O-palmitoylation refers to the addition of lipids to a serine residue *via* an oxyester linkage. Importantly, S-palmitoylation (hereafter referred to as palmitoylation) is the only reversible modification.

The Wnt family is a group of secreted palmitoylated proteins that play a role in embryonic development and carcinogenesis. O-palmitoylation is necessary for Wnt3a transport from the ER for secretion to exosomes (Takada et al. 2006; Gao and Hannoush 2014). Ghrelin, a 28 aminoacid appetite-stimulating peptide hormone secreted by the food-deprived stomach, is another example of O-palmitoylation. Palmitoylation of ghrelin by the Ghrelin O-Acyltransferase (GOAT) is required for growth hormone releasing activity (Yang et al. 2008).

N-palmitoylation occurs on hedgehog proteins (Hh), which are morphogens highly present during embryonic development and tumour growth in adults. Following entry into the lumen of the ER, Hh is cleaved between the glycine and cysteine residues of a glycine–cysteine–phenylalanine (GCF) sequence *via* an auto-processing event, resulting in a cut protein. The resulting protein has now a C-terminal glycine, to which a cholesterol molecule is added, and an N-terminal Cys residue that becomes N-palmitoylated.

By contrast, examples of S-palmitoylated proteins include G-protein-coupled receptors (GPCRs), G α subunits, Src family kinases, cell adhesion proteins (such as integrins and claudins), Ras proteins, endothelial nitric oxide synthase (eNOS) and membrane fusion proteins (Greaves and Chamberlain 2011a).

1.2.1 Regulation of palmitoylation

Palmitoylation has no single sequence requirement other than the presence of a cysteine residue. Although no consensus amino acid sequence has been identified, only specific cysteines are modified, therefore indicating that a specificity of sequence recognition may exist. Indeed, palmitoylated cysteines share some common features: (i) they are often found adjacent to prenylation and myristoylation sites in soluble proteins (up to 20 residues away); and (ii) they are frequently located at the interface of the cytoplasm and membranes or in cytoplasmic C-terminal tails of transmembrane proteins (Nadolski and Linder 2007; Salaun et al. 2010).

Interestingly, while palmitoylation was firstly described over 30 years ago, information about the identity of enzymes that regulate this modification did not emerge until the last decade.

The regulation of the palmitoylation status is determined by two types of enzymes: protein acyltransferases (PATs), which catalyse the addition of palmitate (and other fatty acids) to the substrate; and protein acylthioesterases, responsible for mediating the removal of the fatty acid (Nadolski and Linder 2007; Chamberlain and Shipston 2015).

1.2.1.1 The zDHHC family of palmitoyl acyltransferases

The most important breakthroughs in the search for PATs came from investigations in the yeast *Saccharomyces cerevisiae*, where: (a) the proteins Erf2p and Erf4p were identified as crucial for palmitoylation of Ras2p (Lobo et al. 2002); and (b) Akr1p was identified as a PAT that was sufficient to catalyse palmitoylation of casein kinase Yck2p (Roth et al. 2002). Both Erf2p and Akr1p were shown to share a conserved 51-amino acid DHHC (aspartate-histidine-histidine-cysteine) – cysteine rich (CR) zinc finger-like domain that was essential for palmitoylation (note that in Akr1p, the motif is actually “DYHC” (Mitchell et al. 2006)). This DHHC-CR domain is now known to be the defining characteristic of PATs, and led to the discovery of a family of 24 *ZDHHC* genes in mammalian genomes.

zDHHC enzymes are polytopic membrane proteins containing between four and six transmembrane domains (TMD), with the catalytic domain present on the cytosolic face of the membrane. The majority of these proteins are localised in the ER or Golgi (Ohno et al. 2006), with some exceptions such as zDHHC5, which is present in the plasma membrane (Greaves and Chamberlain 2011a; Gorleku et al. 2011). As all known PATs are integral membrane proteins, the palmitoylation reaction can only occur if the protein substrates are in close proximity to the membrane.

There is no defined general consensus sequence within proteins specifying palmitoylation, however some progress has been made in identifying features in substrate proteins that are recognised by specific zDHHC enzymes. For example, recent work identified a short linear peptide sequence present within multiple proteins that is recognised by zDHHC17 and zDHHC13 and important for palmitoylation of proteins such as SNAP25 and CSP α (Greaves et al., 2009; Lemonidis et al., 2015). In addition, zDHHC5 and zDHHC8 recognise PDZ domains in substrates *via* their PDZ ligand domains (Thomas et al. 2012). Although some substrates are dependent upon a specific zDHHC enzyme for their palmitoylation, such as the yeast Chs3p protein, which is specifically modified by the zDHHC enzyme Swf1p (Lam et al. 2006), other proteins appear to be substrates for multiple zDHHC enzymes. Indeed, over-expression of a number of zDHHC enzymes rescued palmitoylation of VAC8 in a *Saccharomyces cerevisiae* depleted of the zDHHC protein Pfa3 (Roth et al. 2006), and co-expression studies identified zDHHC3, zDHHC7, zDHHC15 and zDHHC17 as enzymes that are active against SNAP25 and CSP α (Greaves et al. 2008; Greaves et al. 2010).

1.2.1.2 Protein thioesterases

Protein depalmitoylation is mediated by acyl protein thioesterase (APTs). Acyl protein thioesterase 1 (APT1) is a cytoplasmic enzyme first identified as a lysophospholipase I (LYPLA1) able to remove palmitate from G α_s (Duncan and Gilman 1998). Later work identified other substrates of APT1, such as H/N-Ras (Dekker et al. 2010), endothelial nitric oxide synthase (eNOS) (Yeh et al. 1999), G α subunits (Duncan and Gilman 2002) and SNAP23 (Flaumenhaft et al. 2007). Through bioinformatics analysis, two additional APT1-related proteins were identified: APT2 (which shares ~64% amino acids with APT1) and APT1-like (APT1L, which has ~31% identity to APT1) (Zeidman et al. 2009). APT2 has been

shown to function as a thioesterase against growth-association protein 43 (GAP43) and H-Ras (Tomatis et al. 2010; Chamberlain and Shipston 2015), while APT1L is highly expressed in adipose tissues and reportedly has depalmitoylation activity against calcium-activated potassium (BK) channels (Tian et al. 2012).

Protein palmitoyl thioesterase 1 (PPT1) is an additional enzyme mediating protein depalmitoylation, which was first described as a thioesterase largely found in cytosolic fractions and active against H-Ras and G α (Camp and Hofmann 1993). However, subsequent studies showed that PPT1 is actually targeted to lysosomes and depalmitoylates proteins undergoing lysosomal degradation (Verkruyse and Hofmann 1996). PPT2 is another lysosomal thioesterase which shares 18% amino acid identity with PPT1, although its physiological function remains unknown and substrates have not yet been identified (Soyombo and Hofmann 1997).

The study of protein depalmitoylation has undergone a major renaissance in the last few years, following identification of additional protein thioesterases within the metabolic serine hydrolase family (mSH), such as ABHD17 identified as a thioesterase for H- and N-Ras (Lin and Conibear 2015) and ABHD16 identified as a thioesterase for PSD95 (Yokoi et al. 2016).

1.2.2 Functions of palmitoylation

The most frequently described function of palmitoylation is to increase the affinity of soluble proteins for membranes, thus affecting protein localisation and function. Other roles of palmitoylation include modifying protein stability, protein trafficking, controlling

interaction with other proteins, as well as targeting proteins to defined membrane domains (Nadolski and Linder 2007; Blaskovic et al. 2013).

Regulation of protein trafficking by palmitoylation-depalmitoylation reactions affects a wide range of cellular proteins (Greaves and Chamberlain 2007), although it has been especially well illustrated for palmitoylated forms of the GTPase Ras (Resh 2006; Nadolski and Linder 2007; Linder and Deschenes 2007). The GTPases N- and H-Ras are key regulators of the mitogen-activated protein kinase (MAPK) cascade and are known to cycle between different intracellular membranes regulated by dynamic palmitoylation. All Ras isoforms undergo a complex series of post-translational modifications: farnesylation, proteolytic removal of the AAX motif at the C-terminal and carboxymethylation of the farnesylated cysteine. Farnesylated H- and N-Ras proteins exhibit a weak membrane affinity and interact with Golgi membranes, where palmitoylation occurs (Swarthout et al. 2005). Palmitoylation at this compartment promotes stable membrane association and facilitates vesicular transport to the plasma membrane (Rocks et al. 2005). At the plasma membrane, Ras is depalmitoylated and released into the cytosol. The process of re-palmitoylation occurs again at the Golgi, resulting in repeated traffic to the plasma membrane (Rocks et al. 2005; Rocks et al. 2010). This cycle is important in maintaining the specific localisation of Ras isoforms on Golgi and plasma membranes (Nadolski and Linder 2007; Salaun et al. 2010; Aicart-Ramos et al. 2011).

Palmitoylation also regulates the trafficking of transmembrane proteins. For example, LRP6 is a co-receptor for Wnt and undergoes palmitoylation at the ER (Abrami et al. 2008). Blocking palmitoylation leads to accumulation of the protein at the ER and prevents delivery to the plasma membrane (Abrami et al. 2008). In this case, palmitoylation was proposed to mediate tilting of the single transmembrane domain of LRP6 in ER membranes

to facilitate hydrophobic matching with the ER membrane, preventing aggregation and facilitating ER exit.

Another role for palmitoylation is the regulation of protein stability, as observed in the case of the *S. cerevisiae* SNARE protein Tlg1 (Valdez-Taubas and Pelham 2005), which mediates vesicle trafficking between the Golgi and endosome compartments (Siniosoglou and Pelham 2001; Coe et al. 1999). Palmitoylation of Tlg1 prevents its ubiquitination by the E3 ubiquitin ligase Tul1 and subsequent degradation at the vacuole (Valdez-Taubas and Pelham 2005). Palmitoylation is thought to change the interaction of Tlg1 with the membrane, allowing it to escape ubiquitination and rapid degradation (Valdez-Taubas and Pelham 2005). A similar interplay between palmitoylation and ubiquitination has been described for several other proteins and the regulation of protein stability is emerging as a major function of palmitoylation (Linder and Deschenes 2007; Chamberlain and Shipston 2015).

1.2.3 Palmitoylation in neurological disorders

Abnormal regulation of palmitoylation has been associated with a number of human diseases. This dysregulation can be caused either by mutations in the palmitoylated proteins or by aberrant expression of the enzymes involved. Several zDHHC enzymes have been linked with human disorders (see Table 1.1): zDHHC5 and 19 with X-linked intellectual disability (Raymond et al. 2007), zDHHC17 and 13 with Huntington's disease (Milnerwood et al. 2013; Singaraja et al. 2011; Sutton et al. 2013), zDHHC8 with schizophrenia, and also zDHHC2, 9, 11 and 14 have been found to be implicated in various forms of human cancer

(Yan et al. 2013; Anami et al. 2010; J. U. Kang et al. 2008; Mansilla et al. 2007; Yamamoto et al. 2007).

Table 1.1. Involvement of zDHHCs and acyl thioesterases in human disease.

Human disease	Enzyme	Experimental model	Evidence	Reference
Schizophrenia	zDHHC8	Human	An SNP (A-allele of rs175174) in <i>ZDHH8</i> gene is associated with an increased risk of schizophrenia. The allele is predicted to encode a truncated protein. Other studies failed in the association of zDHHC8 and schizophrenia.	(Mukai et al. 2008; Mukai et al. 2004; Liu et al. 2002; Chen et al. 2004)
Huntington's disease	zDHHC13 (HIP14L) zDHHC17 (HIP14)	Animal model/ <i>in vitro</i>	<ul style="list-style-type: none"> • zDHHC13 (HIP14L) and zDHHC17 (HIP14) enzymes mediate palmitoylation of huntingtin protein (HTT). • HIP14 is a major PAT for HTT, and HTT also regulates enzymatic activity of HIP14. • Palmitoylation and interaction Htt-HIP14 is reduced in presence of disease-causing mutation in HTT. • Reduced HTT palmitoylation in YAC128 mouse model of HD. 	(Huang et al. 2004; Yanai et al. 2006; Singaraja et al. 2002; Huang et al. 2011; Singaraja et al. 2011; Sutton et al. 2013)
X-linked intellectual disability (XLID)	zDHHC9 zDHHC15	Human Human	<ul style="list-style-type: none"> • Mutations in ZDHH9 cause moderate XLID in males in 4 of 250 families that were studied • A chromosomal translocation event disrupting ZDHH15 identified in a single patient with severe nonsyndromic XLID, epileptic seizures, dysmorphic facial appearance 	(Raymond et al. 2007; Mansouri et al. 2005; Baker et al. 2015)
Cancer	zDHHC2	Human	<ul style="list-style-type: none"> • zDHHC2 expression downregulated in colorectal cancers and gastric adenocarcinoma, • zDHHC2 is also named REAM (reduced expression associated with metastasis) 	(Yan et al. 2013)
	zDHHC9	Human	zDHHC9 is strongly upregulated in adenocarcinomas of the gastrointestinal tract.	(Mansilla et al. 2007; Birkenkamp-Demtroder et al. 2002)
	zDHHC11	Human	Increased copy number of ZDHH11 in bladder cancers, biomarker identifying high risk patients with disease progression	(Kang, Koo, Kwon, Park, and Kim, 2008)

	zDHHC14	Human	Increased expression of zDHHC14 in gastric cancer	(Anami et al. 2010; Oo et al. 2014)
Ischemic stroke	zDHHC17 (HIP14)	Animal model	<ul style="list-style-type: none"> • zDHHC17 contributes to acute ischemic brain injury <i>via</i> a mechanism not related to its palmitoylating activity. zDHHC17 interacts with c-Jun N-terminus kinase (JNK) to form a signalling module for JNK activation. • Enhanced interaction of zDHHC17 with JNK3 in brains from a rat model of transient ischemic stroke. Inhibition of this interaction (before or after the ischemic insult) reduced the infarct size by 80%. 	(Yang and Cynader, 2011)
Alzheimer's disease	zDHHC12	<i>In vitro</i>	zDHHC12 modifies APP metabolism (including A β production)	(Mizumaru et al. 2009)
Infantile NCL	Ppt1	Human	Mutations in <i>PPT1</i> cause infantile NCL	(Vesa et al. 1995)

Microdeletions at the 22q11 locus (also known as DiGeorge Syndrome, Conotruncal Anomaly Face Syndrome (CTAF) or Velo-Cardio Facial Syndrome (VCFS), amongst others) are associated with an increased prevalence of psychiatric disease, including schizophrenia (Liu et al. 2002). The gene encoding for zDHHC8 is one of the genes disrupted by the microdeletions (Liu et al. 2002). Indeed, a single nucleotide polymorphism (SNP) identified in the *ZDHHC8* gene was associated with an increased risk of schizophrenia in the Han-Chinese population (Chen et al. 2004). Although this association was not observed in a number of other population groups (Ota et al. 2013; M. Xu et al. 2010), knock-out of zDHHC8 in mice leads to a deficit in pre-pulse inhibition, which is also seen in patients with schizophrenia, and a decreased complexity of dendritic spines and a reduced number of glutamatergic synapses (Mukai et al. 2008).

Mutations in zDHHC enzymes have also been shown to cause intellectual disability (ID), which is associated with a reduced capacity for cognitive processing. A study of 250 patients with X-linked ID identified four families with mutations in the *ZDHHC9* gene, whereas a separate study identified a disruption in the *ZDHHC15* gene as the cause of ID in a single female patient (Mansouri et al. 2005; Raymond et al. 2007). The mutations in the *ZDHHC9* gene that cause ID either introduce point mutations into the DHHC-CR domain, which have been shown to inhibit enzyme activity (Mitchell et al. 2014), or result in truncation of the enzyme due to premature stop codons.

Alzheimer's disease (AD) is the most common cause of dementia, characterised by memory loss and decline

in other intellectual and cognitive abilities. The major pathogenic feature of AD is the presence of neurotoxic beta-amyloid (A β) (Hardy and Selkoe 2002), generated by the

cleavage of amyloid precursor protein (APP). The proteolytic cleavage of APP is performed by the β -site APP-cleaving enzyme 1 (BACE1) and the multiprotein complex γ -secretase. zDHH12 has been associated with APP regulation and trafficking: the retention of APP in the Golgi due to zDHH12 palmitoylation has been found to inhibit APP metabolism and thus A β formation (Mizumaru et al. 2009). Although there is an evident association between APP processing enzymes and palmitoylation, it is important to note that no genetic link has been found to date (Young et al. 2012).

A potential role of γ -secretase palmitoylation in the regulation of A β depositions in the brain has also been observed. The γ -secretase multiprotein complex consists of four catalytic subunits: presenilin 1 (PS1), presenilin enhancer Gamma-Secretase Subunit 2 (PEN2, PSENEN), anterior pharynx-defective 1 (APH-1) and nicastrin (NCT) (Kaether et al. 2006). Both APH-1 and NCT are palmitoylated, enhancing γ -secretase stability and association with lipid rafts without affecting its activity and the processing of APP (Cheng et al. 2009). However, transgenic mice co-expressing palmitoylation-deficient APH-1 and NCT showed a reduction of amyloid deposits (Meckler et al. 2010).

Another neurological disorder linked to palmitoylation is Huntington's disease (HD). HD is an adult-onset autosomal-dominant neurodegenerative disease, caused by a mutation in the *huntingtin* (*HTT*) gene. The mutation consists on a CAG repeat expansion in exon 1 of the *HTT* gene, which leads to the extension of a normal-length polyglutamine stretch to more than 35 repeats (Macdonald et al. 1993; Aronin et al. 1995). The motor disorder of HD includes both voluntary and involuntary components, such as chorea and dystonia, developing to a state in which voluntary movement is no longer possible. Other clinical features of the disease include slowing of intellectual processes, eventually leading to dementia, as well as depression and changes in personality (De Souza and Leavitt 2014).

HTT encoding protein (HTT) undergoes a number of post-translational modifications, including palmitoylation (Ehrnhoefer et al. 2011). HTT is palmitoylated at cysteine 214 by HIP14 (Huntingtin Interactin Protein 14, or zDHHC17) and HIP14L (HIP14-like, zDHHC13) (Yanai et al. 2006; Sanders and Hayden 2015). The interaction of mutant HTT and its palmitoylating enzymes is dependent on the length of the polyglutamine tract, with mutant HTT showing a decreased palmitoylation profile, which increases inclusion formation (Huang et al. 2004; Yanai et al. 2006). Interestingly, the activity of zDHHC17 is also positively modulated by HTT protein (Huang et al. 2011), suggesting that loss of HTT function may lead to a decrease in zDHHC17 activity, which could contribute to some of the features of HD. The idea that loss of palmitoylation might contribute to HD pathology is supported by work showing that zDHHC17-deficient mice display behavioural and neuropathological deficits similar to those seen in HD mouse models, including loss of medium spiny neurons in the striatum (Singaraja et al. 2011). Moreover, zDHHC13-deficient mice also develop adult-onset, progressive neuropathology, together with movement disorders and altered palmitoylation of SNAP25 (Sutton et al. 2013).

Neuronal Ceroid Lipofuscinoses (NCL) are a group of neurodegenerative disorders defined by the accumulation of autofluorescent lipopigment in cells (Jalanko and Braulke 2009). NCLs are classified as infantile, juvenile and adult depending on the age of symptomatic onset (Mole and Cotman 2015). Mutations in the *PPT1* gene on chromosome region 1p32, which encodes for the lysosomal thioesterase PPT1, cause infantile NCL (E. Hellsten et al. 1993), while mutations in the *DNAJC5* gene encoding CSP α , a highly palmitoylated pre-synaptic chaperone, have been identified as the cause of adult-onset NCL (ANCL) (Nosková et al. 2011; Velinov et al. 2012; Benitez et al. 2011; Cadieux-Dion et al. 2013).

1.3 Palmitoylation in synaptic function

Protein palmitoylation regulates various aspects of neuronal trafficking and function. The reversible nature of palmitoylation allows proteins to travel between different compartments and re-localise in different contexts (Fukata and Fukata 2010).

Neurons are characterised by their highly polarised morphology, unlike many of the cells of the human body. Neurons have two types of processes, long (axon) and branching (dendrites). The shape of neurons reflects their role in communication, where dendrites conduct signals from post-synaptic terminals to the cell body, and axons conduct signals from the cell body to the pre-synaptic terminals (Chklovskii 2004). Such specialised cell shape and function requires a precise trafficking and distribution of proteins. For example, proteins that mediate neurotransmitter synthesis, vesicle fusion and neurotransmitter release accumulate at pre-synaptic termini (axons), whereas neurotransmitter receptors and postsynaptic scaffolds localise on the opposite post-synaptic site (postsynaptic termini, dendrites). This precise distribution and localisation of some of these neuronal proteins is mediated or facilitated by palmitoylation (Fukata and Fukata 2010).

1.3.1 Synaptic vesicle exocytosis

Exocytosis is the fusion of intracellular vesicles with the plasma membrane, and it is essential for life in eukaryotes. Exocytosis takes place over two different pathways: constitutive, which occurs in all eukaryotic cells in the absence of external signals; and regulated, which consists of a more specialised pathway. Regulated exocytosis occurs in response to particular stimuli, such as the release of neurotransmitters at the presynaptic termini, mediated by Ca^{2+} -triggered synaptic vesicle exocytosis (Lin and Scheller 2000).

The lipids and integral membrane proteins that make up synaptic vesicles are initially synthesised in the ER and modified in the Golgi apparatus in the soma of the neurons (Lin and Scheller 2000). The assembly and maturation of synaptic vesicles at the nerve terminal involves a trafficking cycle consisting of various steps, including fusion with the plasma membrane and subsequent endocytosis. In order for efficient Ca^{2+} -secretion coupling to occur, synaptic vesicles need to be docked in active zones, specialised presynaptic areas enriched in voltage-gated Ca^{2+} channels. Synaptic vesicles dock at the presynaptic membrane in active zone, and subsequently undergo a vesicle priming step (Südhof 2004; Rizo and Xu 2015; Lin and Scheller 2000). The priming reaction leaves the vesicles ready to preferentially fuse with the plasma membrane upon Ca^{2+} influx, subsequently producing a postsynaptic signal (Südhof 2013).

The key proteins universally involved in all intracellular fusion reactions, and thus also in neuronal synaptic vesicle exocytosis (Figure 1.1), belong to at least four different families: (i) the SNAREs (SNAP receptors) and associated proteins (N-ethylmaleimide sensitive factor [NSF] and soluble NSF attachment proteins [SNAPs]); (ii) Sec1/Munc18-like (SM) proteins; (iii) small GTPases known as Rabs; and (iv) a group of tethering proteins named CATCHR proteins (complex associated with tethering containing helical rods) (Jahn and Fasshauer 2012; Rizo and Xu 2015). The SNAREs are thought to play an essential role in membrane fusion (Sollner, Whiteheart, et al. 1993), while the other groups are considered SNARE regulators (Rizo and Xu 2015).

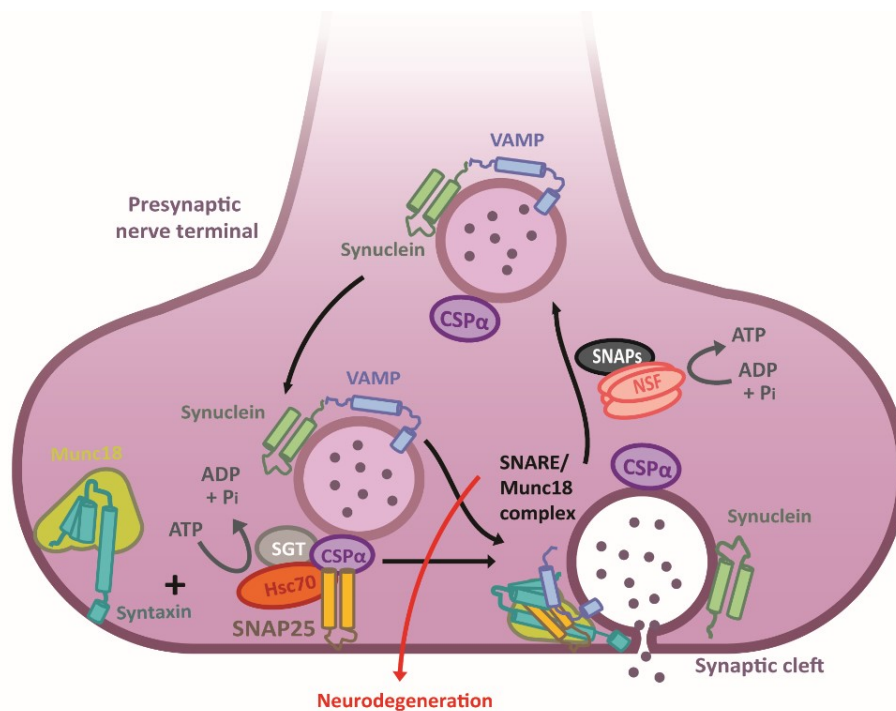


Figure 1.1. Synaptic vesicle exocytosis. The chaperone complex formed by CSP α -Hsc70-SGT binds to SNAP25 on the target membrane, refolding SNAP25 to be SNARE-complex competent. Interaction of SNAP25 with VAMP and syntaxin through their highly-conserved SNARE motifs forms an extremely stable four-helix bundle, known as SNARE-complex, which brings together the vesicle and plasma membranes, facilitating their fusion and release of the vesicle contents.

1.3.2 SNARE proteins and membrane fusion

SNARE proteins are critical for most types of intracellular membrane trafficking. The critical role of SNARE proteins in membrane fusion at the synapse was observed when the proteins were identified as targets of tetanus and clostridial botulinum toxins (Schiavo et al. 2000).

SNAREs are a superfamily of proteins that vary in size and structure, and which share a conserved ~65-residue homologous sequence (the SNARE motif) (Weimbs et al. 1997; Rizo and Xu 2015). SNAREs are present in all eukaryotic cell types, ranging from yeast to humans (Jahn et al. 2003; Ramakrishnan et al. 2012). The SNARE proteins associated with vesicles are named vesicle-SNAREs (v-SNAREs), whereas those proteins present at the target membrane (e.g. the presynaptic plasma membrane) are named t-SNAREs (Sollner et al. 1993; Ramakrishnan et al. 2012). In neuronal synaptic vesicle exocytosis, the v-SNARE is Synaptobrevin-2/VAMP2 (vesicle-associated membrane protein), and the plasma membrane SNARE proteins are SNAP25 (synaptosomal-associated protein of 25 kDa) and syntaxin-1.

SNARE proteins undergo a cycle of assembly and disassembly that drives the membrane fusion reaction. The SNARE complex is highly stable, as reflected by its resistance to denaturing conditions in the presence of the ionic detergent sodium dodecyl sulfate (SDS) (Hayashi et al. 1994; Yang et al. 1999). The interaction of the v-SNARE VAMP2 with the t-SNAREs syntaxin-1 and SNAP25 (Sollner et al. 1993a; Sollner et al. 1993b), brings the two opposing membranes into close proximity and is thought to drive membrane fusion (Weber et al. 1998). During SNARE complex association, the individual helical SNARE motifs of the SNARE proteins interact, starting from their N-termini, to form a parallel four-helix bundle (Lin and Scheller 1997; Poirier et al. 1998). “Zippering” of this *trans*-SNARE complex (also known as a “SNAREpin”) leads to interactions at the membrane-proximal C-terminal ends of the SNAREs to form a *minimal* membrane fusion machinery (Weber et al. 1998). Many other proteins enhance SNARE-driven membrane fusion including SM proteins and the Ca²⁺ sensor synaptotagmin. The SNARE/SM protein complex assembly is maintained by chaperones such as CSP α and synucleins (Südhof 2013). After membrane fusion, the initial *trans*-SNARE complex is converted into a *cis*-SNARE complex and dissociated by the action

of α -SNAP and the ATPase NSF, concluding the cycle and allowing the free SNAREs to be released and start a new round of fusion (Sollner et al. 1993; Lin & Scheller 1997; Montecucco et al. 2005).

SNARE complexes contain a conserved hydrophilic layer of amino acids known as the "0" layer, consisting of an arginine (R) residue and three glutamine (Q) residues (Fasshauer et al. 1998). In light of this observation, it was suggested that SNARE motifs can be classified into four groups: Qa-, Qb-, Qc- and R-SNAREs. Qa- SNAREs include syntaxins, while Qb- and Qc- are homologs of the N-terminal and C-terminal SNARE motifs, respectively, of SNAP25 (Fasshauer et al. 1998; Bock et al. 2001). Thus, all functional SNARE complexes appear to contain Qa, Qb, Qc, and R SNAREs (Fasshauer et al. 1998).

1.3.2.1 Syntaxin

Syntaxins are t-SNARE proteins that typically contain a C-terminal transmembrane domain. The neuronal syntaxin isoform, syntaxin-1, was originally described as an antigen for the monoclonal antibody, HPC-1, which recognises ~35 kDa proteins (now known as syntaxin-1A and 1B) in the plasma membrane in neurons (Bennett et al. 1992; Yoshida et al. 1992).

The syntaxin family consists of 7 genes in yeast and 15 in mammals, and additional diversity is generated by alternative splicing, which generates syntaxins that are differentially expressed during development and that have distinct functions (Teng et al. 2001). Syntaxin-1A is an isoform exclusively found in neuronal and (neuro)endocrine cells, which functions in regulated exocytosis at the plasma membrane.

Syntaxins consist of a single transmembrane domain and a cytoplasmic region which contains a SNARE domain (H3) and a regulatory domain (H_{abc}). The SNARE domain of syntaxin-1 forms a stable complex with VAMP2 and SNAP25 (Sollner et al. 1993; McMahon and Sudhof 1995). The H_{abc} domain contains three α -helices that fold forming a closed configuration, and unfold to expose the SNARE motif to allow interaction during vesicle fusion. In addition to SNAP25 and VAMP2, syntaxin-1 interacts with a number of proteins, including Munc18 (Hata et al. 1993), Munc13 (Betz et al. 1997) and CSP α (Nie et al. 1999).

1.3.2.2 SNAP25

SNAP25 is essential for synaptic vesicle exocytosis in neurons (Banerjee et al. 1996), and also adrenal chromaffin cells (Lawrence et al. 1994) and pancreatic beta cells (Sadoul et al. 1995), which are the main cell types where it is expressed. In contrast, the SNAP25 homologous protein, SNAP23, is ubiquitously expressed and is mainly involved in regulated exocytosis in non-neuronal cells (e.g. Ravichandran et al. 1996) but has also been shown to function in neuronal exocytosis pathways such as those involved in inserting glutamate receptor proteins into the postsynaptic membrane (Suh et al. 2010).

There are two homologous forms of SNAP25: A and B, which differ by only nine amino acids (Bark 2004). The expression of both of these isoforms is exclusive to neuronal and (neuro)endocrine cells.

In the core SNARE complex, syntaxin binds to SNAP25, contributing to a conformational change in SNAP25 which is essential for the formation of the complex (Fasshauer et al. 1997). SNAP25 contributes two α -helices to the SNARE core complex, one SNARE motif from its N-terminal domain and the other from its C-terminal domain (Sutton et al. 1998).

As expected, a SNAP25 knockout (KO) mice shows inhibition of Ca²⁺-triggered exocytosis (Washbourne et al. 2002).

1.3.2.3 VAMP

The vesicle-associated membrane protein (VAMP; also known as synaptobrevin) is a small 19 kDa conserved C-tail anchored proteins, first identified as a neuronal specific protein isolated from a cDNA expression library of *Torpedo californica* electromotor nucleus (Trimble et al. 1988). Different VAMP isoforms have been identified, localised to distinct subcellular compartments and involved in membrane fusion events there (Stegmaier et al. 1999; Sander et al. 2008; Rossetto et al. 1996; Sadler et al. 2015; Advani et al. 1998; Wong et al. 1998). VAMP1 and VAMP2 isoforms are involved in regulated exocytosis in neuronal and other cells (Trimble et al. 1988; Schoch 2001). VAMPs contain four functional domains: an N-terminal proline rich region, and one single transmembrane domain flanked by a variable C-terminal intravesicular tail and a conserved coil-coil region which contains a SNARE motif (Sudhof et al. 1989). The VAMPs contribute directly to the assembly of the SNARE complex by providing one helix to the core complex (Sutton et al. 1998). Indeed, the essential role of VAMP2 in Ca²⁺-dependent membrane fusion has been shown by the 100-fold reduction in Ca²⁺-dependent vesicle fusion in VAMP2 KO mice (Schoch 2001).

1.3.2.4 Palmitoylation of the SNARE machinery

While syntaxin and VAMP possess carboxy-terminal transmembrane domains, SNAP25 membrane binding depends on its palmitoylation (Lin and Scheller 2000).

SNAP25A and SNAP25B are differentially expressed during development, suggesting that they perform different functions (Ravichandran et al. 1996). The isoforms differ by nine amino acids, and interestingly three of these different residues occur within the palmitoylated cysteine-rich domain of SNAP25, suggesting that the different functions of both isoforms might be related, in part, to their different palmitoylation profiles (Prescott et al. 2009). Indeed, SNAP25 is synthesised as a soluble protein, although it is bound to the cytoplasmic face of the plasma membrane. Membrane association of SNAP25 is dependent on palmitoylation of up to four cysteines located within the cysteine-rich domain, which is flanked by the two SNARE motifs (Veit, Söllner, and Rothman 1996; Resh 2006). Golgi-located zDHHC3, 7, and 17 enzymes palmitoylate SNAP25 on residues C85, C88, C90 and C92 (Greaves et al. 2010). SNAP25 palmitoylation is dynamic, suggesting that this modification may not only be an anchor for membrane binding but may also impart other regulatory effects (Greaves and Chamberlain 2011b).

Synaptobrevin/VAMP is palmitoylated at a single cysteine residue located in its transmembrane domain (Veit et al. 2000). The function of palmitoylation in this case is not fully understood. It has been seen that vesicles prepared from adult rat brain can incorporate [³H] palmitate, indicating palmitoylation, as opposite to vesicles from embryonic brains. Therefore, it is possible that regulation of VAMP palmitoylation occurs during development (Veit et al. 2000; Chamberlain and Shipston 2015).

Syntaxin-1a and syntaxin-1b were firstly identified as targets for palmitoylation using an acyl-biotin exchange (ABE) technique in cultured rat embryonic cortical neurons and synaptosomes isolated from whole adult rat brain (Drisdell and Green 2004). The acyl biotin exchange method consists of three steps: in the first step, free cysteines are alkylated by N-ethylmaleimide (NEM); secondly, the fatty acid group at the palmitoylation site is removed

by treatment with hydroxylamine; finally, the depalmitoylated cysteines are labelled with a thiol-reactive biotin, followed by a purification step on streptavidin agarose. Using this method, and in combination with the palmitoylation inhibitor 2-bromopalmitate, palmitoylation of syntaxin-1a and -1b was confirmed by Kang et al. (2008). Other members of the syntaxin family, such as syntaxin-7 and syntaxin-8, have also been reported to be palmitoylated (He and Linder 2009). Like in the case of VAMP, the function of palmitoylation in syntaxin is not known, although it is speculated that palmitoylation could regulate the clustering of the TMD of syntaxin and mediate its association with cholesterol-rich domains (Prescott et al. 2009).

1.3.3 SNARE regulators and chaperones

The SNARE complex is considered the *minimal* machinery required for membrane fusion, since membrane fusion can be recreated *in vitro* by reconstituting SNARE proteins into lipid bilayer vesicles (Weber et al. 1998). However, the process *in vitro* is very slow compared to the process *in vivo*, which is thought to occur in a few hundred microseconds after the Ca²⁺ entrance triggers release of neurotransmitter (Sabatini and Regehr 1996). Thus, in a physiological context, SNARE complex assembly alone does not mediate fusion and other factors are needed to assist the membrane fusion, such as the SM proteins and other regulators.

SM proteins assemble SNARE complexes to catalyse membrane fusion. However, after fusion, SNARE complexes are dissociated by the ATPase NSF and the resulting disassembled SNARE proteins are maintained in a fusion-competent conformation by chaperone complexes.

The synaptic membrane-fusion machinery is controlled by the Ca²⁺-binding protein synaptotagmin, and additionally regulated by a presynaptic protein matrix (the “active zone”) that includes Munc13 and RIM (for Rab3-interacting molecules) proteins as central components.

1.3.3.1 *Munc13-1 and Munc18-1*

A few decades ago, the *Caenorhabditis elegans unc* genes were identified while trying to uncover genes involved in movement (Brenner 1974). A subset of these genes was subsequently identified as being involved in presynaptic neurotransmitter release (Hosono et al. 1987). Mammalian homologues of two of these genes include Munc13 and Munc18 (Brose et al. 1995; Hata et al. 1993). Both proteins are thought to be involved in guiding the SNARE proteins through the initial part of the assembly pathway.

The mammalian homologues of *C. elegans unc-13* were cloned and named Munc13-1, Munc13-2 and Munc13-3 (Brose et al. 1995). These ~200 kDa proteins contain a conserved C-terminal region containing a phorbol-ester-binding C1 domain and a MUN domain (for mammalian homologue of the *C. elegans unc* gene; aa 859-1531), flanked by two calcium-binding C2 domains (Jahn and Fasshauer 2012). The C2 domains are thought to modulate the MUN domain, which interacts with syntaxin 1-SNAP25 heterodimers (Guan et al. 2008) and weakly to Munc18-1 and to the syntaxin-1 SNARE motif (Ma et al. 2011). The C2A domain is also linked to Rab3-interacting molecule (RIM) (Brose et al. 1995), leading to the activation of Munc13, which has been proposed to catalyse the conformational switch of syntaxin 1 from “closed” to “open” (Südhof 2013).

Munc18-1 is an SM protein initially characterised as an essential component of the core fusion machinery, as demonstrated by the binding of the yeast SM protein Sec1p (homolog of *Munc18-1* in yeast exocytosis) to assembled SNARE complexes (Carr et al. 1999). However, Munc18-1 exhibits different binding modes to syntaxin-1 and the assembled SNARE complex, and these interactions are thought to have different regulatory functions. Munc18-1 binds directly to syntaxin-1 in the “closed” conformation of syntaxin-1 (Dulubova et al. 2007), which may be important for trafficking of syntaxin-1 (Medine et al. 2007), and also to the four-helix bundle of the SNARE complex, which is linked to its function in exocytosis (Xu, Su, and Rizo 2010).

Moreover, Munc18-1 can also interact with an extreme N-terminal motif of syntaxin-1 also in the “open” conformation of syntaxin-1 (Dulubova et al. 2007; Medine et al. 2007; Shen et al. 2007). Syntaxin-1 in the open conformation, and in association with Munc18-1, can progress to the ternary SNARE-complex (Rickman et al. 2007).

1.3.3.2 Synaptotagmins

The final stages of neurotransmitter release depend on the concentration of intracellular free Ca^{2+} , which triggers vesicle exocytosis through activation of specific Ca^{2+} sensors, and exhibits two components: a synchronous phase (fast) that occurs less than 0.5 ms after Ca^{2+} influx; and a slower asynchronous phase (Südhof 2013). Synaptotagmin proteins are thought to be the major Ca^{2+} sensors proteins involved in synaptic exocytosis (Südhof 2013; Rizo and Xu 2015). Sixteen synaptotagmins have been identified to be expressed in brain, of which eight are able to bind Ca^{2+} . Most experiments have been performed on synaptotagmin-1 (Sytn1), which has a key function in synaptic vesicle exocytosis (Südhof

2004). However, it has been seen that synaptotagmin-2 and synaptotagmin-9 have a high degree of similarity and also act as Ca^{2+} sensors although with different kinetics, corresponding to the synapses in which they are expressed (Xu, Mashimo, and Südhof 2007).

The sequence of the first synaptotagmin was determined by Perin et al. (1990), and was named synaptotagmin-1. Synaptotagmins are type I transmembrane proteins with a single transmembrane region, a short linker sequence, a short N-terminal intra-vesicular sequence and two cytoplasmic C2 domains (the C2A and C2B domains) (Perin et al. 1990). The C2A and C2B domains of synaptotagmin are able to bind three and two Ca^{2+} ions respectively (Ubach et al. 1998; Fernandez et al. 2001). Moreover, C₂ domains of synaptotagmins can also bind to syntaxin-1, SNARE complexes and the exocytotic chaperone cysteine-string protein alpha (CSP α) (Edelmann et al. 1995; Boal et al. 2011; Südhof 2013) through the C₂A domain, and SNAP25 *via* the C₂B domain (Schiavo et al. 1997). In the absence of Ca^{2+} , synaptotagmin-1 binds to the SNARE complex, but also displays Ca^{2+} dependent interaction with phospholipids, which may facilitate the opening of the fusion pore (Südhof 2004; Martens et al. 2007).

The role of synaptotagmin-1 as a Ca^{2+} sensor for the fast, synchronous release (and not the short, slow component) was supported by observations made using electrophysiological analyses of neurons from synaptotagmin-1 KO mice, which revealed that synaptotagmin-1 is essential for fast Ca^{2+} -triggered exocytosis (Geppert et al. 1994). Moreover, introduction of a point mutation in the C₂A domain of Syt1 that reduced the affinity of Syt1 to bind Ca^{2+} also decreased the affinity of Ca^{2+} to neurotransmitter release (Südhof 2013), providing very strong evidence that Ca^{2+} binding to synaptotagmin-1 is directly linked to synaptic vesicle fusion.

1.3.3.3 Complexins

Complexins are small cytoplasmic proteins that bind to assembled synaptic core complexes and promote the action of synaptotagmin-1 (Südhof 2004). They are thought to have both inhibitory and active roles in neurotransmitter release (Martin et al. 2011).

Firstly, the binding of complexins to the SNARE complex surface may facilitate the initiation and progression of zippering, probably by stabilising the partially zippered SNARE-complex and promoting its activation by synaptotagmin (Jahn and Fasshauer 2012). This role is supported by the observation that KO of both complexins (complexin-1, Cpx1; complexin-2, Cpx2) causes a similar but milder phenotype as synaptotagmin-1 KO (Reim et al. 2001).

The second, inhibitory role of complexins was suggested from observations that led to a model by which Cpx1 inhibits release of synaptotagmin-1 and acts as a clamp, thus blocking the progression of SNARE-zippering. This inhibition is proposed to be released by Ca²⁺ binding to synaptotagmin-1 (Jahn and Fasshauer 2012; Rizo and Xu 2015).

1.3.3.4 The Rab GTPases

Rab proteins are part of a large family of GTP-binding proteins that regulate all stages of intracellular transport. Their primary function is to provide specificity to fusion reactions by marking the site of attachment between donor and acceptor membranes (Grosshans et al. 2006). This process is called membrane attachment, tethering or docking.

In synaptic vesicles, three families of Rab proteins can be found: Rab3 (Rab3A, B, C and D), Rab5 and Rab11, although Rab3 is the most abundant (Südhof 2004). Rab3 undergoes a cycle of synaptic vesicle association and disassociation, which occurs in parallel with the synaptic exocytotic-endocytotic cycle (Fischer von Mollard et al. 1991). Rab3 GTPase shuttles between a soluble GDP-bound form (inactive) and a membrane-bound GTP (active) form. During (or after) synaptic vesicle fusion, GTP/Rab3 is hydrolysed to a soluble GDI-GDP/Rab3 complex, resulting in disassociation of Rab3 from the synaptic vesicles (Araki et al. 1990). The soluble complex is later reattached to synaptic vesicles by a reaction involving GDP to GTP exchange, although this process is poorly understood (Jahn et al. 2003; Südhof 2004).

1.3.3.5 Palmitoylation of SNARE regulators

Synaptotagmin-1 is modified by both palmitoylation and glycosylation. Both of these post-translational modifications are required for correct targeting of the protein to secretory vesicles (Kanno and Fukuda 2008; Prescott et al. 2009), and alteration of the palmitoylation of synaptotagmin-1 in neurons causes an augmented surface expression and diffuse localisation (Kang et al. 2004). Synaptotagmin-1 contains five cysteine residues located within the transmembrane domain and at the boundary with the cytoplasmic region. Although palmitoylation may not occur at all cysteine residues, mutational analyses confirmed that a number of cysteines present at the boundaries of the cytoplasmic region and the transmembrane domain are either directly palmitoylated or relevant for the palmitoylation of other residues within this region (Kang et al. 2004; Heindel et al. 2003).

1.4 Cysteine-string protein alpha (CSP α)

Cysteine-string proteins (CSPs) are a group of cysteine-rich proteins that belong to the DnaJ family of molecular chaperones. They are mainly vesicle-associated and are thought to modulate regulated exocytosis in neuronal and neuroendocrine cells (Chamberlain and Burgoyne 1998a; Zinsmaier et al. 1990; Chamberlain, Henry, and Burgoyne 1996; Chamberlain and Burgoyne 1998b). The importance of CSP α for viability has been shown by analysis of *Drosophila csp* null mutants, with a phenotype exhibiting premature death and impaired neurotransmission, indicating CSP in Ca²⁺-related vesicle release in the nerve terminals (Zinsmaier et al. 1994).

1.4.1 Discovery of CSP and isoforms

CSP was first discovered in *Drosophila melanogaster* by the use of a neuronal-specific monoclonal antibody. Immunohistochemical stainings were performed on *Drosophila* heads, revealing that the antigen recognised by one of the monoclonal antibodies was localised exclusively to synaptic nerve terminals. Subsequent cloning and analysis of the corresponding antigen cDNA revealed that the antigen consisted of three different splice variants of a novel gene. The novel proteins contained a striking enrichment of cysteine residues in a central region, containing a continuous stretch of eleven cysteine residues, which led to the name “cysteine-string” (Zinsmaier et al. 1990).

Efforts to identify potential subunits of neuronal calcium channels led to the independent discovery of CSP in *Torpedo californica* (Gundersen and Umbach 1992). CSPs were subsequently characterised in mammalian species (Mastrogiacomo and Gundersen 1995; Chamberlain and Burgoyne 1996; Coppola and Gundersen 1996) and are also expressed in

Xenopus (Mastrogiacomo et al. 1998), *Caenorhabditis elegans* (*dnaj-14*, Kashyap et al. 2014) and several other species, although there is no yeast isoform.

Three isoforms of CSP are known in *Drosophila*: dCSP1, dCSP2 and dCSP3 (Zinsmaier et al. 1990). The three isoforms are generated by alternative splicing of the same *csp* gene, located on chromosome 3 at position 79E1-2 (Zinsmaier et al. 1994). The *Drosophila* CSPs are 50–60% identical to mammalian CSP α , which is 98–100% identical at the amino acid level in different mammalian species (Chamberlain and Burgoyne 2000). Two mammalian isoforms, CSP1 and CSP2, are generated by differential splicing of the same gene (Chamberlain and Burgoyne 1996; Coppola and Gundersen 1996). CSP1 is the mammalian homologue of *Torpedo* tCSP (Gundersen and Umbach 1992), while CSP2 corresponds to a truncated C-terminal splice variant of CSP1 (Chamberlain and Burgoyne 1996).

In addition to mammalian CSP1 (now referred to as CSP α) and CSP2, two other isoforms were identified from human testis mRNA: CSP β and CSP γ (Evans et al. 2003). CSP β has also been identified in a mouse testis cDNA library, while only a part of human CSP γ mRNA sequence and predicted mouse mRNA could be obtained (Evans et al. 2003). The three CSP proteins expressed in mammals (α , β , γ) are encoded by the *DNAJC5a*, *b* and *g* genes, respectively (Burgoyne and Morgan 2015), which are located on different human chromosomes: 20 (CSP1/ α), 8 (CSP β) and 2 (CSP γ) (Evans et al. 2003). CSP α and CSP β present high homology between sequences, while CSP γ is more distantly related. CSP γ is only expressed in testis, while CSP β is also expressed in auditory hair cell neurons, although the functional roles of these two isoforms are unknown (Fernández-Chacón et al. 2004; Schmitz et al. 2006). On the other hand, CSP α is expressed in most cells and virtually all neurons (Burgoyne and Morgan 2015).

1.4.2 CSP α domains

The protein sequence of CSP α was analysed and five domains were identified: (i) a short N-terminal domain, (ii) a "J" domain, (iii) a linker domain, (iv) a cysteine-rich domain with a high density of cysteine residues, and (v) a C-terminal domain.

The J domain, a highly conserved region between species, has a high degree of homology to a region of the bacterial chaperone protein DnaJ, and is the defining domain of the DnaJ/Hsp70 (heat-shock protein of 70 kDa) family of molecular chaperones (Chamberlain and Burgoyne 2000). The J domain contains a HPD motif (histidine, proline, and aspartic acid) that is essential for interaction with Hsp70 proteins (Chamberlain and Burgoyne 1997).

The linker is also a highly conserved region consisting of 20 amino acids, flanked by the J domain and the cysteine-string region. The function of the linker domain has been associated with regulated exocytosis (Zhang et al. 1999). However, the role of the linker in exocytosis is based on a single mutation (E93V) which overturned the inhibitory effects of over-expression of CSP2 (and not CSP1/ α) on exocytosis (Zhang et al. 1999), thus the exact role of the linker domain is difficult to assess. By contrast, the linker domain is required for other aspects of CSP biology, often in combination with other domains of the protein. For instance, both the cysteine-string domain (CSD) and the linker domain have been shown to be important for CSP self-association (Swayne et al. 2003). Furthermore, the 8 amino acids upstream the CSD, together with the CSD itself, have been shown to be required and sufficient for membrane association of CSP α prior to palmitoylation (Greaves and Chamberlain 2006). The CSD is the defining domain of CSP and contains 14 cysteines (in a span of 24 amino acids), the majority of which are thought to be palmitoylated (Gundersen et al. 1994). Palmitoylation of the CSD is required for membrane attachment and

membrane targeting (Chamberlain and Burgoyne 1998b) , and the hydrophobicity of the CSD is also important for initial membrane binding prior to palmitoylation (Greaves and Chamberlain 2006).

The N-terminal region of CSP α includes a conserved serine residue (Ser-10), which is subject to phosphorylation by protein kinase A and protein kinase B (Evans et al. 2001; Evans et al. 2005). Interestingly, phosphorylation at this site leads to an inhibition of interactions with both syntaxin (Evans et al. 2001) and synaptotagmin (Evans and Morgan 2002) and was also shown to trigger binding to 14-3-3 proteins (Prescott et al. 2008). Interestingly, mutation of serine-10 was shown to modulate the kinetics of exocytosis in PC12 cells (Evans et al. 2001; Chiang et al. 2014). Recent work showed that phosphorylation of serine-10 causes a major conformational change in CSP α , involving an interaction between the phosphorylated serine and lysine-58 in the J domain (Patel et al. 2016), explaining how phosphorylation of this residue can impact protein interactions and function of CSP α . The function of the C-terminal domain of CSP α is poorly defined although it has been shown to be required for efficient palmitoylation of the CSD (Greaves et al. 2008) and also to contain a recognition site for the palmitoylation enzyme zDHHC17 (Lemonidis et al. 2015).

1.4.3 Palmitoylation and membrane interactions of CSP α

Differential protein band sizes of CSP α on SDS gels were firstly reported in 1994 in an immunoblot analysis using CSP antiserum raised in *Torpedo*, where it was seen that the molecular weight of *Torpedo* CSP was greater than the product of *in vitro* translated CSP. As a result, it was proposed that CSP is post-translationally modified *in vivo* (Mastrogiacomo

et al. 1994; Gundersen et al. 1994). Nowadays, due to the extensive palmitoylation of CSP α , this observation is still used to discriminate between palmitoylated and non-palmitoylated forms of the protein, which migrate at 35 and 27 kDa, respectively.

Non-palmitoylated CSP α is barely detectable in mammalian tissues, suggesting that palmitoylation may occur rapidly after synthesis and/or that CSP α remains stably palmitoylated (Gundersen et al. 1996).

Palmitoylation is required for CSP α function since it converts the protein from a soluble to a membrane-associated form. A screen of the 23 murine zDHHC enzymes for palmitoylation activity against CSP α revealed that CSP α is a substrate for zDHHC3, zDHHC7, zDHHC15 and zDHHC17 (Greaves et al. 2008), and studies in *Drosophila melanogaster* showed that disruption of zDHHC17 resulted in a loss of palmitoylation and mislocalisation of CSP α (Ohyama et al. 2007; Stowers and Isacoff 2007).

The hydrophobic cysteine-string domain provides a weak membrane affinity that is required to bring CSP α to membranes where zDHHCs are localised, leading to palmitoylation and a stable membrane anchoring of CSP α and facilitating intracellular sorting (Greaves et al. 2008).

1.4.4 Cellular functions of CSP α

The first role associated to CSP was that of a calcium channel subunit or regulator, and came from a suppression cloning study using CSP anti-sense mRNA, which inhibited activity of N-type voltage-dependent calcium channels expressed in *Xenopus* oocytes (Gundersen and Umbach, 1992). Later analysis of *Csp* null mutants in *Drosophila melanogaster* provided

evidence that CSP was important for neurotransmitter release (Zinsmaier et al. 1994). At the same time, CSP was shown to be localised to synaptic vesicles rather than to the plasma membrane (where Ca^{2+} channels are present) and thus it was proposed that CSP was an essential regulator rather than a subunit of Ca^{2+} channels; specifically that vesicular CSP activated Ca^{2+} channels following vesicle docking at the active zone (Mastrogiacomo et al. 1994). However, there is now a large amount of evidence suggesting that the synaptic function of $\text{CSP}\alpha$ probably does not involve Ca^{2+} channel regulation (Chamberlain and Burgoyne 2000) and instead the function of $\text{CSP}\alpha$ in exocytosis may reflect its association with other exocytotic proteins.

The proposed function of $\text{CSP}\alpha$ in the regulation of calcium channels was questioned by the widespread tissue distribution of $\text{CSP}\alpha$. A number of tissues where $\text{CSP}\alpha$ are expressed do not contain cells with voltage-gated calcium channels, suggesting that the main role of $\text{CSP}\alpha$ in exocytosis is not to regulate those channels (Chamberlain and Burgoyne, 2000). Indeed, studies performed in non-neuronal cells demonstrated a direct role of $\text{CSP}\alpha$ in exocytosis, independent of calcium-channel regulation: over-expression of $\text{CSP}\alpha$ in PC12 and insulin-secreting cells were examined, showing that over-expression does not affect depolarisation-induced calcium influx and suggesting that $\text{CSP}\alpha$ does not have a major effect on calcium-channel activity in the cells studied (Brown et al. 1998; Chamberlain and Burgoyne 1998a).

A number of protein interactions have been identified, which are relevant to the function of $\text{CSP}\alpha$ in exocytosis. The first and best characterised is the interaction of the J domain with Hsc70 proteins (Braun et al. 1996; Chamberlain and Burgoyne 1997), which requires the highly conserved HPD motif of the J domain (Chamberlain et al. 1997), and which stimulates the ATPase activity of Hsc70 (Chamberlain and Burgoyne 1997). The interaction of these

proteins with SGT (small glutamine-rich tetratricopeptide repeat-containing protein) is thought to form a chaperone complex for the regulation of synaptic proteins (Stahl et al. 1999; Tobaben et al. 2001).

Other interactions have also been reported with SNARE proteins, such as syntaxin, VAMP and synaptotagmin. Biochemical and genetic studies using *Drosophila* and mammalian proteins provided good evidence of a direct interaction between CSP and syntaxin: in *Drosophila*, the neurotransmission deficit caused by over-expression of syntaxin is abolished by over-expression of CSP (Nie et al. 1999; Wu et al. 1999). In addition, the recombinant mammalian proteins form complexes *in vitro*, that can be immunoprecipitated from hippocampal homogenates and HeLa cells expressing CSP α and syntaxin (Chamberlain et al. 2001; Magga et al. 2000).

CSP has also been seen to interact with synaptotagmin (Evans and Morgan, 2002) and the SNARE protein VAMP, which has been seen to co-immunoprecipitate with CSP in rat brain membranes (Boal et al. 2004; Leveque et al. 1998).

Interestingly, the ability of CSP to interact with some of these different proteins depends on phosphorylation of Serine-10 of CSP. Indeed, phosphorylation of CSP by protein kinase A (PKA) reduces binding to syntaxin by 10-fold (Evans et al. 2001; Evans et al. 2005). A similar phosphor-regulated interaction is found between CSP and synaptotagmin (Evans and Morgan, 2002).

The more recent identification of another substrate of CSP α , dynamin 1, also suggested a potential role of CSP α in dynamin-mediated synaptic vesicle recycling (Zhang et al. 2012).

More recent studies on CSP α KO mice also highlighted the neuroprotective role of CSP α and its implication in the assembly of the SNARE complex. The levels of SNAP25, SNAP23, α -

synuclein, Hsp70, Hsc70 and assembled SNARE complexes appeared to be reduced in CSP α KO mice (Chandra et al. 2005). The most striking phenotype of the CSP α KO mice was the progressive synaptic degeneration, which highlighted an important function for CSP α as a neuroprotective protein (Fernández-Chacón et al. 2004). Intriguingly, the neurodegeneration and reduced life-span present in CSP α KO mice were reversed by over-expression of α -synuclein. However, the reduction of SNAP25 expression observed in CSP α KO mice was not affected by the over-expression of α -synuclein (Chandra et al. 2005). Finally, further analysis of the CSP α KO mice suggested that SNAP25 is the major client of CSP α , indicating that neurodegeneration in the KO mice can be explained by defective SNAP25 function, which, in turn, causes a failure in SNARE complex assembly (Sharma, Burré, and Südhof, 2011; Sharma et al. 2012).

1.4.5 Role of CSP α in neurodegeneration

In the past few years, a number of studies have found evidence for a direct link between CSP α and human disease. Different research groups have identified mutations in the *DNAJC5* gene encoding CSP α as the cause of adult-onset Neuronal Ceroid Lipofuscinosis (ANCL) (Benitez et al. 2011; Nosková et al. 2011; Velinov et al. 2012; Cadieux-Dion et al. 2013). ANCL is an autosomal-dominant neurodegenerative disease with a broad clinical variability, including movement disorders and progressive dementia, starting at a mean age of onset of 30 years (Nosková et al. 2011). Further investigation of new cases is important in ANCL, since due to its rarity and remarkable clinical variability it is often misdiagnosed (Benitez et al. 2011). Two mutations in *DNAJC5* have been shown to cause ANCL; these mutations result in the substitution of leucine 115 for an arginine or the deletion of leucine 116 (Benitez et al. 2011; Nosková et al. 2011; Velinov et al. 2012; Cadieux-Dion et al. 2013).

Interestingly, both mutations are located within the CSD of CSP α , an essential domain for CSP α palmitoylation and targeting to the membranes (Greaves et al. 2008). In one of the studies where the disease-causing mutations were identified, it was shown that recombinant GFP-CSP α mutant proteins were accumulated in an abnormal localisation, in contrast to the GFP-tagged wild-type protein (Nosková et al. 2011). These findings were supported by the work of Greaves et al. (2012), showing that the mutations mistarget CSP α and furthermore cause the formation of high molecular weight SDS-resistant aggregates. Moreover, the aggregates were reported to be membrane-bound and palmitoylated, and treatment with hydroxylamine, which depalmitoylates proteins, caused the solubilisation of the mutant CSP α aggregates in mammalian cell lines and post-mortem brain samples from patients, suggesting a link between palmitoylation and aggregate formation (Greaves et al. 2012).

ANCL is the only disease known to be caused directly by mutations in CSP α . However, other neurodegenerative diseases have also been linked to alterations in the expression levels or function of CSP α . The observation that progressive neurodegeneration in CSP α KO mice can be rescued by over-expression of α -synuclein (Figure 1.2) is particularly relevant since α -synuclein has been associated with Lewy Bodies, characteristic of Parkinson's disease (Spillantini et al. 1997; Baba et al. 1998) and inclusions in Alzheimer's disease (Norris et al. 2004). Interestingly, CSP α expression is reduced in areas of the forebrain of post-mortem brains from Alzheimer's disease patients (Tiwari et al. 2015). Additionally, CSP α can interact with mutant huntingtin protein, which contains an expanded polyQ region, although it does not interact with the wild type protein (Miller et al. 2003), suggesting that sequestration of CSP α by the mutant huntingtin protein could enhance and accelerate the neurodegenerative process.

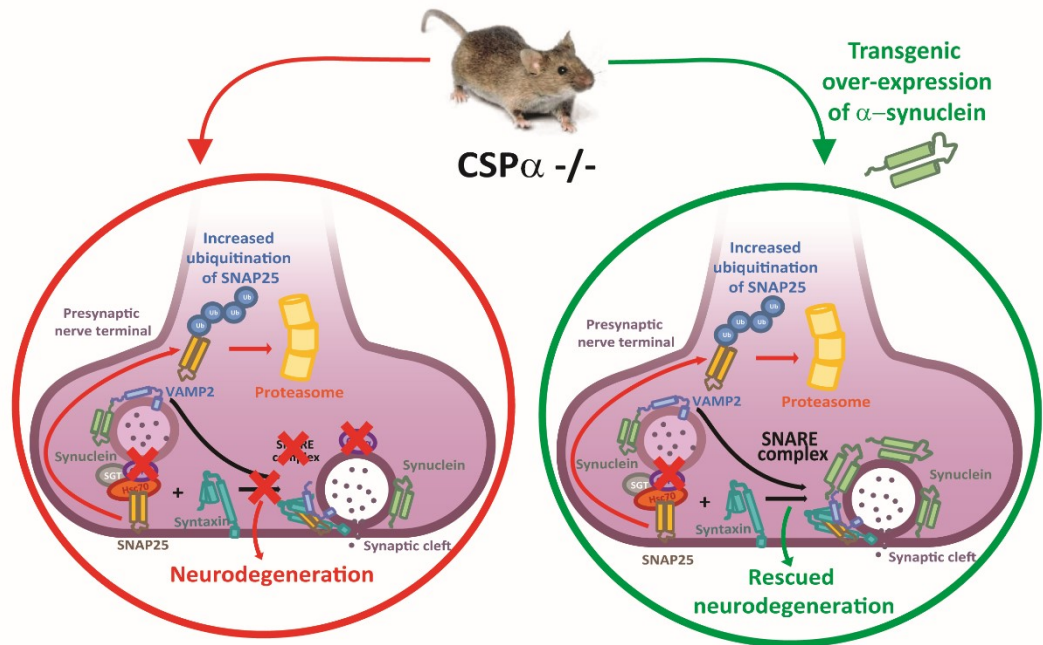


Figure 1.2. CSPα KO mice exhibit an age-dependent progressive neurodegeneration. CSPα KO mice present decreased levels of SNAP25 and impaired SNARE-complex assembly, which leads to neurodegeneration. α-Synuclein is proposed to rescue SNARE-complex assembly by a non-enzymatic mechanism involving binding to phospholipids *via* its N-terminus and to VAMP2 *via* its C-terminus. This results in an enhanced SNARE-protein function that compensates the CSPα deletion. α-Synuclein, however, does not rescue SNAP-25 levels, degradation of this protein is enhanced by the ubiquitin-proteasome system in CSPα deficient synapses.

1.5 Neuronal Ceroid Lipofuscinoses

Neuronal Ceroid Lipofuscinoses (NCL), also referred to as Batten's disease, are a group of neurodegenerative disorders characterized by the accumulation of autofluorescent lipopigment in neurons and other cell types. The NCL family includes different diseases that vary in age of onset (infantile, juvenile and adult), specific neurologic phenotype and degree of progression. While efforts have been made to understand the pathogenesis of the family of NCL disorders, clinical diagnosis and recognition is still challenging and NCL are often misdiagnosed (Mink et al. 2013).

The worldwide incidence (affected persons per live births) is approximately 1 in 100,000 but the rates vary with the United States and northern European populations having a higher incidence with an occurrence of around 1 in 12,500 (Jalanko and Braulke 2009; Neverman et al. 2015; Haltia and Goebel 2013).

The clinical and pathological features differ between the infantile and adult forms of the disease, with most childhood forms being characterized by progressive loss of vision together with cognitive and motor deterioration, epileptic seizures and premature death. On the other hand, adult forms do not present with visual impairment but do display progressive dementia. All forms of NCL however share the presence of autofluorescent ceroid lipopigment granules, which are resistant to lipid solvents and accumulate in the cytoplasm of mainly nerve cells, although they can also be present in other cell types (Haltia 2006).

NCL are generally considered and classified as lysosomal storage disorders (LSDs), since the ceroid lipopigment accumulates in lysosomes and many of the proteins identified as the cause of different types of NCL are lysosomal proteins (Jalanko and Braulke 2009). However, the accumulating material in NCLs is not specific for the disease and has an heterogeneous origin, alternatively of what occurs in LSDs, where lysosomal enzyme dysfunction leads to accumulation of specific metabolites in lysosomes (Jalanko and Braulke 2009). In infantile NCL, the storage material consists mostly of accumulation of ceroid-lipopigments, subunit c of mitochondrial ATP synthase and/or sphingolipid activator proteins A and D (Jalanko and Braulke 2009; Kollmann et al. 2013). Generally, the storage material found in NCLs is autofluorescent and positive for periodic acid-Schiff (PAS) staining (used to detect polysaccharides, glycolipids and glycoproteins), Sudan black B staining (which stains lipoproteins and neutral triglycerides), the Ziehl-Neelsen acid fast stain (used

to stain mycolic acids) and the Luxol Fast Blue (LFB) staining (stains lipoproteins in the myelin sheath) (Cárcel-Trullols et al. 2015). The link between the storage material accumulation in NCLs and the NCL-causing gene products is not clear: the accumulation of autofluorescent material might be the result of a cumulative process.

The first description of a form of NCL in the medical literature was by Dr Otto Christian Stengel in 1826, describing a juvenile-onset disease presenting blindness, loss of speech, progressive dementia and premature death (Haltia 2006; Mink et al. 2013). The report written by Dr Stengel remained hidden for almost a century, until in 1903 Frederick Batten identified patients within a familial setting presenting psychomotor retardation and described the neuropathology of “cerebral degeneration with macular changes” (Batten 1903; Mink et al. 2013). During the following years and until 1914 (Batten 1914), a number of further patients were diagnosed with a similar disorder, reported by Vogt (Vogt 1905; Vogt 1907; Vogt 1909). Patients with a juvenile onset were described by Spielmeyer (Spielmeyer, 1905; Spielmeyer 1908), and patients with a late infantile-onset were reported by Janský (Janský 1908) and Bielschowsky (Bielschowsky 1913). Finally, in 1925 Kufs described an adult-onset with similar intra-neuronal storage and pathological characteristics but without vision loss (Kufs 1925). The final form of infantile-onset form was described by Haltia and Santavuori in 1973 (Haltia et al. 1973). Most of the papers previous to 1969 refer to NCLs as “amaurotic family idiocy”, until the concept of NCL was introduced by Zeman and Dyken (Zeman, 1969).

Information on the biochemical nature of the storage materials accumulated was obtained during the late 80s, showing it was composed of phospholipids, neutral lipids and proteins (Palmer et al. 1986). Finally, the first responsible genomic defects were identified in 1995 (Vesa et al. 1995; The International Batten Disease Consortium 1995). Since then, more NCL

genes have been identified, leading to the formulation of the current classification of NCLs (Williams and Mole 2012; Knoch et al. 2013).

1.5.1 Diagnosis and classification of NCL

Prior to the discovery of the disease-causing genes, the accepted classification of the NCLs was based on the age of symptomatic onset and the ultrastructure abnormalities of the storage material found with electron microscopy. The classification, created by Zeman in 1976 (Zeman, 1976), distinguished four different human NCLs and a canine form: infantile (Haltia-Santavuori or INCL), late-infantile (Jansky-Bielschowsky), juvenile (Spielmeyer-Sjögren) and adult (Kufs) in human, and the canine form named after Koopang (Haltia and Goebel 2013). The characteristic ultrastructural patterns in infantile NCL are granular, while in late-infantile are curvilinear, fingerprint bodies in juvenile and rectilinear in adult NCLs (Mink et al. 2013). Similarly, the age of symptomatic onset in the early infantile form of NCL is after normal birth, with a progressive visual loss leading to complete blindness by the age of 2, presenting premature death at the age of 4. The late infantile form starts its symptomatic manifestation between 2 and 4 years old, with an average age death of 10 to 12 years. The juvenile form of the disease (JNCL) is manifested between 4 and 10 years of age with eventual death in the mid to late 20s (Schulz et al. 2013). Finally, symptoms in ANCL are generally milder and appear around 30 years of age, with progression until death at 40-45 years old (Velinov et al. 2012; Benitez et al. 2011; Nosková et al. 2011; Cadieux-Dion et al. 2013).

With the advances of molecular genetics and the identification of the disease-causing genes, the Zeman's classification became obsolete. It was seen that different mutations in a

Table 1.2. Classification and characteristics of human NCLs.

Disease	Gene	Protein	Clinical phenotype	Eponym
CLN1	<i>CLN1/PPT1</i>	PPT1	IC, LI, J, A	Haltia-Santavuori
CLN2	<i>CLN2/TPP1</i>	TPP1	LIC, J	Jansky-Bielschowsky
CLN3	<i>CLN3</i>	CLN3	J	Spielmeier-Sjogren
CLN4	<i>CLN4/DNAJC5</i>	CSP α	A	Parry
CLN5	<i>CLN5</i>	CLN5	LIV, J, A	Finnish variant late infantile
CLN6	<i>CLN6</i>	CLN6	LIV, A	Lake-Cavanagh early juvenile/Indian variant late infantile, adult Kufs type A
CLN7	<i>CLN7/MFSD8</i>	CLN7/MFSD8	LIV, J, A	Turkish variant late infantile
CLN8	<i>CLN8</i>	CLN8	LIV, progressive mental retardation	Northern epilepsy/progressive epilepsy with mental retardation
CLN9		Unknown	JV	Juvenile variant
CLN10	<i>CLN10/CTSD</i>	CLN10/Cathepsin D (CTSD)	Congenital classic, LI, A	Congenital
CLN11	<i>CLN11/GRN</i>	CLN11/Progranulin/ Proepithelin/Acrogranin	A	Adult variant
CLN12	<i>CLN12/ATP13A2</i>	CLN12/ATPase 13A2/KRPPD/PARK9/HSA9947/RP-37C10.4	J, Kufor-Raheb syndrome	Juvenile variant
CLN13	<i>CLN13/CTSF</i>	CLN13/Cathepsin F	A Kufs type	Adults Kufs type B
CLN14	<i>CLN14/KCTD7</i>	CLN14/Potassium channel tetramerization domain-containing protein 7 (KCTD7)	I, progressive myoclonus epilepsy 3	Infantile

Abbreviations: I, Infantile; IC, Infantile Classic; LI, Late Infantile; LIC, Late Infantile Classic; LIV, Late Infantile Variant; J, Juvenile; JV, Juvenile Variant; A, Adult

References: Cárcel-Trullols et al. 2015; Mole and Cotman 2015; Mink et al. 2013; Haltia and Goebel 2013.

single gene (*CLN1*) could give different phenotypes, including different forms of NCLs with different ages of onset (infantile, late-infantile, juvenile and adult). Therefore, the current and accepted classification of NCLs is purely based on the gene loci (Williams and Mole 2012; Haltia and Goebel 2013). According to this classification, there are 14 genetic forms of NCL (Table 1.2).

Although great efforts have been made in the characterization of the different forms of NCLs, diagnosis is still challenging. The exact number of NCL genes is not known and some families remain without genetic diagnosis (Warrier et al. 2013). Moreover, some genes remain without known identity (such as *CLN9*). Therefore, the NCL disease spectrum will be revisited considering the advances in global genome techniques and its accessibility (Knoch et al. 2013).

1.5.2 Adult Neuronal Ceroid Lipofuscinosis (ANCL)

As mentioned in the previous sections, ANCL corresponds to the adult-onset variation of NCLs. ANCL is associated with the characteristics of intracellular inclusions of autofluorescent material and with progressive neurodegeneration. However, ANCL patients do not present visual loss. Due to its rarity and clinical variability, its diagnosis becomes very challenging and ANCLs are often misdiagnosed (Berkovic et al. 2016).

There are two forms of adult NCL, Type A and Type B, differentiated mainly by their genetic cause and their mode of inheritance, since the symptoms of the two subtypes can sometimes overlap (Schulz et al. 2013). Type A (Kufs Type A) is associated with progressive seizures and uncontrollable muscle jerks (progressive myoclonic epilepsy, PME), difficulties of speech (dysarthria) and with muscle coordination (ataxia). Type A is caused by recessive

mutations in the *CLN6* gene (Arsov et al. 2011; Smith et al. 2013), although rare cases associated with visual loss are linked to the *PPT1/CLN1* gene (Kousi et al. 2012), *CLN5* and *GRN/CLN11* (Smith et al. 2012; Berkovic et al. 2016; Mole and Cotman 2015).

Type B (Parry disease) presents similar symptoms to Type A, except for seizures, which are rare in Type A. Moreover, patients also suffer facial tics or tremors (facial dyskinesia), dementia and changes in behaviour and psychiatric abnormalities. Type B is caused by mutations in *DNAJC5* gene (Velinov et al. 2012; Cadieux-Dion et al. 2013; Benitez et al. 2011; Nosková et al. 2011), encoding for CSP α , and mutations in the *CTSF/CLN13* gene (Smith et al. 2013). ANCL caused by mutations in the *DNAJC5* (also named *CLN4*) gene, encoding CSP α , is the only type inherited in an autosomal-dominant manner.

While extremely rare, there have been some other cases of adult-onset NCL due to changes in the *CTSD/CLN10* (Steinfeld et al. 2006; Siintola et al. 2006) and *CLN3* genes (Mole and Cotman 2015).

1.5.3 Animal models of NCLs and current therapeutic strategies

The current treatments for NCLs depend on the form of the disease. Some of the symptoms can be treated, such as epilepsy. However, for instance, there is no treatment for the dementia associated with NCLs. Specifically, the treatment of ANCL is directed towards each individual and is focused in palliative and psychological support (physical therapy, occupational therapy, speech therapy, feeding gastrostomy, suction and airway management and caregiver support). Moreover, since it is an autosomal-dominant disease, genetic counselling is recommended for the members of the family of an affected individual

(Berkovic et al. 2016). Unfortunately, there are currently no therapies that can change the outcome of the disease.

Current therapeutic strategies in the field of NCLs include small molecule regulators, pharmacological chaperones, immune and receptor modulators, enzyme replacement therapy, stem cell therapy and gene therapy, amongst others. Indeed, there are some current pre-clinical and clinical trials of gene therapy in NCLs, using adeno-associated viral or lentiviral derived vectors for gene delivery (Neverman et al. 2015). However, these therapeutic approaches have been focused on the infantile, late-infantile and juvenile forms of the disease (*CLN1*, *CLN2*, *CLN3*) (Geraets et al. 2016; Neverman et al. 2015).

Mice are the primary model to study NCLs, and there are currently ten mouse models available for the study of different forms of the disease (Cooper et al. 2006; Salek et al. 2011). The models have been mainly obtained by genetic modifications, such as *CLN1/PPT1* (two models), *CLN2/TPP1*, *CLN3* (three models), *CLN5* and *CLN10/CTSD*, or have been obtained by spontaneous mutations, such as *CLN6/ncfl* and *CLN8/mnd*. The mouse models represent all age of onsets of the disease, although there is no model for the autosomal-dominant adult form of the disease (*DNAJC5/CLN4*).

In the case of autosomal-dominant ANCL, a *Caenorhabditis elegans* (*C. elegans*) model has been proposed (Kashyap et al. 2014; McCue et al. 2015). The phenotype of the *C. elegans dnaj-14* mutants presents age-dependent sensorimotor impairment, neurodegeneration and premature death, similarly to CSP α KO mice (Figure 1.2, Fernández-Chacón et al. 2004). While in *Drosophila*, *csp null* mutants present premature death (Umbach et al. 1994), a disease progression is observed in worm, suggesting that the *dnaj-14* worm model could serve as a platform to identify potential treatments.

1.6 Aims of this study

The study of several disorders, such as Alzheimer's disease (AD), Amyotrophic Lateral Sclerosis (ALS), Parkinson's disease (PD) and Huntington's disease (HD) has established a potential mechanistic link between protein aggregation and neurodegeneration (Bourdenx et al. 2015; Kumar et al. 2016; Takalo et al. 2013). Two mutations in the *DNAJC5* gene encoding CSP α have been identified as the cause of the neurodegenerative disorder adult-onset neuronal ceroid lipofuscinosis (ANCL) (Benitez et al., 2011; Nosková et al., 2011). Interestingly, the two disease-causing mutations, a substitution of leucine 115 by arginine (L115R) or a deletion of leucine 116 (Δ L116), have been reported to form high molecular weight SDS-resistant aggregates (Greaves et al. 2012), suggesting that protein aggregation may also be associated with neurodegeneration in ANCL. Indeed, the SDS-resistant CSP aggregates were also detected in post-mortem brain tissue from individuals carrying the L115R mutation (Greaves et al. 2012).

The two disease-causing mutations are located within the CSD of CSP α , a region of the protein that is highly palmitoylated (Gundersen et al. 1994; Chamberlain and Burgoyne 2000). Previous work by Greaves et al. (2012) showed that the aggregation of the ANCL mutants was palmitoylation-dependent. Indeed, the SDS-resistant aggregates were solubilised by hydroxylamine (HA) treatment, which depalmitoylates proteins, suggesting that the aggregates are stabilised by palmitoylation. Moreover, the over-expression of active (but not inactive) zDHHC palmitoyltransferases increased aggregate formation.

Post-translational modifications have been related to protein aggregation in other neurodegenerative disorders, such as Huntington's disease, Parkinson's disease and Alzheimer's disease (Pennuto et al. 2009; Martin et al. 2011; Ren et al. 2014). Indeed, palmitoylation has previously been implicated in neurodegeneration as the formation of

inclusions by mutant huntingtin is increased when palmitoylation of the protein is blocked (Yanai et al., 2006).

Therefore, the over-arching hypothesis of this work is that palmitoylation-induced aggregation of CSP α mutants is the cause of autosomal dominant adult-onset NCL in affected families. Figure 1.3 illustrates the main effects the ANCL mutants are thought to have.

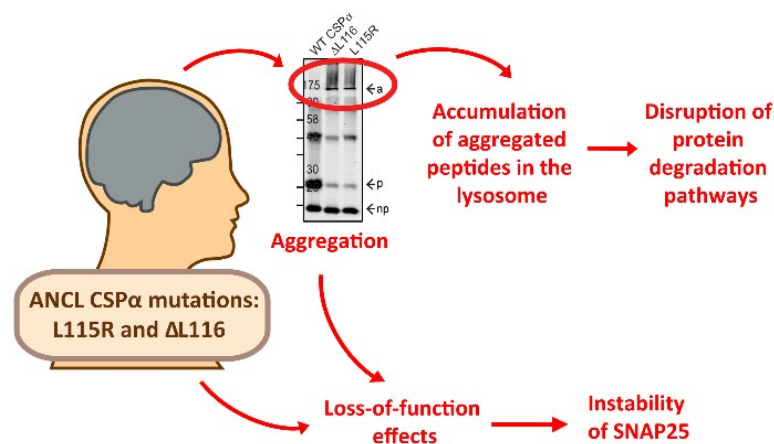


Figure 1.3. Effects of ANCL mutations. According to the hypothesis of this work, ANCL mutations cause aggregation, as seen by (Greaves et al. 2012), which could cause an accumulation of aggregated peptides in the lysosome and, in turn, disrupt protein aggregation pathways. Moreover, either the ANCL mutations themselves or the palmitoylation-induced aggregation might cause loss-of-function effects leading to an instability of SNAP25 expression and function.

In order to develop therapeutic strategies to treat ANCL, it is important to identify pathways and mechanisms that lead to pathogenesis. The present study focuses on three main questions that are important for understanding the ANCL disease process and for developing new and effective treatments:

1. What features of the CSP α protein mediate aggregation in the presence of ANCL mutations? Addressing this question is important as it will provide new insight into the molecular pathway for aggregate formation and may also highlight potential strategies to prevent aggregation.
2. What molecular changes occur in ANCL brain? By identifying changes in the levels of proteins and protein complexes in ANCL brain, it is possible to propose new mechanisms underlying ANCL disease pathology or ongoing compensatory processes. Furthermore, by comparing molecular changes in ANCL brain and brains from patients with other neurodegenerative disorders, it is possible to discriminate ANCL-specific changes from changes that occur more generally in neurodegeneration.
3. What cell pathways control CSP α degradation? Disruption of protein degradation pathways by protein aggregates is one mechanism that has been proposed to lead to neuronal death and neurodegeneration. Thus, it is important to identify the pathways regulating turnover of CSP α and to determine if these pathways are effective at clearing ANCL mutant aggregates or if the expression of aggregates disrupts function of these pathways. Addressing these issues will provide new insight into cell perturbations that could be caused by the presence of ANCL mutants leading to neurodegeneration.

Chapter 2: Materials and methods

2.1 Materials and suppliers

2.1.1 Chemicals

Except otherwise indicated, all reagents were purchased from Sigma-Aldrich Company Ltd. (Dorset, UK) and Life Technologies™ (Paisley, UK).

2.1.2 Molecular biology and biochemical reagents

NativeMark™ Unstained Protein Standard, Precast NativePAGE™ 4-16% Bis-Tris Gel, One Shot® TOP10 Chemically Competent *E. coli*, PureLink™ Quick Plasmid Miniprep Kit, PureLink™ Gel Extraction Kit, SYBR® Safe DNA gel stain, DNA ladder (1 kb) and Lipofectamine®2000 Reagent were purchased from Life Technologies™ Ltd. (Paisley, UK). Gateway BP Clonase™, LR Clonase™, restriction endonucleases and BCA Protein Assay Reagent Kit were purchased from Thermo Fisher Scientific (Waltham, MA, USA). KOD Hot Start DNA Polymerase was supplied by Novagen, Merck Millipore (Darmstadt, Germany). HypperLadder™ 1kb molecular weight marker was purchased from Bionline Reagents Ltd. (London, UK). Prestained Protein Marker (7-175 KDa) was obtained from either New England Biolabs® Inc. (Ipswich, MA, USA) or Cell Signalling Technologies (Denver, MA, USA). NucleoBond® Xtra Midi Kit for DNA plasmid purification was purchased from Macherey-Nagel (Düren, Germany). µMACS™ Epitope Tag Protein Isolation Kit for immunoprecipitation was obtained from Milteyni Biotech (Bergisch Gladbach, Germany). Finally, oligonucleotide primers were synthesised by Sigma-Aldrich Company Ltd. (Dorset, UK). T4 DNA Ligase was obtained from Promega (Southampton, UK).

2.1.3 Electrophoresis and immunoblot equipment

Gel plates, electrophoresis chambers for vertical gels, protein transfer tanks, power supplies, and Polyvinylidene difluoride (PVDF) and nitrocellulose membranes were purchased from Bio-Rad Laboratories (California, U.S.A). Agarose gel electrophoresis horizontal tanks were purchased from Thermo Fisher Scientific (Waltham, MA, USA).

2.1.4 Cell culture media and plasticware

Advanced RPMI 1640 Media, Dulbecco's Modified Eagle Media (DMEM), 0.05 % Trypsin-EDTA, GlutaMAX™ (100X), Heat Inactivated Foetal Bovine Serum (FBS) and G418 antibiotic Geneticin™ were purchased from Life Technologies™ Ltd. (Paisley, UK).

75 cm² flasks and BioCoat Poly-D-Lysine 24-well plates were obtained from Corning Incorporated (Corning, NY, USA). Cellcoat® Poly-D-Lysine 6-well plates were purchased from Greiner Bio-One (Kremsmünster, Austria). Non-treated Polystyrene 100 × 20 mm culture dishes and 12 mm pre-coated Poly-D-Lysine coverslips were obtained from BD Biosciences (Oxford, UK). The 100 mm culture dishes were coated with Poly-D-Lysine (100 ng/ml in sterile distilled H₂O), left overnight under UV-light and rinsed with media before use.

2.1.5 Mammalian cell lines

Rat pheochromocytoma-12 (PC12) and Human Embryonic Kidney 293 (HEK293T) cells were purchased from ATCC (Manassas, VA, USA).

2.1.6 Human Brains

Cortical brain tissue from male adult Neuronal Ceroid Lipofuscinosis (ANCL) patients carrying the L115R mutation was provided by the Washington University School of Medicine in St. Louis Alzheimer's Disease Research Centre (ADRC). Ethically approved for scientific research (Lothian Research Ethical Committee; reference 2003/8/37) cortical tissue from histologically characterized normal and Huntington's disease (HD) patients brain tissue was obtained from the Medical Research Council Sudden Death Brain and Tissue Bank (University of Edinburgh), (Millar et al 2007). All tissue proceeded from anonymized patients and the work was ethically approved by the University of Strathclyde (reference UEC1112/46).

2.1.7 Primers

All primers used in this thesis were purchased from Sigma-Aldrich Company Ltd. (Dorset, UK) and are shown in the following tables.

Table 2.1. Oligonucleotide primers (5'>3') used to “humanise” bovine CSP α constructs by mutating the coding sequence of isoleucine (bovine) into the coding sequence for valine (human). Mismatches to introduce mutations are underlined and ANCL mutations are presented in bold. Reverse primers were synthesised as the reverse complement of the forward sequences.

Primer Name	Target residue	Forward Sequence
HUMAN_WT(I-V)	111	5'-GCCAAGGCCCTGTTT <u>GTC</u> TTCTGCGGCCTCCTCACGTGCTGCTAC
HUMAN_L115R (I-V)	111	5'-GCCAAGGCCCTGTTT <u>GTC</u> TTCTGCGGC CGC CCTCACGTGCTGCTAC
HUMAN_ Δ L116 (I-V)	111	5'-GCCAAGGCCCTGTTT <u>GTC</u> TTCTGCGGCCTC-ACGTGCTGCTAC

Table 2.2. Oligonucleotide primers (5'>3') used to introduce the ANCL mutations into the 14KR mutant. Mismatches to introduce mutations are underlined and deletions presented with a dash; reverse primers were synthesised as the reverse complement for the forward sequences.

Primer Name	Target residue	Forward Sequence
14KR_L115R	115	5'-GCCAGGGCCCTGTTTGTCTTCTGCGGC <u>CGC</u> CCTCACGTGCTGCTAC
14KR_ Δ L116	116	5'-GCCAGGGCCCTGTTTGTCTTCTGCGGCCTC-ACGTGCTGCTAC

Table 2.3. Oligonucleotide primers (5'>3') used to mutate the coding sequence for specific cysteine residues within the cysteine-string domain (CSD) to alanines. Mismatches to introduce mutations are underlined; reverse primers were synthesised as the reverse complement for the forward sequences.

Primer Name	Target residue	Forward Sequence
C(1-3)A	113, 118, 119	5'- CTGTTTGTCTTC <u>CGCCGGCCTCCTCACGGCCGCT</u> ACTGCTGCTG
C(1-3)A_LR	113, 118, 119	5'- GTTTGTCTTC <u>CGCCGGCCTCCTCACGGCCGCT</u> ACTGCTGC
C(1-3)A_ΔL	113, 118, 119	5'- GTTTGTCTTC <u>CGCCGGCCTCACGGCCGCT</u> ACTGCTGC
C(4-7)A	121-124	5'- GTTTGTCTTC <u>CGCCGGCCTCACGGCCGCT</u> ACTGCTGC
C(8-10)A	126-128	5'- TGCTGCTGTCTG <u>GCCGCCGCTTCAACTGCTGCTGC</u>
C(11-14)A	131-136	5'- CTGCTGCTTCAAC <u>GCCGCCGCGGGAAGGCTAAGCCCAAGGCG</u>
C(8-14)A*	126-128, 131-136	5'- CTGGCCGCCGCTTCAAC <u>GCCGCCGCGGGAAGGCTAAGCCCAAGGCG</u>

*C(8-10)A mutant used as template DNA in PCR reaction

Table 2.4. Oligonucleotide primers (5'>3') used to mutate the coding sequence for specific cysteine residues within the CSD to leucines. Mismatches to introduce mutations are underlined; reverse primers were synthesised as the reverse complement for the forward sequences.

Primer Name	Target residue	Forward Sequence
C(4-7)L	121-124	5'- ACGTGCTGCTACCTCCTCCTCCTGCTGCTGCTTCAACTGC
C(4-5)L	121, 122	5'- ACGTGCTGCTACTT <u>GTTGTGCTGCCTGTGCTGC</u>
C(5-6)L	123, 124	5'- TGCTGCTACTGCTGCTT <u>GTTGTGCTGTGCTGCTGC</u>

Table 2.5. Oligonucleotide primers (5'>3') used to mutate the coding sequence for specific non-cysteine residues within the CSD to alanine.

Mismatches to introduce mutations are underlined; reverse primers were synthesised as the reverse complement for the forward sequences.

Primer Name	Target residue	Forward Sequence
G114A	114	5'-CTGTTTGTCTTCTG <u>CGCC</u> CTCCTCACGTGCTG
T117A	117	5'- CTGCGGCCTCCTC <u>GCG</u> TGCTGCTACTGCTGCTG
Y120A	120	5'- CTCCTCACGTGCTG <u>CGC</u> CTGCTGCTGCTGTCTG
L125A	125	5'- TGCTGCTGCTGT <u>GCG</u> TGCTGCTGCTTCAAC
FN129,130A	129, 130	5'- CTGTGCTGCTG <u>CGCCG</u> CTGCTGCTGCGGG
G134A	134	5'-CTTCAACTGCTGCTG <u>CGCG</u> AAGGTAAGCCCAAG

Table 2.6. Oligonucleotide primers (5'>3') used to mutate the coding sequence for PEST regions [regions rich in proline (P), glutamic acid (E), serine (S) and threonine (T)] within the C-terminal domain of CSP α . All residues were mutated into alanine residues. Mismatches to introduce mutations are underlined; reverse primers were synthesised as the reverse complement for the forward sequences.

Primer Name	Target residue	Forward Sequence
E144A	144-147	5'- GCGCCTGAAGGCG <u>CGGCCGGCGGCGTTCTACGTG</u>
S151A	151-157	5'- GTTCTACGTG <u>GCCGCCGCGGATCTGGAGGC</u>
T179A	179-182	5'- GGCATCCG <u>CCGCCGCGGCCCGCCAGCTCACAG</u>

Table 2.7. Oligonucleotide primer (5'>3') used to mutate the coding sequence for lysines in the linker region of GW-pEF-BOS-HA to arginines. Mismatches to introduce mutations are underlined; the reverse primer was synthesised as the reverse complement for the forward sequence.

Primer Name	Target bp	Forward Sequence
HA_KR_CSP_F	3872-3877	5'- TCT ACA AGT TTG TAC <u>AGA AGA</u> GCA GGC TTC ATG GCA

Table 2.8. Oligonucleotide primers (5'>3') used to introduce attB1/attB2 sequences, and START and STOP codons into CSP α truncation mutants. *attB1* and *attB2* sequences are shown in bold; START and STOP codons are underlined.

Primer Name	Mutant	Forward Sequence
GW_CSP_F	attB CSP	5'- GGGG ACA AGT TTG TAC AAA AAA GCA GGC TTC <u>ATG</u> GCA GAC CAG AGA
hCSP_attB1_F	1-136	5'- GGGG ACA AGT TTG TAC AAA AAA GCA GGC TTC ATG GCAGACCAGAGACAGCGCTC
hCSP_14-198_attB1_F	14-198	5'- GGGG ACA AGT TTG TAC AAA AAA GCA GGC TTC <u>ATG</u> GAG TCA TTG TAC CAC GTC CTT GG
hCSP_84-198_attB1_F	84-198	5'- GGGG ACA AGT TTG TAC AAA AAA GCA GGC TTC <u>ATG</u> CTC TAC GTG GCC GAG CAG TTT G
hCSP_113-198_attB1_F	113-198	5'- GGGG ACA AGT TTG TAC AAA AAA GCA GGC TTC <u>ATG</u> TCGGCCTCCTCACGTG
hCSP_136-198_attB1_F	136-198	5'- GGGG ACA AGT TTG TAC AAA AAA GCA GGC TTC <u>ATG</u> TGTAAGCCCAAGGCGCCT
hCSP-STOP-attB2_F	1-198	5'- C CAC ACT GAC GGG TTC AAC <u>TAA</u> CCC AGC TTT CTT GTA C
Primer Name	Mutant	Reverse Sequence
GW_CSP_R	attB CSP	5'- GGG AC CAC TTT GTA CAA GAA AGC TGG GTA GTT GAA CCC ATC GGT
hCSP_STOP_198_attB2_R	All	5'- GGGG-AC-CAC-TTT-GTA-CAA-GAA-AGC-TGG-GTG- <u>TTA</u> GTT GAA CCC GTC AGT GTG GTA G
hCSP_STOP_136_attB2_R	1-136	5'- GGGG-AC-CAC-TTT-GTA-CAA-GAA-AGC-TGG-GTG- TTA ACACTTCCCGCAGCAGC

2.1.8 Plasmids

The EGFP-CSP α (wild type, L115R and Δ L116) plasmid vectors used were designed by the group and used for previous work (Greaves et al. 2012). The human CSP α coding sequence missing the initiating methionine and flanked by HindIII and BamHI restriction sites was synthesized by GeneArt[®] (Invitrogen, MA, USA) and inserted in-frame into the pEGFP-C2 vector, after removal of an intrinsic HindIII restriction site in the CSP α sequence by introducing a silent mutation.

The human CSP α coding sequence with all lysines mutated into arginines (CSP α 14KR) and flanked by HindIII and BamHI was also synthesized by GeneArt (Invitrogen, MA, USA). It was then inserted in-frame into the pEGFP-C2 vector.

The entry plasmid pDONR[™]207 was used in the Gateway cloning system to create entry clones. The destination vector pDest40 was used to obtain the untagged CSP α constructs. The destination vector GW-HA-pEF-BOS was used to obtain N-terminal triple HA tagged CSP α constructs. The entry plasmid vector and both destination vectors were obtained from Invitrogen (Thermo Fisher Scientific, MA, USA). HA-DHHC constructs were provided by Masaki Fukata (Fukata et al. 2004). The HA-PPT1 construct in pHM6 vector was synthesised by Dr Christine Salaun and is unpublished.

2.1.9 Antibodies

2.1.9.1 Primary antibodies

Living Colors[®] A. v. monoclonal GFP monoclonal antibody (JL-8) was purchased from Clontech Laboratories, Inc. (California, USA), produced by hybridoma cells against full-

length *Aequorea victoria* green fluorescent protein (GFP). A dilution of 1:3,000 was used for immunoblotting.

Anti-HA High Affinity monoclonal antibody, purchased from Roche Diagnostics Ltd. (Burgess Hill, West Sussex, UK), was generated by immunisation of rats. This antibody recognises the HA peptide sequence [YPYDVPDY] derived from the human influenza virus haemagglutinin protein. The antibody was used at a dilution of 1:1,000 for immunoblotting.

The polyclonal CSP α antibody obtained from Enzo Life Sciences (Exeter, UK) was raised in rabbit. This antibody recognises a sequence near the C-terminus of the CSP α protein. It was used at a dilution of 1:3,000 for western blotting.

Ubiquitin (VU-1) mouse monoclonal antibody, obtained from Life Sensors (Malvern, PA, USA) was used at a dilution of 1:1,000 for western blotting.

SNAP25 (SMI 81) monoclonal antibody purchased from BioLegend (San Diego, CA, IUSA) (formerly Covance Antibody Products Inc.) was raised in mice immunized with full-length SNAP25. The dilution factor used for use in immunoblotting was 1:10,000.

The monoclonal antibody recognising Syntaxin 1 (HPC-1) was purchased from Sigma-Aldrich Company Ltd. (Dorset, UK). Syntaxin antibody, raised in mice, was derived from a synaptosomal plasma-membrane fraction from adult rat hippocampal and used at a dilution of 1:5,000 for immunoblotting.

Synaptic Systems GmbH (Göttingen, Germany) supplied the monoclonal VAMP2 (synaptobrevin 2) antibody. VAMP2 antibody was produced in mice against the synthetic peptide SATAATVPPAAPAGEG (amino acids 2-17 in rat synaptobrevin 2). The dilution ratio of VAMP2 antibody used for immunoblotting was 1:10,000.

Abcam plc. (Cambridge, UK) provided the purified polyclonal α -synuclein antibody, derived from a peptide from human α -synuclein around the phosphorylation site of tyrosine 133 and raised in rabbit. The antibody was used at a dilution of 1:1,000 for immunoblotting.

Anti-synaptophysin mouse monoclonal antibody, obtained from Merck Millipore (Darmstadt, Germany), was derived from a vesicular fraction of bovine brain. Anti-synaptophysin antibody recognises a pentapeptide repeat structure in the carboxyl-terminal cytoplasmic tail of the protein. It was used at a dilution of 1:1,000 for immunoblotting.

Cell Signaling Technology Inc. (Danvers, MA, USA) provided the monoclonal antibody against PSD95 and the polyclonal antibodies against flotillin-1 and flotillin-2. Anti-PSD95 monoclonal antibody, produced by immunizing rabbits with a synthetic peptide corresponding to residues surrounding Gln53 of human PSD95, was used at a 1:1,000 dilution for immunoblotting. The flotillin-1 and flotillin-2 polyclonal antibodies, purified by peptide affinity chromatography, were raised in rabbits against a synthetic peptide corresponding to residue surrounding Ile368 of human flotillin-1 and Leu294 of human flotillin-2. Anti-flotillin-1 and -2 antibodies were used at a 1:1,000 dilution for immunoblotting.

N1C3 rabbit polyclonal PPT1 antibody, purchased from GeneTex (Irvine, CA, USA), was derived from a recombinant protein encompassing a sequence within the centre region of human PPT1 protein. The dilution used for western blotting was 1:1,000.

2.1.9.2 Secondary antibodies

The goat anti-mouse IgG DyLight™ 680 and 800 conjugated, the goat anti-rabbit IgG DyLight™ 800 conjugated and the Pierce™ goat anti-Rat IgG DyLight 800 conjugated antibodies were obtained from Thermo Fisher Scientific (Waltham, MA, USA). Each of these antibodies is a fluorescence conjugate and is affinity purified using its target antigen.

The peroxidase-conjugated Affinipure Donkey Anti-Mouse IgG used for enhanced chemiluminescence was obtained from Jackson Immuno Research Laboratories Inc. (PA, USA).

2.2 Mammalian cell culture

2.2.1 Culturing PC12 cells

Rat pheochromocytoma-12 (PC12) cells were cultured in 75 cm² flasks in RPMI-1640 advanced medium supplemented with 10% horse serum, 5% foetal bovine serum (FBS) and 1% glutamine. Cells were grown in a humidified atmosphere at 37°C and 7.5% CO₂.

Cells were passaged once a week. For this, the cells were detached from the surface by gently tapping the flask or pipetting. Cells were transferred to a 50-ml Falcon tube and centrifuged for 3 minutes at 150 × g. Medium was then removed and the cells resuspended in 5 ml of Trypsin-EDTA. Following incubation for 5 minutes at 37°C, 5 ml of medium was added to inhibit trypsin and the cell suspension was again centrifuged for 3 to 5 minutes at 150 × g. The supernatant was discarded and the cell pellet was resuspended in 10 ml of medium by pipetting. The cells were then reseeded at a dilution ratio of 1:5 in a final volume of 25 ml in 75 cm² flasks, or in 6 or 24-well plates according to the confluence needed for assay purposes.

2.2.2 Culturing HEK293T cells

Human Embryonic Kidney 293 (HEK293T) cells were grown in Dulbecco's modified Eagle's media (DMEM) with 10% foetal bovine serum and maintained at a humidified atmosphere of 37°C and 5% CO₂.

To passage HEK293T cells, they were briefly washed in 3 ml of Trypsin-EDTA (previously pre-heated at 37°C) and then incubated for 3 minutes at 37°C in 3 ml Trypsin. Cells were detached from the surface of the flask by gentle agitation and pipetting. The cell suspension was then added to a 15-ml Falcon tube and 7 ml of media added. Cells were reseeded at a dilution of 1:15 for 75 cm² flasks and 1:6 for 24-well plates.

2.2.3 Transient transfection of plasmid DNA into mammalian cells

LipofectamineTM2000 reagent (Invitrogen Ltd) was used for all transfections in both PC12 and HEK293T cells. For PC12 cells grown on poly-D-lysine coated 24-well plates, 0.8 µg of DNA was added to 50 µl of serum-free Advanced RPMI media in a sterile 1.5 ml tube. LipofectamineTM2000 was added into 50 µl of serum-free Advanced RPMI media at a 2µl/µg DNA ratio. The DNA and Lipofectamine mixes were then incubated for 5 minutes at room temperature, and subsequently combined and incubated at room temperature for a further 20 minutes. The DNA-Lipofectamine mix was then slowly pipetted onto the cells, which were returned to the incubator for 24 to 48 hours.

HEK293T cells were transfected with 0.5 - 0.8 µg of EGFP-CSPα plasmid and 1.6 – 2.0 µg of the designated HA-tagged zDHHC or PPT1 construct, following the same procedure as described above for PC12 cells. Cells were analysed 24 to 48 hours post-transfection.

2.2.4 Harvesting transfected cells for SDS-PAGE

Cells were placed on ice, washed two times with PBS [1.3 mM NaCl, 28.6 mM KCl, 120 mM Na₂HPO₄, 13.7 mM KH₂PO₄, pH 7.4] and subsequently incubated for 10 minutes in 100 µl SDS Sample Buffer [50 mM Tris (pH 6.8), 0.1 % (w/v) bromophenol blue, 10 % (v/v) glycerol,

2 % (w/v) SDS, 25 mM Dithiothreitol (DTT)]. The cell mixture was then heated to 95°C for 5 minutes and used for subsequent analysis or stored at -20°C.

2.3 Analysis of human brain tissue

2.3.1 Preparation of human brain lysates

A pea-sized sample of brain tissue was homogenized using a Dounce homogenizer in 500 µl of ice-cold lysis buffer composed of 20 mM Hepes, 250 mM sucrose, 1 mM MgCl₂, 2mM EDTA, 1% Triton X-100, and protease inhibitor mixture (Sigma-Aldrich Company Ltd. (Dorset, UK)), pH 7.4. After a 10 minute centrifugation step at 14,000 x g, the supernatant was collected and the protein concentration was determined by BCA Protein Assay.

2.3.2 Quantification of total protein by Bicinchoninic acid (BCA) Protein Assay

The BCA Assay is a biochemical assay used to determine the total concentration of protein in a solution (0.5 µg/ml to 1.5 mg/ml). It is a colorimetric method based on two reactions. First, the reduction of Cu²⁺ to Cu⁺ by protein in an alkaline medium. This reaction (biuret reaction) is dependent on temperature and the amount of protein present in the sample. Secondly, the Cu⁺ cations are chelated with two molecules of bicinchoninic acid (BCA), resulting in a purple-colored complex with a strong absorbance at 562 nm. Thus, the absorbance of this water-soluble complex is nearly linear with increasing protein concentrations and the amount of protein present in a solution can be determined by measuring the absorption spectra and comparing with protein samples of known

concentration. In this case, BSA was used as the protein standard. The assay was performed following the manufacturer's instructions.

2.4 Molecular Biology

2.4.1 Standard molecular biology protocols

All bacterial liquid cultures were grown from bacterial colonies containing the plasmid of interest or from a scraping of a frozen glycerol stock, and were placed into autoclaved Lysogeny Broth (LB) media [10 g/L NaCl, 10 g/L tryptone, 5 g/L yeast extract]. For growth on solid media, LB agar was prepared by adding 20 g/L agar into the LB media previously described. Both the liquid and solid media contained the appropriate concentration of selective antibiotic to ensure plasmid propagation (100 µg/ml of ampicillin, 30 µg/ml of kanamycin or 10 µg/ml of gentamicin).

DNA was kept in Diethylpyrocarbonate (DEPC) water, previously prepared by adding 0.1 % (v/v DEPC) to ultra-pure water and incubating for a period from 2 hours to overnight. The DEPC-treated water was then autoclaved to eliminate traces of DEPC.

2.4.2 DNA amplification by Polymerase Chain Reaction (PCR)

Polymerase chain reaction (PCR) was used to introduce targeted mutations into plasmid DNA. The PCR reaction mix contained 5 µl of 10X KOD Polymerase Buffer, 5 µl of MgSO₄ (25 mM), 4 µl of dNTPs (2 mM each of dATP, dCTP, dGTP and dTTP), 1.5 µl of each primer (10 µM, forward and reverse), 50 ng of template DNA and 1 µl of KOD Hot Start DNA Polymerase (1 U/ µl). 2 µl of DMSO were added to the PCR reaction mix to increase the

yield of PCR fragment obtained. Nuclease-free water was added to give a total volume of 50 μ l.

The ready PCR-mix was then incubated at 95°C for 2 minutes to denature the DNA and heat-activate the KOD Hot Start DNA polymerase. After the initial denaturation, 18 cycles followed consisting in a 20 second denaturation step at 95°C, a 10 seconds annealing step at 55°C and an elongation step at 68°C. The temperature in the annealing step was modified accordingly depending on the reaction and set to be at least 5°C below the melting temperature (T_M) of the primers used. The elongation step was calculated depending on the length of the amplified product with circa 30 seconds per 1 kilobase pair of DNA.

After the reaction finished, PCR products were stored at 4°C for short periods (overnight) and at -20°C for longer periods.

2.4.3 Site-Directed Mutagenesis (SDM)

Site-Directed Mutagenesis (SDM) was used to introduce specific mutations into expression plasmids. For this, specific oligonucleotide primers were designed according to the region of DNA intended to be modified. The primers contained base mismatches to introduce sequence changes of up to 12 base pairs and had a length of 30 to 48 nucleotides, containing 15 to 20 nucleotides up and downstream of the specific mismatch. The plasmid DNA used for SDM was isolated from an *E. coli* strain, therefore the DNA is methylated. Subsequently, a PCR was conducted as explained in Section 2.3.2. In order to eliminate traces of the plasmid DNA and select the mutation-containing synthesized DNA, the PCR product was digested with the methylation sensitive restriction enzyme DpnI. The PCR

product was directly treated with 1 μ l of DpnI and incubated for at least an hour at 37°C. The resulting DNA solution was then stored at -20°C or used for further processing.

2.4.4 Gateway Cloning System

The Gateway cloning system is based on the site-specific recombination characteristics of the bacteriophage λ , used to combine its DNA with the *E. coli* chromosome. With the Gateway system, a DNA sequence is cloned into an entry vector and from there, the DNA fragment can be cloned into any other gateway-compatible destination vector through a recombination reaction.

E. coli and bacteriophage λ share specific recombination sites called *att* (*attP* in phage λ and *attB* in *E. coli*). When the phage infects bacteria, its DNA recombines with the corresponding bacterial DNA through the *att* sites. This reaction, which is catalysed by the bacteriophage λ protein Int (Integrase) and the *E. coli* Integration Host Factor (IHF) protein (BP Clonase™ enzyme mix), results in the integration of the phage DNA into the bacterial genome. After integration, the recombination sites *attB* and *attP*, now called *attL* and *attR* (L stands for left and R stands for right), are flanking the integrated DNA. This is a reversible process and the phage DNA can excise itself from the bacterial genome through the lytic pathway, catalysed by another set of excision and recombination enzymes: the bacteriophage λ Int and Excisionase (Xis) proteins and the *E. coli* Integration Host Factor (IHF) protein (LR Clonase™ enzyme mix), reforming again the *attP* site in the phage and the *attB* site in *E. coli*.

The Gateway system makes use of this phenomenon and recreates an *in vitro* version of these two reactions. In order to increase specificity and efficiency, the original *att*

recombination sites have been modified to remove stop codons and preserve reading frame and orientation.

The first reaction, BP reaction, generates the entry clone by facilitating the recombination of an *attB* substrate (DNA fragment flanked by *attB1* and *attB2* sites) with an *attP* substrate (donor vector containing *attP1* and *attP2*), creating *attP* and *attL* sites. The reaction, catalysed by the BP Clonase™ enzyme mix, generates the entry clone along with a by-product fragment containing a counterselectable marker (*ccdB*). Entry clones contain the kanamycin resistance gene, which allows clone selection on plates.

The LR reaction is catalysed by the LR Clonase™ enzyme mix and enables the recombination of an *attL* substrate (entry clone) with an *attR* substrate (destination vector), creating an expression clone containing an *attB* site. Upon addition of the enzyme mix, the expression clone is produced together with a by-product plasmid containing *ccdB*. Selection of expression clones is possible due to the presence of the ampicillin resistance gene in the destination vector.

2.4.5 Agarose gel electrophoresis

Visualisation of DNA fragments amplified by PCR was performed by agarose gel electrophoresis. Electrophoresis uses an electrical field to move the negatively charged DNA towards a positive electrode through a 1 % (w/v) agarose gel submerged in 1X TAE buffer [40 mM Tris, 1 mM EDTA, pH 8]. SYBR Safe® (Life Technologies™ Ltd., Paisley, UK) was added to the gel at a 1:10,000 dilution in order to intercalate with DNA to allow UV visualisation. After electrophoresis, the DNA samples were visualised under ultraviolet light.

2.4.6 DNA purification from agarose gels

Once the integrity of the DNA was checked through gel electrophoresis, the desired DNA fragment was isolated from the gel for further processing. For this, the agarose gel was removed from the gel tray and cut with a sterile razor blade, slicing the preferred DNA fragment in a minimum volume of agarose. The gel slice containing the DNA fragment was transferred into a 1.5 ml tube and the DNA was isolated using the QIAquick Gel Extraction Kit (Qiagen Ltd, Germany). Following the manufacturer's instructions, the slice was weighed and buffer QI was added at a 3:1 ratio (100 mg of gel corresponds to 100 μ l of buffer). After a 10 minute incubation step at 50°C and vortexing, the agarose was dissolved. Then, one gel volume of isopropanol was added and gently mixed by pipetting. The mixture was subsequently placed into a QIAquick Spin Column and centrifuged for 1 minute at 13,000 x g to bind the DNA. The DNA was washed firstly with 500 μ l Buffer QG, followed by a 1 minute centrifugation step, and secondly with 750 μ l of Buffer PE and centrifuged again for 1 minute. In order to remove residual wash buffer, the column was centrifuged for another extra minute. Subsequently, the column was placed into a clean 1.5 ml tube and the DNA was eluted by adding 35 μ l of DEPC-treated water followed by a one minute centrifugation at 13,000 x g. To ensure success or otherwise of the purification, one tenth of the elution volume was resolved on a 1% agarose gel and against a 1 kb DNA ladder.

2.4.7 Restriction endonuclease digestion of DNA

Restriction endonucleases were used in order to cut the DNA in specific recognition sites. For this, 1-2 μ g of vector DNA was mixed with 1 μ l of the specific FastDigest® restriction

enzyme, 2 μl of 10X FastDigest[®] Buffer (Fermentas, Thermo Fisher Scientific, MA, USA) and DEPC-treated water to a volume of 20 μl . The mixture was then incubated for one hour at 37°C. In order to ensure the success of the digestion, an aliquot of the sample was resolved on by agarose gel electrophoresis.

2.4.8 DNA dephosphorylation and ligation of DNA inserts with plasmid vectors

After restriction digestion, the DNA was ligated to the expression plasmid. Digested DNA contains a 5' phosphate group required for ligation. However, this can also cause self-ligation. In order to avoid this, the digested DNA was dephosphorylated at its 5' end prior to the ligation reaction. For this, 1 μl of Fast Alkaline Phosphatase (FastAP; Fermentas, Thermo Fisher Scientific, MA, USA) was added to the digestion mix and incubated for 10 minutes at 37°C.

In order to obtain a high efficiency in the ligation process, a higher amount of the DNA insert than the plasmid vector was used, with a ratio of 3 insert: 1 vector. 17 μl of 2X ligation buffer and 1 μl of T4 DNA ligase (Promega, WI, USA) were then added to the DNA mixture. The ligation mix was incubated between 1 hour and overnight at room temperature.

2.4.9 Transformation of expression plasmid DNA into One Shot[®]TOP10 cells

In order to replicate the expression plasmid, the vector was transformed into chemically competent One Shot[®] TOP10 *E. coli* cells (Life Technologies, Thermo Fisher Scientific, MA, USA). TOP10 competent cells were stored at -80°C. After the cells were thawed on ice, 5 μl

of the PCR reaction DNA product were added to a 50 µl vial of competent cells and incubated on ice for 20 minutes. After this, the DNA-cell mixture was incubated for 1 minute at 42°C and then immediately placed on ice for 2 minutes. The transformed cells were then incubated in 250 µl of either SOC medium [tryptone 2% (w/v), yeast extract 0.5% (w/v), 8.6 mM NaCl, 2.5 mM KCl, 20 mM MgSO₄, 20 mM Glucose] or liquid LB medium (see 2.3.1) for one hour at 37°C in an orbital shaker set to 200 rpm. Subsequently, the cells were plated on pre-warmed agar plates (see 2.3.1) containing the corresponding selection antibiotic and incubated overnight at 37°C.

2.4.10 Small-scale plasmid purification (mini-prep)

Mini-prep plasmid purification preparations were used to analyse bacterial clones. For this, single colonies of transformed *E. coli* culture were added to 5 mL of LB broth and incubated overnight at 37°C in an orbital shaker set to 200 rpm. The bacterial cultures were then processed and DNA purified according to the manufacturer's protocol.

2.4.11 Large-scale plasmid purification (midi-prep)

Midi-prep plasmid purification preparations were used to obtain high yields and purity of DNA plasmids for transfection of mammalian cells. The plasmid DNA was purified following the manufacturer's instructions. All buffers used during the protocol were provided in the midi-prep kit.

Bacterial cultures were grown overnight (37°C, 200 rpm) in 150 ml of LB with antibiotic. Cultures were then centrifuged for 15 minutes at 6000 × g and the supernatant was

discarded. The cell pellet was completely resuspended by pipetting up and down in 8 ml of resuspension buffer (RES) supplemented with RNase A. 8 ml of lysis buffer LYS was then added to the solution, mixed by inverting the tube 5 times, and incubated at room temperature for 5 minutes. The lysate was neutralized with 12 ml of neutralization buffer (NEU) and loaded into the NucleoBond®Xtra Column Filter, previously equilibrated with 12 ml of equilibration buffer (EQU). 5 ml of EQU buffer was then loaded onto the NucleoBond®Xtra Column Filter to wash out lysate that remained in the filter. The filter was discarded and the NucleoBond®Xtra Column was washed with 8 ml of wash buffer (WASH). The plasmid solution was eluted with 5 ml of elution buffer (ELU) and precipitated by adding 3.5 ml of isopropanol and centrifuged at $15,000 \times g$ for 30 minutes at 4°C . The pellet was washed with 2 ml 70 % ethanol and centrifuged at $5,000 \times g$ for 5 minutes at room temperature. Finally, the pellet was dried at room temperature and reconstituted in 100 to 200 μl of DEPC H_2O . The plasmid yield was determined by spectrophotometry ($\text{A}_{260 \text{ nm}}$).

2.4.12 Spectrophotometric quantification of DNA

Once the nucleic acid sample had been purified, it was subjected to a UV absorption analysis to determine its concentration. Nucleic acids have absorption maxima at 260 nm wavelength if the sample is pure and there is no significant contamination from proteins or organic solvents. The purity of the sample can be determined by the ratio $\text{OD}_{260}/\text{OD}_{280}$. The reading at OD_{260} gives the amount of nucleic acid present in the sample, while the reading at OD_{280} corresponds to the amount of protein. A ratio ~ 1.8 or ~ 2 is considered an indicator of pure DNA and RNA respectively. If the ratio is noticeably lower, it may indicate the presence of protein, phenol or other contaminants that absorb at 280 nm.

The absorbance was measured at 260 nm and 280 nm with the NanoDrop 2000c spectrophotometer (LabTech International Inc., East Sussex, UK). The concentration was obtained in ng/ μ l.

2.4.13 DNA sequencing

All plasmid vectors were sequenced in order to ensure accuracy. The sequencing was performed on both strands by GATC Biotech (Konstanz, Germany).

2.4.14 Glycerol stock preparation

Bacterial glycerol stocks were used for long-term storage of plasmids. By doing this, plasmids can be stored for many years and available to be used at any point without the need of obtaining more competent cells and retransforming. The addition of glycerol stabilises frozen bacteria and prevents damage to the cell membrane.

A glycerol stock was prepared from every mutant construct generated by adding 500 μ l of glycerol 50% (diluted in dH₂O) to 500 μ l of an overnight bacterial culture. The tubes were then thoroughly vortexed and immediately put on dry ice until frozen and kept at -80°C for long storage.

2.5 Generation of mutant constructs

2.5.1 Generation of human CSP α constructs by SDM

Bovine CSP α and human CSP α proteins differ by two aminoacids, one of them in position 111, very close to the cysteine-string domain (CDS) of CSP α . In order to “humanise” the bovine CSP α construct, the coding sequence of isoleucine was changed to valine using SDM.

The steps followed are described in Section 2.3.3. The primers used are shown in Table 1 in Section 2.1.6.

2.5.2 Subcloning of CSP α 14KR into pEGFP-C2 expression vector

The 14KR CSP α construct containing all lysine codons replaced by arginine codons was supplied by GeneArt[®] (Thermo Fisher Scientific, MA, USA) within the pMA vector. The 14KR CSP DNA was flanked with restriction enzyme recognition sites for HindIII (upstream) and BamHI immediately downstream of the CSP α STOP codon.

The pEGFP-C2 expression vector and the 14KR CSP α pMA vector were digested with the appropriate endonucleases. In order to isolate the fragments, the digested samples were resolved on an agarose gel (see Section 2.3.7). The bands corresponding to the DNA fragments of interest were extracted from the gel and purified as explained in Section 2.3.6. Following gel purification, both digested and purified DNA fragments corresponding to 14KR CSP α and pEGFP-C2 were ligated together as explained in Section 2.3.8., and transformed into One Shot[®] TOP10 cells (see Section 2.3.9). Following antibiotic selection, colonies containing the ligated plasmid were isolated and the ligated plasmid was amplified and purified by small-scale plasmid purification (see Section 2.3.10). The reliability of the ligation and resulting DNA plasmid was verified by DNA sequencing as explained in Section 2.3.13. Upon confirmation, the DNA plasmid was amplified by large-scale plasmid purification (2.3.14) and kept at -20°C until used.

2.5.3 Generation of 14KR ANCL mutants using SDM

The ANCL mutations (L115R and Δ L116) were introduced in the EGFP-CSP α 14KR plasmid by SDM, as described in Section 2.3.3. The oligonucleotide primers used for the generation of these constructs are shown in Table 2 (see Section 2.1.7).

2.5.4 Generation of untagged and HA-tagged mutants through the Gateway Cloning system

Untagged and HA-tagged CSP α mutants were generated with the Gateway Cloning system (see Section 2.3.4). Firstly, a donor vector was generated containing CSP α coding sequence through the BP reaction. Once the incorporation of CSP α sequence in the donor vector was confirmed, the donor vector was subjected to the LR recombination reaction, in which the CSP α sequence is incorporated into an appropriate expression vector.

The generation of the donor vector is a common step in order to generate any final expression vector containing the sequence of interest. The substrates of the LR reaction change depending on the destination vector, as explained in the following sections.

2.5.4.1 attB PCR reaction and purification of attB products

In order to create entry clones, a PCR product containing *attB* sites was needed as substrate in a BP reaction with the donor vector (pDONR™). This PCR product was generated by a PCR (see Section 2.3.2) using primers containing the corresponding *attB* sites, as explained in the manufacturer's manual. The oligonucleotide primers used are shown in Table 7 (see Section 2.1.7). The *attB*-PCR reaction mix was subjected to an initial denaturation stage of 2 minutes at 95°C, followed by 5 cycles of 20 seconds at 95°C, 10 seconds at T_M -5°C and 20

seconds at 70°C. T_M indicates the lower melting temperature of the two primers used. After these 5 cycles, the PCR mix followed 30 cycles of 20 seconds at 95°C and 30 seconds at 70°C, with a final extension step of 30 seconds per kilobase at 70°C.

After the PCR reaction, the resulting *attB*-PCR product was purified in order to remove *attB* primers and any *attB* primer-dimers, since these can recombine with the donor vector during the BP reaction. The PCR products (50 μ l) were then purified according to the manufacturer's manual by adding 150 μ l of TE Buffer and 100 μ l of 30% PEG8000/30mM $MgCl_2$. After a vortexing step, the mixture was centrifuged at 15,000 x g for 15 minutes at room temperature. The supernatant was then carefully removed and the pellet was resuspended in 50 μ l of TE buffer. The success of the purification was confirmed in an agarose gel.

2.5.4.2 Creating a CSP α -pDONR207 entry clone plasmid using the BP Recombination Reaction

Once the *attB*-PCR product was purified, the BP reaction was prepared. As explained in 2.3.4, the BP recombination reaction enables the transfer of the *attB*-PCR product (CSP α) to an *attP*-containing donor vector (pDONRTM207), creating an entry clone.

The BP reaction was prepared with 1 μ l of the donor vector (pDONRTM207, 150 ng/ μ l), 1 μ l of BP Clonase II enzyme mix and 3 μ l of the purified *attB*-PCR product. The reaction was incubated for 1 to 24 hours at room temperature. After the incubation, 1 μ l of Proteinase K was added to the mixture and incubated for 10 minutes at 37°C.

Subsequently, *E. coli* TOP10 competent cells were transformed with the resulting entry clone plasmids according to Section 2.3.9. Selection was possible due to antibiotic gentamicin resistance.

A colony was picked and the plasmid amplified and purified by mini-prep. The validity of the product was confirmed by sequencing.

2.5.4.3 Generation of CSP α -pDest40 expression vector (untagged CSP α)

When the accuracy of the entry clone was confirmed, the LR reaction was prepared. The LR recombination reaction allowed the transfer of the CSP α coding sequence into an *attR*-containing destination vector, creating an *attB*-expression clone.

In order to generate untagged CSP α constructs, the destination plasmid pDest40 was used. The pDest40 vector contains a 6 histidine tag at the C-terminal end. However, due to the presence of a STOP codon in the C-terminal of CSP α , the tag was not expressed.

The LR reaction was performed by mixing together 1 μ l of the destination vector (in this case, pDest40; 150 ng/ μ l), 1 μ l of LR Clonase II enzyme mix, 1 μ l of the CSP α -pDONR207 entry clone (150 ng/ μ l) and 2 μ l of TE. The reaction was incubated for 1 to 24 hours at room temperature. After the incubation, 1 μ l of Proteinase K was added and incubated for a further 10 minutes at 37°C.

Finally, *E. coli* TOP10 competent cells were transformed with the resulting expression plasmids according to Section 2.3.9. Selection was possible due to resistance to ampicillin.

A colony was picked and the plasmid was amplified and purified by mini-prep. The validity of the final product was confirmed by sequencing.

2.5.4.4 Generation of CSP α -pEF-BOS-HA expression vector (HA-tagged CSP α)

HA-tagged CSP α was generated following the LR reaction, as explained in the previous Section (see 2.4.2.3). In this case, the destination vector was GW-HA-pEF-BOS, which contains a triple histidine tag at the N-terminal end.

2.5.5 Replacing lysine codons with arginine codons in CSP α

In order to study the degradation pathway of CSP α , all encoded lysines were substituted with arginine codons, creating the mutant 14KR. The CSP α 14KR sequence was then inserted into the GW-HA-pEF-BOS plasmid to obtain an HA-tagged CSP α 14KR mutant. However, there were also two lysine codons present in the linker region of the GW-HA-pEF-BOS plasmid, between the tag and the coding sequence of CSP α 14KR. These codons were mutated to arginines by SDM as explained in Section 2.3.3, using the primers described in Table 8 (see Section 2.1.6).

2.5.6 Introducing cysteine to alanine/leucine mutations in EGFP-CSP and untagged CSP α plasmids using SDM

CSP α contains 14 cysteines within the CSD, from position 113 to 136. Oligonucleotide primers were designed in order to substitute specific codons with alanine or leucine

codons. The oligonucleotide primers used for this purpose are indicated in Table 3 and 4. The procedure for the SDM is explained in Section 2.3.3.

2.5.7 Generation of CSD mutants using SDM

In order to study the effect of the CSD on the degradation pathway of CSP α , all the non-cysteine codons located within the CSD of CSP α were mutated to alanine codons. The mutants were generated using SDM as explained in Section 2.3.3. The oligonucleotides primers used are detailed in Table 5.

2.5.8 Generation of CSP α -PEST mutants using SDM

Three PEST sequences [rich in proline (P), glutamic acid (E), serine (S) and threonine (T)] were identified within the C-terminal of CSP α . To study the possible role that these sequences might have in the degradation pathway of CSP α , three mutants were generated targeting P, E, S and T within the regions 144 to 147, 151 to 157 and 179 to 182 respectively. The mutants were generated individually using SDM (see Section 2.3.3). The oligonucleotide primers used for the generation of these constructs are detailed in Table 6 (see Section 2.1.6).

2.6 Protein biochemistry

2.6.1 Cycloheximide treatment

Cycloheximide (CHX) is an inhibitor of protein synthesis in eukaryotic organisms produced by *Streptomyces griseus*. CHX binds to the E-site of the 60S ribosomal unit and interferes with deacetylated tRNA, thus blocking translational elongation (Schneider-poetsch et al. 2010). CHX was also used to determine the half-life of CSP α and the ANCL CSP α mutants by treating transfected cells with 50 μ g/ml for 6 to 14 hours. Moreover, transfected PC12 cells were treated for 24 hours with CHX to determine the effect of protein depalmitoylation prior to degradation.

2.6.2 Hydroxylamine treatment

The hydroxylamine (HA) treatment is used to cleave off palmitate bound to cysteine residues. HA targets the thiol group of the palmitoylated cysteine, reducing the thioester bond which results in free SH-groups.

To study the palmitoylation state of CSP α mutants, PC12 cell lysates transfected with CSP α constructs were treated with 0.5 M HA (pH 7) or 0.5 M Tris (pH 7), adding 1X Proteinase Inhibitors, for 24 hours. The same protocol was followed for the study of palmitoylation in human brain lysates (50 μ g of protein).

2.6.3 Brefeldin A treatment

Brefeldin A (BFA) is a fungal metabolite produced from *Penicillium brefeldianum*. BFA inhibits the transport of proteins from ER to Golgi, resulting in the disruption of the structure and function of the Golgi apparatus. In contrast, retrograde membrane traffic from Golgi to ER is not affected by BFA, and thus this fungal metabolite causes the formation of a mixed ER-Golgi compartment (Klausner et al. 1992).

In order to study the effects of mixing ER and Golgi membranes on the palmitoylation of these specific mutants, transfected PC12 cells were treated for 4 hours with 30 µg/ml of BFA (Greaves et al. 2008).

2.6.4 Treatment with proteasome and lysosome inhibitors

A total of two lysosome inhibitors and two proteasome inhibitors were used to investigate the degradation pathway of CSP α and ANCL CSP α mutants.

Bafilomycin A1 and Leupeptin are lysosomal inhibitors. Bafilomycin A1 (BF) is produced by *Streptomyces griseus* and is a specific inhibitor of vacuolar type H⁺-ATPase (V-ATPase). It was used at a concentration of 100 nM in transfected cells (Yoshimori et al. 1991). Leupeptin (LP) is an inhibitor of serine, cysteine and threonine proteases (e.g. plasmin, trypsin, papain, calpain, cathepsin B). Leupeptin was used at a concentration of 50 µM (Yang et al. 2013).

MG-132 (MG) is a proteasome inhibitor. It inhibits NF- κ B activation by preventing I κ B degradation. It was used at a concentration of 10 µM (Sharma et al. 2011; Gao et al. 2000).

Lactacystin (LC) is also a proteasome inhibitor, synthesized by bacteria of the genus *Streptomyces*. It also inhibits NF- κ B activation. LC was used in transfected cells at a concentration of 50 μ M (Shirley et al. 2005).

2.6.5 Palmostatin B treatment

Palmostatin B is an inhibitor of palmitoylation. It has been shown to target Ras depalmitoylation by specifically targeting acyl protein thioesterase 1 (APT1) (Hang and Linder 2011).

Together with the proteasome and lysosome inhibitors, transfected cells were treated with 100 μ M of palmostatin B in order to investigate whether degradation of CSP α is linked to depalmitoylation.

2.6.6 Metabolic labelling of proteins and turnover detection using “click chemistry”

Click chemistry is a two-step labelling and detection technique that uses bio-orthogonal molecules to label and detect proteins of interest (Martin and Cravatt 2009). The bio-orthogonal compounds contain functional groups (azides, alkynes, aldehydes and ketones) that can be involved in a chemical reaction without interfering with biological processes. These compounds are not detected directly but through a chemoselective ligation reaction. Click chemistry is based on the copper-catalyzed Huisgen cycloaddition reaction between azides and alkynes. This reaction is used to detect protein S-acylation and involves labelling

S-acylated proteins with a fatty acid azide derivative, followed by incubation with a fluorophore conjugated to an alkyne group (Figure 2.1).

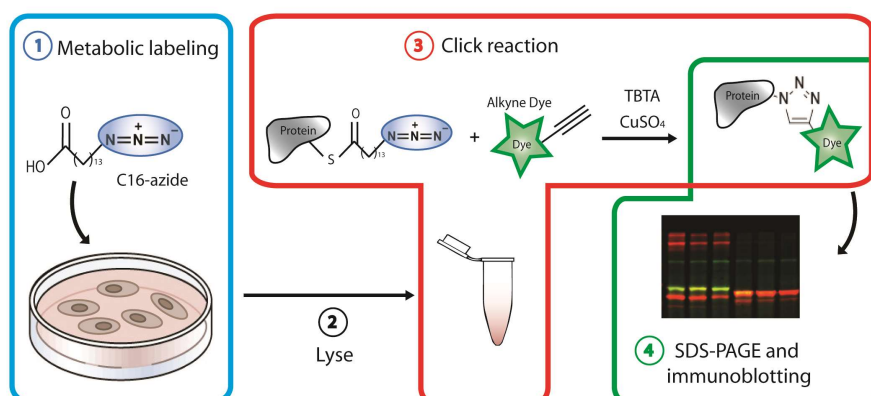


Figure 2.1. Outline of the click-chemistry method to detect attachment of azide-conjugated palmitic acid onto cysteine residues of proteins. HEK293T cells were transfected with an expression vector containing the cDNA encoding the proteins of interest. After 24 h, cells were metabolically labelled with 100 μ M of C16-azide for 4 h and subsequently lysed on ice in 100 μ l of 50 mM Tris (pH 8.0) containing 0.5 % SDS and 1X protease inhibitors. The click reaction mix was added to the lysate [to 100 μ l of cell lysate, 80 μ l of click reaction mix (5 μ M of alkyne dye, 2 mM of CuSO₄ and 0.2 mM TBTA in dH₂O) were added], followed by an incubation of 1 hour at room temperature with end-over-end rotation. The proteins were precipitated with acetone and resuspended in 100 μ l 1X SDS sample buffer containing 25 mM DTT. After separation by SDS-PAGE, the proteins were transferred onto nitrocellulose membranes for immunoblotting analysis and detection of click-signal using the LICOR Odyssey[®] infrared imaging system.

2.6.6.1 Metabolic labelling

The first step of is to label cells by incorporating azide-containing palmitic acid (C16-azide) into palmitoylated proteins. For this, HEK293T cells were serum-starved (24 hours after transfection with an expression vector containing the cDNA encoding the protein of interest) in serum-free DMEM containing 1% (w/v) fatty-acid free bovine serum albumin (BSA) for 30 minutes at 37°C. Following this, media was removed and cells were incubated

in serum-free DMEM supplemented with 1% fatty-acid free BSA containing 100 μ M of C16-azide for 3 to 4 hours at 37°C and 5% CO₂.

2.6.6.2 Cycloheximide chase

After the metabolic labelling, cells were washed twice in warm phosphate buffered saline (PBS) and were incubated for 3 to 6 hours in serum-free DMEM containing 1% fatty-acid free BSA, 100 μ M of unlabelled palmitic acid and 50 μ M of cycloheximide.

2.6.6.3 Cell lysis and azide-alkyne Huisgen cycloaddition reaction (click reaction)

After the chase, cells were washed twice in ice-cold PBS and lysed on ice in 100 μ l of 50 mM Tris (pH 8.0) containing 0.5 % SDS and 1X protease inhibitors.

For the click reaction, the click reaction mix and the ascorbic acid solution were prepared fresh every time. To 100 μ l of cell lysate, 80 μ l of click reaction mix (5 μ M of alkyne dye, 2 mM of CuSO₄ and 0.2 mM TBTA in dH₂O) were added. After vortexing, 20 μ l of 4 mM of ascorbic acid were added, followed by an incubation of 1 hour at room temperature with end-over-end rotation.

2.6.6.4 Acetone precipitation of proteins and preparation for SDS-PAGE

After incubation, proteins were precipitated by adding 600 μ l of ice cold acetone, vortexing and incubating for 20 minutes at -20°C. The proteins were pelleted by centrifugation at 15,000 \times g for 5 minutes at 4 °C. In order to remove any unbound dye from the mixture, the samples were washed with 1 ml of 70% ice cold acetone. This step was repeated two more

times before air-drying the pellet. The resulting pellet was stored at -20°C or resuspended in 100 µl 1X SDS sample buffer containing 25 mM DTT.

2.6.7 Sodium dodecyl sulfate polyacrylamide gel electrophoresis (SDS-PAGE)

SDS-PAGE is a technique used to separate proteins according to their molecular weight (Laemmli, 1970). Sodium dodecyl sulfate (SDS) is an anionic detergent that binds non-covalently to proteins, causing denaturation and conferring a net negative charge. Thus, proteins are able to migrate in one direction towards the anode.

The gel was made by pouring polyacrylamide solutions between a glass cassette sandwich assembled in a casting stand and frame. In this system, two gels are used (resolving gel and stacking gel) to conform a final gel. The main and lower gel is the resolving or separating gel, which is responsible for protein separation. The pore size can be varied to yield the optimal separation of the proteins of interest, and is determined by the total amount of acrylamide present. Gels used were routinely 12%, made by mixing 5 ml of 2X resolving buffer (0.2% (w/v) SDS, 4 mM EDTA, 750 mM Tris, pH 8.9), 4 ml 30% acrylamide/bis-acrylamide, 1 ml dH₂O, 8 µl N,N,N',N'-tetramethyl-ethane-1,2-diamine (TEMED), and 200 µl of 10% ammonium persulfate (APS) solution. TEMED is used for the polymerisation of the acrylamide and bisacrylamide. The reaction is catalyzed by ammonium persulfate (APS). The stacking gel has a lower polyacrylamide concentration and a larger pore size. It is used to improve the resolution of the electrophoresis due to its concentrating effect. It is placed above the resolving gel and prepared by mixing 4 ml of 2X stacking buffer (0.2 % (w/v) SDS, 4 mM EDTA, 250 mM Tris, pH 6.8), 1.2 ml 30 % acrylamide/bis-acrylamide, 2.8 ml dH₂O, 10 µl TEMED and 200 µl 10 % APS. A comb is inserted between the plates into the unpolymerised stacking gel to create wells to load the protein samples.

The protein samples were prepared in SDS sample buffer [50 mM Tris (pH 6.8), 0.1 % (w/v) bromophenol blue, 10 % (v/v) glycerol, 2 % (w/v) SDS, 25 mM Dithiothreitol (DTT)] and denatured at 95°C for 5 minutes. Afterwards, samples were loaded into the gel wells in a gel tank filled with running buffer [25 mM Tris, 250 mM Glycine and 0.1 % SDS (w/v)]. A voltage of 80 V was applied for protein migration through the stacking gel and increased to 150 V for migration through the resolving gel.

2.6.7.1 Immunoblotting using Odyssey[®] infrared imaging system (LI-COR)

After gel electrophoresis, proteins in the gel were transferred onto a nitrocellulose membrane (Nitrocellulose Membrane 0.45 µm pore, Bio-Rad Laboratories Inc., Germany) to make them accessible to antibody detection. The membrane was placed on top of the gel and the two were sandwiched between two pieces of Whatman absorbent paper, all of them previously soaked in transfer buffer [48 mM Tris, 39 mM Glycine, 1.3 mM SDS, 20 % methanol]. The sandwich was tightly clamped within a gel holder cassette to maintain the contact between the gel and the membrane, and put into the Bio-Rad Trans-Blot Cell previously filled with transfer buffer, to which an electrical current was applied. The gel was positioned towards the cathode, allowing the proteins to migrate from the gel to the membrane. The constant current applied was 120 mA overnight.

After the transfer, the nitrocellulose membrane was washed in PBS-T [132 mM NaCl, 10 mM Phosphate, 2.7 mM KCl, 0.02 % (v/v) Tween[®] 20, pH 7.4] and incubated in 5 % (w/v) non-fat milk in PBS-T for 45 minutes to block on an orbital shaker the membrane and prevent non-specific background binding of antibodies to the nitrocellulose. The membrane was then rinsed in PBS-T (5 minutes per wash, 5 times) and probed with the primary antibody against the protein of interest for 1 hour at room temperature on an orbital

shaker or overnight at 4°C with constant gentle shaking. Following this, the membrane was rinsed 5 times in PBS-T for 5 minutes every time and then probed with the secondary antibody solution (1:10,000) for 45 minutes at room temperature with gentle agitation on an orbital shaker. The secondary antibody (DyLight™, Thermo Scientific) is species-specific and is conjugated with an infrared dye that allows detection by image scanning. The membrane was then washed again 5 times in PBS-T (5 minutes per wash) and scanned using a LI-COR® Odyssey Imaging System (LI-COR® Biosciences UK Ltd., Cambridge, UK).

2.6.8 Blue Native polyacrylamide gel electrophoresis (BN-PAGE)

The NativePAGE™Novex®Bis-Tris Gel system (Life Technologies™ Ltd., Paisley, UK) was used to perform BN-PAGE. BN-PAGE is a technique that allows separation of proteins in a native conformation (Schägger and von Jagow 1987). In this case the Coomassie G-250 binds to the proteins maintaining its native state and conferring a net negative charge.

2.6.8.1 Sample preparation

The preparation of the samples was performed on ice. Cells were washed once with PBS before the addition of the precooled (4°C) lysis buffer [NativePAGE™Sample Buffer 1X and 1% of n-dodecyl-β-D-maltoside (DDM) or 1% Digitonin and deionized water]. The cells were lysed by pipetting and the lysate was centrifuged at 20,000 × g for 30 minutes at 4°C. The supernatant was transferred into a sterile tube and stored at -80°C until use.

Two detergents were used to solubilise hydrophobic proteins, depending on the experiment. Digitonin is the mildest detergent and allows the separation of supramolecular complexes. DDM is stronger at delipidating proteins than digitonin. Prior to gel

electrophoresis, 5 % Coomassie G-250 was added to the samples to a final concentration equivalent to 1/4th of the detergent concentration.

2.6.8.2 Gel electrophoresis

Before loading the samples into the gel, the wells were rinsed twice with 1X NativePAGE™ Cathode Buffer. The wells were filled with 1X NativePAGE™ Cathode Buffer for loading and the appropriate volume of the samples was loaded to the wells. After loading, the Upper Buffer Chamber (inner) of the tank was filled with ~200 ml of 1X Dark Blue Cathode Buffer [10 ml NativePAGE™ Running Buffer (20X), 10 ml NativePAGE™ Cathode Additive (20X), 180 ml deionized water]. The Lower (outer) Buffer Chamber was filled with ~600 ml of the 1X Anode Buffer [50 ml NativePAGE™ Running Buffer (20X), 950 ml deionized water]. The gel was run at a voltage of 150 mV for 30 minutes until the dye front migration reached one third of the way through the gel. After that, the 1X Dark Blue Cathode Buffer was replaced with the 1X Light Blue Cathode Buffer [10 ml NativePAGE™ Running Buffer (20X), 1 ml NativePAGE™ Cathode Additive (20X), 189 ml deionized water]. Finally, 150 mV of voltage was applied for a further 60 to 70 minutes.

2.6.8.3 Transfer of separated proteins onto polyvinylidene fluoride (PVDF) and immunoblotting

After BN-PAGE the gel was rinsed in deionized water and washed in 0.1 % SDS solution for 15 minutes. The proteins in the gel were transferred onto a polyvinylidene difluoride (PVDF) membrane (Immobilon® Transfer Membrane, 0.45 µm pore, Merck Millipore) previously soaked in methanol for 2 minutes before transferring into transfer buffer. The

membrane was then placed on top of the gel and between two pieces of filter paper previously soaked in transfer buffer. The transfer proceeded as described for SDS-PAGE.

After the transfer, the PVDF membrane was washed in 8 % acetic acid for 15 minutes and rinsed in deionized water. The membrane was dried at room temperature and re-humidified with methanol before a 1 hour incubation in 5 % non-fat milk in PBS-T. The membrane was washed 5 times with PBS-T (5 minutes per wash) and incubated with the primary antibody for 1 hour at room temperature or overnight at 4°C with constant shaking, followed by a second period of washing in PBS-T. The secondary antibody, also species-specific to the primary antibody, is linked to horseradish peroxidase (HRP). It was diluted at 1:7,500 in PBS-T and added to the PVDF membrane for 1 hour at room temperature. Finally, the membrane was washed 5 times in PBS-T and the proteins were visualised by enhanced chemiluminescence (ECL).

2.6.8.4 Visualisation of proteins by enhanced chemiluminescence (ECL)

ECL is a chemical reaction that produces energy in the form of light. The oxidation of luminol by the HRP in the presence of a peroxide buffer forms an excited state product that emits light. This emission occurs only during the enzyme-substrate reaction and lasts for a few minutes. For this reaction a working solution of ECL was prepared by mixing equal volumes of ECL Solution 1 [100 mM Tris (pH 8.5), 2.45 μ M Luminol, 0.9 μ M Coumaric Acid] and ECL Solution 2 [100 mM Tris (pH 8.5), 0.061 % (v/v) H₂O₂]. The mixed ECL solution was added to the PVDF membrane and the luminescence was detected on light sensitive film (Carestream®Kodak®Biomax®Light film) in a KODAK M35-M X-OMAT processor.

2.6.9 Immunoprecipitation

Post-translational modifications can occur not only in the over expressed proteins, but also in a constitutive manner. Hence, some antibodies, such as anti-ubiquitin, can also detect other ubiquitinated proteins that are not of interest. In order to reduce the background signal, the protein of interest can be immunoprecipitated.

CSP α and mutant CSP α proteins were immunoprecipitated taking advantage of its C-terminal EGFP or HA tag, using the μ MACS™ Epitope Tag Protein Isolation Kit with anti-GFP or anti-HA Microbeads. For that, transfected cells were lysed on ice with 100 μ l of μ MACS lysis buffer (containing 1X protease inhibitors). The lysate was transferred to a 1.5 ml tube and centrifuged for 10 minutes at 10,000 x g at 4°C to sediment the cell debris. The supernatant was transferred to a new tube and 5 μ l of μ MACS anti-GFP or anti-HA microbeads were added to the lysate to magnetically label the protein. The mix was then incubated for at least 30 minutes on ice.

In the meantime, the μ columns were attached to a magnetic platform and equilibrated with 200 μ l of μ MACS Lysis Buffer. After the incubation, the lysate was applied to the column. The column was then washed four times with 200 μ l of μ MACS Lysis Buffer, followed by a final wash with 100 μ l of μ MACS Buffer Wash 2. 20 μ l of pre-heated Elution Buffer (95°C) were added to the column and incubated for 5 minutes at room temperature. To elute the protein, 50 μ l of pre-heated Elution Buffer were added and the eluate was collected as immunoprecipitate.

The immunopurified proteins were kept at -20°C until being analysed by SDS-PAGE.

2.7 Data analysis

The density of protein bands on immunoblots was quantified and background density of the same gel lane subtracted in order to measure relative protein expression. The software Image Studio™ Lite V3.1 (LI-COR Biosciences, Lincoln, NE, USA) was used for quantification of immunoblots visualised by the Odyssey® infrared imaging system (LI-COR). The relative protein levels were calculated using Excel software (Microsoft® Office system). The mean of the measured values was presented with the standard error of the mean (SEM), together with the appropriate statistical analysis, calculated using either Excel software or GraphPad Prism®. The results were plotted using GraphPad Prism® software.

Chapter 3: Analysis of the aggregation of CSP α mutants

3.1 Introduction

A mechanistic link between protein aggregation and neurodegeneration is considered to be well established in several neurodegenerative disorders, such as Alzheimer's disease, Amyotrophic Lateral Sclerosis (ALS), Parkinson's disease and Huntington's disease (Polymenidou and Cleveland 2011). Two mutations in the DNAJC5 gene encoding CSP α , and resulting in a substitution of leucine 115 by arginine (L115R) or a deletion of leucine 116 (Δ L116), have been identified as the cause of adult-onset NCL (ANCL; Benitez et al., 2011; Nosková et al., 2011). Interestingly, these mutations have been shown to cause CSP α to form high molecular weight, SDS-resistant, aggregates (Greaves et al. 2012), providing another potential link between protein aggregation and neurodegenerative disease.

The amino acid changes (L115R and Δ L116) resulting from the disease-causing mutations are located within the cysteine-string domain of the protein. This highly conserved region of CSP α , involved in membrane attachment and intracellular targeting, is extensively modified by palmitoylation (Gundersen et al. 1994). Moreover, aggregation of the ANCL mutants was suggested to be palmitoylation-dependent as it was enhanced by co-expression of zDHHC enzymes and was reduced by treatment with hydroxylamine, which depalmitoylates CSP α (Greaves et al. 2012). These findings emphasised an interesting link between genetic mutations and post-translational modifications, in protein aggregation and neurodegeneration. Post-translational modifications have previously been shown to alter the mechanism of protein aggregation in other neurodegenerative disorders (Wang, Lin, and Qin 2010), such as phosphorylation in Huntington's disease (Humbert et al. 2002) and glycation in Parkinson's disease and Alzheimer's disease (Miranda et al. 2016). Moreover,

palmitoylation itself (or the lack of) has previously been implicated in neurodegeneration as the formation of inclusion bodies containing mutant Huntingtin is increased when palmitoylation of the protein is blocked (Yanai et al. 2006; Sutton et al. 2013; Sanders and Hayden 2015).

In the case of ANCL, both disease-causing mutations result in a loss of palmitoylated monomeric CSP α visible on SDS gels (Greaves et al. 2012). However, palmitoylation (driven by the co-expression of zDHHC palmitoyltransferases) enhances the formation of aggregates of the mutant proteins visualised on SDS gels (Greaves et al. 2012). Moreover, post-mortem prefrontal cortex samples from patients carrying the L115R mutation also show enhanced aggregation of CSP α on SDS gels, which was reduced by treatment with hydroxylamine (Greaves et al. 2012). This chemical induces protein depalmitoylation by cleaving the thioester-linked palmitate groups from modified cysteines and has been extensively used for the study of protein palmitoylation (Fukata and Fukata 2010; Greaves and Chamberlain 2006).

In contrast to the study of Greaves et al. (2012), another group suggested that aggregation of mutant CSP α proteins was palmitoylation-independent as it could be observed with high concentrations of bacterially-produced, non-palmitoylated, recombinant CSP α protein (Zhang and Chandra 2014). This study also suggested that hydroxylamine treatment did not affect the aggregation status of mutant CSP α proteins; however the validity of this result is in question as the conditions employed in these assays were not sufficient to induce full depalmitoylation of the wild-type CSP α protein.

Although the aggregation of ANCL CSP α mutants has been described, how these aggregates are formed and whether they are pathogenic or not is unclear. Even though CSP α has an

intrinsic tendency to self-associate (Swayne et al. 2003), the underlying cause of the aggregation of L115R and Δ L116 mutants is unknown.

The aim of this chapter was to shed light on the aggregation process by identifying amino acids that are important for aggregation of ANCL CSP α mutants.

3.2 Results

3.2.1 Comparison of the migration profile of wild-type CSP α and ANCL mutants

The palmitoylation status of CSP α can be easily assessed by examining its migration profile on SDS gels. The fully palmitoylated form of CSP α migrates at a molecular mass approximately 8 kDa higher than the non-palmitoylated protein (Gundersen et al. 1994; Greaves and Chamberlain 2006; Greaves et al. 2008; Greaves et al. 2012). Therefore it is possible to compare the palmitoylation status of wild-type CSP α and the ANCL mutants by simple immunoblotting analyses.

As discussed, the formation of mutant CSP α aggregates has previously been observed: (i) in post-mortem tissue from patients with ANCL (Greaves et al. 2012); (ii) using purified recombinant proteins expressed in *E. coli* (Zhang and Chandra 2014); and (iii) with tagged proteins expressed in mammalian cells (Greaves et al. 2012; Zhang and Chandra 2014). However, to-date, the formation of aggregates by the ANCL CSP α mutants has only been studied using SDS-PAGE and the aggregates are simply characterised as “SDS-resistant”. It is therefore important to confirm aggregation of the mutants using an alternative approach, as well as to gain insight into the native complexes formed by both wild-type and mutant

CSP α . The expression of wild-type and mutant CSP α and the formation of aggregates in PC12 cells was therefore evaluated through the use of Blue Native gel electrophoresis.

The pheochromocytoma-12 (PC12) is a rat cell line thought to be derived from neuroendocrine adrenal medullary chromaffin cells (Greene and Tischler 1976). PC12 cells can be induced to differentiate to resemble sympathetic neurons functionally and morphologically. Due to this feature, this cell line has been extensively used as a neuronal cell model (e.g. Bai et al. 2007; Bork et al. 2015; Shafer and Atchison 1991; Gordon et al. 2013).

PC12 cells were transfected for 48 hours with EGFP-tagged wild-type and ANCL mutant CSP α plasmids and the cell lysates resolved on Blue Native gels, transferred onto PVDF membranes and immunoblotted using an anti-GFP antibody. There was a clearly distinct migration pattern of the wild-type and mutant EGFP-CSP α proteins, as can be seen in Figure 3.1A. Specifically, both mutant proteins lack the lower molecular weight bands (at ~60 kDa and ~150 kDa) that are prominent for the wild-type protein. Furthermore, the mutant proteins have increased immunoreactivity at a higher molecular weight, providing evidence that they aggregate under native conditions as well as under denaturing conditions.

In addition to examining CSP α migration under native conditions, the effect of the EGFP tag was also assessed in order to ensure that it was not influencing ANCL mutant CSP α aggregation. For this, untagged CSP α constructs expressed in PC12 cell lysates were examined under denaturing conditions. As observed in Figure 3.1B, the formation of aggregates of mutant CSP α was confirmed in the absence of any tag, as well as loss of the immunoreactive band corresponding to monomeric palmitoylated protein. Even though a faint band corresponding to the palmitoylated form of CSP α can be observed in the case of both ANCL mutants, this is likely due to the presence of endogenous CSP α protein in PC12

cells (Greaves et al. 2008; Bai et al. 2007). As previously mentioned, CSP α has an intrinsic tendency to self-associate and form dimers (Bai et al. 2007; Swayne et al. 2003). In this case, dimerization is likely reflected in the immunoreactive band occurring at \sim 58 kDa.

Collectively, these results confirm the different migration patterns of wild-type EGFP-CSP α and the ANCL mutants and emphasise the tendency of the mutants to form high molecular weight aggregates.

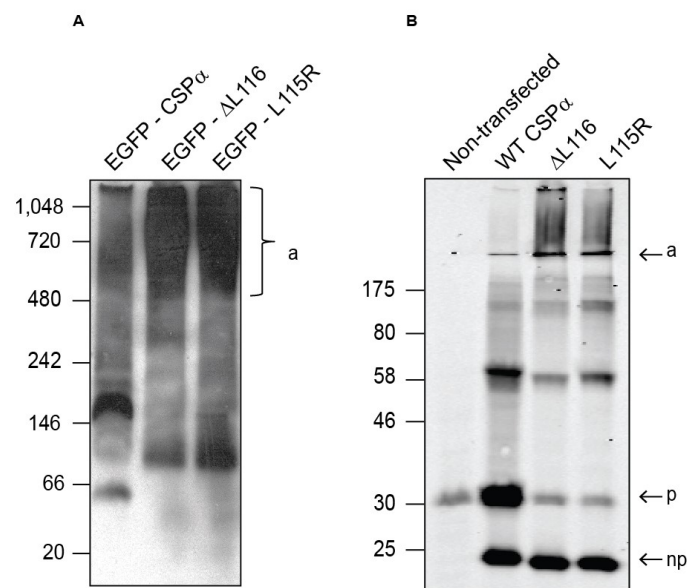


Figure 3.1. Migration profile of wild-type and mutant CSP α . (A) Lysates from PC12 cells expressing EGFP-CSP α constructs were resolved on Blue Native gels, transferred onto PVDF membranes and immunoblotted using an anti-GFP antibody. (B) Untagged CSP α constructs were expressed in PC12 for 48 hours, resolved by SDS-PAGE and transferred to nitrocellulose membranes. The membranes were immunoblotted using an anti-CSP α antibody. The positions of size markers are shown on the left hand side of both panels. *a* indicates aggregates, *p* shows the position of palmitoylated monomeric CSP α , and *np* designates the non-palmitoylated monomers.

3.2.2 Characterisation of the oligomeric properties of the ANCL mutants

Having confirmed that aggregation of the mutant CSP α proteins could be observed both on Blue Native gels and with untagged proteins, an experiment was carried out to determine the time-course of aggregate formation.

PC12 cells were transfected with wild-type and ANCL mutant EGFP-CSP α and treated at the time of transfection with 50 μ g/ml cycloheximide, a translation inhibitor (detailed in *Materials and Methods*, Section 2.6.1), which is extensively used to study post-translational modifications and protein turnover (e.g. Schneider-poetsch et al. 2010; Greaves et al. 2008; Greaves and Chamberlain 2011a; Yang et al. 2013). After an overnight incubation, the media with cycloheximide was removed and substituted with growth medium. PC12 cells were then lysed at different time points following cycloheximide removal (0 minutes, 30 minutes, 1 hour, 2 hours, 3 hours and 4 hours), and lysates resolved by SDS-PAGE and immunoblotted using an anti-GFP antibody.

As shown in Figure 3.2, aggregate formation is a time-dependent process, and was first detected at around the same time (\sim 3 hours) for both mutants. A high molecular weight putative dimer or other oligomeric species (175 kDa) was also observed with wild-type CSP α and both ANCL mutants; formation of this putative dimer occurred on a similar time frame as the aggregation of the mutant proteins. Also at this time point it was possible to observe the palmitoylated form of wild-type CSP α . As the aggregation of the mutant CSP α proteins is time-dependent, this argues against the idea that aggregation is occurring after cell lysis. Furthermore, as aggregation of the mutant proteins occurs on a similar time-scale as palmitoylation of the wild-type protein, it further suggests a link between palmitoylation and aggregation.

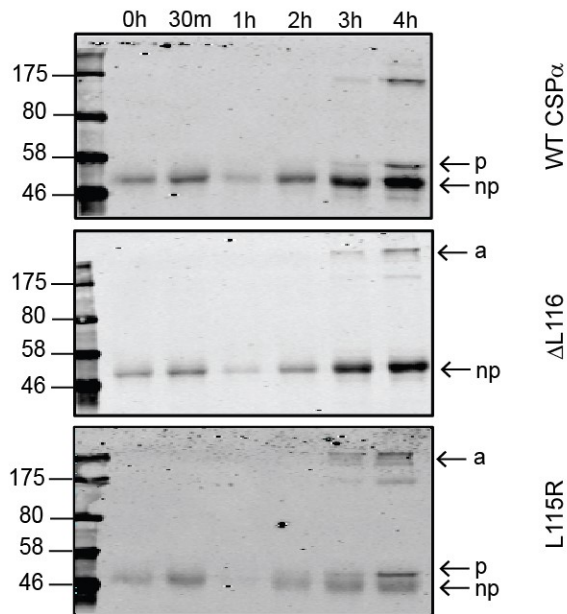


Figure 3.2. The formation of mutant CSP α aggregates is time-dependent. PC12 cells were transfected with EGFP-tagged wild-type/L115R/ Δ L116 CSP α and treated with supplemented RPMI advanced media containing cycloheximide (50 μ g/ml) overnight. The following day, the medium was replaced by supplemented RPMI-1640 advanced medium lacking cycloheximide for the periods indicated. The lysates were resolved by SDS-PAGE and proteins transferred to nitrocellulose membranes. The membranes were then probed with anti-GFP antibody. *a* indicates aggregates, *p* shows position of palmitoylated monomeric CSP α , and *np* designates the non-palmitoylated monomers. Molecular size markers are shown on the left.

3.2.3 Importance of the C-terminus and the cysteine-string domain of CSP α for aggregation of ANCL mutant proteins

The role of the C-terminal region and the cysteine-string domain (CSD) in membrane binding and palmitoylation has been well established (Greaves and Chamberlain 2006), and it serves as a starting point for the study of the key amino acids mediating aggregation of the ANCL mutants.

The C-terminal domain of CSP α corresponds to residues 136 to 198 of the protein. As reported by Greaves and Chamberlain (2006), CSP α truncation mutants lacking the C-terminal domain are membrane-bound but not palmitoylated. Furthermore, these mutants are also mislocalised, accumulating on ER membranes.

In order to determine whether membrane association of CSP α mutants in the absence of palmitoylation was sufficient to trigger their aggregation, EGFP-tagged truncation mutants lacking the C-terminus (CSP₁₋₁₃₆) were examined. The ANCL mutations (L115R and Δ L116) were truncated after amino acid 136 and transfected into PC12 cells. After 48 hours, the cells were lysed and the cell lysates were resolved by SDS-PAGE and examined by immunoblotting (Figure 3.3A). For wild-type CSP α , it can clearly be seen that removal of the C-terminal domain blocked palmitoylation as there was no band-shift observed, in agreement with previous work (Greaves and Chamberlain 2006). In the case of the ANCL mutants, aggregation was still visible for the 1-136 truncation mutants.

For quantification of aggregation, the density of the aggregate band was expressed as a ratio of the sum of the dimeric and monomeric forms of the proteins (non-palmitoylated and palmitoylated) and the mean values are presented together with the standard error of the mean (SEM) and the corresponding significance value (Figure 3.3B). The quantitative analysis showed that removal of the C-terminus from both ANCL mutants significantly decreased the ratio of aggregated to monomeric protein. This suggests either that the C-terminus of CSP α is important for aggregation of the ANCL mutants or that palmitoylation of the CSD is playing a role.

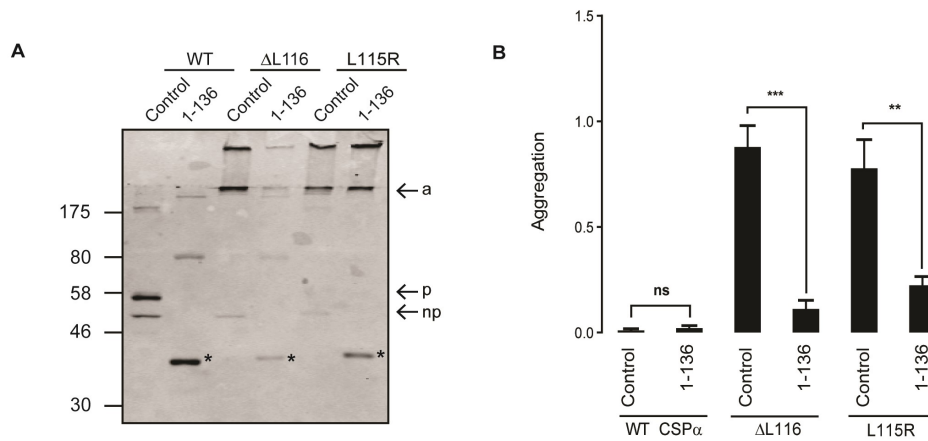


Figure 3.3. Effect of C-terminal truncation on aggregation of ANCL mutants. A) PC12 cells were transfected with wild-type/L115R/ Δ L116 CSP α with or without the indicated C-terminal truncation. Cells were lysed after 48 hours and resolved by SDS-PAGE. The proteins were then transferred onto nitrocellulose membranes and probed with anti-GFP antibody. Position of molecular weight markers is shown on the left; arrowheads indicate aggregates (*a*), palmitoylated CSP α (*p*), non-palmitoylated CSP α (*np*) and the asterisks indicate the 1-136 band. **B)** Quantification was performed by densitometry using Image Studio Software, the graph shows the mean ratio of aggregated to monomeric plus oligomeric forms of each protein (n=5) together with SEM (error bars). Statistical analysis was completed with unpaired two samples Student's T test, asterisks denote a significant difference (ns=non-significant, ** $p < 0.01$, *** $p < 0.001$) from the corresponding control CSP α construct (wild-type, Δ L116 or L115R).

Though quantification shows a decrease in aggregation in the case of L115R₁₋₁₃₆, the aggregates appear clearly visible in panel A. Thus, it is important to note that the quantification in this case could be performed as a percentage of aggregation in relation to total protein. In that case, it is possible that the statistics would no longer be significant.

Altogether, these data suggest either that the C-terminus of CSP α is important for aggregation of the ANCL mutants or that palmitoylation of the CSD is playing a role, especially in the case of the Δ L116 mutant. However, considering the visible aggregation in

the L115R₁₋₁₃₆, it is possible that some aggregation occurs in absence of palmitoylation, as suggested by (Zhang and Chandra 2014).

3.2.4 Analysis of the effects of cysteine mutations on aggregation and palmitoylation of the L115R and Δ L116 CSP α mutants

Analysis of the 1-136 mutants showed the importance of the C-terminal domain of CSP α for aggregation of the L115R and Δ L116 mutants. At first consideration, this result might suggest that aggregation of the CSP α mutants is driven by the C-terminus. However, as discussed, the 1-136 mutant CSP α , although membrane-associated, does not undergo palmitoylation (Greaves and Chamberlain 2006). Therefore, this result is also consistent with previous work suggesting that palmitoylation of the CSD drives aggregation of the L115R and Δ L116 mutants (Greaves et al. 2012). To better define the link between aggregation and palmitoylation, specific cysteine residues in the CSD were substituted in blocks of 3-4 to alanines. The specific cysteine-to-alanine substitutions that were generated are shown in Figure 3.4. In addition, leucine substitutions of cysteines 4-7 were also generated as preserving hydrophobicity at these positions was shown to be important for initial membrane interaction of CSP α and subsequent palmitoylation of the remaining cysteines by membrane-localised zDHHC enzymes (Greaves et al. 2008; Greaves and Chamberlain 2006). These cysteine substitutions were generated in wild-type and both ANCL CSP α mutants.

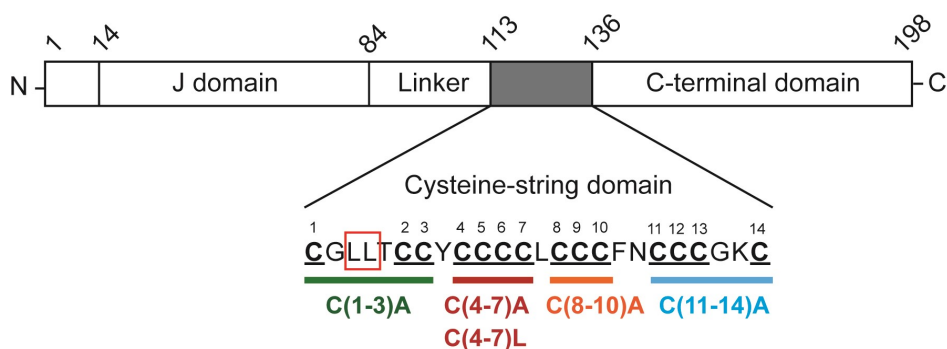


Figure 3.4. Cysteine substitutions on the cysteine-string domain. Schematic diagram of CSP α showing positions of the different domains of the protein and highlighting the positions of amino acids L115R and L116 (indicated with a red box) within the CSD. The cysteines present in the CSD are numbered from 1 to 14 and the different group substitutions are indicated in different colours.

The blocks of cysteine substitutions were introduced into both EGFP-tagged constructs and untagged constructs, which were transfected into PC12 cells for 48 hours. Lysates from the transfected cells were resolved by SDS-PAGE and transferred to nitrocellulose for immunoblotting analysis.

The effects of cysteine substitutions at either end of the CSD in wild-type, L115R and Δ L116 proteins are presented first. Previous work showed that C(1-3)A and C(11-14)A mutants are membrane-associated and efficiently palmitoylated on the remaining cysteines (Greaves and Chamberlain 2006). Figure 3.5 presents representative immunoblots of wild-type, L115R and Δ L116 proteins containing C(1-3)A substitutions expressed in PC12 cells, and corresponding quantification of the ratio of aggregates to monomeric plus dimeric forms of the protein (which corresponds to the sum of monomeric non-palmitoylated and palmitoylated bands, and the putative dimeric band at \sim 175 kDa). As can be seen, cysteine

substitutions at positions 1-3 led to a faster migration on SDS gels of the palmitoylated protein compared to the wild-type palmitoylated protein, consistent with the reduced number of palmitoylation sites (Figure 3.5).

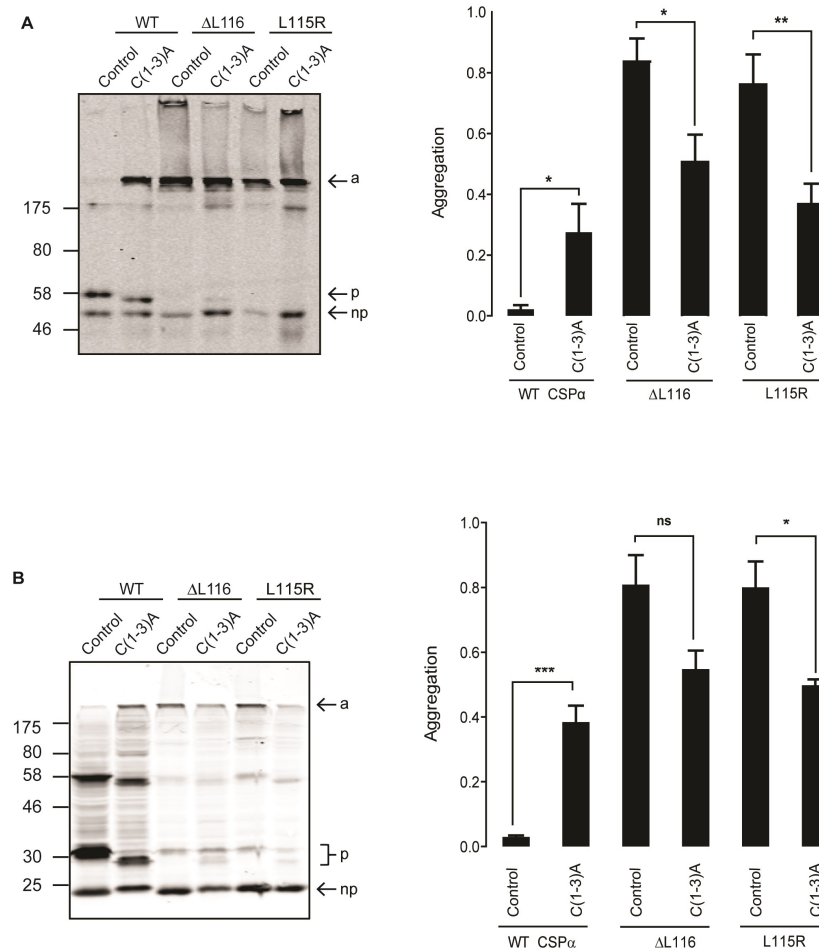


Figure 3.5. Effect of the C(1-3)A substitutions on aggregation of CSPα. PC12 cells were transfected with EGFP-tagged **(A)** and untagged **(B)** CSPα constructs for 48 hours and resolved by SDS-PAGE. Proteins were transferred onto nitrocellulose membranes and probed with anti-GFP antibody (A) and anti-CSPα antibody (B). *a* indicates aggregates, *p* shows position of palmitoylated monomeric CSPα, and *np* designates the non-palmitoylated monomers. Position of molecular weight markers is shown on the left hand side. In both cases, quantification is performed as a ratio of aggregated to the monomeric plus dimeric forms of the proteins (n=4 for EGFP-tagged proteins; n=4 for untagged proteins), shown together with SEM (error bars). The data were analysed using an unpaired two samples Student's T test; asterisks denote a significant difference (ns=non-significant, * $p < 0.05$, ** $p < 0.01$, *** $p < 0.001$) from the respective control CSPα construct (wild-type, ΔL116 or L115R).

However, in agreement with previous work (Greaves and Chamberlain 2006), there was no obvious change in the efficiency of palmitoylation of the remaining cysteines in wild-type CSP α carrying C(1-3)A substitutions, i.e. the ratio of palmitoylated to unpalmitoylated protein was similar for wild-type CSP α with or without substitution of C(1-3)A. Introducing the C(1-3)A substitutions into the ANCL mutants did not have a major effect on their migration profile (Figure 3.5A). Although there was a significant reduction in the level of aggregation of the ANCL mutants containing the C(1-3)A substitutions for both EGFP-tagged and untagged proteins (Figure 3.5B), there was only a very small amount of palmitoylated monomeric Δ L116 and L115R mutants observed and substantially less than seen with the C(1-3)A-substituted wild-type CSP α .

Furthermore, analysis of the effects of the C(1-3)A substitutions on ANCL mutant proteins was complicated by the fact that these substitutions actually induced aggregate formation by wild-type CSP α . Given that the ANCL-causing mutations are located within the cysteines 1-3, it is sensible to think that this small motif (the first 7 residues of the CSD) might protect CSP α from aggregation and mutations in this region can drive aggregation.

Similar to the C(1-3)A substitutions, introduction of the C(11-14)A substitutions into wild-type CSP α did not affect the overall palmitoylation efficiency of the remaining cysteines, although the palmitoylated band migrated faster, consistent with the removal of a number of palmitoylation sites (Figure 3.6). Substitution of the cysteines at positions 11-14 was not observed to have any major effect on the migration profile of the EGFP-tagged or untagged CSP α ANCL mutants, suggesting that these residues are not central to the aggregation process.

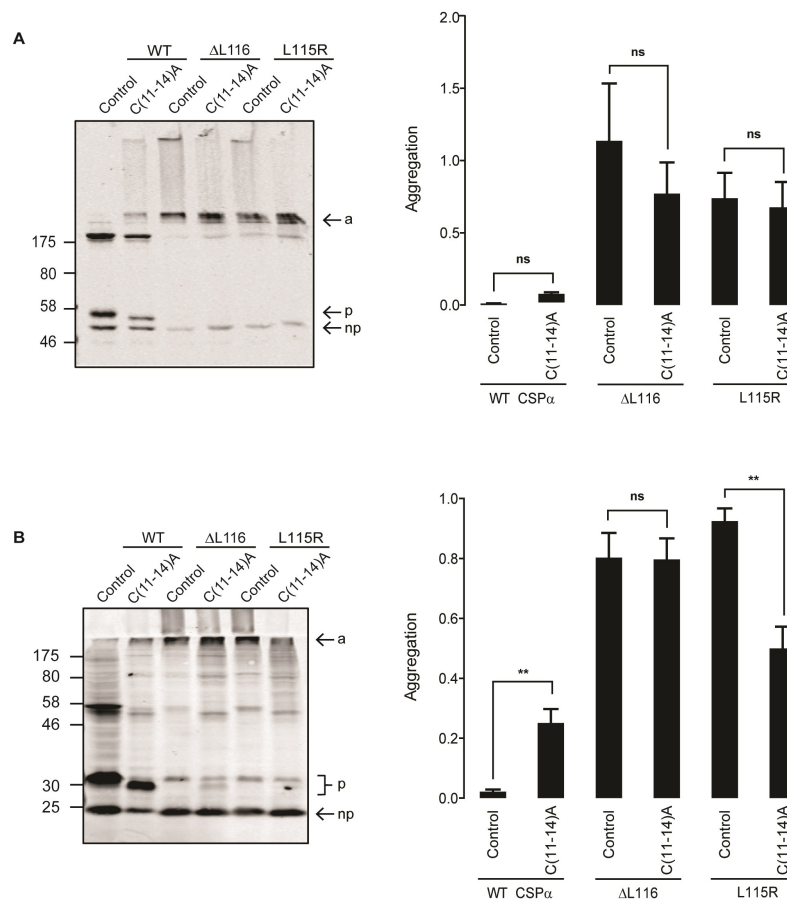


Figure 3.6. Effect of C(11-14)A substitutions on the aggregation of CSP α . EGFP-CSP α (**A**) and untagged CSP α (**B**) constructs were transfected into PC12 cells for 48 hours. Lysates were resolved by SDS-PAGE, transferred onto nitrocellulose membranes and probed with anti-GFP antibody (A) and anti-CSP α antibody (B). Position of molecular weight markers is shown on the left hand side. *a* indicates aggregates, *p* shows position of palmitoylated monomeric CSP α , and *np* designates the non-palmitoylated monomers. In both cases, quantification is presented as a ratio of aggregate to monomer plus dimer ($n=4$ in both cases), shown together with SEM (error bars) and analysis by Student's T test (ns = non-significant; ** $p<0.01$).

In contrast to the cysteine residues that flank the CSD, substitution of cysteines in the core of this domain had a major effect on aggregation of the ANCL mutants. As with the other cysteine mutants studied, substitution of cysteines 8-10 to alanines led to a band-shift in wild-type CSP α consistent with removal of palmitoylated residues but did not affect the efficiency of palmitoylation of the remaining cysteines (Figure 3.7).

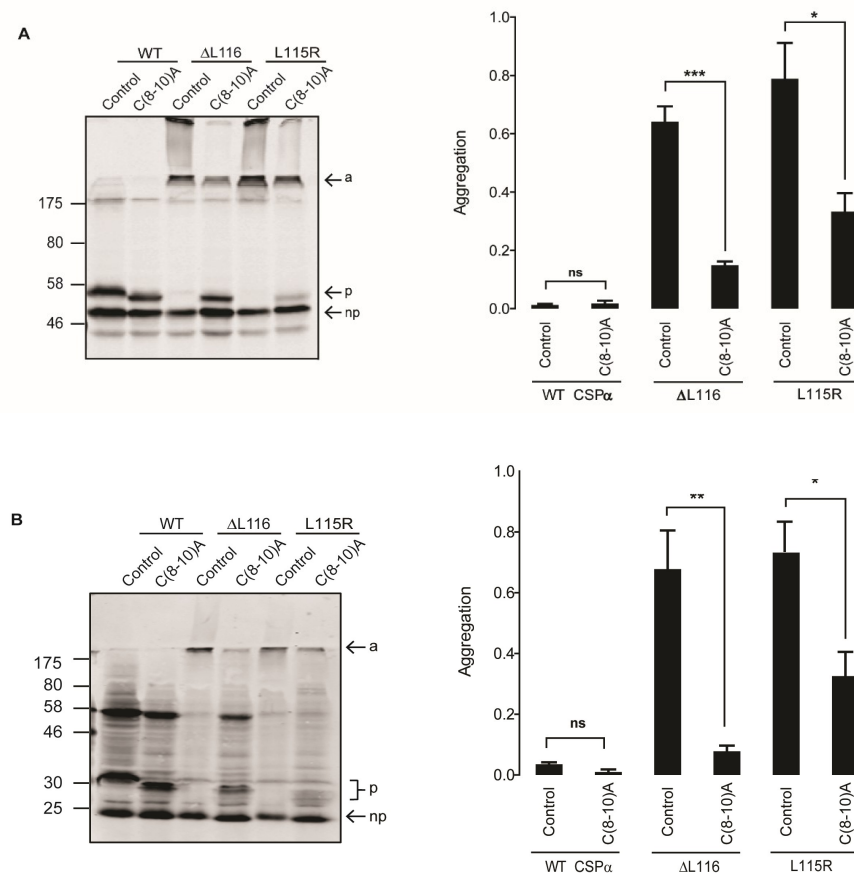


Figure 3.7. Effect of C(8-10)A mutations on the aggregation of CSP α . PC12 cells were transfected with the EGFP-tagged (A) and untagged (B) CSP α constructs for 48 hours and subsequently lysed and resolved by SDS-PAGE. Proteins were transferred onto nitrocellulose membranes and probed with anti-GFP antibody (A) and anti-CSP α antibody (B). *a* indicates aggregates, *p* shows position of palmitoylated monomeric CSP α , and *np* designates the non-palmitoylated monomers. Positions of size markers are shown on the left hand side. In both cases, quantification is presented as a ratio of aggregated to the monomeric and dimeric forms of the proteins (n=4), shown together with SEM (error bars) and analysed by Student's T test (ns = non-significant; * p <0.05; ** p <0.01, *** p <0.001).

Substitution of these cysteines had a clear effect on the ANCL mutants by reducing their aggregation and also increasing levels of a monomeric palmitoylated band, which was more prominent with the Δ L116 mutant than the L115R mutant (Figure 3.7). However, despite the reduction in aggregation of the ANCL mutants when these cysteine residues were substituted, aggregation was not abolished (Figure 3.7).

As previously reported, replacement of the cysteine residues at positions 4-7 of the CSD with alanines decreased the overall efficiency of palmitoylation of the remaining cysteines in wild-type CSP α (Figure 3.8; compare immunoreactivity of palmitoylated and non-palmitoylated monomeric bands of wild-type CSP α and C(4-7)A) (Greaves and Chamberlain 2006). This is thought to reflect a role for this cluster of cysteines (and their hydrophobicity) in membrane association prior to palmitoylation. Interestingly, substitution of these cysteines caused a complete loss of aggregation and recovered the palmitoylated monomeric band of the ANCL mutants to a similar level as seen for wild-type CSP α bearing the C(4-7)A substitutions (Figure 3.8). The palmitoylation band shift was smaller for the EGFP-tagged L115R mutant with C(4-7)A substitutions and more diffuse for the untagged version of this protein (Figure 3.8), suggesting that this ANCL mutant may have an underlying disruption in palmitoylation that is uncovered when its aggregation is prevented.

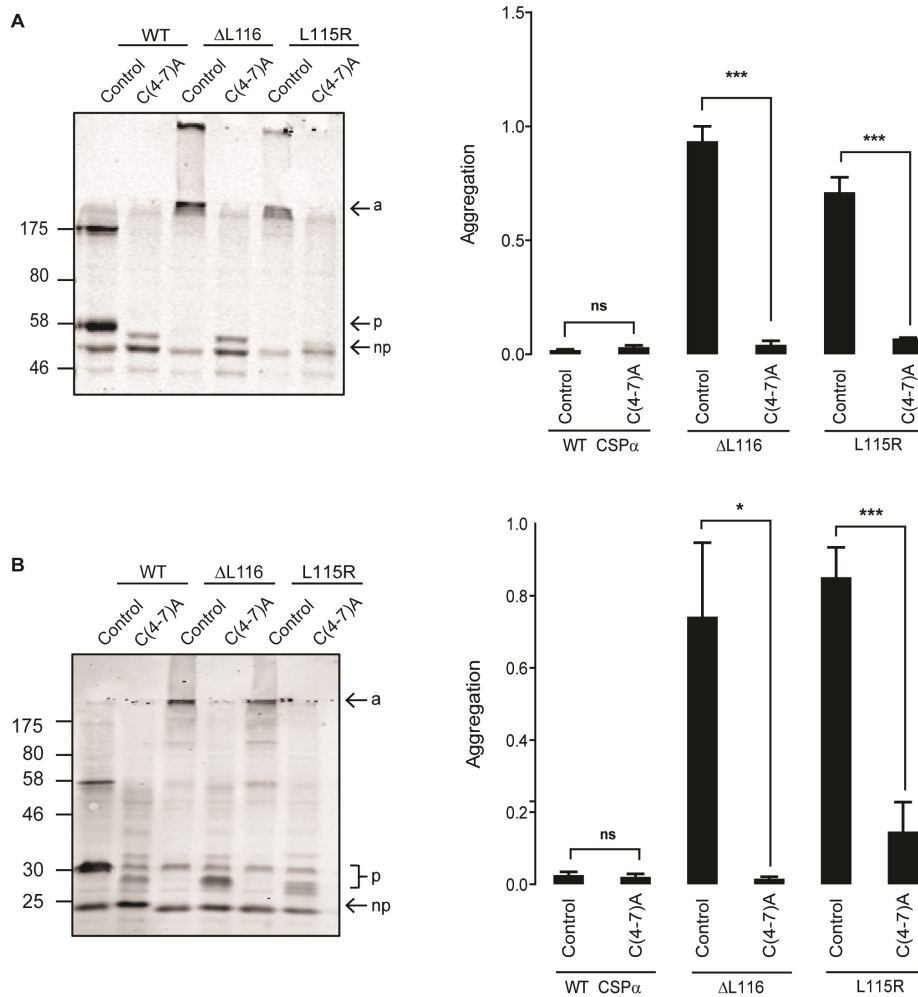


Figure 3.8. C(4-7)A substitutions abolish aggregation of the ANCL mutants. EGFP-CSPα (**A**) and untagged CSPα (**B**) wild-type and ΔL116/L115R constructs with or without the C(4-7)A substitution were transfected into PC12 cells for 48 hours. Lysates were resolved by SDS-PAGE, transferred onto nitrocellulose membranes and probed with antibodies against GFP or CSPα. The non-palmitoylated monomers (*np*), palmitoylated monomers (*p*) and aggregates (*a*) are marked by arrows. The position of molecular weight marker is shown on the left hand side. In both (**A**) and (**B**) cases, the quantification analysis shows the mean ratio of aggregated to monomeric and dimeric forms of each protein (n=4) and is shown together with SEM (error bars). Statistical tests were completed using an unpaired two samples Student's T test, asterisks denote a significant difference compared with the control (wild-type, ΔL116 or L115R) CSPα construct (ns=non-significant, ** $p < 0.05$, *** $p < 0.001$).

However, an issue to consider is that wild-type CSP α with C(4-7)A substitutions is not efficiently palmitoylated on its remaining cysteines and is more cytosolic than wild-type CSP α (Greaves and Chamberlain 2006). Thus, it is possible that loss of aggregation of the ANCL mutants carrying C(4-7)A substitutions is due to reduced membrane association rather than a specific role of these cysteines in the aggregation process. Previous work from Greaves and Chamberlain (2006) showed that membrane association (but not palmitoylation) could be preserved when cysteines 4-7 are replaced by more hydrophobic leucine residues. CSP α carrying C(4-7)L substitutions associates tightly with membranes but localises to the ER, which prevents its palmitoylation due to physical separation from its partner zDHHC enzymes, which are Golgi-localised (Greaves et al. 2008). Therefore, to determine if the loss of aggregation of the ANCL CSP α mutants with C(4-7)A substitutions was simply due to a loss of membrane association, the effects of C(4-7)L substitutions were also examined. Consistent with previous work (Greaves et al. 2008), only a very faint band representing palmitoylated C(4-7)L protein was detected and the bulk of this protein was non-palmitoylated (Figure 3.9). Importantly, introducing cysteine to leucine substitutions at these positions in the ANCL mutants led to a complete loss of aggregation (Figure 3.9) similar to that seen with the C(4-7)A mutants, further emphasising the importance of these cysteines (rather than membrane association) for aggregation of ANCL CSP α mutants.

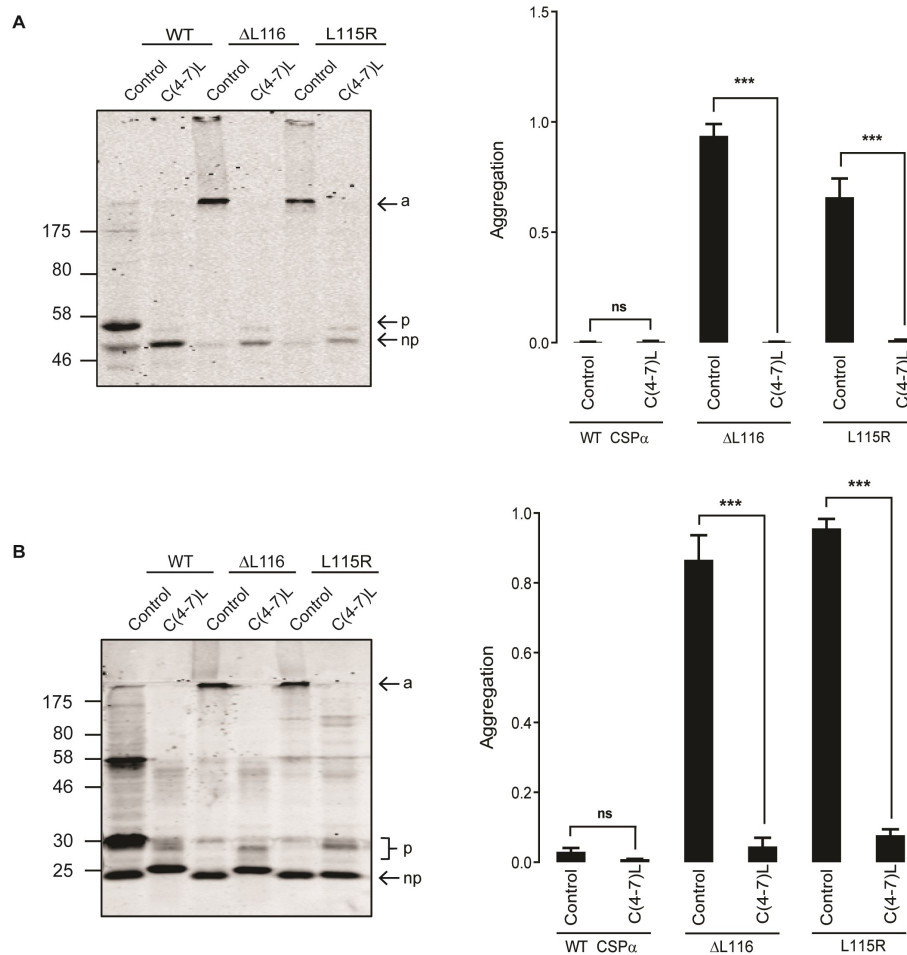


Figure 3.9. C(4-7)L substitutions block aggregation of the ANCL mutants. EGFP-CSPα (A) and untagged CSPα (B) wild-type and ΔL116/L115R constructs with or without the C(4-7)L substitution were transfected into PC12 cells for 48 hours and subsequently analysed by immunoblotting with anti-GFP or anti-CSPα antibodies. The non-palmitoylated monomers (*np*), palmitoylated monomers (*p*) and aggregates (*a*) are marked by arrowheads. The position of molecular marker is shown on the left hand side. In both cases, averaged data of the aggregate to monomer and dimer ratio ($n=4$) is shown together with SEM. Statistical tests were completed using an unpaired two sample Student T test, asterisks denote a significant difference compared with the control (wild-type, ΔL116 or L115R) CSPα construct (ns=non-significant, *** $p<0.001$).

3.3 Analysis of the effects of zDHHC enzyme co-expression on aggregation of ANCL mutant CSP α

Previous work from our group showed that co-expression of active zDHHC enzymes (-3, -7 or -17) led to increased aggregation of ANCL CSP α mutants (Greaves et al. 2012) consistent with a role for palmitoylation in the aggregation process. However, it is important to ensure that this aggregation of ANCL mutants is not caused by some indirect (palmitoylation-independent) effect of zDHHC enzyme over-expression (as suggested by Zhang and Chandra (2014)). To investigate this issue, HEK293T cells were co-transfected with HA-zDHHC3 and wild-type or ANCL mutant CSP α with or without C(4-7)A substitutions. As expected, palmitoylation of wild-type CSP α was increased when co-expressed with zDHHC3 (Figure 3.10). Moreover, aggregation of the ANCL mutants was also enhanced by zDHHC3 co-expression, as previously reported (Greaves et al. 2012) (Figure 3.10). However, no formation of high molecular weight SDS-resistant aggregates was detected for ANCL CSP α mutants carrying the C(4-7)A substitutions when co-expressed with zDHHC3 (Figure 3.10). This result suggests that over-expression of zDHHC enzymes does not induce aggregation of ANCL mutants *via* some indirect effect but instead that aggregation is *directly* linked to increased palmitoylation of the mutants. This analysis further emphasises the importance of cysteines 4-7 for ANCL mutant CSP α aggregation.

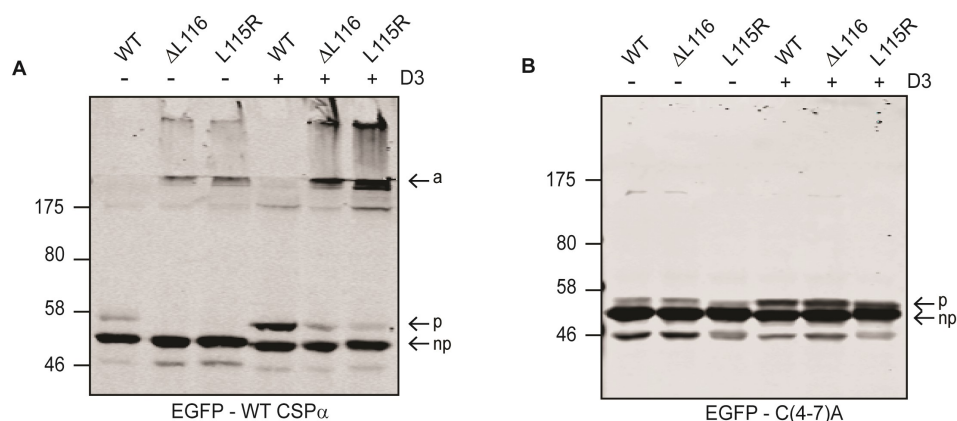


Figure 3.10. Effect of palmitoylation on aggregation of ANCL mutants. HEK293T cells were transfected for 24 hours with wild-type, L115R or Δ L116 EGFP-CSP α with or without HA-zDHH3 as indicated. Cells were then lysed and examined by immunoblotting with anti-GFP. The positions of the molecular weight markers are shown on the *left*, and the arrowheads indicate the aggregated (*a*), palmitoylated monomeric (*p*) and non palmitoylated monomeric (*np*) forms of the protein.

Overall, these results confirm that palmitoylation enhances the formation of ANCL CSP α aggregates and that absence of palmitoylation at cysteines 4 to 7 prevents aggregation from occurring.

However, C(4-7)A and C(4-7)L mutants are only weakly palmitoylated (Greaves and Chamberlain 2006) and therefore it was important to show that loss of aggregation triggered by the mutation of these cysteines does not simply reflect a loss of palmitoylation of the entire CSD. It has previously been shown that addition of brefeldin A (BFA) to cells expressing C(4-7)L mutant CSP α (which is mislocalised to the ER membrane) results in palmitoylation of the protein due to the mixing of ER and Golgi membranes, where the CSP α mutant and zDHH3 enzymes are localised, respectively (Greaves et al. 2008). Therefore, in order to promote palmitoylation of the proteins containing C(4-7)L

substitutions, BFA was added to transfected PC12 cells. BFA inhibits ARF1, a protein that mediates vesicular transport from the ER. BFA treatment thus disrupts ER-to-Golgi transport, promoting a loss of Golgi integrity and causing the fusion of ER and Golgi membranes. Hence, zDHHC enzymes are now able to palmitoylate the C(4-7)L construct (Figure 3.11). The band at ~58 kDa induced following BFA treatment of cells expressing WT_{C(4-7)L}, ΔL116_{C(4-7)L} and L115R_{C(4-7)L} indicates that the proteins have undergone palmitoylation (Figure 3.11). Importantly however, no aggregates were detected even after BFA treatment. Thus, even though the C(4-7)L mutants undergo palmitoylation in the presence of BFA, no aggregation is observed. These results emphasize once more the *direct* role that cysteines 4-7 play in the formation of aggregates.

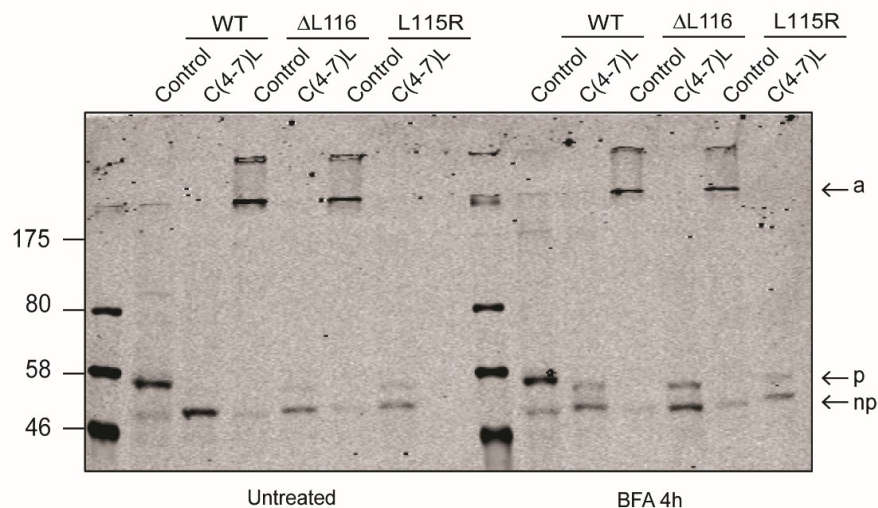


Figure 3.11. Palmitoylation of C(4-7)L constructs does not lead to aggregation. PC12 cells transfected with the wild-type and ANCL mutant EGFP-CSPα constructs with or without the C(4-7)L substitution were treated with 30 μg/ ml of BFA as described in Section 2.6.3. The samples were then resolved by SDS- PAGE and transferred to nitrocellulose for immunoblotting analysis using an antibody against GFP. *a* indicates aggregates, *p* shows position of palmitoylated monomeric CSPα, and *np* designates the non-palmitoylated monomers. Positions of molecular mass standards are shown on the left.

3.4 Further analysis of the Cys(4-7) region of the CSD

Having identified cysteines 4-7 as crucial in the aggregation process, further mutational analysis of this region was performed, examining the effects of double rather than quadruple substitutions. Through site-directed mutagenesis, two new mutants were generated: C(4-5)L and C(6-7)L. Cysteines were substituted to leucines instead of alanines to preserve membrane association (Greaves and Chamberlain 2006). The cysteine substitutions were generated in EGFP-CSP α on either a wild-type or ANCL mutant background. Thus, the constructs obtained were the following: WT_{C(4-5)L}, Δ L116_{C(4-5)L}, L115R_{C(4-5)L}, WT_{C(6-7)L}, Δ L116_{C(6-7)L} and L115R_{C(6-7)L}. PC12 cells were transfected for 48 hours with these constructs and resulting lysates were resolved by SDS-PAGE. Proteins were detected by immunoblotting using anti-GFP antibody. The results obtained are shown in Figure 3.12 and Figure 3.13.

The C(4-5)L substitutions reduced (but did not abolish) aggregation of both ANCL CSP α mutants (Figure 3.12). Furthermore, there was a partial rescue of a palmitoylated monomeric band for both Δ L116 and L115R mutants. The change in migration of the L115R_{C(4-5)L} protein relative to L115R was noticeable for two reasons: the appearance of a high molecular weight band that is likely a dimer (175 kDa) and a single immunoreactive band that migrated at a size intermediate between non-palmitoylated and palmitoylated wild-type CSP α protein carrying the C(4-5)L substitutions (Figure 3.12). One possibility to explain the migration of this single band is that the palmitoylation of the L115R mutant with C(4-5)L substitutions is highly efficient (per molecule) but the number of palmitoylated cysteines in each molecule is lower than the other C(4-5)L mutants. Notwithstanding this, the interpretation of results from the ANCL mutants with C(4-5)L substitutions was

somewhat confounded by the observation that the C(4-5)L mutant led to aggregation of the wild-type protein (Figure 3.12).

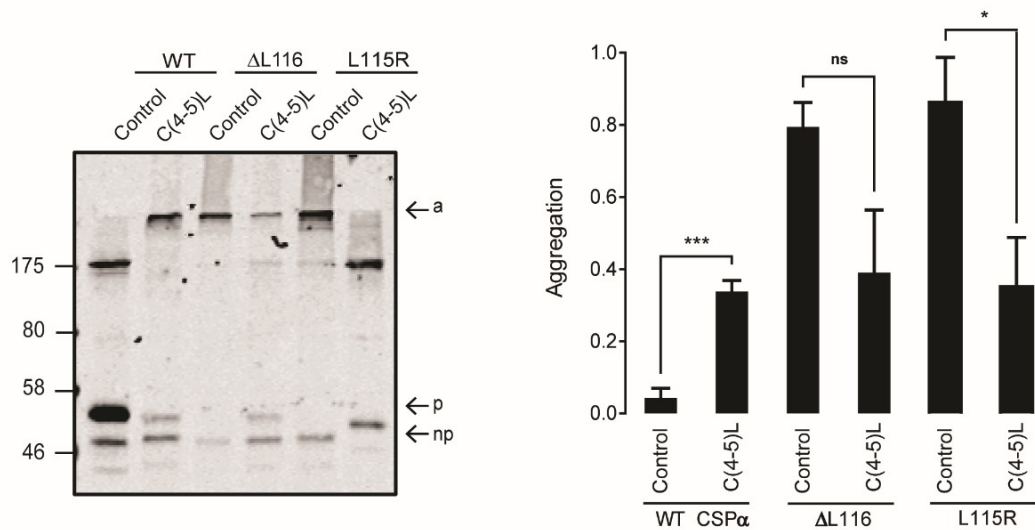


Figure 3.12. Effect of the C(4-5)L substitutions on the aggregation of wild-type and ANCL mutant CSPα. PC12 cells were transfected for 48 hours with the indicated EGFP-CSPα constructs before being lysed and analysed by SDS-PAGE, followed by immunoblotting with anti-GFP. Averaged data \pm SEM for the ratio of aggregates to monomeric plus dimeric CSPα (n=4) is shown; quantification was performed by densitometry using Image Studio Software. Asterisks denote a significant difference in aggregation of the C(4-5)L mutants compared with the corresponding control CSPα constructs (wild-type/ Δ L116/L115R) by two samples unpaired Student's T test analysis (ns=non-significant, * p <0.05, *** p <0.001). The positions of molecular weight standards are shown on the left; arrowheads indicate aggregates (a), palmitoylated CSPα (p) and non-palmitoylated CSPα (np).

Figure 3.13 shows the effects of the C(6-7)L substitutions on aggregation and palmitoylation of the ANCL mutants. In contrast to the C(4-5)L substitutions (Figure 3.12), the C(6-7)L substitutions did not have any effect on aggregation or palmitoylation of wild-type CSPα. Conversely, introduction of these cysteine mutations into the Δ L116 and L115R mutants led to a marked loss of aggregation and a partial recovery of palmitoylation. However, the

effects of the C(6-7)L substitutions of aggregation of the ANCL mutants was less than that seen with the C(4-7)L substitutions (Figure 3.9).

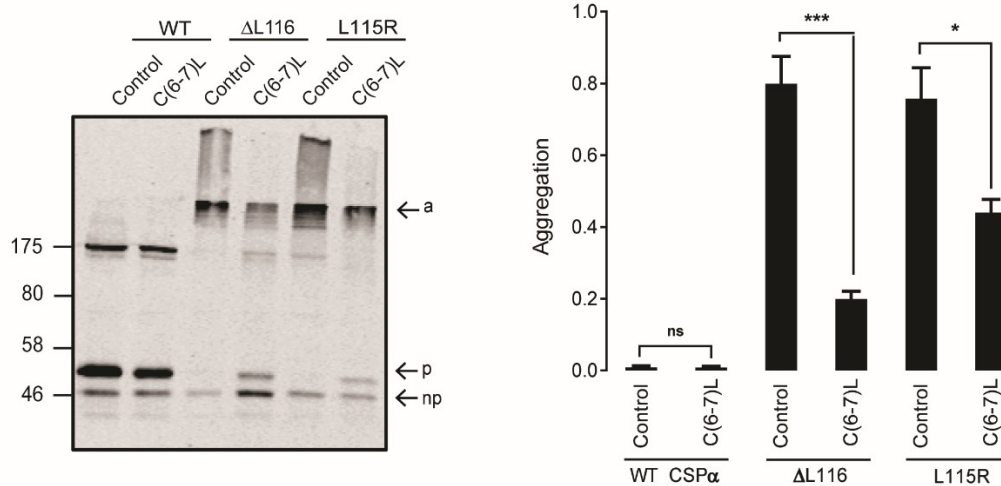


Figure 3.13. Effect of C(6-7)L substitutions on the aggregation of wild-type and ANCL mutant CSPα.

PC12 cells were transfected for 48 hours with the indicated EGFP-CSPα constructs before being lysed and analysed by SDS-PAGE. The proteins were transferred onto nitrocellulose membranes and probed with anti-GFP antibody. Averaged data \pm SEM for the ratio of aggregates to monomers+dimers ($n=4$) is shown, quantified by densitometry using Image Studio Software. Statistical analysis were completed using two samples unpaired Student's T test, asterisks denote a significant difference (ns=non-significant, $*p<0.05$, $***p<0.001$) from the respective control CSPα construct (wild-type/ Δ L116/L115R). The positions of molecular weight standards are shown on the left; arrowheads indicate aggregates (a), palmitoylated monomeric CSPα (p) and non-palmitoylated monomeric CSPα (np).

Collectively, the analyses of the effects of C(4-5)L and C(6-7)L substitutions suggest that all cysteines within this region are important for the aggregation of L115R and Δ L116 mutants, as this was only partly reduced by the C(4-5)L and C(6-7)L substitutions but abolished with the C(4-7)L substitutions.

3.5 Comparison of palmitoylation dynamics of wild-type and ANCL mutant CSP α

Given the clear links between specific cysteines and aggregation of the ANCL CSP α mutants, and the demonstration that palmitoylated cysteines in the core of CSD are key to the aggregation process, the effects of ANCL mutations on palmitoylation dynamics of CSP α were studied in more detail using click chemistry. Click chemistry is a two-step labelling and detection technique that uses bio-orthogonal molecules, which contain functional groups, to label and detect proteins of interest (Martin and Cravatt 2009). In the first step, cells are labelled by incorporating azide-containing palmitic acid (C16-azide) into palmitoylated proteins. In a second step, after the metabolic labelling and cell lysis, the incorporated C16-azide reacts with an infrared alkyne dye in a copper-catalysed reaction named azide-alkyne Huisgen cycloaddition. The reaction between the azide and alkyne forms a conjugate that can be visualised by gel fluorescence using an infrared imaging system (LI-COR). As a first step, the turnover rate of palmitoylation on wild-type CSP α was examined as it is not clear if palmitoylation of this protein is dynamic or not. As a comparison, SNAP25 was included, since this protein is known to undergo palmitoylation-depalmitoylation cycles (Greaves and Chamberlain 2011b). For this, HEK293T cells expressing HA-zDHHC3 together with EGFP-CSP α or EGFP-SNAP25 were labelled with palmitic acid azide for four hours. The label was then removed and replaced with media containing cycloheximide to block new protein synthesis for either 3 or 6 hours. Cell lysates were then incubated with an infrared dye conjugated to an alkyne group, which fluorescently labelled palmitoylated proteins by a click reaction. Figure 3.14 demonstrates that, while SNAP25 showed a progressive decrease in palmitoylation over a six and three-hour chase period, CSP α palmitoylation remained constant. Indeed, there was no loss of palmitoylation of wild-type CSP α even after 6 hours, indicating that CSP α is stably palmitoylated. In order to rule out possible changes in protein

expression that could occur during the experiment, the palmitoylation signal (click signal) was normalised to the protein signal (anti-GFP).

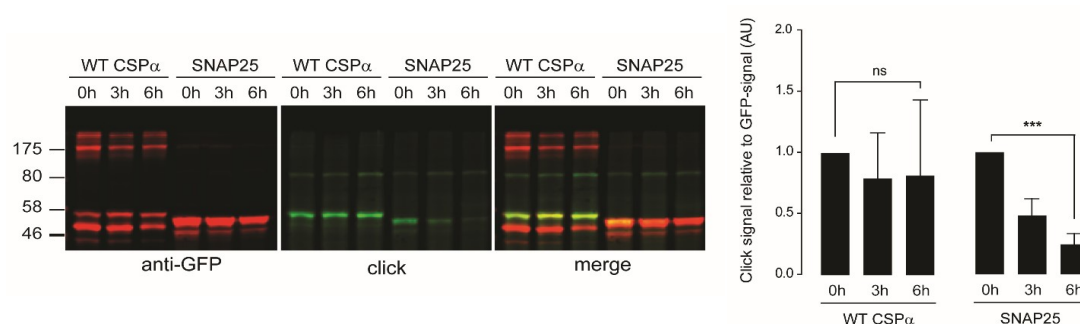


Figure 3.14. Analysis of CSP α palmitoylation turnover by click chemistry. HEK293T cells were co-transfected with HA-zDHHC3 and either EGFP-tagged wild-type CSP α or SNAP25 for 24 hours. Cells were then labelled with 100 μ M of palmitic acid azide. Following removal of the label, cells were incubated in media containing 100 μ M of unlabelled palmitic acid and 50 μ M of CHX to block synthesis of newly synthesised protein for 3 hours or 6 hours. After lysis, incorporation of palmitic acid azide was detected by click chemistry reaction with an alkyne infrared dye. Proteins were separated by SDS-PAGE and analysed by immunoblotting using an anti-GFP antibody. Position of molecular weight markers is shown on the left. The graph shows quantification of azide-C16 incorporation into CSP α or SNAP25, performed by densitometry and expressed as a ratio of click signal to anti-GFP signal. The calculated values of palmitic acid azide incorporation at 0 hours were normalised to 1 for each construct and the chase values were expressed relative to the initial value. Statistical analyses were completed with one-way ANOVA ($n=3$), asterisks denote a significant difference ($ns=non-significant$, $*** p<0.001$).

Having shown that palmitoylation of wild-type CSP α was stable, the turnover of ANCL CSP α mutants was subsequently examined, as described above. Figure 3.15 shows that there was no loss of click signal for wild-type CSP α even after a 6 hour chase period, consistent with the protein being stably palmitoylated (as shown in Figure 3.14). In contrast, there was a marked and significant loss of click signal on palmitoylated monomers of the ANCL CSP α

mutants. This suggests either that the palmitoylated mutant monomers have a faster rate of depalmitoylation than wild-type CSP α or that the palmitoylated monomers are being consumed into high molecular weight aggregates in a time-dependent manner.

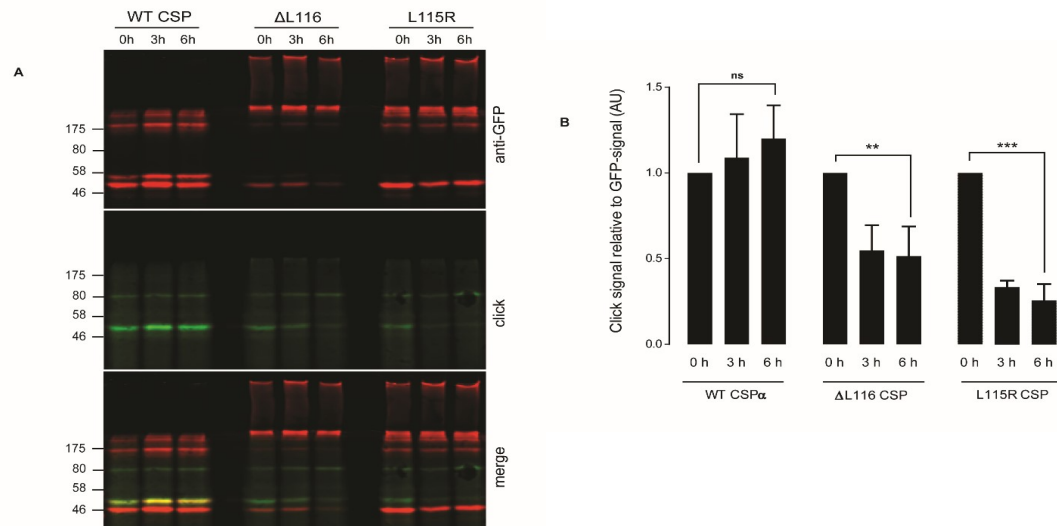


Figure 3.15. Palmitoylated monomers of ANCL CSP α mutants are more short-lived than wild-type protein. HEK293T cells were co-transfected with HA-zDHH3 and wild-type, Δ L116 or L115R EGFP-CSP α for 24 hours. Cells were then labelled with 100 μ M palmitic acid azide. After the metabolic labelling, cells were incubated with 100 μ M unlabelled palmitic acid and 50 μ M of cycloheximide for 3 to 6 hours as indicated. Following cell lysis, incorporation of palmitic acid azide was detected by click chemistry reaction with alkyne infrared dye. Proteins were resolved by SDS-PAGE and analysed by immunoblotting. **A)** Representative image showing GFP immunoreactivity of wild-type, Δ L116 and L115R CSP α (*top panel*), azide-C16 incorporation (*middle panel*) and a merge (*bottom panel*). Position of molecular weight markers is shown on the left. **B)** The graph shows quantification of palmitic acid azide incorporation into the EGFP-CSP α constructs. Quantification was performed by densitometry and is expressed as a ratio of click signal to anti-GFP signal. The calculated values of palmitic acid azide incorporation into the EGFP-CSP α constructs at 0 h were normalised to 1 for each construct and the chase values were expressed relative to this. Statistical analyses were completed with one-way ANOVA (n=3), asterisks denote a significant difference (ns=*non-significant*, ** $p < 0.01$, *** $p < 0.001$).

To distinguish between these two possibilities, HEK293T were transfected for 24 hours with EGFP-tagged SNAP25 and wild-type/ Δ L116/L115R CSP α and labelled with palmitic acid azide for a 4-hour period. After labelling, the media was removed and cells were incubated in media containing cycloheximide (CHX) and palmostatin B (an inhibitor of protein thioesterases that mediate protein depalmitoylation) for 3 to 6 hours, in order to block new protein synthesis and inhibit depalmitoylation. Cell lysates were then incubated with an alkyne dye and subjected to a click chemistry reaction in order to detect the incorporation of palmitic acid azide. The results are shown in Figure 3.16.

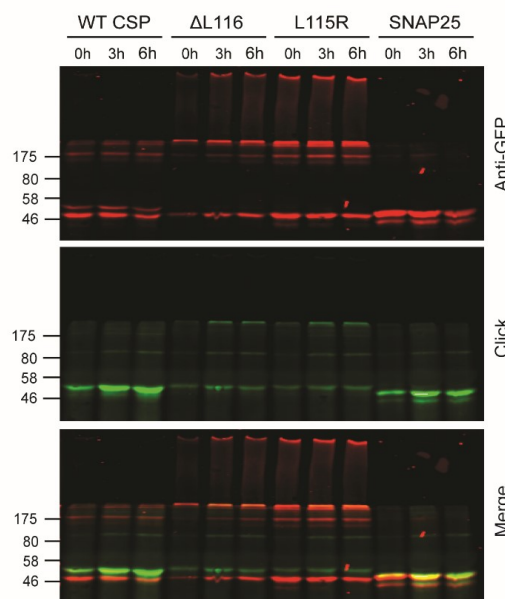


Figure 3.16. Effect of depalmitoylation inhibition on turnover of palmitoylation on ANCL mutant CSP α . HEK293T cells co-expressing HA-zDHHC3 and EGFP-tagged SNAP25 or wild-type/ Δ L116/L115R CSP α were labelled with 100 μ M palmitic acid azide for 4 hours. After labelling, cells were incubated with 100 μ M unlabelled palmitic acid, 50 μ M of cycloheximide and 100 μ M of palmostatin B for a period of 3 hours to 6 hours. Following cell lysis, incorporation of palmitic acid azide was detected by click chemistry reaction with an alkyne infrared dye. Proteins were resolved by SDS-PAGE and analysed by immunoblotting using an anti-GFP antibody. The figure shows a representative image showing detection of wild-type, Δ L116 and L115R CSP α (*top panel*), palmitic acid azide incorporation (*middle panel*) and a merge (*bottom panel*). Position of molecular weight markers is shown on the left.

SNAP25 appeared to be stably palmitoylated even after 6 hours, indicating that palmostatin B was active. Wild-type CSP α showed no change in palmitoylation during incubation with palmostatin B as expected since the palmitoylation of this protein was stable. In the case of the ANCL CSP α mutants, palmostatin B appeared to block palmitoylation turnover of monomeric protein, suggesting that the ANCL mutants have a faster rate of depalmitoylation than wild-type CSP α . However, there was also an increase in aggregation detected over the time-course of the experiment, which could further highlight a link between palmitoylation of the ANCL mutants and their aggregation.

3.6 Discussion

The work in this chapter provides clear evidence that the CSD is essential for the aggregation of the ANCL mutants. Furthermore, through systematic mutation of the CSD, it was found that aggregation can be prevented by alanine substitutions of specific cysteines (C4-7 and to a lesser extent C8-10), implicating these palmitoylated residues in the formation of the high molecular weight SDS-resistant aggregates.

We can be confident that the aggregates are formed inside cells because they were also seen on Blue Native gels (Figure 3.1) and their formation was clearly time-dependent (Figure 3.3). This is important as it rules out any artefactual effects of SDS/denaturation on the aggregation process and supports the notion that these aggregated complexes exist in cells prior to lysis. The profile of WT and ANCL mutants was clearly distinct on Blue Native gels with major immunoreactive bands around 50 kDa and 150 kDa for WT CSP α and at ~100 kDa for the mutants. The ANCL mutants also showed strong immunoreactivity at higher molecular weights (>700 kDa), presumably representing aggregation. The

immunoreactive band around 50 kDa for WT CSP α probably represents the monomeric form of CSP α (the size of WT CSP α together with the EGFP tag corresponds to 48 kDa), while the band at around 150 kDa probably represents a dimer or trimer. The bands at ~100 kDa formed by the mutant proteins could denote other oligomeric species than those seen for WT CSP α . For example, the size difference could reflect a difference in the palmitoylation status of the ANCL mutant proteins relative to WT CSP α . However, although the migration profile of CSP α on denaturing gels is well described, this is the first report of CSP α analysis under native gel conditions. It will therefore be important in future work to confirm the identity of immunoreactive CSP α bands on Blue Native gels by using hydroxylamine treatment and by analysis of a panel of CSP α mutants.

To understand the molecular basis for the aggregation of ANCL CSP α mutants, a series of truncations and amino acid substitutions were constructed and analysed. The C-terminal domain of CSP α corresponds to residues 136 to 198, and this region of the protein is essential for palmitoylation of the protein (Greaves and Chamberlain 2006). Specifically, removal of the C-terminus of CSP α increases membrane affinity and leads to accumulation of the protein on ER membranes in a non-palmitoylated state (Greaves and Chamberlain 2006). This mutant (CSP₁₋₁₃₆) therefore served as a platform to differentiate the effects of membrane binding and palmitoylation on aggregation of the ANCL mutants. Figure 3.3 shows that, when the C-terminal of CSP α is lacking, the aggregates are still present but significantly reduced in comparison to the full-length ANCL mutant proteins. This result is therefore consistent with previous observations (Greaves et al. 2012) highlighting the role of palmitoylation in enhancing aggregation. Although this result in isolation could also reflect an active role for the C-terminal domain of CSP α in the aggregation process, we do not favour this view given the previously described links between palmitoylation and aggregation (Greaves et al. 2012).

As previous results (Greaves et al. 2012) and results in this chapter were pointing to the involvement of palmitoylation in the aggregation process, the importance of different cysteine residues within the CSD was subsequently analysed. For this, different constructs were generated, in which specific cysteines were substituted with alanines. Thus, groups of 3 to 4 cysteines were replaced at a time and tested to observe their effects on palmitoylation and aggregation of the ANCL mutants.

The role of cysteines 1-3 in aggregation is unclear as substitution of these residues led to aggregation of wild-type CSP α . Due to their localisation (surrounding the disease-causing mutations, L11R and Δ L116), it is possible that the effects observed upon substitution of these cysteines is due to a conformational change. Also, while it was clear that aggregation of the ANCL mutants was partially reduced by the C(1-3)A mutation, there was very little rescue of a palmitoylated monomeric form, suggesting some defect in the overall folding of these mutants.

From previous research by Greaves and Chamberlain (2006), it is known that efficient palmitoylation of the CSD of CSP α is dependent on cysteines 4-7, whereas substitution of C(1-3), C(8-10) or C(11-14) does not affect palmitoylation of the remaining cysteines in the CSD or intracellular targeting of CSP α . The essential role of cysteines 4-7 for efficient palmitoylation of the CSD appears to relate to a requirement of these cysteines (and in particular their hydrophobic character) for initial membrane binding of CSP α prior to palmitoylation (Greaves et al. 2008). Given the crucial role that cysteines 4-7 play in membrane binding and palmitoylation of CSP α , it was interesting to test how these residues affect aggregation. In this case, cysteines in positions 4-7 were initially substituted with alanines. These substitutions completely abolished aggregation of the ANCL mutants

(Figure 3.8). Even in the presence of over-expressed palmitoyl acyltransferases (zDHHC3), no aggregation of these mutants was observed (Figure 3. 11).

It was suggested that the overall hydrophobicity of the N-terminal half of the CSD, which includes cysteines 4-7, plays an important role in initial membrane binding, explaining the loss of membrane association and palmitoylation of CSP α when these cysteines were substituted with alanines (Greaves and Chamberlain 2006). Thus, it was possible that alanine replacement of cysteines 4-7 could lead to a loss of aggregation by preventing membrane association of CSP α , rather than any specific role of these cysteines in the aggregation process. To explore this issue, cysteines in position 4-7 were also replaced by leucines, since this was previously shown to allow stable membrane binding of CSP α , albeit in the absence of palmitoylation (Greaves and Chamberlain 2006). The result obtained (Figure 3.9) was essentially identical to that seen with substitution of these cysteines with alanines, and no aggregation of the ANCL mutants was observed. This rules out the possibility that the C(4-7)A substitutions block aggregation of the L115R and Δ L116 mutants by preventing accumulation on membranes. Another possibility was that C(4-7) substitutions prevent aggregation because of a loss of palmitoylation of all cysteines in the CSD rather than just a loss of C(4-7). To address this issue, brefeldin A (BFA) was used. As previously explained (Section 3.3), BFA causes the fusion of ER and Golgi membranes by disrupting ER-to-Golgi vesicle transport. The increased hydrophobicity of the C(4-7)L mutant was proposed to lead to a stronger membrane affinity, resulting in the protein being trapped on abundant ER membranes and physically separated from its partner zDHHC enzymes at the Golgi (Greaves and Chamberlain 2006). BFA was previously shown to allow palmitoylation of C(4-7)L, presumably by mixing ER-localised C(4-7)L mutant and Golgi-localised zDHHC enzymes (Greaves et al. 2008). However, as seen in Figure 3.11, even when the palmitoylation of the C(4-7)L mutants was induced by BFA treatment, the

ANCL mutants still did not aggregate, implying that loss of aggregation of the ANCL mutants containing C(4-7)L substitutions is not caused by a complete absence of palmitoylation on the remaining cysteines but instead suggesting that cysteines 4-7 are integral to the aggregation process. However, it is not possible to say whether palmitoylation of the cysteines at positions 4-7 drives aggregation of the ANCL mutants, or whether the process is triggered simply by the presence of these residues.

Alanine substitution of cysteines 8-10 caused a marked reduction in aggregation and recovery of palmitoylation (Figure 3.7). In this case, the palmitoylation pattern of the C(8-10)A mutant of L115R was quite interesting: for EGFP-tagged L115R, the palmitoylated band was clearly a lower molecular weight than the corresponding palmitoylated band of WT CSP α ; and for the untagged L115R there appeared to be multiple palmitoylated bands present in a smear. These observations may suggest that palmitoylation of the L115R mutant is different from the wild-type protein and that this difference in palmitoylation could be a driver for CSP α aggregation. Finally, cysteines at the end of the CSD (11-14) could be removed without affecting aggregation of the ANCL mutants. All other blocks of cysteines affected aggregation in some way, even though removal of cysteines at positions 4-7 had the greatest effect and completely blocked aggregation of the ANCL mutants.

Therefore, to better assess the role of the C(4-7) region in aggregation, additional mutants were generated. This time, substitutions were introduced in groups of two residues: C(4-5)L and C(6-7)L. However, combination of two cysteine-to-leucine mutations in this region reduced but did not abolish aggregation (Figure 3.12 and 3.13). Thus, it seems likely that mutation of three or four cysteines in this region is necessary to eliminate all aggregation.

How might cysteines 4-7 contribute to the aggregation of ANCL mutants? ANCL mutations could promote a structural change in the CSD, leading to a change in the folding of the

downstream region containing C(4-7). This could be sufficient in itself to promote aggregation, or could require palmitoylation of the misfolded region to drive the aggregation process. ANCL CSP α aggregates have been found in *E. coli*, where no lipid post-translational modifications occur, indicating that palmitoylation is not required for aggregation (Zhang and Chandra 2014). In contrast, Greaves et al. (2012) found evidence of the aggregation of ANCL mutants being sustained by palmitoylation, since co-expression of zDHHC enzymes increased aggregation of ANCL mutants, an observation in agreement with this work.

In the hypothesis that the region containing C(4-7) is misfolded, the ANCL mutants could aggregate *in vitro* without being palmitoylated: the absence of an effective reducing agent would facilitate the formation of disulphide bonds between different CSP α molecules.

Interestingly, the formation of ANCL aggregates was tested under reducing conditions (Zhang and Chandra 2014) and oligomerization was still observed for non-palmitoylated protein. These findings suggest that the formation of disulphide bonds by free cysteines is not the trigger for aggregation. However, Swayne et al. (2003) found that the region of CSP α containing amino acids between 83 and 136 is important for self-association, also even in the presence of reducing agents. The CSD domain, and thus cysteines 4-7 and the ANCL mutations, are located within that region. One possibility is that the ANCL mutations increase the intrinsic tendency of CSP α to self-associate. Thus, it would be interesting to test *in vitro* (without palmitoylation) the effects of increasing reducing agent concentration on the aggregation of ANCL mutants lacking cysteines 4-7. Alternatively, the characterization of cysteine residues and disulphide bonds in proteins could also be performed by liquid chromatography/electrospray ionization tandem mass spectrometry (LC/ESI-MS/MS).

By contrast, the observation that the aggregates are dissolved by HA treatment (Greaves et al. 2012) is clear evidence that the aggregates are palmitoylated. Palmitate chains on different mutant CSP α proteins could cluster together through lipid-lipid interactions, mediated by a misfolded CSD in the mutant proteins. Moreover, inefficient palmitoylation of CSP α monomers might trigger their aggregation and dimers could also be part of the aggregation process. This would explain why some cysteine substitutions reduced aggregation but caused the formation of dimers, such as C(1-3)A and C(4-5)L (Figure 3.5 and 3.12).

Specific cysteines residues in the CSD of wild-type CSP α can be substituted without having an effect on membrane sorting (e.g. C(1-3), C(8-10) and C(11-14)) (Greaves and Chamberlain 2006). This suggests that the extensive palmitoylation of CSP α is not essential for membrane binding and intracellular sorting but instead might be important in order to maintain the correct membrane orientation of the protein required to support its function (Greaves and Chamberlain 2006). The fact that C(4-7) are integral to the aggregation process raises the possibility of targeting this region of the protein as a therapeutic strategy. Thus, perhaps hydrophobic small molecule inhibitors that are designed to interact with the misfolded CSD of ANCL mutants could be used to prevent their aggregation and hence neurodegeneration (if the two processes are linked). To advance this work it will be important to generate structural information on the CSD of both WT CSP α and ANCL mutants.

Considering aggregation of CSP α as the cause of ANCL, it will be important in follow up work to show that the ANCL mutants form aggregates inside cells and that the C(4-7) mutation can prevent this, as seen in immunoblotting experiments. One way to observe fluorescence-tagged molecules in intact living cells is by Fluorescence Correlation

Spectroscopy (FCS) and use of this approach would be important to confirm that ANCL mutants form aggregates inside cells, and that specific cysteines are important in this process. It will also be interesting to study how ANCL mutations might affect the intracellular localisation of CSP α . Previous studies by (Greaves et al. 2012) showed that localisation of ANCL mutants was altered in PC12 cells in comparison to the wild-type protein. Moreover, during the development of this thesis, confocal microscopy was used to analyse the accumulation of the mutant proteins within the cell (neurons) and whether the accumulation of the mutant CSP α causes alterations in the organelle structure (e.g. lysosomes). Since the results were inconclusive (and thus excluded from the thesis), it is a line of investigation worth pursuing in the future, perhaps with different cell lines and different tags.

As ANCL CSP α aggregation is linked to palmitoylation of the protein, the turnover of palmitoylation of wild-type and mutant CSP α proteins was compared. It was found that wild-type CSP α is stably palmitoylated. Conversely, both Δ L116 and L115R mutants presented a different turnover rate. Again, these observations confirm the different behaviour of the wild-type and ANCL proteins and suggest that either (a) the mutants have a faster rate of depalmitoylation than the wild-type; or (b) the palmitoylated monomers are being consumed into high molecular weight aggregates. Experiments performed with palmostatin B did not distinguish clearly between these two possibilities and further analyses should be undertaken to generate a better understanding of this.

Another area of investigation that would be interesting in follow up work is to disrupt the aggregates into their monomeric proteins while preserving palmitoylation. Since the aggregates have been proven to be SDS-resistant, different detergents could be used to selectively extract and isolate proteins. Also, it has previously been seen that treatment with

trifluoroacetic acid (TFA) is able to dissolve SDS-resistant aggregates (Burra and Thakur 2015; Sagné et al. 1996). Thus, CSP α and the aggregates could be purified by immunoprecipitation and treated with TFA, which could help to identify the palmitoylation state of ANCL mutant monomers within the aggregates and provide further clues to the role of palmitoylation in the aggregation process.

Finally, an interesting point of consideration that can be relevant for the disease process is to determine the composition of the aggregates. For example, it has been proposed that protein aggregates formed in other neurodegenerative diseases, such as Alzheimer's disease, Parkinson's disease and Huntington's disease, may sequester cellular factors such as chaperones and transcription factors and that this may contribute to the disease process (Yang and Hu 2016). ANCL CSP α aggregates could be isolated by immunoprecipitation, trypsinized, and the released peptides identified by mass spectrometry (MS) to identify if aggregates contain wild-type CSP α and/or other sequestered cellular factors.

Chapter 4: Analysis of molecular changes in ANCL brains

4.1 Introduction

Neuronal Ceroid Lipofuscinoses (NCLs) are a group of neurodegenerative disorders with the hallmark feature of accumulation of autofluorescent lipopigment in neurons and other cells (Jalanko and Braulke 2009). Several forms of this disease have been identified, characterised by age of symptomatic onset. NCL is the most common neurodegenerative disease in childhood, with most types having an autosomal-recessive inheritance pattern (Oresic et al. 2009). However, NCL can also occur in adulthood and be autosomal-dominant (Nosková et al. 2011; Velinov et al. 2012; Benitez et al. 2011; Cadieux-Dion et al. 2013). Shared clinical features between all NCL types include mental and motor deterioration, epileptic seizures and a decrease in life expectancy (Mink et al. 2013).

Over 430 mutations in 14 NCL genes (CLN1 to CLN14) have been identified as the cause of the different forms of NCL (Mole and Cotman 2015). Even though there are common clinical and pathological features between the different types of NCL, the proteins encoded by the mutated genes in these different NCL disorders often have distinct intracellular functions and localisations (Cárcel-Trullols et al. 2015). Thus, it is not clear whether these proteins act in common disease pathways and if there might be potential interactions between the identified proteins.

Mutations in the *DNAJC5* gene encoding CSP α have been identified as the cause of autosomal-dominant adult-onset NCL (ANCL; Nosková et al. 2011; Velinov et al. 2012; Benitez et al. 2011; Cadieux-Dion et al. 2013). CSP α has also been linked to other neurodegenerative diseases (Burgoyne and Morgan 2015). For example, CSP α expression is

reduced in post-mortem cortex and hippocampal samples from Alzheimer's disease patients (Tiwari et al. 2015; Donnelier et al. 2015), and recent work suggested that CSP α may play a role in Tau spread in this disease (Fontaine et al. 2016). Further connection between CSP α and other forms of neurodegeneration include the observation of reduced SNARE complex levels in brains from Alzheimer's and Parkinson's disease patients (Sharma, Burré and Südhof 2012), similar to that seen in CSP α knockout mice (Sharma, Burré, Bronk, et al. 2012), and the fact that CSP α interacts with mutant huntingtin containing an expanded polyglutamine tract but not with the wild-type protein (Miller et al. 2003).

The aim of this chapter is to attempt to further understand the ANCL disease process by investigating molecular changes occurring in ANCL post-mortem brain tissue. As a comparator, brain samples from Huntington's disease (HD) patients were also analysed to identify ANCL-specific changes and perturbations that might be more generally linked to neurodegeneration. HD is caused by a dominant mutation in the *huntingtin* (HTT, IT15) gene. The mutation leads to the extension of a polyglutamine stretch and a toxin gain-of-function of the mutant Htt protein, together with possible loss-of-function effects (Macdonald et al. 1993; Aronin et al. 1995). The main clinical feature of HD is "chorea", an abnormal "dance-like" movement of the limbs, although the movement abnormalities in HD include both voluntary and involuntary motor functions (De Souza and Leavitt 2014; A. Sharp and Ross 1996). Other clinical features include slowing of intellectual processes, eventually leading to dementia, and changes in the personality of the patients (Sharp and Ross 1996). HD is also of interest from a palmitoylation perspective as Htt is palmitoylated by the Huntingtin-Interacting Protein 14 (HIP14, aka zDHHC17) and HIP14L (HIP14-like, aka zDHHC13) (Young et al. 2012; Yanai et al. 2006; Sanders and Hayden 2015). Mutant Htt has a loss of palmitoylation, and preventing this modification increases toxicity of Htt and its formation on intracellular inclusions (Huang et al. 2004; Yanai et al. 2006). In addition, it

was reported that zDHHC17 is also positively regulated by the Htt protein and that this regulation is lost with mutant Htt (Huang et al. 2011). This observation raises the possibility that loss of zDHHC17 function could contribute to pathogenesis in HD.

4.2 CSP α expression and aggregation in normal and disease human brain

Brain lysates were prepared from three different *DNAJC5* mutation carriers, four control individuals and five HD patients. The prefrontal cortex lysates were prepared as described in Section 2.3 in *Materials and Methods* and protein levels of the lysates were determined by BCA assays. Equal amounts of protein were resolved by SDS-PAGE and subjected to immunoblotting analysis with a range of antibodies. Expression levels and migration profiles of several proteins were examined but only those antibodies that gave reliable signals are presented in this chapter.

It should be noted that, while equal amounts of proteins were examined, no loading control was used. This analysis was performed on brain tissue from individual patients (rather than a cell line or an in-bred mouse line), and therefore it is not clear what the most appropriate loading controls should be since protein expression is predicted to vary somewhat from person to person. However, the results obtained display changes in protein expression without a consistent trend between individual samples, providing confidence in the data presented.

As a first step to studying molecular changes occurring in ANCL, the expression levels and aggregation of CSP α in ANCL brains were examined and compared to brain tissue from patients with HD. Figure 4.1 shows that the expression levels of palmitoylated CSP α are similar between control brains and HD patients. However, it can be seen that there is more

accumulation of CSP α protein at a high molecular weight in samples from ANCL patients, confirming previous observations made by Greaves et al. (2012) (aggregates can be more clearly seen in Figure 4.2).

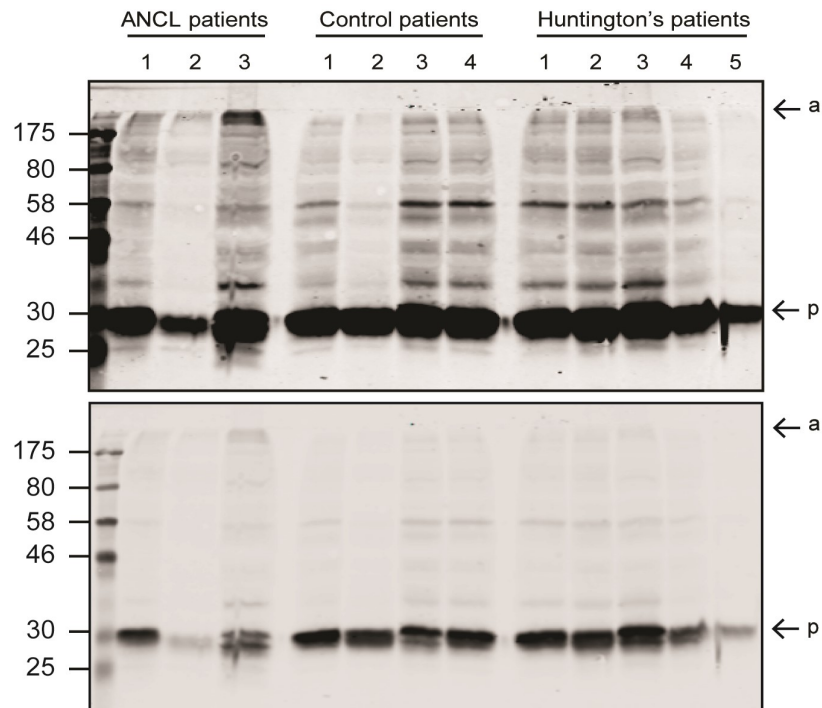


Figure 4.1. CSP α expression in ANCL and HD brain. Prefrontal cortex lysates from control patients (four different individuals), *DNAJC5* mutation carriers (three different individuals) and Huntington's disease patients (five different individuals) were resolved by SDS-PAGE and transferred onto nitrocellulose membranes for immunoblotting analysis using anti-CSP α antibody. Position of molecular mass standard is shown on the left. Palmitoylated monomeric CSP α is indicated by *p* and CSP α aggregates are designated by *a*. The *top panel* is presented at an exposure to allow better visualisation of high molecular weight bands, whereas the *bottom panel* is a different exposure of the same immunoblot to facilitate comparison of protein levels of monomeric CSP α .

To further investigate the aggregates present in ANCL brain samples and their dependence on palmitoylation, the lysates were treated with hydroxylamine (HA) to mediate CSP α depalmitoylation. Thus, brain lysates were treated with 0.5 M HA or 0.5 M Tris as a control (procedure described in Section 2.6.2). The results shown in Figure 4.2 confirm that the

aggregates are only present in the brain lysates from ANCL patients and not the control samples. Additionally, the immunoreactivity of the aggregates was reduced upon HA treatment, indicating that the aggregates are likely to be stabilised by palmitoylation. Altogether, these results confirm the aggregation and palmitoylation profile of ANCL CSP α observed in PC12 cells and HEK293T cells in Chapter 3 and in the work by Greaves et al. (2012).

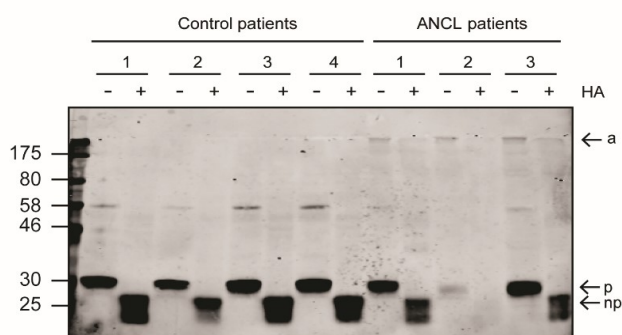


Figure 4.2. Effects of hydroxylamine treatment of brain lysates from control and ANCL patients on CSP α migration profile. Prefrontal cortex lysates from control (four different individuals) and *DNAJC5* mutation carriers (three separate individuals) were treated with hydroxylamine (+) or Tris (-) and resolved by SDS-PAGE. The proteins were then transferred onto nitrocellulose membranes for immunoblotting analysis using anti-CSP α . Position of molecular mass standard is shown on the left. Palmitoylated CSP α monomer is indicated with by *p*, non-palmitoylated CSP α monomer is shown by *np* and aggregated CSP α is designated with *a*.

4.3 Expression of SNARE proteins in ANCL and HD human brains

Unlike many of the other mutant proteins known to cause NCL, CSP α does not have a known lysosomal function nor has it been linked to lysosomal trafficking/sorting. Instead, CSP α is a synaptic vesicle protein thought to function as a chaperone in exocytosis (Chamberlain and Burgoyne 2000; Fernández-Chacón et al. 2004; Burgoyne and Morgan

2015). CSP α forms a chaperone complex with the 70-kDa heat shock cognate protein (Hsc70) and the small glutamine-rich tetratricopeptide repeat (TPR)-containing protein (SGT) on synaptic vesicles (Tobaben et al. 2001), and exerts its co-chaperone activity on SNAP25 by stabilising the protein and enhancing its ability to form SNARE-complexes (Sharma et al. 2011). SNARE complexes formed by SNAP25 and its SNARE partner at the plasma membrane syntaxin 1 together with the vesicle protein VAMP2 (Vesicle-Associated Protein 2) drive the exocytosis of synaptic vesicles in neurons (Poirier et al. 1998; Sutton et al. 1998). Indeed, reduced levels of SNAP25 and SNARE complex are thought to underlie the neurodegeneration seen in CSP α knockout mice (Sharma et al. 2011).

Therefore, in order to establish possible mechanisms by which mutant CSP α leads to neurodegeneration in ANCL patients, the expression levels of the individual SNARE proteins SNAP25, syntaxin 1 and VAMP2 were assessed by immunoblotting (Figure 4.3A).

Densitometry analyses of immunoreactive signals from the three different SNARE proteins showed that there were no significant changes in their expression in ANCL or HD brain samples compared with controls.

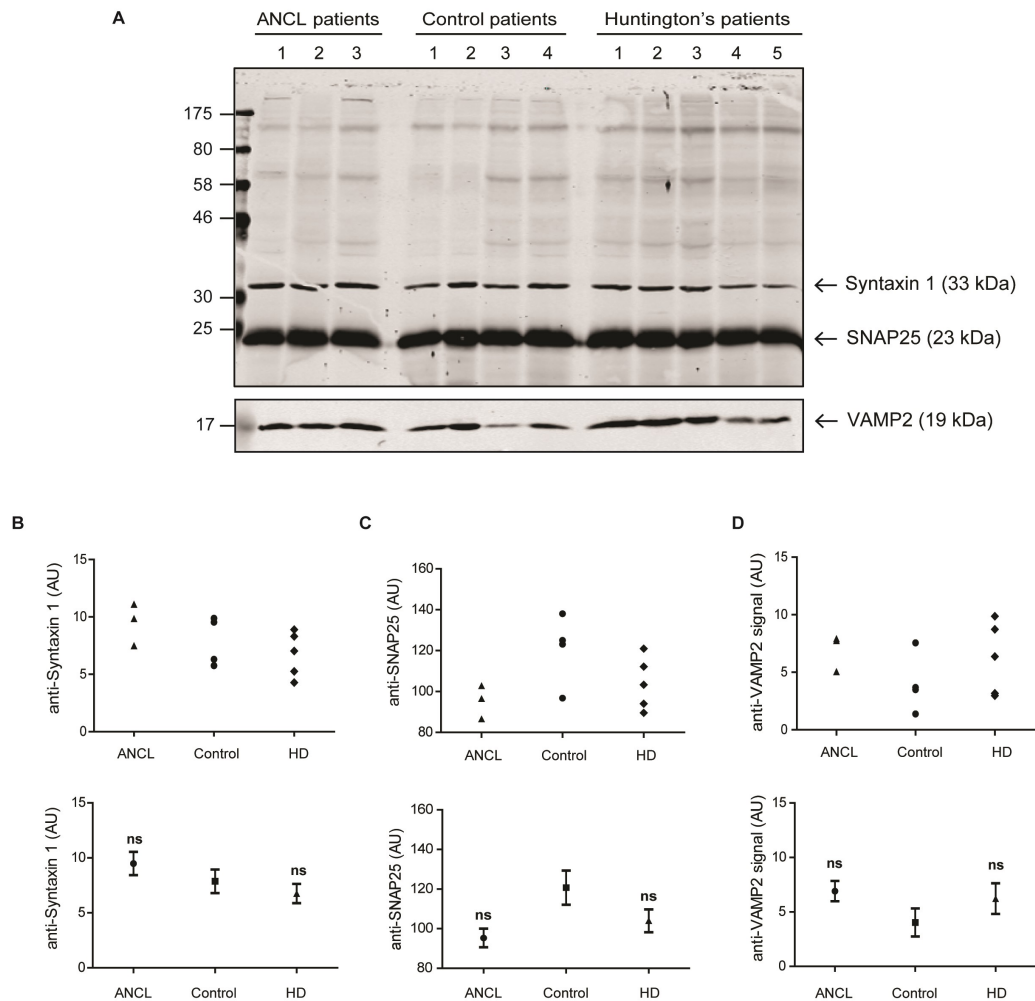


Figure 4.3. Expression levels of SNARE proteins in ANCL and HD brain. Prefrontal cortex lysates from control (four different individuals), *DNAJC5* mutation carriers (three separate individuals) and Huntington's disease patients (five distinct individuals) were incubated in SDS-sample buffer at 95°C for 5 minutes. The lysates were then resolved by SDS-PAGE and transferred onto nitrocellulose membranes for immunoblotting analysis using anti- α -Syntaxin 1, anti-SNAP25 and anti-VAMP2. **A)** Representative immunoblots with position of molecular size standards shown on the left hand side. Quantification of syntaxin 1 (**B**), SNAP25 (**C**) and VAMP2 (**D**) expression was performed by densitometry and presented as individual values (*top*) and averaged values (*bottom*) completed with statistical analyses (Student's T test, ns=non-significant).

Although there was no observed change in expression of the synaptic SNARE proteins, it is possible that the assembly into functional SNARE complexes might be disrupted. Since the syntaxin-SNAP25-VAMP complex is extremely stable, being resistant to SDS denaturation (Hayashi et al. 1994) and temperatures up to 90°C (Yang et al. 1999), the levels of SNARE complex were assessed by treating lysates at a lower temperature (37°C) before immunoblotting with antibodies against syntaxin 1 and SNAP25 (Figure 4.4).

Interestingly, when samples were treated at this lower temperature, the immunoreactive signal from monomeric SNAP25 was significantly decreased in ANCL brains in comparison with control brains (Figure 4.4A). Similarly, the SNAP25 signal in HD brain lysates was also significantly diminished compared to control. In contrast, there was no significant difference in the signal from monomeric syntaxin 1 (Figure 4.4B) or VAMP2 (Figure 4.4C) in these samples.

The SDS-resistant SNARE complex can only be detected using some antibodies, as certain epitopes are masked in this complex. It was found in this study that the assembled SNARE-complex could be detected using the anti-syntaxin 1 antibody, as observed by the presence of an immunoreactive just band above the 58 kDa marker (Figure 4.4D). In contrast, it could not be detected with the anti-SNAP25 and anti-VAMP2 antibodies. No significant difference was observed between the levels of assembled SNARE-complex in ANCL or HD brain lysates relative to controls, although there did appear to be a trend towards higher complex levels in HD brains.

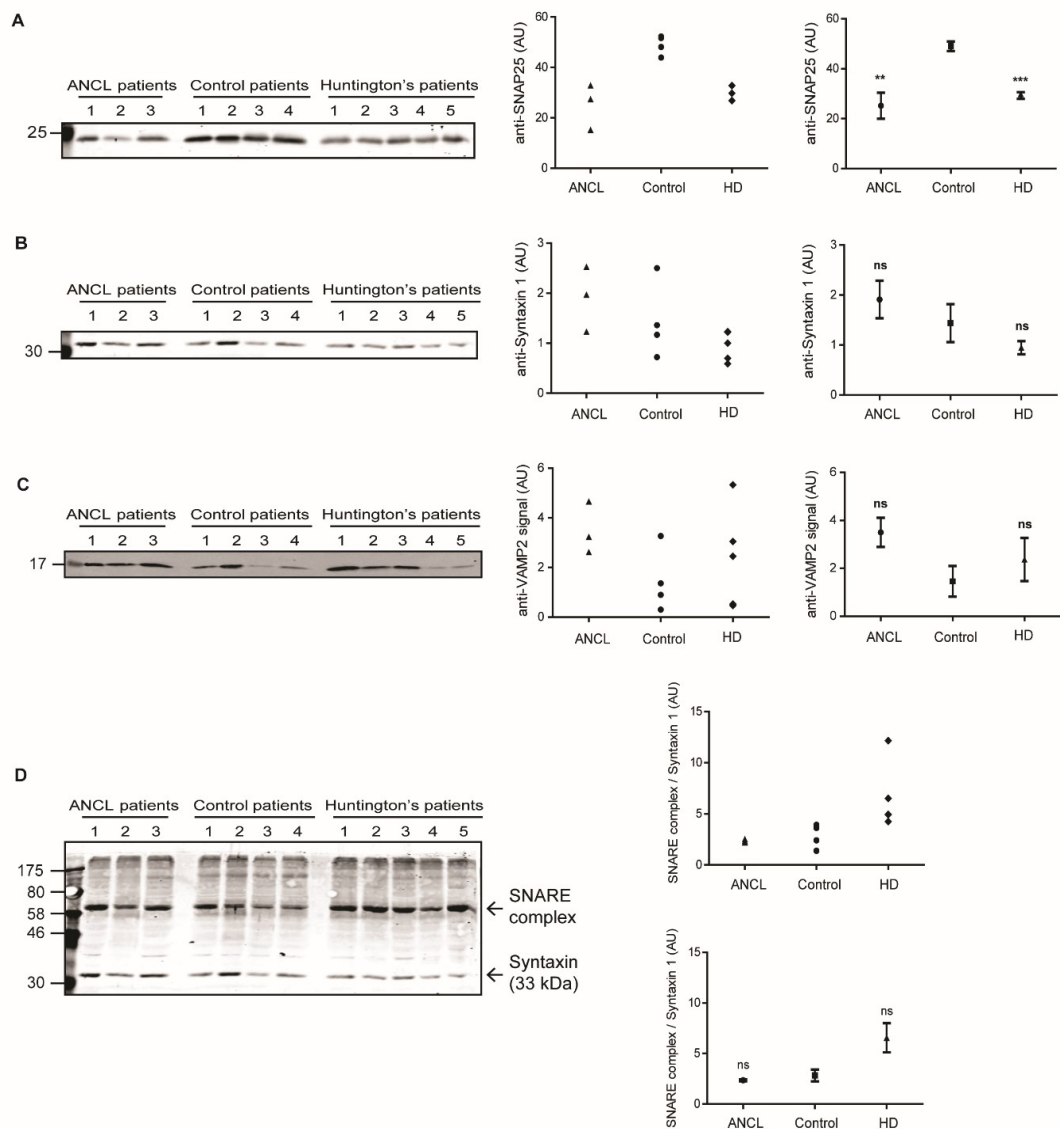


Figure 4.4. Detection of syntaxin 1, SNAP25, VAMP2 and assembled SNARE-complex in non-boiled ANCL and HD brain lysates. Prefrontal cortex lysates from control (four different individuals), *DNAJC5* mutation carriers (three separate individuals) and Huntington's disease patients (five distinct individuals) were incubated in SDS-sample buffer at 37°C for 5 minutes. The lysates were resolved by SDS-PAGE and transferred onto nitrocellulose membranes for immunoblotting analysis using anti-syntaxin 1, anti-SNAP25 and anti-VAMP2. Positions of molecular size standards are shown on the left hand side. **A)** Representative SNAP25 expression in human brains and densitometric quantification expressed as individual values (*left graph*) and averaged values (*right graph*) completed with statistical analyses (Student's T test), denoting statistical significance in relation to control patients (** $p > 0.01$, *** $p > 0.001$). **B)** Representative syntaxin 1 expression in human brains. Quantification was performed by densitometry and expressed as individual values (*left graph*) or averaged values together with Student's T test (*right graph*) (ns=non-significant). **C)** Representative

VAMP2 expression in human brains. Quantification was performed by densitometry and is expressed as individual values (*left graph*) and averaged values together with Student's T test (*right graph*). D) Assembled SNARE-complex expression in human brains, detected with anti-syntaxin 1 antibody. Quantification was performed by densitometry and expressed as individual values (*top graph*) or averaged values (*bottom graph*) completed with Student's T test (ns=non-significant).

4.4 Expression levels of other synaptic and palmitoylated proteins in ANCL and HD brains

Having examined the expression of CSP α and its major target (SNAP25 and the SNARE complex), the expression profile of other synaptic proteins in ANCL and HD brains was analysed. To understand the molecular changes occurring in ANCL brains in more detail and whether there are any marked similarities or differences with HD, the expression of a number of other proteins was studied. Specifically, proteins with known synaptic functions (e.g. PSD95, synaptophysin, AMPA and NMDA receptors, and vGLUTs) or other palmitoylated proteins (e.g. flotillins) were examined. In addition, α -synuclein expression was also examined as previous work showed that over-expression of this protein could rescue neurodegeneration in CSP α KO mice (Chandra et al. 2005). However, due to difficulties achieving successful antibody recognition, only the immunoblots corresponding to α -synuclein, PSD95, synaptophysin and flotillins are shown in this chapter.

Alpha-synuclein (α -synuclein) is an abundant presynaptic protein that associates with synaptic vesicles and has previously been linked to neurodegeneration in CSP α null mice. Specifically, over-expression of α -synuclein rescues neurodegeneration in CSP α null mice, whereas simultaneous knock-out of both proteins leads to a more severe phenotype (Sharma, Burré, Bronk, et al. 2012; Chandra et al. 2005; Fernández-Chacón et al. 2004). Mutations in α -synuclein are also associated with Parkinson's disease (PD), for example,

Ala30Pro (Krüger et al. 1998), Ala53Thre (Polymeropoulos et al. 1997) or triplication of the α -synuclein gene (Singleton et al. 2003). Likewise, α -synuclein is present in Lewy Bodies, characteristic of PD (Spillantini et al. 1997; Baba et al. 1998), as well as in inclusions in other neurodegenerative diseases such as Alzheimer's disease (AD) (Norris et al. 2004). Therefore, due to the association of α -synuclein with neurodegeneration, and its clear links with neurodegeneration in CSP α null mice, the expression of this protein was assessed in ANCL and HD post-mortem brains (Figure 4.5).

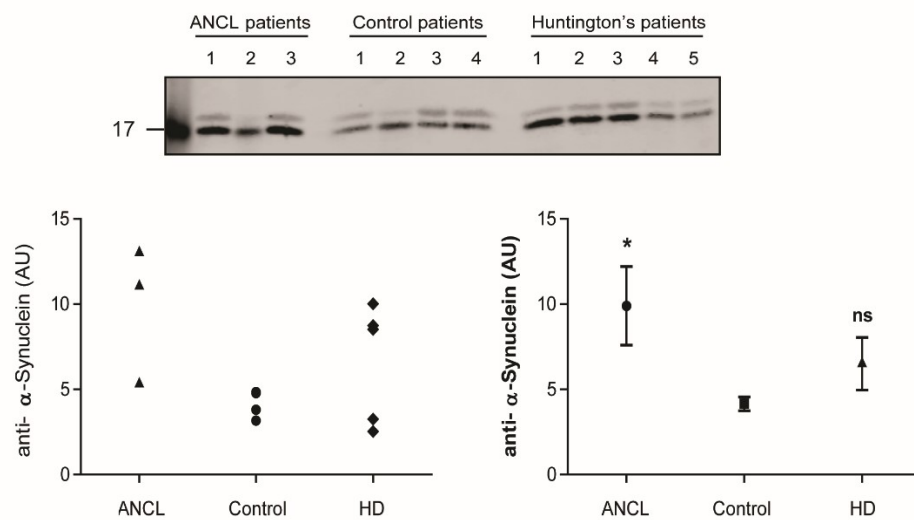


Figure 4.5. Expression of α -synuclein in ANCL and HD brain. Prefrontal cortex lysates from control (four different individuals), *DNAJC5* mutation carriers (three separate individuals) and Huntington's disease patients (five distinct individuals) were resolved by SDS-PAGE and transferred onto nitrocellulose membranes for immunoblotting analysis using anti- α -synuclein (~14 kDa). Position of molecular weight marker is shown on the left hand side. Quantification was performed by densitometry and is expressed as individual values (*left graph*) and averaged values (*right graph*) completed with statistical analyses (Student's T test), denoting statistical significance in relation to control patients (ns=non-significant, * $p>0.05$).

As seen in Figure 4.5, the levels of α -synuclein were significantly higher in ANCL brains in comparison to the controls, whereas there was no significant change in HD brains (but an upwards trend was present).

PSD95 (postsynaptic density protein of 95 kDa), a membrane-associated guanylate kinase (MAGUK), is the most abundant scaffolding protein in the post-synaptic density (PSD; (Cheng et al. 2006)). PSD95 plays a role in function and development of excitatory synapses, and the synaptic targeting and scaffolding activity of PSD95 depends on the palmitoylation of two cysteines in its N-terminal domain (Topinka and Brecht 1998; El-Husseini et al. 2002). The expression of PSD95 in post-mortem brains from ANCL and HD patients was compared to control brains. Figure 4.6 shows that there was no significant difference in PSD95 expression in ANCL or HD patients compared with control individuals. Nevertheless, PSD95 expression was clearly substantially increased in two of the three ANCL patients and mean PSD95 expression was almost two-fold higher in this group compared with controls and HD patients.

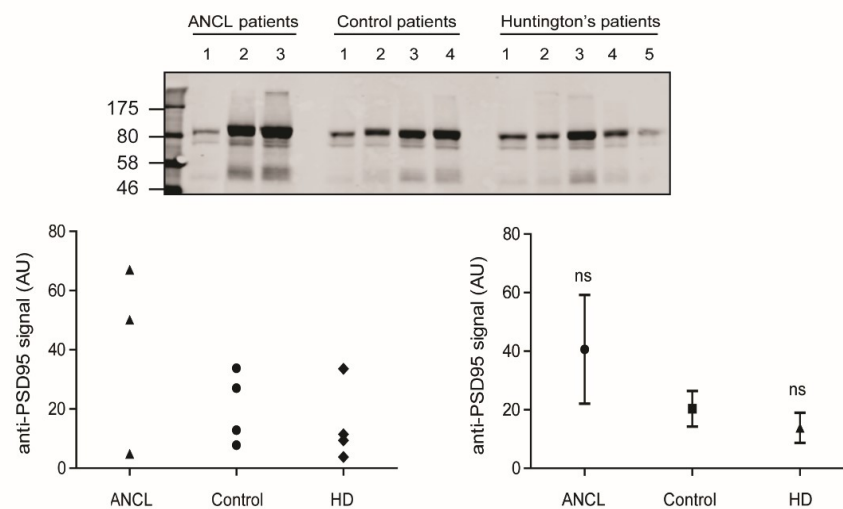


Figure 4.6. Expression of PSD95 in ANCL and HD brain. Prefrontal cortex lysates from control (four different individuals), *DNAJC5* mutation carriers (three separate individuals) and Huntington's disease patients (five distinct individuals) were resolved by SDS-PAGE and transferred onto nitrocellulose membranes for immunoblotting analysis using anti-PSD95. Position of molecular mass

standards is shown on the left hand side. Quantification was performed by densitometry and is expressed as individual values (*left graph*) and averaged values (*right graph*) completed with statistical analyses (Student's T test), denoting statistical significance in relation to control patients (ns=non-significant).

Synaptophysin (p38/SYP) is an integral membrane glycoprotein (Wiedenmann and Franke 1985), widely used as a marker to study the distribution and quantification of synapses in the brain (Navone et al. 1986). While the exact function of synaptophysin is unknown, it was proposed to be involved in the regulation of SNARE proteins assembly, based on its interaction with VAMP2 (Washbourne et al. 1995; Calakos and Scheller 1994; Edelman et al. 1995) and other synaptic termini proteins (Valtorta et al. 2004). Synaptophysin was also shown to be required for VAMP2 retrieval during endocytosis (Gordon et al. 2011). Synaptophysin is highly expressed and a major component of synaptic vesicles (Takamori et al. 2006). Analysis of synaptophysin levels in brain lysates revealed a significant increase of synaptophysin expression in ANCL brains compared to control and HD brains (Figure 4.7).

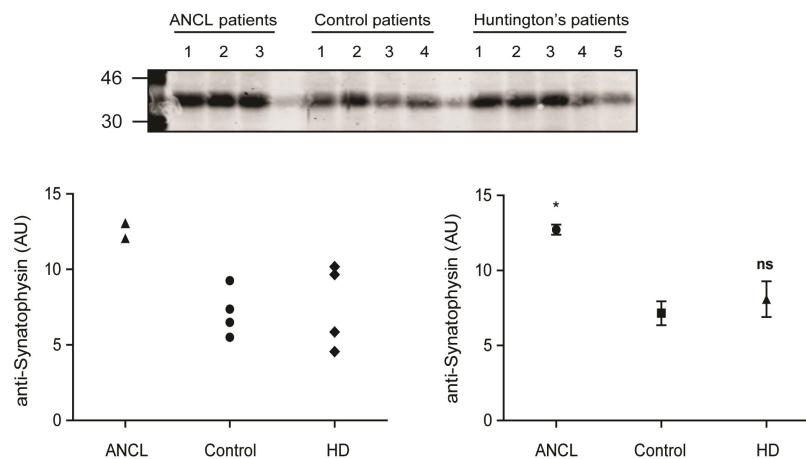


Figure 4.7. Synaptophysin expression in ANCL and HD brain. Prefrontal cortex brain lysates from control individuals, *DNAJC5* mutation carriers and Huntington's disease patients were resolved by SDS-PAGE and transferred onto nitrocellulose membranes for immunoblotting analysis using anti-synaptophysin antibody. Position of molecular mass standard is shown on the left. Quantification

was performed by densitometry and is expressed as individual values (*left graph*) and averaged values (*right graph*) completed with statistical analyses (Student's T test), denoting statistical significance in relation to control patients (ns=non-significant, ** $p > 0.01$).

Subsequently, the expression of other membrane proteins was examined. Flotillins were of particular interest as they are ubiquitously-expressed palmitoylated proteins. Flotillins associate with cholesterol-rich membranes and may play a role in micro-domain formation and endocytosis (Glebov et al. 2006; Hansen and Nichols 2009; Otto and Nichols 2011). Flotillins have also been implicated in the modulation of cadherin-mediated cell-cell adhesion, playing an important role in synapse organisation and function (Takeichi 2007; Togashi et al. 2002) as well as regulating dendritic spine morphogenesis and axon regeneration (Blackmore and Letourneau 2006). In the context of neurodegenerative disease, flotillins have been seen to be implicated in regulation of amyloid precursor protein (APP), which leads to formation of beta amyloid ($A\beta$), highly accumulated in AD (Schneider et al. 2008). Moreover, the expression of flotillin (and other palmitoylated proteins) in ANCL and HD brains is of interest as it is a major palmitoylated protein and palmitoylation has been suggested to be disrupted in both conditions.

Figure 4.8 shows the immunoblot and quantification of the expression levels of flotillin-1 (A) and flotillin-2 (B) in ANCL, HD and control brain lysates. Interestingly, both flotillin-1 and flotillin-2 had a significant increase in ANCL lysates relative to controls and there was also a significant increase in flotillin-2 expression in HD lysates and an upwards trend of flotillin-1 in HD.

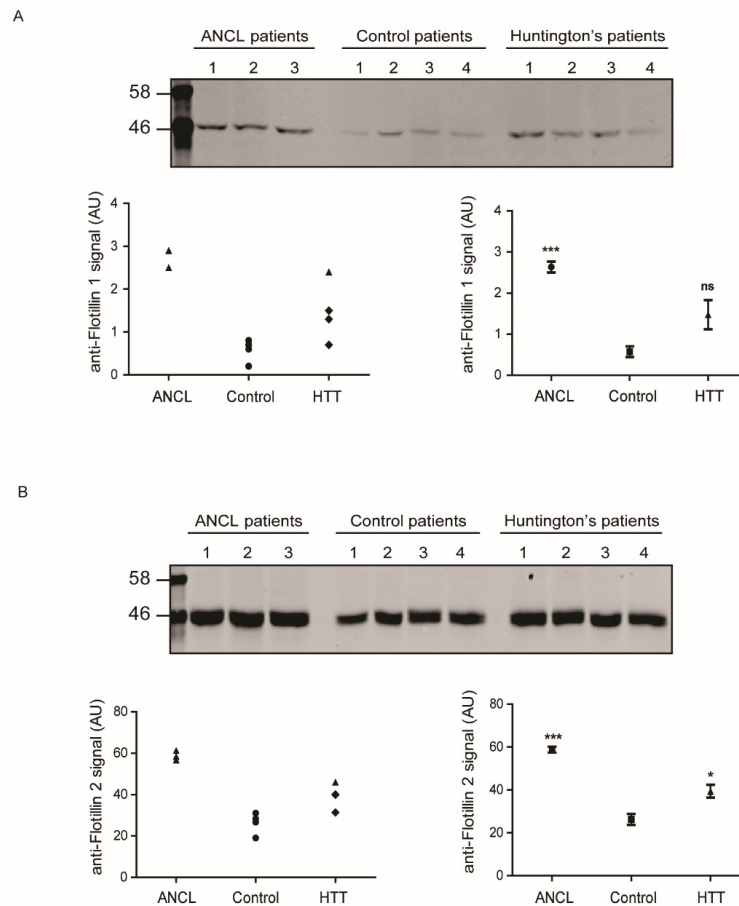


Figure 4.8. Expression of flotillin-1 and flotillin-2 in ANCL and HD brain. Prefrontal cortex lysates from control, *DNAJC5* mutation carriers, and HD patients were resolved by SDS-PAGE and transferred onto nitrocellulose membranes for immunoblotting analysis using anti-flotillin-1 (A) and anti-flotillin-2 (B) antibodies. Position of molecular mass standards is shown on the left hand side. Quantification was performed by densitometry and is expressed as individual values (*left graphs*) and averaged values (*right graph*) completed with statistical analyses (Student's T test), denoting statistical significance in relation to control patients (ns=non-significant, * $p < 0.05$, *** $p < 0.005$).

4.5 ANCL patient brains show a dramatic increase in PPT1 expression

PPT1 (palmitoyl-protein thioesterase 1) is a lysosomal enzyme that catalyses the removal of thioester-linked fatty acyl groups from cysteine residues during lysosomal degradation. Mutations in the *PPT1* gene cause the infantile form on NCL (INCL/CLN1) (Hellsten et al. 1993; Vesa et al. 1995). The post-mortem prefrontal cortex sections from ANCL and HD patients and control individuals were analysed by immunoblotting using an anti-PPT1 antibody. The resulting immunoblot and corresponding quantification are shown in Figure 4.9. Strikingly, the expression of PPT1 in ANCL brains is substantially higher than in control and HD brains.

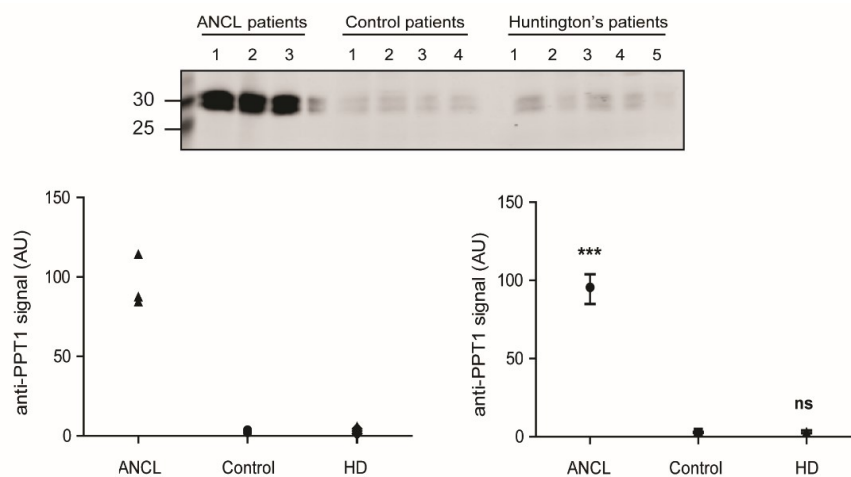


Figure 4.9. Aberrant increased expression profile of PPT1 in human brains carrying the *DNAJC5* mutation. Prefrontal cortex lysates from control (four different individuals), *DNAJC5* mutation carriers (three separate individuals) and Huntington's disease patients (five distinct individuals) were resolved by SDS-PAGE and transferred onto nitrocellulose membranes for immunoblotting analysis using anti-PPT1. Position of molecular weight marker is shown on the left hand side. Quantification was performed by densitometry and is expressed as individual values (*left graph*) and averaged values (*right graph*) completed with statistical analyses (Student's T test), denoting statistical significance in relation to control patients (** $p > 0.001$).

These results confirm the aberrant increased PPT1 expression in ANCL brains described by Henderson et al. (2015), who examined post-mortem tissue from one L115R and one Δ L116 patient. The increase in PPT1 expression reported by Henderson et al. was quantified to be of 21-fold in comparison to control through LC-MS/MS based label free quantification (LFQ).

4.6 Effects of ANCL mutant CSP α on PPT1 expression in cell culture

Having observed a major increase in PPT1 expression in ANCL brains, and considering that mutations in CSP α and PPT1 are the cause of different forms of NCL, it was investigated if the effects of ANCL mutant proteins on PPT1 expression could also be observed in cell lines transfected with these proteins.

To test if ANCL mutants can cause the accumulation of PPT1 in commonly used cell lines, PC12 cells were co-transfected with HA-PPT1 and EGFP (empty vector) or EGFP-tagged wild-type/ Δ L116/L115R CSP α .

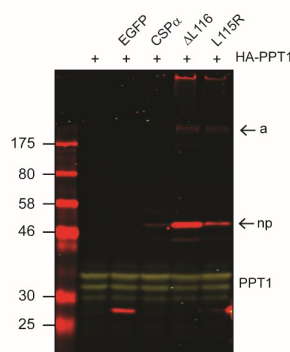


Figure 4.10. Co-expression of HA-PPT1 and EGFP-tagged wild-type/ Δ L116/L115R CSP α . PC12 cells were co-transfected with HA-PPT1 and either EGFP-tagged wild-type/ Δ L116/L115R CSP α or EGFP empty vector. Forty-eight hours after transfection, cell lysates were resolved by SDS-PAGE and transferred onto nitrocellulose membranes and probed with anti-HA and anti-GFP antibodies. Position of the molecular weight markers is shown on the left hand side. *a* indicates aggregates, *np* designates non-palmitoylated monomeric CSP α .

Figure 4.10 shows that levels of HA-PPT1 (in green) were unaffected by the presence of wild-type or ANCL mutant CSP α . While wild-type CSP α is not well expressed, the non-palmitoylated band and the aggregates can be observed for Δ L116 and L115R CSP α . These results indicate that expression levels of PPT1 are not noticeably affected by the ANCL CSP α mutants in a 48-hour co-transfection assay, and that PPT1 expression presumably increases over many years in ANCL brain.

In a converse experiment, it was investigated if PPT1 co-expression affected wild-type and mutant CSP α proteins. This experiment was performed in HEK293T cells to maximise protein expression levels. Cells were transfected with EGFP-CSP α constructs and HA-zDHHC3 with or without HA-PPT1 for 48 hours (HA-zDHHC3 is included to mediate palmitoylation of the CSP α proteins).

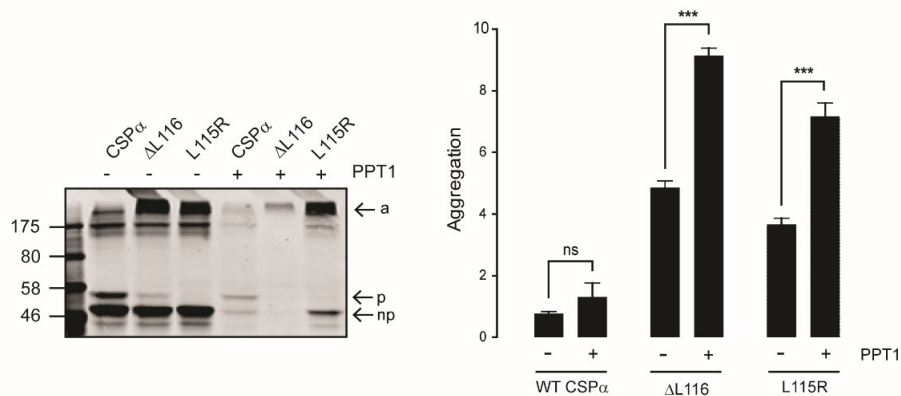


Figure 4.11. Effect of PPT1 on relative aggregation of ANCL mutants. HEK293T cells were co-transfected with EGFP-tagged wild-type/ Δ L116/L115R CSP α with HA-zDHHC3 in presence and absence of HA-PPT1. After 48 hours, cells were lysed and resolved by SDS-PAGE. Proteins were transferred onto nitrocellulose membranes and probed with anti-GFP antibody. Position of the molecular weight markers is shown on the left hand side. *a* indicates aggregates, *p* specifies position of palmitoylated monomeric CSP α , and *np* designates the non-palmitoylated monomers. Quantification was performed by densitometry using Image Studio Software (n=5). The graph shows the values of aggregated protein in relation to total protein in the presence and absence of over-expressed PPT1. Statistical analysis were completed with Student's T test, asterisks denote a significant difference (ns=non-significant, *** $p < 0.001$).

Figure 4.11 shows that although PPT1 co-expression led to a decrease in levels of all CSP α proteins, there was also a significant increase in aggregation of ANCL CSP α in the presence of PPT1 relative to the total amount of protein. This result might indicate a possible link between increased PPT1 expression in ANCL brain and mutant CSP α aggregation.

4.7 Discussion

Fourteen genes have been identified as the cause of the different forms of NCL. The functions of the majority of these gene products encompass lysosomal enzymatic activities (CLN2/TPP1, CLN10/CTSD), vesicle trafficking (CLN3) and regulation of lipid modifications (CLN1/PPT1) (Palmer et al. 2013; Cárcel-Trullols et al. 2015), which correlate with the classification of NCL as lysosomal storage disorders. Moreover, the neurological symptoms present in NCL match with the fact that several NCL proteins are localised at or near the neuronal synapse (CLN1/PPT1, CLN3, DNAJC5/CSP α) (Cotman et al. 2013). However, little is known about the potential interactions or shared pathways of the mutated NCL genes.

The identification of potential common pathways between the different forms of NCL and also other forms of neurodegeneration can provide valuable information into the disease mechanisms and shed light into possible therapeutic approaches.

The study of post-mortem brains has become an important mechanism to help understand the neurobiology of neurodegenerative and psychiatric diseases, especially in light of the new opportunities to apply genomic and proteomic approaches. The examination of post-mortem brains can provide information on potential diagnosis, combination of diseases, and biochemical data to define a disease.

Therefore, in this chapter, post-mortem brains from ANCL patients were studied to identify expression changes of other neuronal and palmitoylated proteins. Furthermore, these ANCL samples were compared to brain tissue from HD patients to identify potential common pathways linked to neurodegeneration and to provide a better understanding of the molecular mechanisms by which CSP α L115R and Δ L116 mutations might cause ANCL.

Aggregation of L115R-CSP α and Δ L116-CSP α was confirmed in ANCL brains (Figure 4.1), and shown to be hydroxylamine-sensitive (Figure 4.2), as previously reported by Greaves et al. (2012). Moreover, aggregation of CSP α was confirmed to be a characteristic feature of ANCL brains and was not present in HD brains.

CSP α is an abundant vesicle associated protein that functions in regulated exocytosis in neuronal and neuroendocrine cells (Chamberlain and Burgoyne 2000). Through its DnaJ domain it is thought to regulate synaptic vesicle exocytosis by functioning as a chaperone within a complex formed with Hsc70 and SGT (Chamberlain and Burgoyne 1997; Chamberlain et al. 1997; Tobaben et al. 2001). Analysis of CSP α knock-out mice, a model of neurodegeneration, helped to identify SNAP25 as a major substrate of CSP α and further showed that SNARE complex levels were reduced in the absence of CSP α (Sharma, Burré, and Südhof 2011; Zhang et al. 2012; Sharma et al. 2012). Due to the direct link between SNAP25, SNARE complex assembly and CSP α , the expression profile of SNAP25 and its SNARE partners syntaxin 1 and VAMP2 were examined in ANCL brains. The brain lysates were incubated at either 95°C to disrupt the SNARE complex or 37°C to maintain the complex. The amount of each SNARE protein detected in control, ANCL and HD brains at 95°C was not significantly different. However, at 37°C a significant reduction in SNAP25 levels was detected in ANCL and HD brain lysates, whereas the amount of assembled SNARE complex was not different. It is not clear why there was a difference in detection of

monomeric SNAP25 expression between samples treated at 95°C and 37°C when there was no change in levels of SDS-resistant SNARE complexes containing syntaxin 1 (most of which will also contain SNAP25). One possibility is that it could reflect an increased association of SNAP25 with SDS-resistant SNARE complexes that do not contain syntaxin 1a (the isoform recognised by the specific antibody used in this study), including complexes with syntaxin 1b or endosomal SNARE proteins (Aikawa et al. 2006a; Aikawa et al. 2006b). This issue could be investigated further by undertaking SNAP25 immunoprecipitation experiments and testing for SNARE protein co-precipitation. Whatever the effects on SNAP25 expression, it was clear that these were not sufficient to perturb synaptic SNARE complex assembly.

Following the study of the SNARE proteins, other synaptic proteins were examined. As previously mentioned in this chapter, deletion of CSP α in mice leads to neurodegeneration. However, over-expression of transgenic α -synuclein rescues this neurodegeneration in CSP α -deficient mice (Chandra et al. 2005) and triple knock-out mice lacking synucleins (α -, β - and γ -synuclein) exhibit decreased SNARE-complex assembly (Burré et al. 2010). Indeed, α -synuclein interacts directly with VAMP2 promoting SNARE-complex assembly (Burré et al. 2010). Therefore, it was reasonable to test the expression of α -synuclein in ANCL and HD post-mortem brains. Remarkably, the expression of α -synuclein was shown to be increased in ANCL brains in comparison to control and HD individuals. This observation is intriguing as α -synuclein is known to compensate for loss of CSP α function in knockout mice (Chandra et al. 2005). Together, these results might suggest that (a) the CSP α disease-causing mutations have a loss-of-function effect, which is rescued by over-expression of α -synuclein, therefore meaning that the assembly of SNAREs is not affected; or (b) the increased expression of α -synuclein represents some intracellular accumulation of the protein as this protein is found

in inclusions in PD and AD (Spillantini et al. 1997; Baba et al. 1998; Norris et al. 2004), although these possibilities warrant further investigation.

The expression of the post-synaptic protein PSD95 was subsequently assessed. This protein was of interest as it is a major scaffold at glutamatergic synapses, important for synaptic assembly and maintenance. Although an increase of PSD-95 expression was detected in ANCL post-mortem brains, statistical analysis revealed that this increase was not significant. However, corresponding immunoblots clearly showed a marked increase in expression (relative to controls) in two of the three ANCL brain samples analysed (Figure 4.6). Thus, it would be interesting to examine the expression of PSD95 in a higher number of brains in order to establish a reasonable conclusion regarding its expression levels.

In addition, the expression of synaptophysin was also assessed. This protein is a major component of synaptic vesicles (Wiedenmann and Franke 1985) and is frequently used as a synaptic marker. The expression of synaptophysin was significantly higher in ANCL brains compared to HD and control brains. The reason for this is not clear but again it could be a compensatory mechanism to overcome a CSP α loss-of-function effect or it could reflect a change in the number of synaptic vesicles, vesicle turnover or targeting of vesicle proteins. It will be interesting in future work to examine in more detail the expression of other synaptic vesicle proteins to determine if levels of vesicle proteins are widely affected. While reduced levels of synaptophysin and other synaptic proteins has been reported in AD and PD brains, as well as in brain tissue from dementia patients (Sharma, Burré and Südhof 2012), it is possible that the increase observed in ANCL brains is due to a compensatory effect; for example, it could reflect a reduced capability for SNARE protein retrieval following exocytosis as synaptophysin is reported to regulate reinternalization of VAMP2 after exocytosis (Gordon, Leube, and Cousin 2011).

A particularly interesting finding of this chapter was the increased expression of the lipid raft proteins flotillin-1 and flotillin-2 in ANCL brains. Similar to CSP α (and SNAP25, PSD95), these proteins are also palmitoylated. Expression of flotillin-1 and -2 was significantly increased in ANCL brains and flotillin-2 was also significantly increased in HD brains (whereas the increase in flotillin-1 expression in HD did not reach statistical significance). Interestingly, these observations are in accordance with previous studies showing over-expression of flotillins in AD and PD (Bodin et al. 2014). Flotillin-1 has previously been reported to be upregulated in PD brains (Jacobowitz and Kallarakal 2004). Moreover, flotillins also associate directly (flotillin-1) and indirectly (flotillin-2) with a dileucine motif in BACE1 (β -site amyloid precursor protein-cleaving enzyme 1), a protease that participates in the cleavage of the amyloid precursor protein in AD (John et al. 2014). Thus, the identification of increased expression of flotillins in ANCL and HD further expands the links between these proteins and neurodegeneration.

It will be of interest in future work to examine if the upregulation of proteins such as flotillins, α -synuclein and synaptophysin is a compensatory mechanism to overcome the loss of CSP α function and/or the toxic effects of mutant aggregates. This could be studied by over-expressing these proteins in CSP α knockout mice or examining their effects on mutant mice expressing ANCL CSP α . Conversely, rather than being a compensatory effect, these observed protein changes could also reflect pathological changes contributing to disease progression. While comparison of ANCL and HD post-mortem brains did not show a consistent link between the two neurodegenerative disorders, some perturbed protein expression profiles are shared between ANCL patients (and AD or PD patients), such as α -synuclein and flotillin upregulation, and these might therefore be general cell response mechanisms to neurodegeneration or pathogenic changes contributing to these diseases.

This study has been performed only in prefrontal cortex sections of post-mortem brains. Thus, it would be interesting to study other regions of the brain in order to understand whether the changes observed are universal or if they are specific to brain regions (such as the prefrontal cortex) that are significantly affected in ANCL.

Finally, perhaps the most remarkable aberrant expression profile found in ANCL was the one of PPT1. As recently seen by Henderson et al. (2015), PPT1 was massively upregulated in ANCL post-mortem brains. Interestingly, mutations in PPT1 cause an infantile form of NCL (Hellsten et al. 1993; Vesa et al. 1995). Thus, it is possible that a common mechanism exists between the two forms of NCL (infantile and adult) but that the diseases progress at different rates.

In the same study, Henderson et al. (2015) found that CSP α is a substrate of PPT1. However, even though the expression of PPT1 was tremendously upregulated, the relative activity of PPT1 was not increased. The observation that PPT1 expression is affected by CSP α mutations is consistent with the findings of Greaves et al. (2012) who proposed that ANCL is associated with palmitoylated CSP α aggregates which may be resistant to PPT1. Thus, perhaps cells respond to an inability to degrade palmitoylated CSP α aggregates/peptides by expressing higher levels of an enzyme required for the degradation of palmitoylated proteins. In this case, infantile NCL would arise due to a loss of PPT1 function against all palmitoylated proteins, whereas ANCL would proceed more slowly linked to an inability of PPT1 to degrade a specific palmitoylated protein (mutant CSP α). To investigate the links between CSP α and PPT1 further, co-expression experiments were performed. Although expression of wild-type or mutant CSP α did not affect expression levels of co-expressed PPT1, these experiments were performed over a short time period and in future work it would be interesting to test the effects of stable over-expression of

CSP α on PPT1 expression. Interestingly, an increase in relative aggregation of ANCL mutants was detected when PPT1 was over-expressed. This might reflect a disruption of lysosome function by PPT1 over-expression, although the results are difficult to interpret as PPT1 co-expression also led to a loss in total levels of wild-type and mutant CSP α . Even though it is evident that PPT1 is involved in the pathological mechanisms of ANCL, the links between ANCL CSP α and PPT1 are yet far from clear. Research on the implications of inhibition or over-expression of PPT1 on ANCL CSP α aggregation might shed light on potential therapeutic approaches.

Although the analysis of post-mortem brain tissue can give interesting insights into disease mechanisms, there are a number of caveats that should be noted: (a) as previously mentioned, while equal amounts of proteins were examined, it is useful to have appropriate loading controls for immunoblotting analyses. However, as this analysis was performed on brain tissue from individual patients (rather than a cell line or an in-bred mouse line), it is not clear what the most appropriate loading controls should be as protein expression is predicted to vary somewhat from person to person. Confidence in the results presented is increased by the fact that only a subset of proteins examined displayed expression changes and there was not a consistent trend in protein levels between individual samples; for example, synaptophysin expression was the same in all three ANCL samples (Figure 4.7), whereas PSD-95 expression was substantially higher in ANCL patients 2 and 3 than patient 1 (Figure 4.6), and α -synuclein expression was lower in ANCL patient 2 than patients 1 and 3 (Figure 4.5). These differences clearly show that observed changes are not caused by differences in protein loadings or the integrity of individual protein samples. Nevertheless, future work should aim to recapitulate the findings presented here through analysis of larger sample sizes; (b) although brain samples are taken from similar brain regions, there will inevitably be differences in the exact region of brain that samples

are collected from; (c) age and sex differences may impact results; and (d) medications taken by the patients could have a major effect on the expression of specific proteins. All samples analysed in this work were from male patients with similar age (in their 50s) and samples were obtained from Medical Research Council (MRC) brain banks (HD and controls) and from the Washington University School of Medicine in St. Louis ADRC for ANCL.

Chapter 5: The degradation mechanism of CSP α

5.1 Introduction

The central hypothesis of this thesis is that the aggregates formed by L115R and Δ L116 CSP α mutants are cytotoxic and contribute to the neurodegeneration process in ANCL. This hypothesis is supported by the fact that aggregation of misfolded proteins is a common feature in many neurodegenerative diseases (Bossy-Wetzel et al. 2004) and that these aggregates are generally thought to cause toxicity in neuronal cells (although larger aggregates such as inclusions in Huntington's disease may be protective) (Gestwicki and Garza 2012; Wang et al. 2014; Bossy-Wetzel et al. 2004). One mechanism whereby this toxicity might occur is *via* the protein aggregates "clogging up" the cellular degradation machinery.

Indeed, impairment of protein degradation systems has been seen in the most common neurodegenerative diseases, such as Alzheimer's disease (AD), Parkinson's disease (PD) and Huntington's disease (HD) (Gestwicki and Garza 2012; Pan et al. 2008; McKinnon and Tabrizi 2014; Majd et al. 2015). More specifically, Parkinson's disease-linked LRRK2 mutations are associated with protein degradation defects in lysosomes (Wang et al. 2014) and the ubiquitin-proteasome system, due to PD-associated mutations in the ubiquitin E3 ligase Parkin (Bossy-Wetzel et al. 2004). Moreover, reduction of proteasome peptidase activity has been reported in brains of AD patients and in a mouse model of Amyotrophic Lateral Sclerosis (ALS) (McKinnon and Tabrizi 2014). These findings, amongst others, have drawn attention to the modulation of the degradation processes of misfolded proteins as a potential therapeutic strategy in neurodegeneration (Scheper and Hoozemans 2015; Zhu et al. 2013; Lin and Qin 2013).

In the case of NCL, research has, thus far, focused mainly on the infantile and juvenile forms of the disease. NCL are generally classified as lysosomal storage disorders, since they are characterised by the accumulation of autofluorescent lipopigment in lysosomes (Kollmann et al. 2013). Indeed, it has been seen that the autophagy-lysosome pathway is involved in the neuropathology of a mouse model of infantile (Thelen et al. 2012) and juvenile (Cao et al. 2006) NCL.

However, under the broad NCL classification umbrella, each specific disorder is caused by mutations in distinct genes (Kollmann et al. 2013). Thus, the precise molecular pathways implicated in the development of the adult form of the disease may differ from those involved in the infantile and juvenile forms (Kollmann et al. 2013; Palmer et al. 2013). Although investigations have been made in the case of the infantile and juvenile forms of NCL (Thelen et al. 2012; Cao et al. 2006), there is a lack of knowledge on the potential link between ANCL and an impairment of the cellular degradation machinery.

At present, there is no information available on the pathways that mediate degradation of wild-type CSP α and how ANCL mutations and aggregation affect the degradation process. Therefore, the original aim of this chapter was to characterise the mechanisms involved in the degradation of wild-type CSP α and the ANCL mutants. However, most of the work presented in this chapter is focused on mechanisms governing turnover of wild-type CSP α .

5.2 Effect of proteasomal and lysosomal inhibitors on CSP α expression levels

The main routes by which proteins and organelles are cleared from eukaryotic cells are the ubiquitin-proteasome system (UPS) and the autophagy-lysosome pathway (ALP) (Ciechanover 2005). It is speculated that the ANCL aggregates might interfere with the

cellular degradation machinery, as seen in other neurodegenerative diseases (Rubinsztein 2006; Pan et al. 2008). Thus, a first essential step was to characterise the degradation pathway(s) that regulate turnover of CSP α .

Three different inhibitors of protein degradation pathways were used to assess the mechanism of turnover of wild-type CSP α . Leupeptin hemisulfate (LP) and Bafilomycin-A1 (BF) are lysosomal inhibitors (Yang et al. 2013; Yoshimori et al. 1991), while MG-132 inhibits the proteasome (Gao et al. 2000).

PC12 cells expressing wild-type EGFP-tagged CSP α were treated with either 50 μ M of LP, 100 nM of BF or 10 μ M of MG-132 overnight, as described in Section 2.6.4. Following this, cells were lysed and resolved by SDS-PAGE, before being transferred to nitrocellulose membranes for immunoblot analyses.

The results of this assay suggest that wild-type CSP α is normally degraded by the proteasome as treatment with MG-132 led to a marked increase in CSP α expression (Figure 5.1A, 5.1B). In contrast, the lysosomal inhibitors (LP and BF) did not have any consistent effect on CSP α expression levels. Interestingly, the major effect of MG-132 treatment was on the levels of the non-palmitoylated band (Figure 5.1C). These observations implicate the proteasome in the degradation of wild-type CSP α , with the non-palmitoylated form of the protein being the primary target for degradation *via* this route.

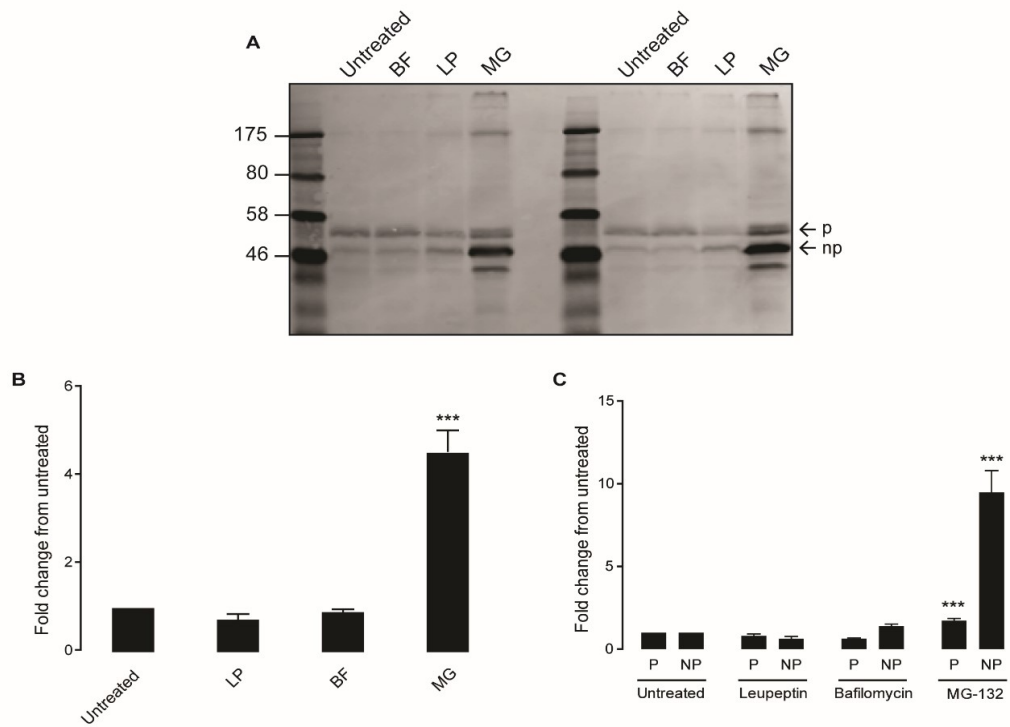


Figure 5.1. CSP α expression levels are increased by incubation of PC12 cells with MG-132. PC12 cells were transfected with EGFP-tagged wild type CSP α for 48 hours and treated for overnight with leupeptin (LP; 50 μ M), bafilomycin A1 (BF; 100 nM) and MG-132 (MG; 10 μ M) as described in Section 2.5.4. **A**) After lysis, proteins were resolved by SDS-PAGE and transferred onto nitrocellulose membranes (gel shows samples from two separate experiments). The membranes were immunoblotted using an anti-GFP antibody. Position of size of molecular weight markers is shown on the left hand side. *p* shows position of palmitoylated monomeric CSP α , and *np* designates the non-palmitoylated monomers. Quantification was performed by densitometry using Image Studio Software (n=4). **B**) Graph showing total levels of CSP α in treated versus untreated cells (palmitoylated + non-palmitoylated). **C**) Graph showing the levels of palmitoylated (P) and non palmitoylated (NP) CSP α in treated versus untreated cells. Statistical analyses were completed with one-way ANOVA, asterisks denote a significant difference (***) $p < 0.001$ in CSP α expression in treated versus untreated cells.

5.3 CSP α ANCL mutants are degraded *via* proteasome

Once the degradation pathway of the wild-type protein was established, it was important to test whether ANCL mutant CSP α proteins were also degraded *via* the proteasome. For this, the same experimental approach described above (Figure 5.1) was applied to the ANCL mutants. As can be seen in Figure 5.2, both the Δ L116 and L115R mutants also showed stronger immunoreactivity following cell treatment with MG-132. Furthermore, for both mutants, it can be seen that the intensity of the non-palmitoylated band (*np*) was greatly increased following MG-132 treatment, consistent with the results obtained with the wild-type protein. In addition, a faint band corresponding to the palmitoylated monomer (*p*) can be observed for the ANCL mutants treated with MG-132, together with a possible dimer (band at \sim 175 kDa). Interestingly, high molecular weight aggregates also significantly increased in abundance following MG-132 treatment. This might suggest that aggregates are also degraded *via* the proteasome or that the increased stability of monomeric CSP α ANCL mutants leads to increased aggregate formation.

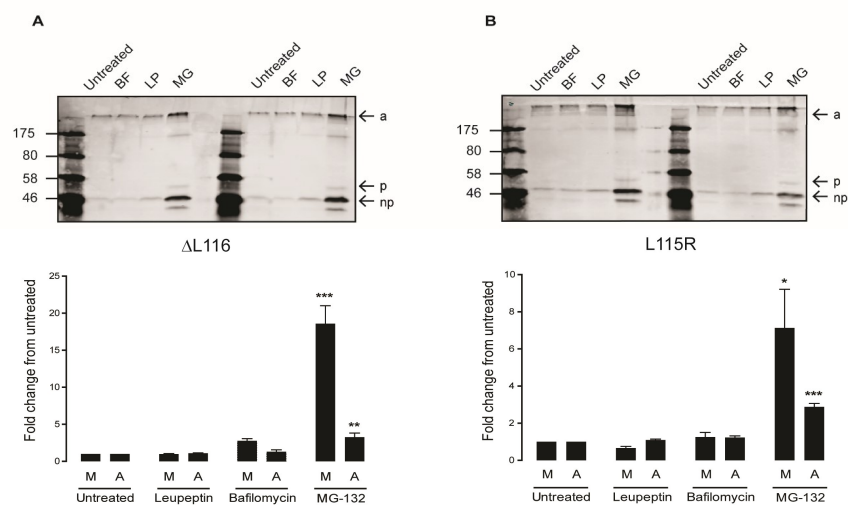


Figure 5.2. Expression of ANCL CSP α mutants is increased by incubation of PC12 cells with MG-132. PC12 cells were transfected with EGFP-tagged (A) Δ L116 and (B) L115R CSP α for 48 hours and treated overnight with leupeptin (LP; 50 μ M), bafilomycin A1 (BF; 100 nM) or MG-132 (MG; 10 μ M) as described in Section 2.6.4. The lysates from PC12 cells expressing EGFP-CSP α constructs were

resolved by SDS-PAGE, transferred to nitrocellulose membranes and immunoblotted using an anti-GFP antibody. The position of size markers is shown on the left hand side. *a* indicates aggregates, *p* designates palmitoylated monomeric CSP α , and *np* shows the position of the non-palmitoylated monomers. Quantification was performed by densitometry using Image Studio Software (n=4 for Δ L116 and n=3 for L115R). The graphs show the values of aggregates (A) and monomeric CSP α (M; palmitoylated + non-palmitoylated) in treated versus untreated cells. Statistical analyses were completed with one-way ANOVA, asterisks denote a significant difference (* $p < 0.05$, ** $p < 0.01$, *** $p < 0.001$) from untreated CSP α .

To confirm that CSP α is degraded by the proteasome, PC12 cells were treated with a structurally-unrelated proteasomal inhibitor, lactacystin. As can be seen in Figure 5.3, the effect of lactacystin on CSP α expression is similar to that observed with MG-132, with increased immunoreactivity of the monomeric non-palmitoylated bands for wild-type and the ANCL mutants. Moreover, aggregation of the ANCL mutants was also enhanced by treatment with both proteasome inhibitors.

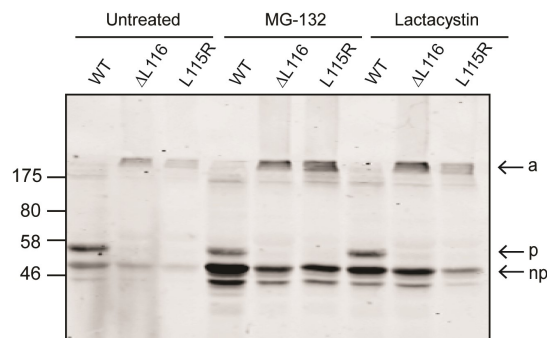


Figure 5.3. Effect of different proteasomal inhibitors on the expression of wild-type and ANCL mutant CSP α . PC12 cells were transfected with wild-type/L115R/ Δ L116 CSP α EGFP-tagged constructs for a total of 48 hours, including overnight incubation with MG-132 (10 μ M) or lactacystin (5 μ M) prior to cell lysis. Proteins were then resolved by SDS-PAGE and immunoblotted with anti-GFP. *a* indicates aggregates, *p* designates palmitoylated monomeric CSP α , and *np* shows the position of the non-palmitoylated monomers. The position of molecular weight markers is shown on the left hand side.

5.4 Analysis of the role of lysine residues in CSP α proteasomal degradation

It is well established that most proteins are modified by ubiquitination as a targeting signal for proteasomal degradation (Rubinsztein 2006; Ciechanover 2005). Thus, having shown that CSP α degradation is likely to occur *via* the proteasome (Figure 5.1, 5.2 and 5.3), it was reasoned that ubiquitination could be driving CSP α degradation. The attachment of ubiquitin to proteins to trigger proteasomal degradation was first reported by Hershko et al. (1980, 1984). Since then, the ubiquitin-proteasome system has been extensively studied and the mechanism by which ubiquitinated proteins are targeted to the proteasome is considered to be well described (Varshavsky 1997; Hershko and Aaron 1998; McKinnon and Tabrizi 2014; Grice and Nathan 2016).

Ubiquitination (or ubiquitylation) is a post-translational modification consisting of the attachment of ubiquitin to a substrate protein. Ubiquitin, a 76-residue protein, forms a bond between its carboxyl-terminal glycine residue (G76) and a lysine residue of the substrate protein (Pickart 2001). The canonical signal for proteasomal degradation is a polyubiquitin chain anchored to the ϵ -amino group of a substrate lysine residue (Chau et al. 1989). This reaction is catalysed by three enzymes: a ubiquitin-activating enzyme (E1), a conjugating enzyme (E2), and a ligase (E3) (Pickart 2001). Polyubiquitinated proteins are then recognised and degraded by the 26S proteasome (Voges et al. 1999).

A series of experiments were performed to test the role of ubiquitination in the degradation of CSP α . As a first step, a CSP α mutant without lysines was generated (see Section 2.5.2). All fourteen lysine residues in CSP α were substituted with arginine, generating the EGFP-tagged CSP α -14KR mutant. Moreover, the ANCL mutations (Δ L116 and L115R) were also introduced into CSP α -14KR by site-directed mutagenesis, as described in

Section 2.4.3. PC12 cells were then transfected with these 14KR constructs and protein expression was assessed by immunoblotting (Figure 5.4).

The overall migration pattern of the 14KR mutants appeared to be very similar to the respective control proteins (wild-type, Δ L116 and L115R). Aggregation was visible in the case of the mutants (14KR- Δ L116, Δ L116, 14KR-L115R and L115R), as well as a loss of monomeric palmitoylated band (~60 kDa). There was no consistent change in the expression levels or expression pattern on 14KR-CSP α compared with the respective proteins containing lysine residues, implying that lysine ubiquitination may not be important for proteasomal degradation of CSP α .

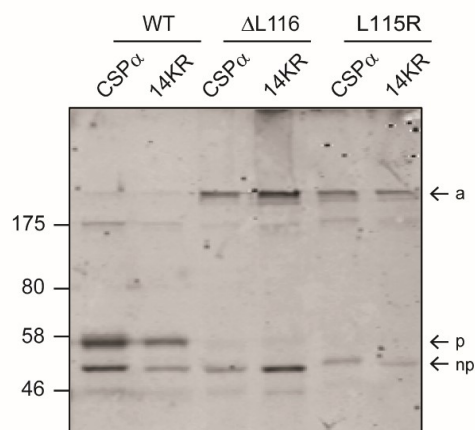


Figure 5.4. Analysis of the effect of 14KR mutations on the migration profile of wild-type and ANCL mutant CSP α on SDS gels. EGFP-CSP α 14KR wild-type and Δ L116/L115R constructs and their respective controls (wild-type CSP α , Δ L116 and L115R) were transfected into PC12 cells for 48 hours. Lysates were resolved by SDS-PAGE, transferred onto nitrocellulose membranes and probed with an antibody against GFP. Positions of the molecular weight markers are shown on the left hand side. *a* indicates aggregates, *p* designates palmitoylated monomeric CSP α , and *np* shows the position of the non-palmitoylated monomers.

Having determined that the 14KR substitutions had no gross effect on the migration profiles of wild-type and ANCL mutant CSP α , an experiment was performed to examine if MG-132

treatment affected the expression of the proteins lacking lysines. For this, PC12 cells were transfected with EGFP-tagged wild-type CSP α and 14KR, treated overnight with MG-132, and cell lysates examined by immunoblotting. The density of the palmitoylated and non-palmitoylated monomeric bands was quantified by densitometry and expressed as a ratio of the MG-treated samples to the untreated (Figure 5.5).

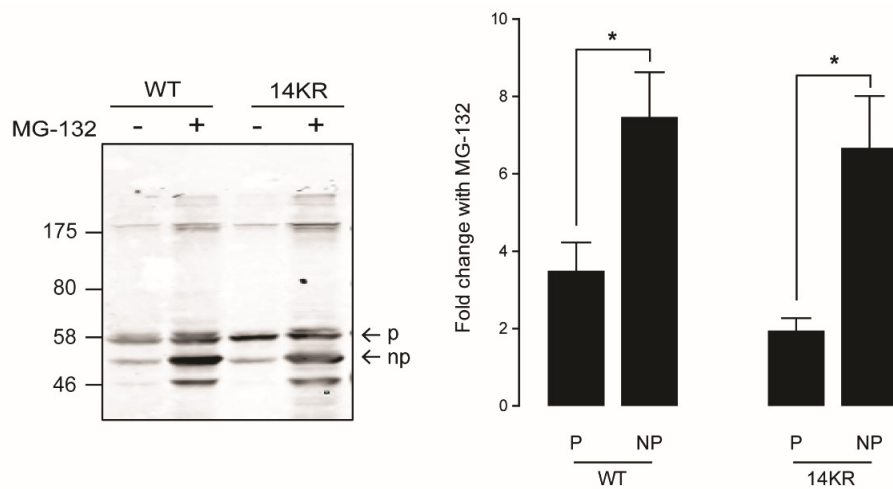


Figure 5.5. Effect of MG-132 on CSP α -14KR expression. EGFP-CSP α wild-type and 14KR constructs were transfected into PC12 cells for 48 hours, including overnight treatment with MG-132 (10 μ M) prior to cell lysis as indicated in Section 2.5.4. Lysates were then resolved by SDS-PAGE, transferred onto nitrocellulose membranes and probed with anti-GFP. Positions of size markers are shown on the left hand side. *p* and *np* indicate palmitoylated and non palmitoylated CSP α monomeric forms, respectively, and *a* indicates aggregates. Intensity of protein bands was quantified by densitometry using Image Studio Software (n=4). The values for palmitoylated and non palmitoylated monomers from treated cells were divided by the values of monomers from untreated cells to create a ratio. Statistical analysis were completed with Student T-test, asterisks denote a significant difference (* $p < 0.05$) between the palmitoylated (P) and non palmitoylated (NP) form of the protein.

As can be seen in Figure 5.5, the effect of MG-132 on the 14KR mutant was very similar to the effect on the wild-type protein. In both cases, treatment with the inhibitor caused an increase in the amount of monomeric protein, but specifically the non-palmitoylated form.

The lack of effect of the 14KR mutation on CSP α sensitivity to MG-132 was unexpected. It was possible that the EGFP tag was in some way contributing to the degradation itinerary of CSP α (e.g. lysines in EGFP could also act as ubiquitin acceptors). In order to dismiss a potential effect of the EGFP tag on the characterisation of the degradation pathway of CSP α , untagged mutants were generated. Thus, untagged wild-type CSP α , Δ L116, L115R and 14KR were transfected into PC12 cells for 48 hours and treated overnight with different proteasome and lysosome inhibitors. Cells were lysed and protein expression was assessed by immunoblotting with an antibody against CSP α .

The pattern of bands seen in Figure 5.6 is consistent with the one seen in EGFP-tagged constructs (Figure 5.1, 5.2, 5.5). Aggregation was clearly present for the L115R and Δ L116 mutants but not wild-type CSP α or the 14KR mutant (Figure 5.6B and 5.6C versus 5.6A), and the 14KR CSP α (Figure 5.6D) showed a similar immunoreactive pattern to WT CSP α (Figure 5.6A). For all proteins examined, MG-132 had the greatest effect on CSP α expression. Moreover, the band at \sim 25 kDa, corresponding to the non-palmitoylated protein (*np*) was specifically increased following MG-132 treatment in comparison to the monomeric palmitoylated band (*p*, band at <30 kDa) in all cases. This experiment clearly shows that MG-132 increases CSP α expression levels in the absence of any lysine residues on the CSP α protein and that the results obtained so far with EGFP-tagged protein are consistent with untagged CSP α proteins.

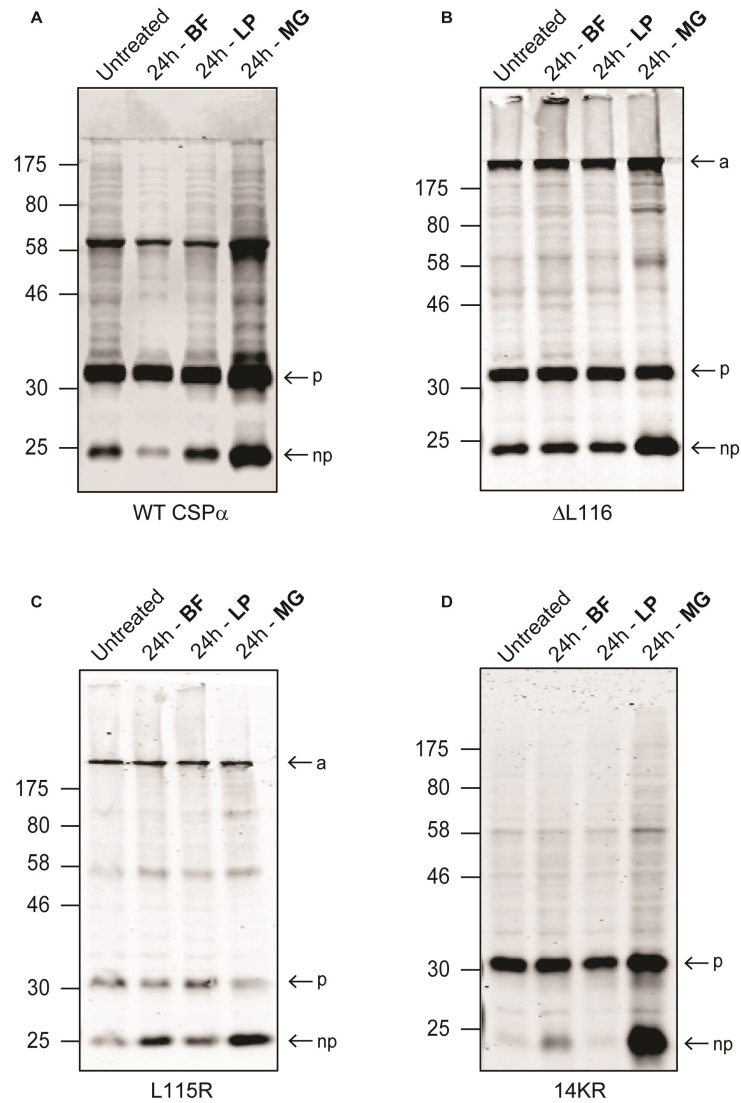


Figure 5.6. Effect of proteasome and lysosome inhibitors on untagged CSP α constructs. PC12 cells were transfected with untagged (A) wild-type, (B) Δ L116, (C) L115R and (D) 14KR CSP α constructs for 48 hours and treated overnight with the indicated inhibitors, as detailed in Section 2.6.4. After treatment, cells were lysed and proteins were resolved by SDS-PAGE, followed by transfer onto nitrocellulose membranes. The membranes were immunoblotted using an anti-CSP α antibody. The positions of the size markers are shown on the left hand side. *a* indicates aggregates, *p* specifies position of palmitoylated monomeric CSP α , and *np* designates the non-palmitoylated monomers.

5.5 Analysis of the mechanisms whereby proteasomal inhibition leads to a selective increase of non-palmitoylated CSP α

So far, the experiments shown in this chapter have provided evidence that CSP α is degraded by the proteasome. Remarkably, the major effects seen with proteasomal inhibitors are on non-palmitoylated CSP α , with this form of the protein showing a marked increase in expression compared with palmitoylated CSP α following MG-132/lactacystin treatment. There are several reasons that could explain why levels of non-palmitoylated CSP α are selectively increased following proteasomal degradation, and the two possibilities considered to be most likely were: (i) proteasomal degradation of CSP α is preceded by depalmitoylation of the protein; or (ii) newly-synthesised non-palmitoylated CSP α has a shorter half-life than palmitoylated CSP α , i.e., palmitoylation stabilises the protein.

If proteasomal degradation of CSP α requires prior depalmitoylation of the protein, then the effects of MG-132 on accumulation of non-palmitoylated CSP α should be prevented by palmostatin B, a general and non-selective inhibitor of protein thioesterases (depalmitoylation enzymes). Thus, PC12 cells were transfected with EGFP-tagged and untagged wild-type CSP α for 48 hours and treated with the proteasome inhibitors (MG-132 and LC) with or without palmostatin B (PalmB), as described in Sections 2.6.4 and 2.6.5. The results of the experiment are shown in Figure 5.7.

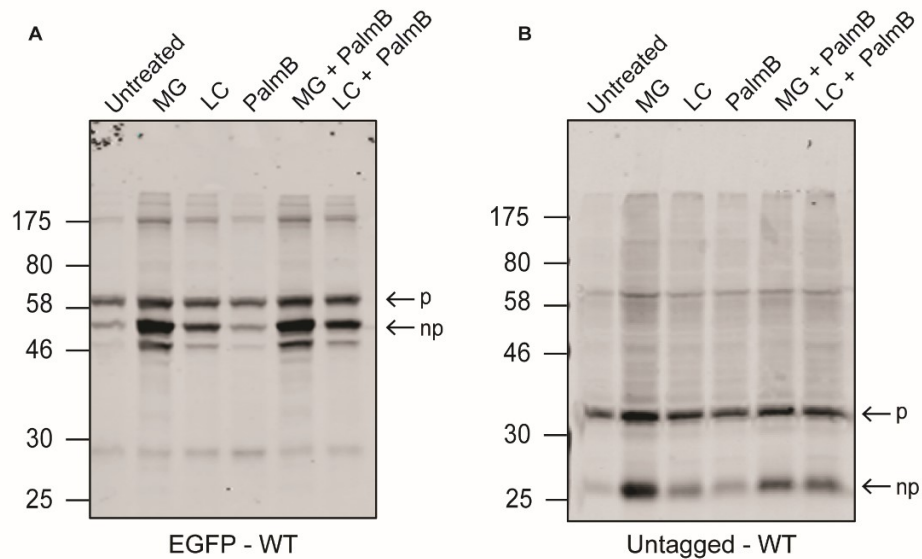


Figure 5.7. Palmostatin B does not affect the accumulation of non-palmitoylated CSP α induced by proteasomal inhibitors. PC12 cells were transfected with (A) EGFP-tagged and (B) untagged wild-type CSP α constructs for 48 hours. The cells were treated overnight with proteasome inhibitors (MG-132 [10 μ M] and lactacystin [50 μ M]) and a depalmitoylation inhibitor (palmostatin B [100 μ M]), as indicated and explained in Sections 2.6.4 and 2.6.5. The cell lysates were resolved by SDS-PAGE and transferred onto a nitrocellulose membrane for further analyses by western blot. The proteins were detected using anti-GFP and anti-CSP α antibodies. The palmitoylated bands are indicated with *p*, and *np* designates the non-palmitoylated protein. Positions of the molecular weight markers are indicated on the left hand side.

As previously seen, the proteasome inhibitors (MG-132 and LC) caused an accumulation of protein, especially in the non-palmitoylated form (*np*) for both EGFP-tagged and untagged CSP α (Figure 5.7). Addition of palmostatin B alone had no obvious effect on the levels of the palmitoylated and non-palmitoylated immunoreactive CSP α bands (Figure 5.7; this is consistent with data in Chapter 3 showing that turnover of palmitoylation on CSP α at steady-state is minimal). Furthermore, palmostatin B also had no effect on the accumulation of non-palmitoylated CSP α following treatment with either MG-132 or lactacystin (Figure 5.7). This result suggests that accumulation of non-palmitoylated CSP α

following treatment with proteasomal inhibitors does not reflect conversion of palmitoylated to non-palmitoylated protein prior to proteasomal degradation. The ability of palmostatin B to block protein depalmitoylation was shown in Chapter 3 of this thesis (Figure 3.16).

Finally, it was investigated if the non-palmitoylated CSP α seen on SDS gels represents newly-synthesised protein that has not yet undergone palmitoylation. To do this, transfected cells were treated with cycloheximide to block new protein synthesis. As can be seen in Figure 5.8 (left panel), cycloheximide treatment led to a loss of immunoreactivity for non-palmitoylated CSP α in transfected cell samples. This suggests either that this newly-synthesised pool of protein has been degraded and/or converted to palmitoylated protein. In addition, Figure 5.8 also shows the presence of an immunoreactive band corresponding in size to non-palmitoylated CSP α appearing after MG-132 treatment of non-transfected cells (asterisk), implying that the rapid turnover of non-palmitoylated protein is also seen with endogenous CSP α .

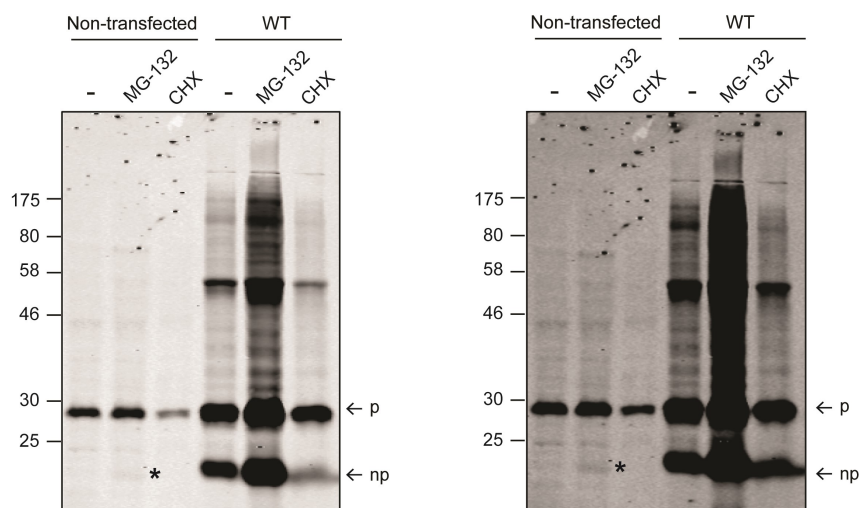


Figure 5.8. Effect of cycloheximide (CHX) and MG-132 on CSP α expression. Non-transfected PC12 cells and cells expressing untagged wild-type CSP α were treated overnight with CHX (Section 2.6.1) and MG-132 (Section 2.6.4). After lysis, proteins were resolved by SDS-PAGE and transferred onto

nitrocellulose membranes for further immunoblot analysis using an anti-CSP α antibody. The palmitoylated band is indicated with *p*, and *np* designates the non-palmitoylated protein. Positions of the molecular weight markers are indicated on the left hand side. The two images shown are the same but the intensity of the image on the right has been increased to highlight the appearance of a band corresponding in size to non-palmitoylated CSP α in non-transfected cell samples treated with MG-132 (asterisks).

The combined results of the experiments performed thus far with MG-132, palmostatin B and cycloheximide suggest that: (a) non-palmitoylated CSP α protein is degraded by the proteasome; and (b) this non-palmitoylated CSP α represents immature protein (newly-synthesised) rather than CSP α that has been depalmitoylated as part of a proteasomal degradation mechanism; and (c) non-palmitoylated CSP α has a faster rate of turnover (is less stable) than the palmitoylated protein.

5.6 Analysis of the importance of specific domains in CSP α for targeting to the proteasome

Having identified the proteasomal pathway as playing a major role in degradation of (non-palmitoylated) CSP α , and shown that targeting to this pathway does not require lysine ubiquitination, potential signals that do target CSP α for proteasomal degradation were investigated. Although ubiquitination is the most common signal for proteasomal degradation (Chau et al. 1989), the results shown in Figure 5.5 and 5.6 suggest that other signals regulate movement of CSP α to this pathway.

There is already evidence that specific proteins are being degraded in a ubiquitin-independent manner (Asher et al. 2006; Eroles and Coffino 2014). One mechanism by which

this might happen is *via* the presence of intrinsically unstructured regions (degrons) which target the protein for degradation *via* the proteasome (Dyson and Wright 2005; Fortmann et al. 2015). Different online platforms can be used for the prediction of unstructured regions in proteins (Dyson and Wright 2005; Prilusky et al. 2005). In this case, PrDOS was used (Ishida and Kinoshita 2007) to predict potential disordered regions in the sequence of CSP α that could be targeting the protein for degradation. After inserting the amino acid sequence of CSP α in the server, the platform returned a prediction on the order and disorder state of the protein. Figure 5.9 shows the two-state prediction corresponding to CSP α . The main disordered regions covered the extreme N-terminus of the protein (amino acids 1-12) and most of the C-terminus of the protein (amino-acids 142-198).

2-state prediction

1	MADQRQ RSL S	T SGESLYHVL	GLDKNATSDD	IKKSYRKLAL	KYHPDKNPDN	50
51	PEAADKFKEI	NNAHAILTDA	TKRNIYDKYG	SLGLYVAEQF	GEENVNTYFV	100
101	LSSWWAKALF	VFCGLLTCCY	CCCCLCCCFN	CCCGKCKPKA	P E G E E T E F Y V	150
151	SPED LEAQLQ	S D E R E A T D T P	I V I Q P A S A T E	T T Q L T A D S H P	S Y H T D G F N	200

Red: disordered residues

Black: ordered residues

Figure 5.9. Prediction of CSP α disordered regions. PrDOS server was used for the prediction of disordered regions in CSP α . The amino acid sequence was inserted in the online server (<http://prdos.hgc.jp>). The results are presented as the amino acid sequence of CSP α with the residues in red indicating the predicted disordered regions and the residues in black representing the ordered residues.

In addition to these disordered regions, it is possible that there are novel sequences in CSP α that target the protein for degradation. Thus, an initial strategy that was adopted to investigate regions of CSP α that control proteasomal targeting was to analyse N- and C-

terminal truncations and their expression levels in the absence and presence of MG-132. These truncations removed part or all of the disordered regions identified in Figure 5.9.

PC12 cells were transfected with EGFP-tagged constructs encoding truncated versions of CSP α : CSP₁₋₁₃₆, CSP₁₋₁₄₆, CSP₁₋₁₅₆, CSP₈₇₋₁₉₈, CSP₁₀₆₋₁₉₈. The transfected cells were treated with MG-132 overnight prior to cell lysis, followed by immunoblotting analysis (Figure 5.10).

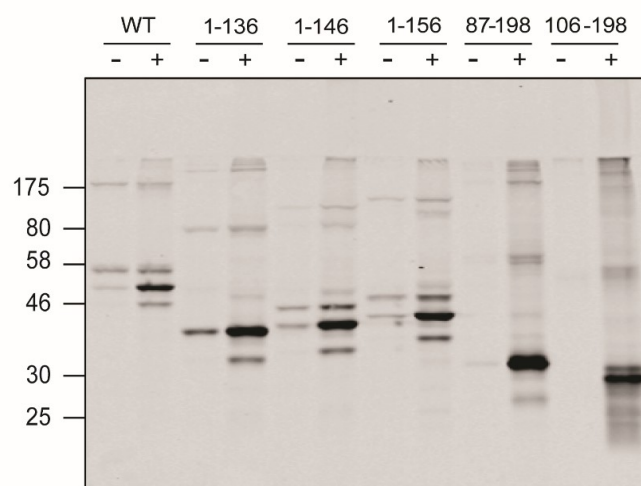


Figure 5.10. EGFP-tagged C-terminal and N-terminal truncated CSP α mutants are degraded via the proteasome. EGFP-tagged wild-type CSP α construct and the indicated truncated CSP α mutants were transfected into PC12 cells for 48 hours. MG-132 (10 μ M) was added overnight prior to cell lysis. The cell lysates were resolved by SDS-PAGE and transferred onto nitrocellulose membranes. The membranes were probed with anti-GFP antibody. Position of size markers is shown on the left hand side.

MG-132 treatment was found to increase expression of all mutants (C-terminal and N-terminal truncations). The band shift corresponding to the palmitoylated and non-palmitoylated protein can be observed in the case of wild-type CSP α , CSP₁₋₁₄₆, CSP₁₋₁₅₆ and CSP₁₀₆₋₁₉₈ (Figure 5.10). In all of these cases, upon treatment with MG-132, the lower (non-

palmitoylated) band increased in intensity in comparison to the untreated cells. These results suggest that the predicted disordered regions in the N-terminal and C-terminal do not function as essential degrons for CSP α degradation at the proteasome. CSP₁₋₁₃₆ is tightly membrane-associated but does not undergo palmitoylation (Greaves and Chamberlain 2006). As this mutant also accumulated after inhibition of the proteasome, it is reasonable to conclude that membrane association without palmitoylation does not protect CSP α from proteasomal degradation. No immunoreactive bands were detected with the 87-198 and 106-198 truncations since these mutants are rapidly cleared from cells due to their small size (and lack of palmitoylation; Greaves and Chamberlain 2006).

To complement the experiments performed with EGFP-tagged CSP α mutants, untagged CSP α constructs were also examined. However, as the CSP α antibody recognises an epitope present in the extreme C-terminus of the protein, this analysis was limited to N-terminal truncations. A group of untagged N-terminal truncation mutants was generated (CSP₁₄₋₁₉₈, CSP₈₄₋₁₉₈, CSP₁₁₃₋₁₉₈, CSP₁₃₆₋₁₉₈) and analysed by immunoblotting following cell treatment with or without MG-132. The results are shown in Figure 5.11.

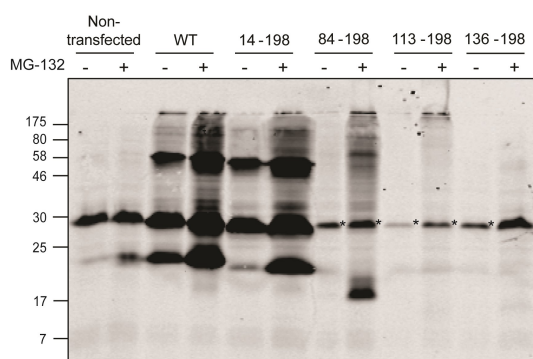


Figure 5.11. Untagged truncated CSP α mutants are degraded *via* the proteasome. PC12 cells were transfected for 48 hours with untagged wild-type CSP α and the indicated truncation mutants. The cells were treated with MG-132 (10 μ M) overnight, followed by cell lysis. The cell lysates were then resolved by SDS-PAGE and transferred onto nitrocellulose membranes. The membranes were probed

with anti-CSP α antibody. Position of molecular weight markers is shown on the left hand side. Asterisks designate the palmitoylated endogenous protein.

It is clear from Figure 5.11 that the addition of MG-132 leads to the accumulation of a non-palmitoylated band for wild-type CSP α and the 14-198 mutant (lacking the N-terminal unstructured region). For the 84-198 mutant, no obvious band is detected in the untreated sample, whereas MG-132 treatment leads to the appearance of an immunoreactive band at ~20 kDa, showing that this mutant is also subject to proteasomal degradation (Figure 5.11). In contrast, no immunoreactive bands were detected with the 113-198 or 136-198 truncation mutants, even in the presence of MG-132. The fact that these mutants are not detected might be due to a rapid clearance from cells as a result of their small size (and lack of palmitoylation; Greaves and Chamberlain 2006).

5.7 Analysis of the effects of mutations in the cysteine-string domain on CSP α proteasomal degradation

Analysis of the truncation mutants above suggested that CSP α disordered regions do not target the protein for proteasomal degradation (although we cannot rule out that there is more than one unstructured region that function as degrons in CSP α). Moreover, as discussed, the mutant CSP₁₋₁₃₆, which is membrane associated but non-palmitoylated (Greaves and Chamberlain 2006), undergoes degradation *via* the same pathway. Therefore, this result suggests that membrane association does not prevent rapid degradation of CSP α by the proteasome. As the rate of degradation of CSP α is linked with its palmitoylation, it was possible that the cysteine-string domain was involved in proteasomal targeting.

Unfortunately, none of the mutants examined above remove the cysteine-string domain, with the exception of the 136-198 mutant, which did not give rise to any detectable protein expression.

Therefore, the cysteine-string domain of CSP α was analysed in order to determine its importance in degradation of the protein, as well as to better define the link between degradation and palmitoylation. Thus, the different cysteine mutants that were generated in Chapter 3 were analysed here in MG-132 experiments. In addition, another EGFP-tagged plasmid was introduced in this experiment: C(8-14)A, which combines the 8-10 and 11-14 cysteine mutations. Figure 5.12A shows the migration profile of the different EGFP-tagged constructs after treatment with the proteasome inhibitor MG-132. The migration pattern corresponding to similar untagged constructs is shown in Figure 5.12B. For all mutants, and especially for the untagged constructs, it can be seen that the palmitoylated band migrates at a lower molecular weight in comparison to the palmitoylated wild-type band, in line with the loss of palmitoylation of the mutated cysteines. Also, treatment with MG-132 appears to induce accumulation of non-palmitoylated CSP α for all mutants. Importantly, the migration pattern and the effect of the inhibitor is consistent for the EGFP-tagged and untagged mutants. As with the 1-136 truncation mutant, the membrane-associated but non-palmitoylated C(4-7)L mutant also shows sensitivity to MG-132, further emphasising that membrane association in the absence of palmitoylation does not protect CSP α from proteasomal degradation.

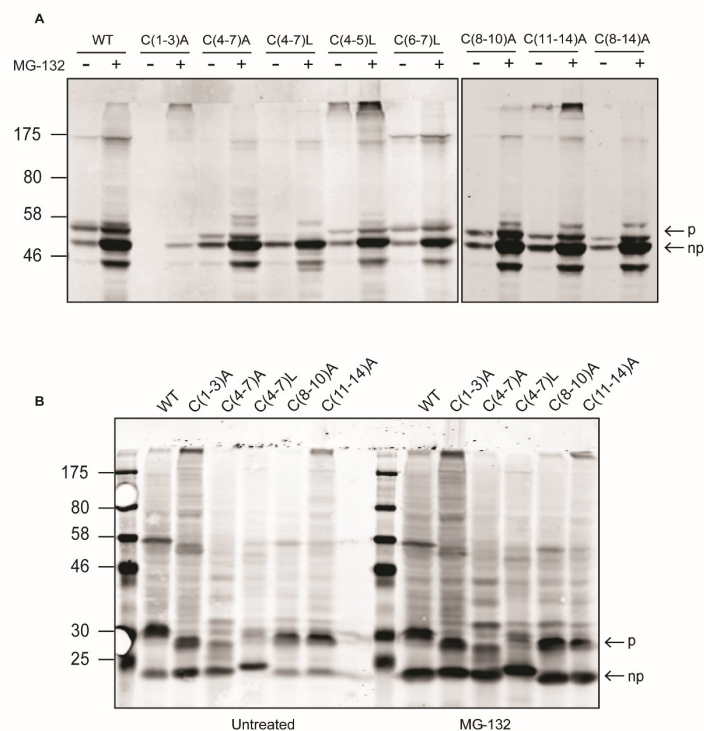


Figure 5.12. Effect of cysteine mutations in the CSD on degradation of CSP α via proteasome. PC12 cells transfected for 48 hours with GFP-tagged **(A)** and untagged **(B)** cysteine mutants were treated overnight with MG-132 (10 μ M). The cell lysates were then resolved by SDS-PAGE and transferred onto nitrocellulose membranes. The membranes were immunoblotted using anti-GFP **(A)** or anti-CSP α **(B)** antibodies. Position of the molecular weight markers is shown on the left hand side. *p* specifies position of palmitoylated monomeric CSP α , and *np* designates the non-palmitoylated monomers.

Having examined the effect of cysteine substitutions in the CSD, the remaining non-cysteine residues in this region were also mutated to identify possible signals targeting CSP α for proteasomal degradation. Figure 5.13A shows a diagram of CSP α indicating the different domains of the protein. The amino acid sequence of the CSD is detailed, displaying the 14 cysteine residues and highlighting non-cysteines in green boxes. The amino acid substitutions of these non-cysteines were introduced into EGFP-tagged constructs using site-directed mutagenesis (Section 2.4.3) and named as follows: CSP α -G114A, CSP α -T117A,

CSP α -Y120A, CSP α -L125A, CSP α -FN129A and CSP α -G134A. The constructs were transfected into PC12 cells and treated with MG-132 as in the previous experiments. Figure 5.13B shows that none of the non-cysteine mutations in the CSD had any effect on the increased expression of CSP α following MG-132 treatment.

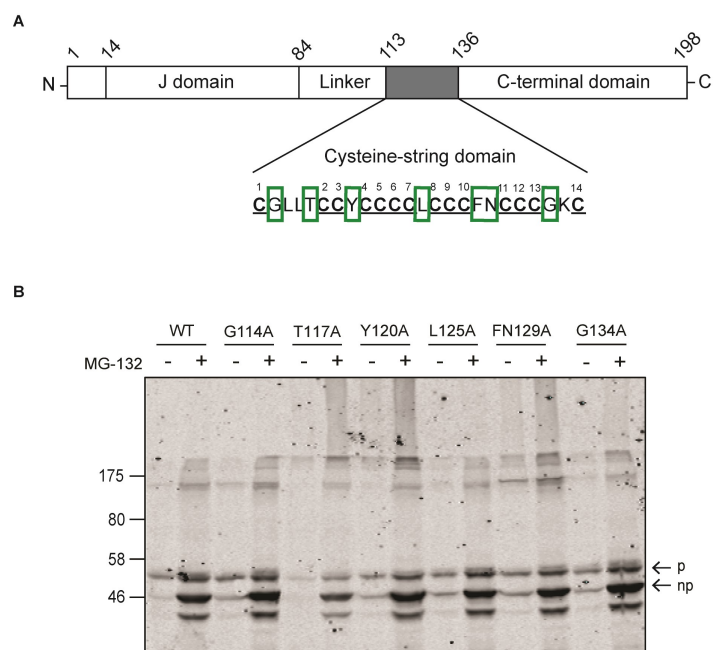


Figure 5.13. Effect of substitution of non-cysteine residues within the CSD on CSP α degradation. A) Schematic diagram of the domains of CSP α and their location in the protein. The amino acids in the CSD are shown, highlighting the cysteine residues (numbered consecutively). The green squares indicate the non-cysteine residues that were mutated into alanines. **B)** The resulting EGFP-tagged mutant constructs and wild-type EGFP-tagged CSP α were transfected into PC12 for 48 hours. Cells were treated with MG-132 (10 μ M) overnight. Lysates were then resolved by SDS-PAGE, transferred onto nitrocellulose membranes and immunoblotted with anti-GFP antibody. Position of the molecular weight markers is shown on the left hand side. *p* shows position of palmitoylated monomeric CSP α , and *np* indicates the non-palmitoylated monomers.

5.8 PEST sequences are not responsible for CSP α degradation

Some peptide motifs have been proposed to function as degradation signals (Rechsteiner and Rogers 1996). Examples of these motifs include KFREQ regions for lysosomal degradation (Dice 1990) and PEST sequences, thought to target peptides for degradation *via* the 26S proteasome (Rogers et al. 1986). PEST motifs are regions of the protein rich in proline (P), glutamate (E), serine (S) and threonine (T). In order to investigate whether CSP α contained any PEST motifs, the online platform *EMBOSS-pest finder* was used (Rice et al. 2000). The results of the prediction are shown in Figure 5.14.

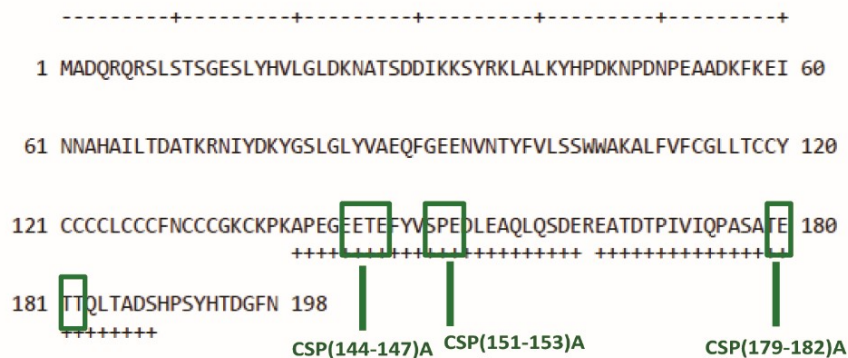


Figure 5.14. Identification of potential PEST sequences in CSP α . Sequences rich in Proline (P), Glutamic Acid (E), Serine (S) and Threonine (T) were identified in the CSP α amino acid sequence using EMBOSS-pest online platform (<http://emboss.bioinformatics.nl/cgi-bin/emboss/help/pepfind>). The identified sequences are indicated with an underlying “+” symbol. The green frames designate the mutations introduced in order to test the importance of PEST motifs on the degradation of CSP α .

Two potential PEST motifs were identified in CSP α (Figure 5.14), and different mutants were generated in order to target the identified sequences. Blocks of 3 to 4 residues were mutated into alanine residues through site-directed mutagenesis (Section 2.4.3). The

resulting untagged and EGFP-tagged plasmids [CSP(144-147)A, CSP(151-153)A and CSP(179-182)A] were expressed in PC12 cells and treated with or without MG-132 as before.

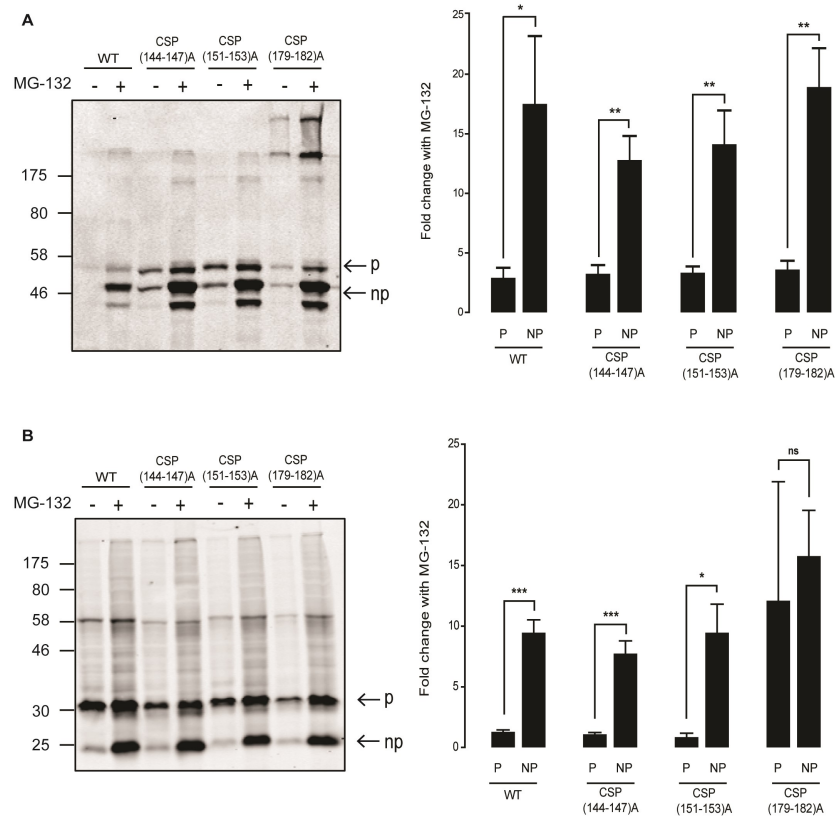


Figure 5.15. PEST sequences do not drive proteasomal degradation on CSP α . PC12 cells were transfected for 48 hours with the indicated EGFP-tagged (A) or untagged (B) wild-type CSP α and PEST mutants. After an overnight treatment with MG-132, cell lysates were resolved by SDS-PAGE and transferred onto nitrocellulose membranes. The membranes were probed with anti-GFP or anti-CSP α . The positions of the size markers are shown on the left hand side. Quantification was performed by densitometry using Image Studio Software (n=4). For each construct, the fold change is expressed as a ratio of monomeric forms of the protein (palmitoylated and non-palmitoylated) in treated versus untreated samples. Statistical analyses were completed with unpaired (two sample) Student T-test, asterisks denote a significant difference (* $p < 0.05$, ** $p < 0.005$, *** $p > 0.001$, ns= non-significant) between the palmitoylated (P) and non palmitoylated (NP) form of the protein.

Figure 5.15A shows that mutations in the PEST sequences of CSP α did not prevent degradation *via* the proteasome as the intensity of the non-palmitoylated monomeric bands is increased in the mutants treated with MG-132. Figure 5.15B shows the results of the same experiment performed with untagged constructs. The observed pattern of bands is consistent with the EGFP-tagged constructs: the PEST mutations generated do not affect sensitivity of CSP α to MG-132. Moreover, the quantification of both experiments is consistent, showing the same pattern even though the significance values are slightly different.

5.9 Unusual ubiquitination profile of CSP α

As efforts to identify signals in CSP α mediating proteasomal targeting were unsuccessful, subsequent analyses examined the ubiquitination profile of CSP α . As previously mentioned in this chapter (Section 5.4), ubiquitination is an accepted signal for proteasomal degradation. The canonical mechanism consists of the addition of a polyubiquitin chain to a ϵ -NH₂ group of a lysine residue in the substrate protein. However, there is evidence of other types of ubiquitin chains (Kravtsova-Ivantsiv and Ciechanover 2012; McDowell and Philpott 2013). The non-canonical ubiquitin mechanisms include bonds between ubiquitin and non-lysine residues, such as cysteine (Cadwell and Coscoy 2005), threonine (Tait et al. 2007; Vosper et al. 2009) and serine (Tait et al. 2007). As the CSP α -14KR mutant showed no difference to wild-type CSP α in terms of MG-132 sensitivity, it is likely that lysine ubiquitination does not play a role in CSP α degradation. Furthermore, additional analysis performed above indicates that there is unlikely to be any single degron in CSP α that mediates proteasomal targeting.

Ubiquitination of CSP α oligomers has been previously reported by Zhang and Chandra (2014). However, the results in Figure 5.5 and 5.6 suggest that ubiquitination does not occur on lysines, since the CSP α lysine-less mutant appears to be degraded *via* the proteasome. Thus, it was hypothesised that CSP α could be ubiquitinated in a non-canonical manner. To further test this idea, the ubiquitination state of the 14KR CSP α mutant was assessed.

PC12 cells were transfected with EGFP-tagged wild-type, 14KR CSP α constructs, or pEGFP-C2 empty vector. The cells were treated with MG-132 overnight and immunoprecipitated using anti-GFP microbeads, as described in Section 2.6.9. Figure 5.16 shows the immunoprecipitated EGFP and EGFP-tagged CSP α constructs after detection with anti-GFP (A) and anti-ubiquitin (B) antibodies. Both palmitoylated and non-palmitoylated bands can be observed for wild-type and 14KR CSP α (indicated with the arrowheads) and dimeric bands can be seen at ~175 kDa. Moreover, the non-palmitoylated band is increased upon proteasomal inhibition. Figure 5.16B shows the signal for ubiquitination for the same samples. Ubiquitination is detected as a smear, not to be confounded with the aggregates seen in the case of the ANCL mutants. A high molecular weight band is observed in MG-132-treated cells transfected with wild-type CSP α . Moreover, a visible smear is also detected for the 14KR CSP α mutant. However, EGFP empty vector also seems to show a faint smear albeit less visible compared to the CSP α constructs.

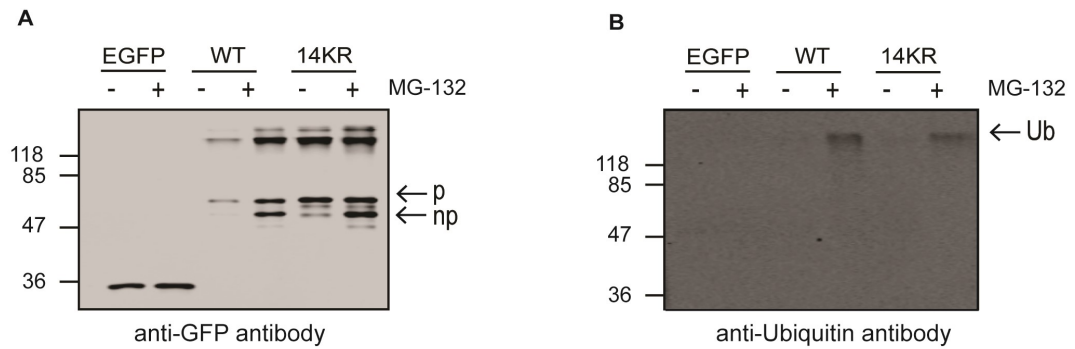


Figure 5.16. Ubiquitination of EGFP-tagged CSP α constructs. PC12 cells were transfected with pEGFP-C2 empty plasmid, EGFP-wild type and EGFP-14KR CSP α constructs for 48 hours. After a 24-hour treatment with MG-132, the cells were lysed. The lysates were then immunoprecipitated using anti-GFP magnetic microbeads and the immunoprecipitated lysates were resolved by SDS-PAGE, transferred onto nitrocellulose membranes and immunoblotted using antibodies against GFP (**A**) and ubiquitin (**B**). The position of the molecular marker is shown on the left hand side. *p* shows position of palmitoylated monomeric CSP α , *np* indicates the non-palmitoylated monomers and *ub* indicates the presence of ubiquitin molecules.

In order to rule out any confounding effect caused by the EGFP tag, the same experiment was also performed using HA-tagged constructs. The pef-BOS-HA expression vector contains two lysines in the linker region (between the tag and the coding sequence of CSP α 14KR) that were mutated into arginines through site-directed mutagenesis, as detailed in Section 2.5.5. Thus, the resulting HA-14KR CSP α construct lacks any lysines. PC12 cells were transfected with EGFP-tagged and HA-tagged wild-type and 14KR CSP α for 48 hours. After an overnight treatment with MG-132, the proteins were immunoprecipitated and resolved by SDS-PAGE. The immunoblots obtained are shown in Figure 5.17.

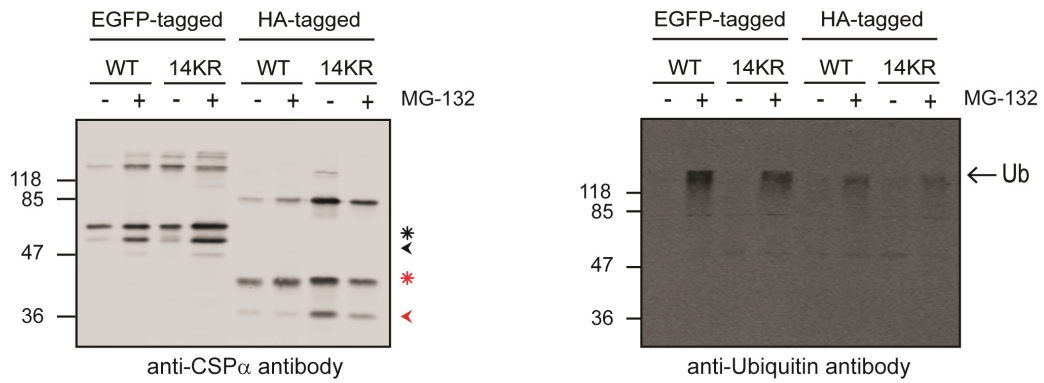


Figure 5.17. Evidence that CSP α is ubiquitinated in absence of lysines. EGFP-tagged and HA-tagged wild-type and 14KR CSP α constructs were transfected in PC12 cells for 48 hours. The cells were treated with the proteasome inhibitor MG-132 overnight. After this treatment, the cell lysates were immunoprecipitated using anti-HA and anti-GFP microbeads. The immunoprecipitated lysates were then resolved by SDS-PAGE, transferred onto nitrocellulose membranes and immunoblotted using anti-ubiquitin and anti-CSP α antibodies. The molecular weight is indicated on the left hand side. *ub* indicates the presence of ubiquitin molecules, arrowheads designate non-palmitoylated monomers, asterisks indicate palmitoylated monomers (black for EGFP-tagged constructs and red for HA-tagged).

The effect of the proteasome inhibitor is clearer in the case of the EGFP-tagged constructs in comparison to the HA-tagged. As seen previously, the inhibitor causes an accumulation of the non-palmitoylated EGFP-tagged proteins. By contrast, the pattern of the HA-tagged constructs is slightly different and no increase in non-palmitoylated monomer was seen with MG-132 treatment. The reason for this is not clear but may be due to more efficient immunoprecipitation of the palmitoylated HA-tagged CSP α than the non-palmitoylated form. However, a smear corresponding to the presence of ubiquitin molecules is clearly present in Figure 5.17B in all samples treated with the inhibitor. Even in the complete absence of lysines (HA-14KR mutant), the smear is visible. Overall, these results suggest that ubiquitination of CSP α does occur, is enhanced by MG-132 treatment and is independent of any lysine residues. However, it cannot be ruled out at this stage that the

ubiquitination signal is due to a co-precipitating protein or background binding to the GFP microbeads.

5.10 ANCL mutants also undergo ubiquitination

To extend the analyses of CSP α ubiquitination, the ANCL CSP α mutants were also examined using both HA-tagged and EGFP-tagged constructs. PC12 cells were transfected for 48 hours and treated with MG-132 overnight. After immunoprecipitation, the proteins were resolved by SDS-PAGE and transferred to nitrocellulose membranes. The immunoblots obtained are shown in Figure 5.18. Quantification was performed for the HA-tagged constructs in order to dismiss potential effects of the larger EGFP tag (Figure 5.18C). The data were normalised to untreated cells and presented as fold change in ubiquitination for each construct in comparison to each control (wild-type, Δ L116 and L115R untreated).

The migration patterns in Figures 5.18A and B are broadly similar with previous results, although the profile of immunoprecipitated protein is not identical to protein in cell lysates: in particular, the GFP antibody is not effective at precipitating ANCL mutant aggregates. Ubiquitination was present in all samples and there was no difference in signal between wild-type and ANCL CSP α mutants. This result might indicate that: (i) the aggregates are ubiquitinated, as suggested by Henderson et al. (2016); or (ii) that there are other protein components clustered with the ANCL aggregates that are indeed palmitoylated.

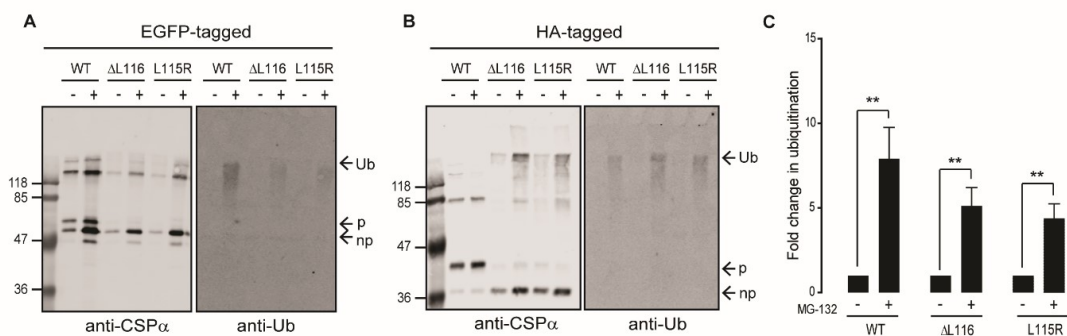


Figure 5.18. Ubiquitination of the ANCL CSP α mutants. PC12 cells were transfected with EGFP (**A**) and HA-tagged (**B**) wild-type and ANCL CSP α constructs for 48 hours. After an overnight treatment with MG-132, the cells were lysed. Lysates were immunoprecipitated using anti-GFP and anti-HA microbeads. The resulting immunoprecipitated proteins were resolved by SDS-PAGE and transferred onto nitrocellulose membranes for immunoblotting, using anti-CSP α and anti-ubiquitin antibodies. **C**) Quantification of the HA-tagged constructs was performed by densitometry and is expressed as a fold-difference of ubiquitin levels between the untreated and treated samples. The data were normalised to untreated cells, and statistical analysis were completed with unpaired two samples Student's T test; asterisks denote a significant difference (** $p < 0.01$) from the respective control CSP α construct (wild-type, Δ L116 or L115R).

5.11 Discussion

A common characteristic feature of many different neurodegenerative disorders is an abnormal folding of proteins, which can cause aggregation and accumulation in cells. These aggregates, in turn, can trigger degenerative signals (Bence et al. 2001; Metcalf et al. 2012). Interestingly, there appears to be an important link between protein aggregation, protein turnover and disruption of the cellular degradation machinery (Gestwicki and Garza 2012). Thus, the work in this chapter initially set out to examine the pathways mediating CSP α turnover with a view to providing new understanding about how ANCL mutants might disrupt degradative pathways. However, the analyses that were carried out focused

predominantly on the mechanisms underlying turnover of wild-type CSP α , although it is hoped that this new knowledge will contribute ultimately to an increased understanding of degradation of the ANCL mutants.

Experiments using degradation pathway inhibitors were undertaken in PC12 cells expressing EGFP-tagged CSP α . The results of these experiments suggest that CSP α and the monomeric forms of the ANCL mutants are degraded *via* the proteasome (Figure 5.1, 5.2 and 5.6). These results were confirmed with two different proteasome inhibitors (Figure 5.3). However, it is possible that proteasomal degradation is specific to non-palmitoylated CSP α , as MG-132 and lactacystin led to a selective enhancement in the levels of this form of the protein and had very little effect on the palmitoylated pool of the protein. Thus, the pathway for degradation of non-palmitoylated CSP α may have been uncovered more readily than palmitoylated CSP α due to the rapid turnover of the non-palmitoylated form of the protein. Experiments with palmostatin B confirmed that the increased accumulation of non-palmitoylated CSP α with MG-132 treatment was likely to reflect a stabilisation of the protein and essentially ruled out any influence on the results of a possible depalmitoylation step *en route* to proteasomal degradation.

One possibility to explain the low turnover of palmitoylated CSP α is that palmitoylation prevents CSP α degradation. In fact, one of the known functions of palmitoylation is the regulation of protein stability (Linder and Deschenes 2007). Regulation of protein degradation can be achieved by limiting ubiquitination of proteins as a result of palmitoylation. One example is the case of the *S. cerevisiae* SNARE protein Tlg1 (Valdez-Taubas and Pelham 2005), which mediates vesicle fusion in the secretory pathway (Siniosoglou and Pelham 2001; Coe et al. 1999). Tlg1 is palmitoylated on two cysteines nearby its transmembrane domain, preventing the interaction of the SNARE protein with

the E3 ubiquitin ligase Tul1. When palmitoylation is blocked, either by mutation of the two cysteine residues in Tgl1 or by deletion of the zDHHC enzyme Swf1, Tul1-mediated ubiquitination of Tgl1 is increased and the protein is targeted to the vacuole for degradation (Valdez-Taubas and Pelham 2005).

Interestingly, the ubiquitin ligase Tul1 has specificity for proteins that contain acidic residues adjacent to transmembrane domains (Reggiori and Pelham 2002). It is possible that palmitoylation stabilises Tgl1 by preventing acidic residues adjacent to the transmembrane domain from penetrating the bilayer. In absence of palmitoylation, the acidic residues are proposed to come in contact with the membrane, triggering Tul1-mediated ubiquitination; indeed non-palmitoylated Tgl1 can be stabilised by deletion of membrane-proximal acidic residues (Valdez-Taubas and Pelham 2005).

Another example of regulation of protein stability by palmitoylation is the case of the anthrax-toxin receptor (ATR) or tumour endothelial marker-8 (TEM8) (Abrami et al. 2006), which is a substrate for not only palmitoylation but also ubiquitination. Both of these post-translational modifications have opposite effects on the half-life of ATR and TEM8. The anthrax toxin is composed of three different polypeptides: lethal factor (LF), edema factor (EF) and protective antigen (PA) (Abrami et al. 2005). Since PA is the only subunit of the toxin able to bind to target cells, LF and EF require this factor to be transported into the target cell cytosol. PA can bind two receptors, both type I transmembrane proteins, named ATR/TEM8 and capillary morphogenesis gene 2 (CMG2). A proteolytic cleavage of the receptor complex leads to the heptamerization of PA. Following heptamerization, the toxin-receptor complex becomes associated with lipid rafts at the cell surface, which facilitates its internalisation. However, it has been seen that palmitoylation of the cytoplasmic tail of the receptor prevents association with lipid rafts and provokes premature ubiquitination

(Linder and Deschenes 2007). The palmitoylation profile of the anthrax-toxin receptors was evaluated by Abrami et al. (2006) and found that the post-translational modification was essential to prevent premature targeting of the receptors to the lysosome. Moreover, the non-palmitoylated receptors appeared to be highly enhanced in lipid raft sections in comparison to the wild-type mutant receptors. This observation indicates that palmitoylation negatively regulates association to lipid rafts, and suggests that the receptor is depalmitoylated during heptamerization in order to facilitate association with rafts. Moreover, when the toxin-receptor complex is associated to rafts, the receptors become available to the E3 ubiquitin ligase Cbl, which modifies the cytoplasmic tail of the receptor, facilitating endocytosis. Thus, cells expressing palmitoylation-defective mutant receptors are more resistant to the anthrax toxin due to a lower number of surface receptors and a premature ubiquitination and internalisation of PA (Abrami et al. 2006).

In the case of CSP α , a mutagenic approach was taken in order to understand the mechanisms by which CSP α turnover is triggered, and the post-translational modifications that might be involved in this process. As previously mentioned, the main signal for proteasomal degradation is the ubiquitination of lysines (Hershko et al. 1980; Hershko et al. 1984). To examine whether ubiquitination was triggering CSP α proteasome-mediated degradation, a lysine-less mutant was generated (CSP α -14KR). Surprisingly, treatment with MG-132 suggested that the CSP α -14KR mutant was also degraded by the proteasome, suggesting that the destruction signal for CSP α is not lysine ubiquitination. Importantly, the same results were obtained with EGFP-tagged and untagged CSP α , and this rules out any confounding effects of the EGFP tag on CSP α turnover.

Since lysine ubiquitination was ruled out as the signal mediating proteasomal destruction of non-palmitoylated CSP α , it was reasoned that the presence of intrinsically unstructured

regions might instead target the protein for degradation (Dyson and Wright 2005; Fortmann et al. 2015). A search using an online prediction platform identified two potential disordered regions in CSP α : a short region in the N-terminus of the protein and a large region of the C-terminus of CSP α (downstream of the CSD). Thus, a mutagenic approach was taken to examine how these unstructured regions affect CSP α degradation. Moreover, expression of C-terminal and N-terminal CSP α truncation mutants can give additional information on the effect of palmitoylation and membrane association on the degradation of CSP α . Thus, EGFP-tagged mutants 1-136, 1-146, 1-156, 87-198 and 106-198 and untagged 14-198, 84-198, 113-198, 136-198 mutants were analysed (Figure 5.10, 5.11). The truncation mutants showed that elimination of the two predicted disordered regions in the C and N-terminal of CSP α did not change the sensitivity of the protein to MG-132. Moreover, the band pattern observed in the mutants was similar to the full-length wild-type CSP α , displaying an increased immunoreactivity in the non-palmitoylated band. As some of these mutants are known to associate with membranes in the absence of palmitoylation (e.g. 1-136; (Greaves and Chamberlain 2006)), these results also reveal that membrane association is not sufficient to stabilise CSP α and presumably that palmitoylation has a direct effect on protein stability.

The role of palmitoylation in the degradation pathway of CSP α was further investigated by the generation of mutations in the CSD. However, even though the palmitoylation profile of these CSP α mutants was altered, expression of all the mutants showed sensitivity to MG-132 (Figure 5.12). Therefore, there are no specific cysteines within the CSD that are essential for proteasomal degradation but it would be interesting in future work to examine the effect of mutating all cysteines simultaneously to test the specific requirement for palmitoylation in general rather than palmitoylation of specific cysteines. For a more comprehensive assessment of the role of the CSD region in proteasomal degradation of

CSP α , the non-cysteine residues in this domain were also substituted by alanines (Figure 5.13). However, none of these amino acid substitutions affected the accumulation of non-palmitoylated monomer following inhibition of the proteasome. The mutations of the cysteines in the CSD also confirmed that membrane association does not protect CSP α from degradation as the C(4-7)L mutant, which is membrane-associated but not palmitoylated (similar to the 1-136 mutant), was also MG-132 sensitive.

Another possible explanation for the accumulation of non-palmitoylated CSP α following proteasomal inhibition could be the presence of a chaperone that targets the non-palmitoylated protein to the proteasome, while avoiding interactions with zDHHC enzymes. CHIP (C-terminus of Hsp70-interacting protein), an E3 ligase, is an example of co-chaperone able to facilitate protein degradation (Lilienbaum 2013). Interestingly, CSP α has been reported to be involved in the proteasome-mediated degradation of cystic fibrosis transmembrane conductance regulator (CFTR) by facilitating association with Hsp70/Hsc70 and CHIP E3 ligase (Schmidt et al. 2009). In the same study it was reported that CSP α can directly bind to CHIP. Thus, it would be interesting to investigate whether the interaction of CHIP with CSP α is directly related to CSP α proteasome-mediated degradation, for example by using proteasome inhibitors in combination with co-expression experiments.

Having determined that ubiquitination, unstructured regions, or specific residues within the CSD do not prevent degradation, it was reasoned that sequences rich in proline (P), glutamate (E), serine (S) and threonine (T) (also known as PEST sequences) could also be a signal for proteasome-mediated degradation of CSP α , as reported for other proteins (Rogers, Wells, and Rechsteiner 1986; Rechsteiner and Rogers 1996). Two potential PEST sequences were identified within CSP α (Figure 5.15) and although these were located in the C-terminus of the protein (which had previously been truncated without effect) it was

decided to mutate these PEST sequences and blocks of 3 to 4 residues within the motifs were mutated to alanines. The resulting PEST mutants were examined in the presence and absence of MG-132. As seen previously, the proteasome inhibitor caused an overall increase of the immunoreactivity of all mutants, especially for the non-palmitoylated band. Altogether, these results indicate that the PEST sequences identified in CSP α do not trigger its degradation *via* the proteasome.

Overall, the exhaustive analysis of CSP α amino acid sequence did not result in the identification of a region or motif triggering CSP α degradation. As discussed above, it would be interesting to examine effects of mutating all cysteines in the CSD or combining different mutations (as the presence of more than one proteasomal targeting sequence in CSP α would increase the complexity of this analysis). Nevertheless, the results in this chapter show for the first time that CSP α is degraded by the proteasome, and specifically that it is the non-palmitoylated form of the protein that follows this pathway. Recently, CSP α was shown to undergo ubiquitination (Zhang and Chandra 2014). In this chapter, however, CSP α -14KR was shown to be degraded by the proteasome despite lacking lysine residues. Could CSP α be ubiquitinated on non-lysine residues? To test this idea, an anti-ubiquitin antibody was used to detect the presence of ubiquitin molecules in CSP α , and the results suggest that EGFP-wild type CSP α is indeed ubiquitinated. Furthermore, CSP α -14KR also appeared to be ubiquitinated as observed for the high-molecular weight smear (Figure 5.16).

In order to rule out the effect of the EGFP-tag, HA-tagged plasmids were generated. All lysines present in the pef-BOS-HA vector were substituted by arginines to ensure that the tag would not have an effect on the detection of ubiquitin molecules. Indeed, the HA-tagged constructs were also ubiquitinated (Figure 5.17, 5.18). Although these results are

interesting, future work should confirm that the ubiquitination detected is specifically associated with CSP α and not a co-precipitated protein.

Apart from lysines, ubiquitination can also occur on cysteines, threonines and serines (Tait et al. 2007). Therefore, it will be important in the future to further delineate the non-canonical ubiquitination pathway of CSP α . For example, by incubating the immunoprecipitated protein with β -mercaptoethanol or DTT in order to break potential thio-ester bonds (and detect cysteine-ubiquitination). Moreover, co-expression experiments with specific E3 ligases, such as CHIP, could provide information on the ubiquitination status of CSP α and factors that regulate CSP α ubiquitination.

Moreover, in order to allow proteasomal unfolding, ubiquitin must occur near a region of structural instability. Close proximity of the ubiquitin modification to an unstructured region of the protein will allow effective proteasomal unfolding (Prakash et al. 2004). Thus, analysis of the ubiquitination status of residues in CSP α that surround unstructured regions could be an experiment to perform in the future.

Another point of consideration is that while ANCL is considered a lysosomal storage disorder due to accumulation of fluorescent material in lysosomes, non-palmitoylated CSP α appears to be degraded *via* the proteasome. Similar observations have also been reported in other NCL diseases. Actually, Cln6 protein mutants, implicated in late-infantile NCL and autosomal recessive form of adult-NCL (Kufs' disease) (Arsov et al. 2011), are degraded as misfolded proteins *via* the proteasome (Oresic et al. 2009). However, the link between proteasome-mediated degradation of ANCL CSP α protein and lysosomal deposition of fluorescent material is still not well established. The work in this chapter showed an increased presence of ANCL aggregates following MG-132 treatment but it remains to be

seen if this reflects aggregate degradation *via* the proteasome or simply the increased levels of monomeric CSP α leading to increased aggregate formation.

Moreover, considering aggregation of CSP α as the possible cause of ANCL, targeting of the pathway that clears the aggregates from cells might be considered a therapeutic approach for the treatment of the disease. This is the case for other neurodegenerative disorders, such as Alzheimer's disease (Zhu et al. 2013) and Parkinson's disease (Pan et al. 2008).

It will therefore be important in the future to generate more knowledge on the mechanisms facilitating CSP α ubiquitination and triggering CSP α proteasome-mediated degradation, and to interrogate further the mechanisms mediating degradation of palmitoylated monomeric CSP α and the ANCL aggregates.

Chapter 6: General discussion

The main conclusions from this study are: (i) aggregation of disease-causing CSP α mutants can be prevented by substitution of specific cysteine residues; (ii) ANCL mutants exhibit a change in the lifetime of palmitoylated monomers; (iii) the expression of several proteins is altered in ANCL brains and some of these changes are specific to ANCL (e.g. PPT1, α -synuclein), whereas others may occur more generally in neurodegenerative disease (e.g. flotillins); and (iv) non-palmitoylated CSP α is rapidly degraded by the proteasome, potentially as mechanism to limit expression of a cytosolic pool of this protein.

Cysteines 4-7 are essential for aggregation of CSP α mutants that cause ANCL

The first conclusion drawn from this study is that the aggregation of the ANCL-causing CSP α mutants (L115R and Δ L116) can be prevented by substitutions of cysteines 4 to 7 in the cysteine-string domain (CSD), thus indicating that these palmitoylated cysteines are central to the formation of high molecular weight SDS-resistant aggregates.

Other cysteines within the CSD were also substituted, although the effects of this on aggregation were not as pronounced as the substitution of cysteines 4-7. Replacement of cysteines 11-14 was the only cysteine modification that did not have any effect on the aggregation of the ANCL mutants. Replacement of cysteines 1-3 for alanines partially reduced aggregation, however there was no rescue of the palmitoylated monomeric form of the protein. Furthermore, the overall interpretation of these results was difficult since substantial aggregation of the ANCL mutants was still observed and substitution of these cysteines also promoted the formation of aggregates in the wild-type protein. On the other

hand, substitution of cysteines 8 to 10 caused a marked reduction in aggregation while also promoting a change in the palmitoylation profile of the ANCL mutants, which was similar to that seen with C(4-7) substitutions but of smaller magnitude.

Previous research from Greaves and Chamberlain (2006) showed that efficient palmitoylation of the CSD of CSP α is dependent on cysteines 4-7. Indeed, the role of cysteines 4-7 for efficient palmitoylation of the CSD is proposed to be related to a requirement of these cysteines (and their hydrophobic character) for initial membrane binding prior to palmitoylation (Greaves et al. 2008). In order to rule out the possibility that reduced membrane association was the responsible for loss of aggregation of the C(4-7)A protein, these were also replaced with leucines, which allow tighter membrane association of the non-palmitoylated protein (Greaves and Chamberlain 2006). Indeed, it was seen that replacement of cysteines 4-7 by leucines also prevented aggregation. The possibility that substitution of cysteines 4-7 abolished aggregation due to a loss of overall palmitoylation of CSP α (rather than a loss of palmitoylation of only cysteines 4-7) was also tested by treatment with BFA. BFA causes the fusion of the ER and Golgi membranes, thus facilitating palmitoylation of the C(4-7)L mutant (Greaves et al. 2008). Interestingly, BFA treatment did not promote aggregation of ANCL CSP α mutants lacking cysteines 4-7, concluding that aggregation of the ANCL mutants is not caused by a complete absence of palmitoylation on the remaining cysteines but rather that cysteines 4-7 are integral to the aggregation process.

Based on the results of the analyses of cysteine substitutions, it is proposed that the palmitoylated cysteines in the central core of the CSD (i.e. cysteines 4 to 10) are responsible for the formation and/or stability of the SDS-resistant aggregates. The ANCL mutations could promote a structural change in the CSD, leading to a change in the folding of the

region containing cysteines 4-7. This structural change could promote the clustering of hydrophobic palmitate chains in the centre of the CSD *via* lipid-lipid interactions, hence preventing correct membrane interactions. Another possibility is the alteration of the overall palmitoylation profile of CSP α by the ANCL mutations. As palmitoylation is important to maintain the correct function and, possibly, membrane topology of the protein, inefficient palmitoylation of certain cysteines within this domain could disrupt correct membrane interactions and, in doing so, lead to aggregation.

Links between palmitoylation and aggregation of the ANCL CSP α mutants

The palmitoylation of the ANCL aggregates and the importance of palmitoylation for formation and stability of these structures was shown by Greaves et al. (2012). However, Greaves et al. (2012) showed that recombinant ANCL CSP α mutants form high molecular weight oligomers *in vitro* in the absence of palmitoylation. It remains to be determined, however, whether the aggregates formed *in vitro* are the same as those that form in cells. Indeed, it has been seen that oligomerisation of wild-type CSP α (which has an intrinsic tendency to self-associate (Swayne et al. 2003)) is limited to the formation of dimers in cells (Chamberlain and Burgoyne 1998), but large high-molecular weight oligomers are formed by bacterially-produced non-palmitoylated CSP α (Swayne et al. 2003). Thus, it will be important in future work to investigate the properties of cellular ANCL CSP α aggregates and *in vitro* aggregates to determine if their properties are the same. As the aggregates formed by the ANCL mutant CSP α in cells are membrane-associated (Greaves et al. 2012), and since membrane association of CSP α is mediated by palmitoylation, it is implied that the aggregates are also palmitoylated. The results of Chapter 4 showing the destabilisation of the ANCL CSP α aggregates in post-mortem ANCL brains treated with hydroxylamine

confirms the observations of Greaves et al. (2012), but contrasts with the results of Zhang and Chandra (2014), who did not see any effect on aggregation upon hydroxylamine treatment. It should be pointed out, though, that the conditions used for hydroxylamine treatment in the work of Zhang and Chandra (2014) were not sufficient to mediate complete depalmitoylation of wild-type CSP α , so it is unclear if closely-packed ANCL mutant aggregates could be effectively depalmitoylated under these same conditions. zDHHC knockdown experiments could provide further insight into the importance of palmitoylation for ANCL CSP α mutant aggregation.

Palmitoylated monomers of ANCL CSP α mutants are more short-lived than monomers of wild-type CSP α

In an effort to uncover further differences between wild-type CSP α and the ANCL mutants, the stability of palmitoylation of these proteins was investigated. This analysis was performed given the almost complete lack of a palmitoylated monomeric pool of the ANCL CSP α mutants. Through click chemistry, the turnover of wild-type CSP α was first investigated. This analysis revealed that, in comparison to SNAP25, the turnover rate of wild-type CSP α was very low and, indeed, undetectable. Thus, it is considered that the wild-type protein is stably palmitoylated.

However, turnover of palmitoylation of the ANCL mutant proteins appeared to be enhanced compared with the wild-type protein. Indeed, there was a marked time-dependent loss of click signal on palmitoylated monomers of the ANCL CSP α mutants, suggesting either that the mutants have a faster rate of depalmitoylation than the wild-type CSP α , or that the palmitoylated monomers are being consumed into high molecular weight

aggregates. Although palmostatin B was employed to try and distinguish between these possibilities, the results were inconclusive.

An important development in the future work will be to determine conditions that lead to disruption of ANCL CSP α aggregates, as this will allow the exact palmitoylation status of incorporated monomers to be examined.

Study of post-mortem brains and aberrant protein expression

The results presented in Chapter 4 of this thesis show that the pathology caused by the *DNAJC5* mutations does not only affect CSP α and that other proteins might also be affected. For instance, upregulation of α -synuclein was found in post-mortem brains from ANCL patients, and this protein is also linked to PD and AD (Singleton et al. 2003; Norris et al. 2004). Moreover, upregulation of flotillin-1 and flotillin-2, found also in PD and AD (Jacobowitz and Kallarakal 2004; John et al. 2014), was a common feature of both ANCL and HD post-mortem brains. Although the potential mechanistic link between different neurodegenerative disorders, such as ANCL and HD, is not clear, the fact that they share common up-regulated proteins might shed light on potential common mechanisms of neurodegeneration.

Perhaps the most compelling finding of the analysis performed on post-mortem brains, however, was the markedly increased expression of PPT1, specifically in ANCL samples (Chapter 4, Henderson et al. (2015)). Indeed, the finding that PPT1 was massively increased in ANCL post-mortem brains emphasised the suggested link between palmitoylation and aggregation of ANCL CSP α mutants. Likewise, this observation is consistent with the

previous proposal by Greaves et al. (2012) that ANCL is associated with accumulation of palmitoylated CSP α aggregates that are, in turn, resistant to PPT1 action.

The findings from analysis of post-mortem tissues allow speculation about the possible role of CSP α mutations in the ANCL disease process. Upregulation of PPT1 is perhaps more suggestive of a toxic gain-of-function effect of mutant CSP α , caused by accumulation of PPT1-resistant aggregates that perturb lysosomal function. In contrast, the increased expression of α -synuclein may arise due to a loss-of-function effect of mutant CSP α , as over-expression of α -synuclein has previously been shown to rescue the neurodegeneration phenotype in CSP α knockout mice; thus, up-regulation of this protein may be a compensatory mechanism to overcome a defect in CSP α function. It will be interesting in future work to try and replicate some of these protein changes in cell models of ANCL, such as neuronal cells engineered to stably over-express ANCL CSP α mutants. This may help to understand the processes leading to altered protein expression patterns. Finally, with respect to the possible gain-of-function effect of ANCL mutant CSP α , it is interesting that Henderson et al. (2015) came to the conclusion that aggregates were unlikely to be toxic to cells as they were only present at very low levels. However it is likely that epitope masking prevents an accurate assessment of aggregate levels in brain and more accurate analysis of the extent of endogenous ANCL mutant CSP α aggregation is an important area of future work.

Non-palmitoylated CSP α is rapidly degraded *via* the proteasome

In Chapter 5 of this thesis, the degradation pathway of CSP α was examined. The experiments performed using different degradation pathway inhibitors showed that both

mutant and wild-type CSP α are degraded by the proteasome. Remarkably, the amount of non-palmitoylated CSP α was significantly increased upon proteasomal inhibition. In contrast, levels of palmitoylated CSP α were largely unaffected by either proteasomal or lysosomal inhibitors. These results suggest that non-palmitoylated protein is rapidly degraded, whereas palmitoylated CSP α is somehow stabilised. As discussed, this system may exist to prevent accumulation of high levels of cytosolic CSP α , which could interfere with cytosolic chaperone complexes.

In spite of intense efforts, a *degron* or sequence for proteasomal degradation was not identified in CSP α . The removal of the C- and N-termini did not alter the MG-132-sensitivity of CSP α , neither did the removal of specific cysteines from the CSD. However, deeper examination into the degradation pathway of CSP α showed that CSP α does not only undergo palmitoylation but also ubiquitination, although, CSP α ubiquitination profile appeared to be non-canonical. While ubiquitination occurs normally on lysines, the lysine-less CSP α mutant (14KR) appeared to be also degraded by the proteasome and showed signs of ubiquitination. Therefore, it is possible that CSP α is ubiquitinated on residues other than lysines. It will be of interest in future work to examine mutants that lack all cysteines in the CSD to rule out any role for cysteines in proteasomal degradation. It will also be important to undertake more detailed mutagenesis to determine whether there are multiple *degrons* in CSP α that need to be collectively removed in order to block proteasomal degradation.

Analysis of the degradation pathways that control CSP α expression levels was initiated with the aim of identifying changes in the turnover of mutant aggregates, which might lead to their accumulation *in vivo*. Although this issue was not resolved within the work performed, it should remain an active area of investigation. It is possible that palmitoylation of CSP α

diverts the protein from a proteasomal degradation pathway towards a slower lysosomal degradation. Lysosomal degradation of palmitoylated CSP α and mutant aggregates would be more consistent with the lysosomal pathology seen in NCL diseases, and so this is an avenue that clearly warrants further study.

Concluding remarks

The correlation between protein aggregation and neurodegeneration is clearly-defined for a number of neurodegenerative disorders, such as AD, PD and HD (Polymenidou and Cleveland 2011). The results presented in this work further emphasise the link between protein aggregation and neurodegeneration. Moreover, a potential common mechanism of aberrant protein expression in different types of neurodegeneration is shown through the study of post-mortem human brains.

The present study extends the work of Greaves et al. (2012), emphasising the relation between palmitoylation and ANCL and expanding on the proposal of targeting the palmitoylation machinery in order to neutralise the effects of the ANCL mutations.

Considering aggregation of CSP α as the cause of ANCL, and zDHHC enzymes as the cause of aggregation of mutant CSP α (*via* palmitoylation), zDHHC enzymes may be considered as potential drug targets for the treatment of the disease. Moreover, having identified 4 cysteines as essential for the aggregation process, further analysis of which zDHHC enzymes palmitoylate cysteines 4 to 7 constitutes a promising research path.

The finding of aberrant expression of PPT1 shows a potential link between the adult and infantile forms of ANCL, as suggested by Henderson et al. (2015). However, further research

on the interactions between CSP α and PPT1 is needed in order to understand how the accumulation of PPT1 might affect the aggregation of ANCL CSP α .

On another hand, while targeting palmitoylation might deliver a higher therapeutic benefit, activation of the ubiquitin-proteasome system could also become an attractive therapeutic target to enhance the turnover of pathogenic CSP α mutants in ANCL brain.

Chapter 7: References

- Abrami, L. et al., 2008. Palmitoylation and ubiquitination regulate exit of the Wnt signaling protein LRP6 from the endoplasmic reticulum. *PNAS*, 105(14), pp.5384–5389.
- Abrami, L., Leppla, S.H. & Gisou Van Der Goot, F., 2006. Receptor palmitoylation and ubiquitination regulate anthrax toxin endocytosis. *Journal of Cell Biology*, 172(2), pp.309–320.
- Abrami, L., Reig, N. & Van Der Goot, F.G., 2005. Anthrax toxin: The long and winding road that leads to the kill. *Trends in Microbiology*, 13(2), pp.72–78.
- Advani, R.J. et al., 1998. Seven novel mammalian SNARE proteins localize to distinct membrane compartments. *Journal of Biological Chemistry*, 273(17), pp.10317–10324.
- Aicart-Ramos, C., Valero, R.A. & Rodriguez-Crespo, I., 2011. Protein palmitoylation and subcellular trafficking. *Biochimica et biophysica acta*, 1808(12), pp.2981–94. Available at: <http://www.ncbi.nlm.nih.gov/pubmed/21819967> [Accessed December 25, 2013].
- Aikawa, Y., Lynch, K.L., et al., 2006. A Second SNARE Role for Exocytic SNAP25 in Endosome Fusion. *Molecular Biology of the Cell*, 17(5), pp.2113–2124.
- Aikawa, Y., Xiaofeng, X. & Martin, F.J.T., 2006. SNAP25, but Not Syntaxin 1A, Recycles via an ARF6-regulated Pathway in Neuroendocrine Cells. *Molecular Biology of the Cell*, 17(2), pp.711–722.
- Anami, K. et al., 2010. Search for transmembrane protein in gastric cancer by the Escherichia coli ampicillin secretion trap: Expression of DSC2 in gastric cancer with

intestinal phenotype. *Journal of Pathology*, 221(3), pp.275–284.

Araki, S. et al., 1990. Regulation of reversible binding of smg p25A, a ras p21-like GTP-binding protein, to synaptic plasma membranes and vesicles by its specific regulatory protein, GDP dissociation inhibitor. *Journal of Biological Chemistry*, 265(22), pp.13007–13015.

Aronin, N. et al., 1995. CAG expansion affects the expression of mutant Huntingtin in the Huntington's disease brain. *Neuron*, 15, pp.1193–1201. Available at: <http://www.sciencedirect.com/science/article/pii/089662739590106X> [Accessed January 5, 2014].

Arsov, T. et al., 2011. Kufs disease, the major adult form of neuronal ceroid lipofuscinosis, caused by mutations in *cln6*. *American Journal of Human Genetics*, 88(5), pp.566–573. Available at: <http://dx.doi.org/10.1016/j.ajhg.2011.04.004>.

Asher, G., Reuven, N. & Shaul, Y., 2006. 20S proteasomes and protein degradation “by default.” *BioEssays*, 28(8), pp.844–849.

Baba, M. et al., 1998. Aggregation of alpha-synuclein in Lewy bodies of sporadic Parkinson's disease and dementia with Lewy bodies. *The American journal of pathology*, 152(4), pp.879–84.

Bai, L., Swayne, L.A. & Braun, J.E.A., 2007. The CSPalpha/G protein complex in PC12 cells. *Biochemical and Biophysical Research Communications*, 352(1), pp.123–129.

Baker, K. et al., 2015. Epilepsy, cognitive deficits and neuroanatomy in males with ZDHHC9 mutations. *Annals of Clinical and Translational Neurology*, 2(5), p.n/a-n/a. Available at:

<http://www.pubmedcentral.nih.gov/articlerender.fcgi?artid=4435709&tool=pmcentrez&rendertype=abstract>.

Banerjee, A. et al., 1996. SNAP-25 is required for a late postdocking step in Ca²⁺-dependent exocytosis. *Journal of Biological Chemistry*, 271(34), pp.20227–20230.

Bark, C., 2004. Developmentally Regulated Switch in Alternatively Spliced SNAP-25 Isoforms Alters Facilitation of Synaptic Transmission. *Journal of Neuroscience*, 24(40), pp.8796–8805. Available at: <http://www.jneurosci.org/cgi/doi/10.1523/JNEUROSCI.1940-04.2004>.

Bence, F.N., Roopal, M.S. & Kopito, R.R., 2001. Impairment of the Ubiquitin-Proteasome System by Protein Aggregation. *Science*, 292(May), pp.1552–1555.

Benitez, B. a et al., 2011. Exome-sequencing confirms DNAJC5 mutations as cause of adult neuronal ceroid-lipofuscinosis. *PloS one*, 6(11), p.e26741. Available at: <http://www.pubmedcentral.nih.gov/articlerender.fcgi?artid=3208569&tool=pmcentrez&rendertype=abstract> [Accessed December 29, 2013].

Bennett, M.K., Calakos, N. & Scheller, R.H., 1992. Syntaxin : A Synaptic Protein Implicated in Docking of Synaptic Vesicles at Presynaptic Active Zones. *Science*, 257(13), pp.255–259.

Berkovic, S.F. et al., 2016. Diagnosis and misdiagnosis of adult neuronal ceroid lipofuscinosis (Kufs disease). *Neurology*, 87(6), pp.579–584.

Betz, A. et al., 1997. Direct Interaction of the Rat unc-13 Homologue Munc13-1 with the N Terminus of Syntaxin Direct Interaction of the Rat unc-13 Homologue Munc13-1 with the N Terminus of Syntaxin. *The Journal of Biological Chemistry*, 272(4), pp.2520–

2526.

Birkenkamp-Demtroder, K. et al., 2002. Gene expression in colorectal cancer. *Cancer Research*, 62(15), pp.4352–4363.

Blackmore, M. & Letourneau, P.C., 2006. L1, beta1 integrin, and cadherins mediate axonal regeneration in the embryonic spinal cord. *Journal of neurobiology*, 66(14), pp.1564–83. Available at: <http://www.ncbi.nlm.nih.gov/pubmed/17058193> [Accessed October 27, 2016].

Blaskovic, S., Blanc, M. & van der Goot, F.G., 2013. What does S-palmitoylation do to membrane proteins? *The FEBS journal*, 280(12), pp.2766–74. Available at: <http://www.ncbi.nlm.nih.gov/pubmed/23551889> [Accessed December 16, 2013].

Boal, F. et al., 2011. A charged prominence in the linker domain of the cysteine-string protein Csp α mediates its regulated interaction with the calcium sensor synaptotagmin 9 during exocytosis. *The FASEB Journal*, 25(1), pp.132–43. Available at: <http://www.ncbi.nlm.nih.gov/pubmed/20847230>.

Boal, F. et al., 2004. The variable C-terminus of cysteine string proteins modulates exocytosis and protein-protein interactions. *Biochemistry*, 43(51), pp.16212–16223.

Bock, J.B. et al., 2001. A genomic perspective on membrane compartment organization. *Nature*, 409(February), pp.839–841.

Bodin, S. et al., 2014. Flotillins in intercellular adhesion - from cellular physiology to human diseases. *Journal of Cell Science*, 127(24), pp.5139–5147. Available at: <http://jcs.biologists.org/cgi/doi/10.1242/jcs.159764>.

- Bork, K. et al., 2015. Neuroprotective and neuroregenerative effects of nimodipine in a model system of neuronal differentiation and neurite outgrowth. *Molecules*, 20(1), pp.1003–1013.
- Bossy-Wetzell, E., Schwarzenbacher, R. & Lipton, S. a, 2004. Molecular pathways to neurodegeneration. *Nature medicine*, 10 Suppl(July), pp.S2–S9.
- Bourdenx, M. et al., 2015. Protein aggregation and neurodegeneration in prototypical neurodegenerative diseases: Examples of amyloidopathies, tauopathies and synucleinopathies. *Progress in Neurobiology*. Available at: <http://dx.doi.org/10.1016/j.pneurobio.2015.07.003>.
- Braun, J.E.A., Wilbanks, S.M. & Scheller, R.H., 1996. The cysteine string secretory vesicle protein activates Hsc70 ATPase. *Journal of Biological Chemistry*, 271(42), pp.25989–25993.
- Brenner, S., 1974. The genetics of *Caenorhabditis elegans*. *Genetics*, 77(1), pp.71–94.
- Brose, N. et al., 1995. Mammalian homologues of *Caenorhabditis elegans* unc-13 gene define novel family of C2-domain proteins. *Journal of Biological Chemistry*, 270(42), pp.25273–25280.
- Brown, H. et al., 1998. Cysteine string protein (CSP) is an insulin secretory granule-associated protein regulating beta-cell exocytosis. *EMBO Journal*, 17(17), pp.5048–5058.
- Burgoyne, R.D. & Morgan, A., 2015. Cysteine string protein (CSP) and its role in preventing neurodegeneration. *Seminars in Cell and Developmental Biology*, 40, pp.153–159. Available at: <http://dx.doi.org/10.1016/j.semcdb.2015.03.008>.

- Burra, G. & Thakur, A.K., 2015. Anhydrous trifluoroacetic acid pretreatment converts insoluble polyglutamine peptides to soluble monomers. *Data in Brief*, 5, pp.1066–1071.
- Burré, J. et al., 2010. Alpha-synuclein promotes SNARE-complex assembly in vivo and in vitro. *Science*, 329(5999), pp.1663–7. Available at: <http://www.sciencemag.org/content/329/5999/1663%5Cnhttp://www.sciencemag.org/content/329/5999/1663.abstract>.
- Cadieux-Dion, M. et al., 2013. Recurrent mutations in DNAJC5 cause autosomal dominant Kufs disease. *Clinical Genetics*, 83(6), pp.571–575.
- Cadwell, K. & Coscoy, L., 2005. Ubiquitination on nonlysine residues by a viral E3 ubiquitin ligase. *Science (New York, N.Y.)*, 309(5731), pp.127–30. Available at: <http://www.ncbi.nlm.nih.gov/pubmed/15994556>.
- Calakos, N. & Scheller, R.H., 1994. Vesicle-associated membrane protein and synaptophysin are associated on the synaptic vesicle. *Journal of Biological Chemistry*, 269(40), pp.24534–24537.
- Camp, L.A. & Hofmann, S.L., 1993. Purification and Properties of a Palmitoyl-Protein Thioesterase That Cleaves Palmitate From H-Ras. *Biochemistry*, 268(30), pp.22566–22574.
- Cao, Y. et al., 2006. Autophagy is disrupted in a knock-in mouse model of juvenile neuronal ceroid lipofuscinosis. *Journal of Biological Chemistry*, 281(29), pp.20483–20493.
- Cárcel-Trullols, J., Kovács, A.D. & Pearce, D.A., 2015. Cell biology of the NCL proteins: What they do and don't do. *Biochimica et Biophysica Acta - Molecular Basis of Disease*,

1852(10), pp.2242–2255. Available at:
<http://dx.doi.org/10.1016/j.bbadis.2015.04.027>.

Carr, C.M. et al., 1999. Sec1p binds to SNARE complexes and concentrates at sites of secretion. *Journal of Cell Biology*, 146(2), pp.333–344.

Chamberlain, L.H. et al., 2001. The synaptic vesicle protein, cysteine-string protein, is associated with the plasma membrane in 3T3-L1 adipocytes and interacts with syntaxin 4. *Journal of cell science*, 114(Pt 2), pp.445–455.

Chamberlain, L.H. & Burgoyne, R.D., 1997. Activation of the ATPase activity of heat-shock proteins Hsc70/Hsp70 by cysteine-string protein. *The Biochemical Journal*, 322, pp.853–8. Available at:
<http://www.pubmedcentral.nih.gov/articlerender.fcgi?artid=1218266&tool=pmcentrez&rendertype=abstract>.

Chamberlain, L.H. & Burgoyne, R.D., 2000. Cysteine-string protein: the chaperone at the synapse. *Journal of neurochemistry*, 74(5), pp.1781–9. Available at:
<http://www.ncbi.nlm.nih.gov/pubmed/10800920>.

Chamberlain, L.H. & Burgoyne, R.D., 1998a. Cysteine string protein functions directly in regulated exocytosis. *Molecular biology of the cell*, 9(8), pp.2259–67. Available at:
<http://www.pubmedcentral.nih.gov/articlerender.fcgi?artid=25479&tool=pmcentrez&rendertype=abstract>.

Chamberlain, L.H. & Burgoyne, R.D., 1996. Identification of a novel cysteine string protein variant and expression of cysteine string proteins in non-neuronal cells. *Journal of Biological Chemistry*, 271(13), pp.7320–7323.

- Chamberlain, L.H. & Burgoyne, R.D., 1998b. The cysteine-string domain of the secretory vesicle cysteine-string protein is required for membrane targeting. *Biochemical Journal*, 335(2), pp.205–209. Available at: <http://www.biochemj.org/bj/335/bj3350205.htm>.
- Chamberlain, L.H., Henry, J. & Burgoyne, R.D., 1996. Cysteine string proteins are associated with chromaffin granules. *Journal of Biological Chemistry*, 271(32), pp.19514–19517.
- Chamberlain, L.H., Robert, D. & Burgoyne, R.D., 1997. The Molecular Chaperone Function of the Secretory Vesicle Cysteine String Proteins The Molecular Chaperone Function of the Secretory Vesicle Cysteine String Proteins *. *Journal of Biological Chemistry*, 272(50), pp.31420–31426. Available at: <file:///E:/luis mayorga/articulos/Chamberlain97.pdf>.
- Chamberlain, L.H. & Shipston, M.J., 2015. The physiology of protein S-acylation. *Physiological reviews*, 95(2), pp.341–76. Available at: <http://physrev.physiology.org/content/95/2/341>.
- Chandra, S. et al., 2005. α -Synuclein cooperates with CSP α in preventing neurodegeneration. *Cell*, 123(3), pp.383–396.
- Chau, V. et al., 1989. A multiubiquitin chain is confined to specific lysine in a targeted short-lived protein. *Cell*, 243(1576–1583).
- Chen, W.Y. et al., 2004. Case-control study and transmission disequilibrium test provide consistent evidence for association between schizophrenia and genetic variation in the 22q11 gene ZDHHC8. *Human Molecular Genetics*, 13(23), pp.2991–2995.
- Cheng, D. et al., 2006. Relative and Absolute Quantification of Postsynaptic Density

Proteome Isolated from Rat Forebrain and Cerebellum. *Molecular & Cellular Proteomics*, 5(6), pp.1158–1170. Available at: <http://www.mcponline.org/cgi/doi/10.1074/mcp.D500009-MCP200>.

Cheng, H. et al., 2009. S-Palmitoylation of gamma-secretase subunits nicastrin and aph-1. *Journal of Biological Chemistry*, 284(3), pp.1373–1384.

Chiang, N. et al., 2014. Phosphomimetic mutation of cysteine string protein-alpha Increases the rate of regulated exocytosis by modulating fusion pore dynamics in PC12 cells. *PLoS ONE*, 9(6), p.e99180.

Chklovskii, D., 2004. Synaptic connectivity and neuronal morphology: two sides of the same coin. , 43, pp.609–617.

Ciechanover, A., 2005. Proteolysis: from the lysosome to ubiquitin and the proteasome. *Nature reviews. Molecular cell biology*, 6(1), pp.79–87.

Coe, J.G. et al., 1999. A role for Tlg1p in the transport of proteins within the Golgi apparatus of *Saccharomyces cerevisiae*. *Molecular biology of the cell*, 10(July), pp.2407–2423.

Cooper, J.D., Russell, C. & Mitchison, H.M., 2006. Progress towards understanding disease mechanisms in small vertebrate models of neuronal ceroid lipofuscinosis. *Biochimica et Biophysica Acta - Molecular Basis of Disease*, 1762(10), pp.873–889.

Coppola, T. & Gundersen, C., 1996. Widespread expression of human cysteine string proteins. *FEBS Letters*, 391(3), pp.269–272.

Cotman, S.L. et al., 2013. Neuronal ceroid lipofuscinosis: Impact of recent genetic advances and expansion of the clinicopathologic spectrum topical collection on genetics.

Dekker, F.J. et al., 2010. Small-molecule inhibition of APT1 affects Ras localization and signaling. *Nature Chemical Biology*, 6(6), pp.449–456. Available at: <http://dx.doi.org/10.1038/nchembio.362><http://www.nature.com/doi/finder/10.1038/nchembio.362>.

Dice, J.F., 1990. Peptide sequences that target cytosolic proteins for lysosomal proteolysis. *Science*, 15(8), pp.305–309.

Diez-Ardanuy, C. et al., 2017. A cluster of palmitoylated cysteines are essential for aggregation of cysteine-string protein mutants that cause neuronal ceroid lipofuscinosis. *Scientific Reports*, 7(January), pp.1–10. Available at: <http://dx.doi.org/10.1038/s41598-017-00036-8>.

Donnelier, J. et al., 2015. Increased Expression of the Large Conductance, Calcium-Activated K⁺ (BK) Channel in Adult-Onset Neuronal Ceroid Lipofuscinosis. *PLoS One*, 10(4), p.e0125205. Available at: <http://www.ncbi.nlm.nih.gov/pubmed/25905915>.

Drisdell, R.C. & Green, W.N., 2004. Labeling and quantifying sites of protein palmitoylation. *BioTechniques*, 36(2), pp.276–285.

Dulubova, I. et al., 2007. Munc18-1 binds directly to the neuronal SNARE complex. *PNAS*, 104(8), pp.2697–2702. Available at: http://www.ncbi.nlm.nih.gov/entrez/query.fcgi?cmd=Retrieve&db=PubMed&dopt=Citation&list_uids=17301226<http://www.pnas.org/content/104/8/2697.full.pdf>.

Duncan, J.A. & Gilman, A.G., 2002. Characterization of *Saccharomyces cerevisiae* acyl-protein thioesterase 1, the enzyme responsible for G protein alpha subunit

- deacylation in vivo. *Journal of Biological Chemistry*, 277(35), pp.31740–31752.
- Duncan, J. a & Gilman, A.G., 1998. A Cytoplasmic Acyl-Protein Thioesterase A Cytoplasmic Acyl-Protein Thioesterase That Removes Palmitate from G Protein alpha Subunits and p21 RAS. *Journal of Biological Chemistry*, 273(25), pp.15830–15837.
- Dyson, H.J. & Wright, P.E., 2005. Intrinsically unstructured proteins and their functions. *Nature reviews. Molecular cell biology*, 6(3), pp.197–208.
- Edelmann, L. et al., 1995. Synaptobrevin binding to synaptophysin: a potential mechanism for controlling the exocytotic fusion machine. *The EMBO journal*, 14(2), pp.224–31.
- Ehrnhoefer, D.E., Sutton, L. & Hayden, M.R., 2011. Small changes, big impact: posttranslational modifications and function of huntingtin in Huntington disease. *The Neuroscientist : a review journal bringing neurobiology, neurology and psychiatry*, 17(5), pp.475–92.
- El-Husseini, A.E.D. et al., 2002. Synaptic strength regulated by palmitate cycling on PSD-95. *Cell*, 108(6), pp.849–863.
- Englund, P., 1993. The structure and biosynthesis of glycosyl phosphatidylinositol protein anchors. *Annu Rev Biochemistry*, 62, pp.121–138.
- Erales, J. & Coffino, P., 2014. Ubiquitin-independent proteasomal degradation. *Biochimica et Biophysica Acta - Molecular Cell Research*, 1843(1), pp.216–221.
- Evans, G.J.O. et al., 2001. Phosphorylation of cysteine string protein by protein kinase A: Implications for the modulation of exocytosis. *Journal of Biological Chemistry*, 276(51), pp.47877–47885.

- Evans, G.J.O. et al., 2006. Protein kinase B/Akt is a novel cysteine string protein kinase that regulates exocytosis release kinetics and quantal size. *Journal of Biological Chemistry*, 281(3), pp.1564–1572.
- Evans, G.J.O. & Morgan, A., 2002. Phosphorylation-dependent interaction of the synaptic vesicle proteins cysteine string protein and synaptotagmin I. *The Biochemical Journal*, 364(2), pp.343–7. Available at: <http://www.pubmedcentral.nih.gov/articlerender.fcgi?artid=1222577&tool=pmcentrez&rendertype=abstract>.
- Evans, G.J.O., Morgan, A. & Burgoyne, R.D., 2003. Tying everything together: the multiple roles of cysteine string protein (CSP) in regulated exocytosis. *Traffic*, 4(10), pp.653–9.
- Fasshauer, D. et al., 1997. A structural change occurs upon binding of syntaxin to SNAP-25. *Journal of Biological Chemistry*, 272(7), pp.4582–4590.
- Fasshauer, D. et al., 1998. Conserved structural features of the synaptic fusion complex: SNARE proteins reclassified as Q- and R-SNAREs. *Proceedings of the National Academy of Sciences of the United States of America*, 95(26), pp.15781–6. Available at: <http://www.pubmedcentral.nih.gov/articlerender.fcgi?artid=28121&tool=pmcentrez&rendertype=abstract>.
- Fernández-Chacón, R. et al., 2004. The synaptic vesicle protein CSP α prevents presynaptic degeneration. *Neuron*, 42(2), pp.237–251.
- Fernandez, I. et al., 2001. Three-dimensional structure of the synaptotagmin 1 C2B-domain: Synaptotagmin 1 as a phospholipid binding machine. *Neuron*, 32(6), pp.1057–1069.
- Fischer von Mollard, G., Südhof, T.C. & Jahn, R., 1991. A small GTP-binding protein

- dissociates from synaptic vesicles during exocytosis. *Nature*, 349(6304), pp.79–81.
- Flaumenhaft, R. et al., 2007. SNAP-23 and syntaxin-2 localize to the extracellular surface of the platelet plasma membrane. *Blood*, 110(5), pp.1492–1501.
- Fontaine, S.N. et al., 2016. DnaJ / Hsc 70 chaperone complexes control the extracellular release of neurodegenerative- associated proteins. *The EMBO journal*, 35(14), pp.1–13.
- Fortmann, K.T. et al., 2015. A Regulated, Ubiquitin-Independent Degron in I κ B α . *Journal of molecular biology*, 427(17), pp.2748–56. Available at: <http://www.ncbi.nlm.nih.gov/pubmed/26191773>.
- Fukata, M. et al., 2004. Identification of PSD-95 palmitoylating enzymes. *Neuron*, 44(6), pp.987–996.
- Fukata, Y. & Fukata, M., 2010. Protein palmitoylation in neuronal development and synaptic plasticity. *Nature reviews. Neuroscience*, 11(3), pp.161–75. Available at: <http://www.ncbi.nlm.nih.gov/pubmed/20168314> [Accessed December 13, 2013].
- Gao, X. & Hannoush, R.N., 2014. Single-cell imaging of Wnt palmitoylation by the acyltransferase porcupine. , 10(january).
- Gao, Y. et al., 2000. Inhibition of ubiquitin-proteasome pathway-mediated I kappa B alpha degradation by a naturally occurring antibacterial peptide. *The Journal of clinical investigation*, 106(3), pp.439–48. Available at: <http://www.jci.org/articles/view/9826>.
- Geppert, M. et al., 1994. Synaptotagmin I: A major Ca²⁺ sensor for transmitter release at a central synapse. *Cell*, 79(4), pp.717–727.

- Geraets, R.D. et al., 2016. Moving towards effective therapeutic strategies for Neuronal Ceroid Lipofuscinosis. *Orphanet journal of rare diseases*, 11(1), p.40. Available at: <http://ojrd.biomedcentral.com/articles/10.1186/s13023-016-0414-2>.
- Gestwicki, J.E. & Garza, D., 2012. *Protein quality control in neurodegenerative disease* 1st ed., Elsevier Inc. Available at: <http://dx.doi.org/10.1016/B978-0-12-385883-2.00003-5>.
- Glebov, O.O., Bright, N. a & Nichols, B.J., 2006. Flotillin-1 defines a clathrin-independent endocytic pathway in mammalian cells. *Nature Cell Biology*, 8(1), pp.46–54. Available at: <http://www.nature.com/doifinder/10.1038/ncb1342>.
- Gordon, J., Shohreh, A. & White, K.M., 2013. General overview of neuronal cell culture. *Methods Mol Biol*, 1078, pp.9–21. Available at: <http://link.springer.com/10.1007/978-1-62703-640-5>.
- Gordon, S.L., Leube, R.E. & Cousin, M. a., 2011. Synaptophysin Is Required for Synaptobrevin Retrieval during Synaptic Vesicle Endocytosis. *Journal of Neuroscience*, 31(39), pp.14032–14036. Available at: <http://www.jneurosci.org/content/31/39/14032.full>.
- Gorleku, O. a et al., 2011. Endoplasmic reticulum localization of DHHC palmitoyltransferases mediated by lysine-based sorting signals. *The Journal of biological chemistry*, 286(45), pp.39573–84.
- Greaves, J. et al., 2012. Palmitoylation-induced aggregation of cysteine-string protein mutants that cause neuronal ceroid lipofuscinosis. *The Journal of biological chemistry*, 287(44), pp.37330–9.
- Greaves, J. et al., 2008. Palmitoylation and membrane interactions of the neuroprotective

chaperone cysteine-string protein. *The Journal of biological chemistry*, 283(36), pp.25014–26. Available at:

<http://www.pubmedcentral.nih.gov/articlerender.fcgi?artid=2882233&tool=pmcentrez&rendertype=abstract> [Accessed December 29, 2013].

Greaves, J. et al., 2010. Palmitoylation of the SNAP25 protein family: specificity and regulation by DHHC palmitoyl transferases. *The Journal of biological chemistry*, 285(32), pp.24629–38. Available at:

<http://www.pubmedcentral.nih.gov/articlerender.fcgi?artid=2915699&tool=pmcentrez&rendertype=abstract> [Accessed January 6, 2014].

Greaves, J. et al., 2009. The Hydrophobic Cysteine-rich Domain of SNAP25 Couples with Downstream Residues to Mediate Membrane Interactions and Recognition by DHHC Palmitoyl Transferases. *Molecular Biology of the Cell*, 20, pp.1845–1854.

Greaves, J. & Chamberlain, L.H., 2011a. DHHC palmitoyl transferases: substrate interactions and (patho)physiology. *Trends in biochemical sciences*, 36(5), pp.245–53. Available at: <http://www.ncbi.nlm.nih.gov/pubmed/21388813> [Accessed December 29, 2013].

Greaves, J. & Chamberlain, L.H., 2011b. Differential palmitoylation regulates intracellular patterning of SNAP25. *Journal of cell science*, 124(Pt 8), pp.1351–1360.

Greaves, J. & Chamberlain, L.H., 2006. Dual Role of the Cysteine-String Domain in Membrane Binding and Palmitoylation-dependent Sorting of the Molecular Chaperone Cysteine-String Protein. *Molecular Biology of the Cell*, 17(November), pp.4748–4759.

Greaves, J. & Chamberlain, L.H., 2007. Palmitoylation-dependent protein sorting. *The*

Journal of cell biology, 176(3), pp.249–54. Available at: <http://www.pubmedcentral.nih.gov/articlerender.fcgi?artid=2063950&tool=pmcentrez&rendertype=abstract> [Accessed December 29, 2013].

Greene, L.A. & Tischler, A.S., 1976. Establishment of a noradrenergic clonal line of rat adrenal pheochromocytoma cells which respond to nerve growth factor. *Proceedings of the National Academy of Sciences of the United States of America*, 73(7), pp.2424–8.

Grice, G.L. & Nathan, J.A., 2016. The recognition of ubiquitinated proteins by the proteasome. *Cellular and Molecular Life Sciences*, 73(3), pp.3497–3506. Available at: <http://link.springer.com/10.1007/s00018-016-2255-5>.

Grosshans, B.L., Ortiz, D. & Novick, P., 2006. Rabs and their effectors: achieving specificity in membrane traffic. *Proceedings of the National Academy of Sciences of the United States of America*, 103(32), pp.11821–7. Available at: <http://www.ncbi.nlm.nih.gov/pubmed/16882731>.

Guan, R., Dai, H. & Rizo, J., 2008. Binding of the Munc13-1 MUN Domain to Membrane-Anchored SNARE complexes. *Biochemistry*, (6), pp.1474–1481.

Gundersen, C.B. et al., 1994. Extensive lipidation of a Torpedo cysteine string protein. *Journal of Biological Chemistry*, 269(30), pp.19197–19199.

Gundersen, C.B. & Umbach, J.A., 1992. Suppression cloning of the cDNA for a candidate subunit of a presynaptic calcium channel. *Neuron*, 9(3), pp.527–537.

Gundersen, C.B., Umbach, J.A. & Mastrogiacomo, A., 1996. Cysteine-string protein: a cycle of acylation and deacylation? *Life Sciences*, 58(22), pp.2037–2040.

- Haltia, M. et al., 1973. Infantile type of so-called neuronal ceroid-lipofuscinosis. *J Neurol Sci*, 18(3), pp.269–285. Available at: <http://www.ncbi.nlm.nih.gov/pubmed/4121459>.
- Haltia, M., 2006. The neuronal ceroid-lipofuscinoses: From past to present. *Biochimica et Biophysica Acta - Molecular Basis of Disease*, 1762(10), pp.850–856.
- Haltia, M. & Goebel, H.H., 2013. The neuronal ceroid-lipofuscinoses: A historical introduction. *Biochimica et Biophysica Acta - Molecular Basis of Disease*, 1832(11), pp.1795–1800. Available at: <http://dx.doi.org/10.1016/j.bbadis.2012.08.012>.
- Hang, H.C. & Linder, M.E., 2011. Exploring protein lipidation with chemical biology. *Chemical Reviews*, 111, pp.6341–6358.
- Hansen, C.G. & Nichols, B.J., 2009. Molecular mechanisms of clathrin-independent endocytosis. *Journal of Cell Science*, 122(11), pp.1713–1721. Available at: <http://jcs.biologists.org/cgi/doi/10.1242/jcs.033951>.
- Hardy, J. & Selkoe, D.J., 2002. The amyloid hypothesis of Alzheimer's disease: progress and problems on the road to therapeutics. *Science (New York, N.Y.)*, 297(5580), pp.353–356. Available at: <http://www.ncbi.nlm.nih.gov/pubmed/12130773>.
- Hata, Y., Slaughter, C.A. & Sudhof, T.C., 1993. Synaptic vesicle fusion complex contains unc-18 homologue bound to syntaxin. *Nature*, 366, pp.347–366.
- Hayashi, T. et al., 1994. Synaptic vesicle membrane fusion complex: action of clostridial neurotoxins on assembly. *The EMBO journal*, 13(21), pp.5051–61. Available at: <http://www.pubmedcentral.nih.gov/articlerender.fcgi?artid=395451&tool=pmcentrez&rendertype=abstract>.

- He, Y. & Linder, M.E., 2009. Differential palmitoylation of the endosomal SNAREs syntaxin 7 and syntaxin 8. , 50.
- Heindel, U., Schmidt, M.F.G. & Veit, M., 2003. Palmitoylation sites and processing of synaptotagmin I, the putative calcium sensor for neurosecretion. *FEBS Letters*, 544(1–3), pp.57–62.
- Hellsten, E. et al., 1993. Refined assignment of the infantile neuronal ceroid lipofuscinosis (INCL, CLN1) locus at 1p32: incorporation of linkage disequilibrium in multipoint analysis. *Genomics*, 16(3), pp.720–725.
- Hellsten, E. et al., 1993. Refined Assignment of the Infantile Neuronal Ceroid Lipofuscinosis (INCL, CLN1) Locus at 1p32: Incorporation of Linkage Disequilibrium in Multipoint Analysis. *Genomics*, 16(3), pp.720–725.
- Henderson, M.X. et al., 2015. Neuronal ceroid lipofuscinosis with DNAJC5/CSPa mutation has PPT1 pathology and exhibit aberrant protein palmitoylation. *Acta Neuropathologica*, pp.1–17.
- Henderson, M.X. et al., 2016. Neuronal ceroid lipofuscinosis with DNAJC5/CSPalpha mutation has PPT1 pathology and exhibit aberrant protein palmitoylation. *Acta Neuropathologica*, 131(4), pp.621–637.
- Hershko, A. et al., 1984. ATP-dependent degradation of ubiquitin-protein conjugates. *Proc Natl Acad Sci U S A*, 81(6), pp.1619–1623. Available at: http://www.ncbi.nlm.nih.gov/entrez/query.fcgi?cmd=Retrieve&db=PubMed&dopt=Citation&list_uids=6324208 %5Cnfile:///Users/nrehjerpe/Documents/Papers2/Articles/1984/Hershko/HershkoProc Natl Acad Sci U S AATP-dependent degradation of

ubiquitin-protein conjugates1.

Hershko, A. et al., 1980. Proposed role of ATP in protein breakdown: conjugation of protein with multiple chains of the polypeptide of ATP-dependent proteolysis. *Proceedings of the National Academy of Sciences of the United States of America*, 77(4), pp.1783–6.

Hershko, A. & Aaron, C., 1998. The Ubiquitin System. *Annu. Rev. Biochem.*, 67, pp.425–479.

Hosono, R., Sassa, T. & Kuno, S., 1987. Mutations affecting acetylcholine levels in the nematode *Caenorhabditis elegans*. *J Neurochem*, 49, pp.1820–1823. Available at: http://www.ncbi.nlm.nih.gov/entrez/query.fcgi?cmd=Retrieve&db=PubMed&dopt=Citation&list_uids=3681298.

Huang, K. et al., 2004. Huntingtin-interacting protein HIP14 is a palmitoyl transferase involved in palmitoylation and trafficking of multiple neuronal proteins. *Neuron*, 44(6), pp.977–86. Available at: <http://www.ncbi.nlm.nih.gov/pubmed/15603740>.

Huang, K. et al., 2011. Wild-type HTT modulates the enzymatic activity of the neuronal palmitoyl transferase HIP14. *Human molecular genetics*, 20(17), pp.3356–65.

Humbert, S. et al., 2002. The IGF-1/Akt pathway is neuroprotective in Huntington's disease and involves huntingtin phosphorylation by Akt. *Developmental Cell*, 2(6), pp.831–837.

Ishida, T. & Kinoshita, K., 2007. PrDOS: Prediction of disordered protein regions from amino acid sequence. *Nucleic Acids Research*, 35(SUPPL.2), pp.460–464.

Jacobowitz, D.M. & Kallarakal, A.T., 2004. Flotillin-1 in the substantia Nigra of the Parkinson brain and a predominant localization in catecholaminergic nerves in the rat brain. *Neurotoxicity Research*, 6(4), pp.245–257.

- Jahn, R. & Fasshauer, D., 2012. Molecular machines governing exocytosis of synaptic vesicles. *Nature*, 490(7419), pp.201–207. Available at: <http://dx.doi.org/10.1038/nature11320>.
- Jahn, R., Lang, T. & Südhof, T.C., 2003. Membrane fusion. *Cell*, 112(4), pp.519–533.
- Jalanko, A. & Braulke, T., 2009. Neuronal ceroid lipofuscinoses. *Biochimica et biophysica acta*, 1793(4), pp.697–709. Available at: <http://www.ncbi.nlm.nih.gov/pubmed/19084560> [Accessed December 19, 2013].
- John, B.A. et al., 2014. Flotillins bind to the dileucine sorting motif of β -site amyloid precursor protein-cleaving enzyme 1 and influence its endosomal sorting. *FEBS Journal*, 281(8), pp.2074–2087.
- Kaether, C., Haass, C. & Steiner, H., 2006. Assembly, trafficking and function of gamma-secretase. *Neurodegenerative Diseases*, 3(4–5), pp.275–283.
- Kang, J.U. et al., 2008. Gain at chromosomal region 5p15.33, containing TERT, is the most frequent genetic event in early stages of non-small cell lung cancer. *Cancer Genetics and Cytogenetics*, 182(1), pp.1–11.
- Kang, R. et al., 2008. Neural palmitoyl-proteomics reveals dynamic synaptic palmitoylation. *Nature*, 456(7224), pp.904–909. Available at: <http://dx.doi.org/10.1038/nature07605>.
- Kang, R. et al., 2004. Presynaptic trafficking of synaptotagmin I is regulated by protein palmitoylation. *Journal of Biological Chemistry*, 279(48), pp.50524–50536.
- Kanno, E. & Fukuda, M., 2008. Increased plasma membrane localization of O-glycosylation-deficient mutant of synaptotagmin I in PC12 cells. *Journal of Neuroscience Research*,

86(5), pp.1036–1043.

Kashyap, S.S. et al., 2014. *Caenorhabditis elegans* dnj-14, the orthologue of the DNAJC5 gene mutated in adult onset neuronal ceroid lipofuscinosis, provides a new platform for neuroprotective drug screening and identifies a SIR-2.1-independent action of resveratrol. *Human Molecular Genetics*, 23(22), pp.5916–5927.

Klausner, R.D., Donaldson, J.G. & Lippincott-Schwartz, J., 1992. Brefeldin A: Insights into the control of membrane traffic and organelle structure. *Journal of Cell Biology*, 116(5), pp.1071–1080.

Kmoch, S. et al., 2013. Bioinformatic perspectives in the neuronal ceroid lipofuscinoses. *Biochimica et Biophysica Acta - Molecular Basis of Disease*, 1832, pp.1831–1841.

Kollmann, K. et al., 2013. Cell biology and function of neuronal ceroid lipofuscinosis-related proteins. *Biochimica et Biophysica Acta - Molecular Basis of Disease*, 1832(11), pp.1866–81. Available at: <http://www.ncbi.nlm.nih.gov/pubmed/23402926> [Accessed December 16, 2013].

Kousi, M., Lehesjoki, A.E. & Mole, S.E., 2012. Update of the mutation spectrum and clinical correlations of over 360 mutations in eight genes that underlie the neuronal ceroid lipofuscinoses. *Human Mutation*, 33(1), pp.42–63.

Kravtsova-Ivantsiv, Y. & Ciechanover, a., 2012. Non-canonical ubiquitin-based signals for proteasomal degradation. *Journal of Cell Science*, 125(3), pp.539–548.

Krüger, R. et al., 1998. Ala30Pro mutation in the gene encoding alpha-synuclein in Parkinson's disease. *Nature genetics*, 18(2), pp.106–108.

- Kumar, V. et al., 2016. Protein aggregation and neurodegenerative diseases: From theory to therapy. *European Journal of Medicinal Chemistry*. Available at: <http://dx.doi.org/10.1016/j.ejmech.2016.07.054>.
- Lam, K.K.Y. et al., 2006. Palmitoylation by the DHHC protein Pfa4 regulates the ER exit of Chs3. *Journal of Cell Biology*, 174(1), pp.19–25.
- Lawrence, G.W., Weller, U. & Dolly, J.O., 1994. Botulinum A and the light chain of tetanus toxins inhibit distinct stages of Mg-ATP-dependent catecholamine exocytosis from permeabilised chromaffin cells. *European Journal of Biochemistry*, 222(2), pp.325–333.
- Lemonidis, K., Sanchez-Perez, M.C. & Chamberlain, L.H., 2015. Identification of a novel sequence motif recognized by the ankyrin repeat domain of zDHHC17/13 S-acyltransferases. *Journal of Biological Chemistry*, 290(36), pp.21939–21950.
- Leveque, C. et al., 1998. Interaction of cysteine string proteins with the α 1A Subunit of the P/Q-type calcium channel. *Journal of Biological Chemistry*, 273(22), pp.13488–13492.
- Lilienbaum, A., 2013. Relationship between the proteasomal system and autophagy. *International Journal of Biochemistry and Molecular Biology*, 4(1), pp.1–26.
- Lin, D.T.S. & Conibear, E., 2015. Enzymatic protein depalmitoylation by acyl protein thioesterases. *Biochemical Society transactions*, 43(2), pp.193–8. Available at: <http://www.ncbi.nlm.nih.gov/pubmed/25849916>.
- Lin, F. & Qin, Z.-H., 2013. Degradation of misfolded proteins by autophagy: is it a strategy for Huntington's disease treatment? *Journal of Huntington's disease*, 2(2), pp.149–57. Available at: <http://www.ncbi.nlm.nih.gov/pubmed/25063512>.

- Lin, R.C. & Scheller, R.H., 2000. Mechanisms of synaptic vesicle exocytosis. *Annu Rev Cell Dev Biol*, 16, pp.19–49.
- Lin, R.C. & Scheller, R.H., 1997. Structural organization of the synaptic exocytosis core complex. *Neuron*, 19(5), pp.1087–1094.
- Linder, M.E. & Deschenes, R.J., 2007. Palmitoylation: policing protein stability and traffic. *Nature reviews. Molecular cell biology*, 8(1), pp.74–84. Available at: <http://www.nature.com/nrm/journal/v8/n1/full/nrm2084.html?ref=SevSevil.Com?message=remove&ref=SevSevil.Com>.
- Liu, H. et al., 2002. Genetic variation in the 22q11 locus and susceptibility to schizophrenia. *Proceedings of the National Academy of Sciences of the United States of America*, 99(26), pp.16859–16864.
- Lobo, S. et al., 2002. Identification of a Ras palmitoyltransferase in *Saccharomyces cerevisiae*. *The Journal of biological chemistry*, 277(43), pp.41268–73. Available at: <http://www.ncbi.nlm.nih.gov/pubmed/12193598> [Accessed January 4, 2014].
- Ma, C. et al., 2011. Munc13 mediates the transition from the closed syntaxin-Munc18 complex to the SNARE complex. *Nature structural & molecular biology*, 18(5), pp.542–9. Available at: <http://dx.doi.org/10.1038/nsmb.2047>.
- Macdonald, M.E. et al., 1993. A Novel Gene Containing a Trinucleotide That Is Expanded and Unstable on Huntington ' s Disease Chromosomes. *Cell*, 72, pp.971–983.
- Magga, J.M. et al., 2000. Cysteine string protein regulates G protein modulation of N-type calcium channels. *Neuron*, 28(1), pp.195–204. Available at: http://www.sciencedirect.com/science?_ob=GatewayURL&_origin=inwardhub&_urlv

ersion=4&_method=citationSearch&_piikey=S0896627300000969&_version=1&md5=161e4eb5a86286eeee624e2b9fe64ff1%5Cnpapers3://publication/uuid/784A1E06-D2F6-4EC3-B107-D4FF4187AF0F.

Majd, S., Power, J.H. & Grantham, H.J.M., 2015. Neuronal response in Alzheimer's and Parkinson's disease: the effect of toxic proteins on intracellular pathways. *BMC neuroscience*, 16, p.69. Available at: <http://www.pubmedcentral.nih.gov/articlerender.fcgi?artid=4619058&tool=pmcentrez&rendertype=abstract>.

Mansilla, F. et al., 2007. Differential expression of DHH9 in microsatellite stable and instable human colorectal cancer subgroups. *British journal of cancer*, 96(12), pp.1896–1903.

Mansouri, M.R. et al., 2005. Loss of ZDHH15 expression in a woman with a balanced translocation t(X;15)(q13.3;cen) and severe mental retardation. *European journal of human genetics : EJHG*, 13(8), pp.970–977.

Martens, S., Kozlov, M.M. & McMahon, H.T., 2007. How synaptotagmin promotes membrane fusion. *Science*, 316(5828), pp.1205–1208. Available at: http://www.ncbi.nlm.nih.gov/entrez/query.fcgi?cmd=Retrieve&db=PubMed&dopt=Citation&list_uids=17478680.

Martin, B.R. & Cravatt, B.F., 2009. Large-Scale Profiling of Protein Palmitoylation in Mammalian Cells. *Nature Methods*, 6(2), pp.135–138.

Martin, J.A. et al., 2011. Complexin has opposite effects on two modes of synaptic vesicle fusion. *Current Biology*, 21(2), pp.97–105. Available at:

<http://dx.doi.org/10.1016/j.cub.2010.12.014>.

Martin, L., Latypova, X. & Terro, F., 2011. Neurochemistry International Post-translational modifications of tau protein : Implications for Alzheimer ' s disease. *Neurochemistry International*, 58(4), pp.458–471. Available at: <http://dx.doi.org/10.1016/j.neuint.2010.12.023>.

Mastrogiacomo, A. et al., 1998. A Xenopus cysteine string protein with a cysteine residue in the J domain. *Biochimica et Biophysica Acta - Molecular Cell Research*, 1401(3), pp.239–241.

Mastrogiacomo, A. et al., 1994. Cysteine string proteins: a potential link between synaptic vesicles and presynaptic Ca²⁺ channels. *Science*, 263, pp.981–982.

Mastrogiacomo, A. & Gundersen, C.B., 1995. The nucleotide and deduced amino acid sequence of a rat cysteine string protein. *Molecular Brain Research*, 28(1), pp.12–18.

McCue, H. V et al., 2015. Expression profile of a Caenorhabditis elegans model of adult neuronal ceroid lipofuscinosis reveals down regulation of ubiquitin E3 ligase components. *Scientific reports*, 5(April), p.14392. Available at: <http://www.pubmedcentral.nih.gov/articlerender.fcgi?artid=4585785&tool=pmcentrez&rendertype=abstract>.

McDowell, G.S. & Philpott, A., 2013. Non-canonical ubiquitylation: Mechanisms and consequences. *International Journal of Biochemistry and Cell Biology*, 45(8), pp.1833–1842. Available at: <http://dx.doi.org/10.1016/j.biocel.2013.05.026>.

McKinnon, C. & Tabrizi, S.J., 2014. The Ubiquitin-Proteasome System in Neurodegeneration. *Antioxidants & redox signaling*, 0(0), pp.1–20. Available at:

<http://www.ncbi.nlm.nih.gov/pubmed/24437518>.

McMahon, H.T. & Sudhof, T.C., 1995. Synaptic core complex of synaptobrevin, syntaxin, and SNAP25 forms high affinity alpha-SNAP binding site. *Journal of Biological Chemistry*, 270(5), pp.2213–2217.

Meckler, X. et al., 2010. Reduced Alzheimer's disease β -amyloid deposition in transgenic mice expressing S-palmitoylation-deficient A β 1-42 and nicastrin. *Journal of Neuroscience*, 30(48), pp.16160–16169. Available at: <http://www.pubmedcentral.nih.gov/articlerender.fcgi?artid=2999009&tool=pmcentrez&rendertype=abstract>.

Medine, C.N. et al., 2007. Munc18-1 prevents the formation of ectopic SNARE complexes in living cells. *Journal of cell science*, 120, pp.4407–4415.

Metcalf, D.J. et al., 2012. Autophagy and misfolded proteins in neurodegeneration. *Experimental Neurology*, 238(1), pp.22–28. Available at: <http://dx.doi.org/10.1016/j.expneurol.2010.11.003>.

Millar, T., Walker, T., Arango, J-C., Ironside, J.W., Harrison, D.J., MacIntyre, D.J., Blackwood, D., Smith, C., Bell, J., 2007. Tissue and organ donation for research in forensic pathology: the MRC Sudden Death Brain and Tissue Bank. *The Journal of pathology*, 213(September), pp.369–375.

Miller, L.C. et al., 2003. Cysteine String Protein (CSP) Inhibition of N-type Calcium Channels Is Blocked by Mutant Huntingtin. *Journal of Biological Chemistry*, 278(52), pp.53072–53081.

Milnerwood, A.J. et al., 2013. Memory and synaptic deficits in Hip14/DHHC17 knockout

mice. *Proceedings of the National Academy of Sciences of the United States of America*, 110(50), pp.20296–20301. Available at: <http://eutils.ncbi.nlm.nih.gov/entrez/eutils/elink.fcgi?dbfrom=pubmed&id=24277827&retmode=ref&cmd=prlinks%5Cnpapers3://publication/doi/10.1073/pnas.1222384110>.

Mink, J.W. et al., 2013. Classification and natural history of the neuronal ceroid lipofuscinoses. *Journal of Child Neurology*, 28(9), pp.1101–5. Available at: <http://www.ncbi.nlm.nih.gov/pubmed/23838030> [Accessed December 11, 2013].

Mitchell, D.A. et al., 2014. Mutations in the X-linked intellectual disability gene, zDHHC9, alter autopalmitoylation activity by distinct mechanisms. *Journal of Biological Chemistry*, 289(26), pp.18582–18592.

Mitchell, D. a et al., 2006. Protein palmitoylation by a family of DHHC protein S-acyltransferases. *Journal of lipid research*, 47(6), pp.1118–27. Available at: <http://www.ncbi.nlm.nih.gov/pubmed/16582420> [Accessed December 13, 2013].

Mizumaru, C. et al., 2009. Suppression of APP-containing vesicle trafficking and production of β -amyloid by AID/DHHC-12 protein. *Journal of Neurochemistry*, 111(5), pp.1213–1224.

Mole, S.E. & Cotman, S.L., 2015. Genetics of the neuronal ceroid lipofuscinoses (Batten disease). *Biochimica et Biophysica Acta - Molecular Basis of Disease*, 1852(10), pp.2237–2241. Available at: <http://dx.doi.org/10.1016/j.bbadis.2015.05.011>.

Montecucco, C., Schiavo, G. & Pantano, S., 2005. SNARE complexes and neuroexocytosis: How many, how close? *Trends in Biochemical Sciences*, 30(7), pp.367–372.

- Mukai, J. et al., 2004. Evidence that the gene encoding ZDHHC8 contributes to the risk of schizophrenia. *Nature Genetics*, 36(7), pp.725–731. Available at: <http://www.ncbi.nlm.nih.gov/pubmed/15184899> <http://www.nature.com/doi/10.1038/ng1375>.
- Mukai, J. et al., 2008. Palmitoylation-dependent neurodevelopmental deficits in a mouse model of the 22q11 microdeletion. *Nature Neuroscience*, 11(11), pp.1302–1310.
- Nadolski, M.J. & Linder, M.E., 2007. Protein lipidation. *The FEBS journal*, 274(20), pp.5202–10. Available at: <http://www.ncbi.nlm.nih.gov/pubmed/17892486> [Accessed December 13, 2013].
- Navone, F. et al., 1986. Protein p38: An integral membrane protein specific for small vesicles of neurons and neuroendocrine cells. *Journal of Cell Biology*, 103(6 I), pp.2511–2527.
- Neverman, N.J. et al., 2015. Experimental therapies in the neuronal ceroid lipofuscinoses. *Biochimica et Biophysica Acta - Molecular Basis of Disease*, 1852(10), pp.2292–2300. Available at: <http://dx.doi.org/10.1016/j.bbadis.2015.04.026>.
- Nie, Z. et al., 1999. Overexpression of cysteine-string proteins in Drosophila reveals interactions with syntaxin. *Journal of Neuroscience*, 19(23), pp.10270–10279. Available at: http://www.ncbi.nlm.nih.gov/entrez/query.fcgi?cmd=Retrieve&db=PubMed&dopt=Citation&list_uids=10575024.
- Norris, E.H., Giasson, B.I. & Lee, V.M.-Y., 2004. Alpha-synuclein: normal function and role in neurodegenerative diseases. *Current topics in developmental biology*, 60, pp.17–54.

Nosková, L. et al., 2011. Mutations in DNAJC5, encoding cysteine-string protein alpha, cause autosomal-dominant adult-onset neuronal ceroid lipofuscinosis. *American journal of human genetics*, 89(2), pp.241–52. Available at: <http://www.pubmedcentral.nih.gov/articlerender.fcgi?artid=3155175&tool=pmcentrez&rendertype=abstract> [Accessed December 12, 2013].

Ohno, Y. et al., 2006. Intracellular localization and tissue-specific distribution of human and yeast DHHC cysteine-rich domain-containing proteins. *Biochimica et biophysica acta*, 1761(4), pp.474–83. Available at: <http://www.ncbi.nlm.nih.gov/pubmed/16647879> [Accessed June 10, 2014].

Ohyama, T. et al., 2007. Huntingtin-interacting protein 14, a palmitoyl transferase required for exocytosis and targeting of CSP to synaptic vesicles. *The Journal of cell biology*, 179(7), pp.1481–96. Available at: <http://www.pubmedcentral.nih.gov/articlerender.fcgi?artid=2373489&tool=pmcentrez&rendertype=abstract> [Accessed December 16, 2013].

Oo, H.Z. et al., 2014. Overexpression of ZDHHC14 promotes migration and invasion of scirrhous type gastric cancer. *Oncology Reports*, 32(1), pp.403–410.

Oresic, K., Mueller, B. & Tortorella, D., 2009. Cln6 mutants associated with neuronal ceroid lipofuscinosis are degraded in a proteasome-dependent manner. *Bioscience reports*, 29(3), pp.173–81. Available at: <http://www.pubmedcentral.nih.gov/articlerender.fcgi?artid=2674128&tool=pmcentrez&rendertype=abstract>.

Ota, V.K. et al., 2013. ZDHHC8 gene may play a role in cortical volumes of patients with schizophrenia. *Schizophrenia Research*, 145(1–3), pp.33–35. Available at:

<http://dx.doi.org/10.1016/j.schres.2013.01.011>.

Otto, G.P. & Nichols, B.J., 2011. The roles of flotillin microdomains - endocytosis and beyond. *Journal of Cell Science*, 124(23), pp.3933–3940.

Palmer, D.N. et al., 1986. Ceroid Lipofuscinosis in Sheep. *The Journal of biological chemistry*, 261(4), pp.1766–1772.

Palmer, D.N. et al., 2013. NCL disease mechanisms. *Biochimica et biophysica acta*, 1832(11), pp.1882–93. Available at: <http://www.ncbi.nlm.nih.gov/pubmed/23707513> [Accessed December 16, 2013].

Pan, T. et al., 2008. The role of autophagy-lysosome pathway in neurodegeneration associated with Parkinson's disease. *Brain*, 131(8), pp.1969–1978.

Patel, P. et al., 2016. Phosphorylation of Cysteine String Protein Triggers a Major Conformational Switch. *Structure*, 24(8), pp.1380–1386. Available at: <http://linkinghub.elsevier.com/retrieve/pii/S0969212616301344>.

Pennuto, M., Palazzolo, I. & Poletti, A., 2009. Post-translational modifications of expanded polyglutamine proteins : impact on neurotoxicity. *Human Molecular Genetics*, 18(1), pp.40–47.

Perin, M.S. et al., 1990. Phospholipid binding by a synaptic vesicle protein homologous to the regulatory region of protein kinase C. *Nature*, 345(18), pp.260–263. Available at: <http://www.ncbi.nlm.nih.gov/pubmed/16290341><http://link.springer.com/10.1007/BF01177222><http://linkinghub.elsevier.com/retrieve/pii/0021979780905019><http://scitation.aip.org/content/aip/journal/pof2/10/9/10.1063/1.869740><http://www.sciencedire>.

- Pickart, C.M., 2001. Mechanisms underlying ubiquitination. *Annual Review of Biochemistry*, 70(1), pp.503–33. Available at: <http://www.ncbi.nlm.nih.gov/pubmed/11583613>.
- Poirier, M.A. et al., 1998. The synaptic SNARE complex is a parallel four-stranded helical bundle. *Nat. Struct. Biol.*, 5(9), pp.765–769. Available at: <http://www.ncbi.nlm.nih.gov/pubmed/9731768>.
- Polymenidou, M. & Cleveland, D.W., 2011. The seeds of neurodegeneration: Prion-like spreading in ALS. *Cell*, 147(3), pp.498–508. Available at: <http://dx.doi.org/10.1016/j.cell.2011.10.011>.
- Polymeropoulos, M.H. et al., 1997. Mutation in the α -Synuclein Gene Identified in Families with Parkinson's Disease. *Science*, 276(June), pp.2045–2047.
- Prakash, S. et al., 2004. An unstructured initiation site is required for efficient proteasome-mediated degradation. *Nature structural & molecular biology*, 11(9), pp.830–837.
- Prescott, G.R. et al., 2009. Palmitoylation of the synaptic vesicle fusion machinery. *Journal of Neurochemistry*, 110(4), pp.1135–1149.
- Prescott, G.R. et al., 2008. Phosphorylation of cysteine string protein on Serine 10 triggers 14-3-3 protein binding. *Biochemical and Biophysical Research Communications*, 377(3), pp.809–814. Available at: <http://dx.doi.org/10.1016/j.bbrc.2008.10.069>.
- Prilusky, J. et al., 2005. FoldIndex(c): A simple tool to predict whether a given protein sequence is intrinsically unfolded. *Bioinformatics*, 21(16), pp.3435–3438.
- Ramakrishnan, N.A., Drescher, M.J. & Drescher, D.G., 2012. The SNARE complex in neuronal and sensory cells. *Mol Cell Neurosci.*, 50(1), pp.58–69.

Ravichandran, V., Chawla, A. & Roche, P.A., 1996. Identification of a novel syntaxin- and synaptobrevin/VAMP-binding protein, SNAP-23, expressed in non-neuronal tissues. *The Journal of Biological Chemistry*, 271(23), pp.13300–13303. Available at: <http://eutils.ncbi.nlm.nih.gov/entrez/eutils/elink.fcgi?dbfrom=pubmed&id=8663154&retmode=ref&cmd=prlinks%0Apapers2://publication/uuid/E3307C36-78F5-492E-9DD4-CE7D23DF9582>.

Raymond, F.L. et al., 2007. Mutations in ZDHHC9, which encodes a palmitoyltransferase of NRAS and HRAS, cause X-linked mental retardation associated with a Marfanoid habitus. *American journal of human genetics*, 80(5), pp.982–987. Available at: <http://linkinghub.elsevier.com/retrieve/pii/S0002929707609549%5Cpapers3://publication/doi/10.1086/513609>.

Rechsteiner, M. & Rogers, S.W., 1996. PEST sequences and regulation by proteolysis. *Trends in Biochemical Sciences*, 21(7), pp.267–271.

Reggiori, F. & Pelham, H.R.B., 2002. A transmembrane ubiquitin ligase required to sort membrane proteins into multivesicular bodies. *Nature Cell Biology*, 4(2), pp.117–123. Available at: <http://www.nature.com/doi/10.1038/ncb743%5Cpapers3://publication/doi/10.1038/ncb743>.

Reim, K. et al., 2001. Complexins regulate a late step in Ca²⁺-dependent neurotransmitter release. *Cell*, 104(1), pp.71–81.

Ren, R. et al., 2014. Proteomics of protein post-translational modifications implicated in neurodegeneration. *Translational Neurodegeneration*, 3(23), pp.1–13.

- Resh, M.D., 2013. Covalent Lipid Modifications of Proteins. *Curr Biol*, 10(23), pp.431–435.
- Resh, M.D., 2006. Palmitoylation of ligands, receptors, and intracellular signaling molecules. *Science's STKE : signal transduction knowledge environment*, 2006(359), p.re14.
Available at: <http://www.ncbi.nlm.nih.gov/pubmed/17077383>.
- Rice, P., Ian, L. & Bleasby, A., 2000. The European Molecular Biology Open Software Suite
EMBOSS: The European Molecular Biology Open Software Suite. *Trends in genetics : TIG*, 16(6), pp.276–277.
- Rickman, C. et al., 2007. Functionally and Spatially Distinct Modes of munc18-Syntaxin 1 Interaction *. *Journal of Biological Chemistry*, 282(16), pp.12097–12103.
- Rizo, J. & Xu, J., 2015. The Synaptic Vesicle Release Machinery. *Annual Review of Biophysics*, 44(1), pp.339–367. Available at:
<http://www.annualreviews.org/doi/abs/10.1146/annurev-biophys-060414-034057>.
- Rocks, O. et al., 2005. An Acylation Cycle Regulates Localization and Activity of Palmitoylated Ras Isoforms. *Science*, 307(5716), pp.1746–1752. Available at:
<http://www.sciencemag.org/cgi/doi/10.1126/science.1105654>.
- Rocks, O. et al., 2010. The palmitoylation machinery is a spatially organizing system for peripheral membrane proteins. *Cell*, 141(3), pp.458–471.
- Rogers, S., Wells, R. & Rechsteiner, M., 1986. Acid Sequences Common to Rapidly Degraded Proteins : The PEST Hypothesis. *Science*, 234, pp.364–368.
- Rossetto, O. et al., 1996. Vamp/synaptobrevin isoforms 1 and 2 are widely and differentially expressed in nonneuronal tissues. *Journal of Cell Biology*, 132(1–2), pp.167–179.

- Roth, A.F. et al., 2006. Global analysis of protein palmitoylation in yeast. *Cell*, 125(5), pp.1003–13. Available at: <http://www.pubmedcentral.nih.gov/articlerender.fcgi?artid=2246083&tool=pmcentrez&rendertype=abstract> [Accessed December 21, 2013].
- Roth, A.F. et al., 2002. The yeast DHHC cysteine-rich domain protein Akr1p is a palmitoyl transferase. *The Journal of cell biology*, 159(1), pp.23–8. Available at: <http://www.pubmedcentral.nih.gov/articlerender.fcgi?artid=2173492&tool=pmcentrez&rendertype=abstract> [Accessed January 4, 2014].
- Rubinsztein, D.C., 2006. The roles of intracellular protein-degradation pathways in neurodegeneration. *Nature*, 443(7113), pp.780–786.
- Sabatini, B.L. & Regehr, W.G., 1996. Timing of neurotransmission at fast synapses in the mammalian brain. *Nature*, 384, pp.170–172.
- Sadler, J.B.A., Bryant, N.J. & Gould, G.W., 2015. Characterization of VAMP isoforms in 3T3-L1 adipocytes: implications for GLUT4 trafficking. *Molecular biology of the cell*, 26(3), pp.530–6. Available at: <http://www.pubmedcentral.nih.gov/articlerender.fcgi?artid=4310743&tool=pmcentrez&rendertype=abstract>.
- Sadoul, K. et al., 1995. SNAP-25 is expressed in islets of Langerhans and is involved in insulin release. *Journal of Cell Biology*, 128(6), pp.1019–1028.
- Sagné, C. et al., 1996. SDS-resistant aggregation of membrane proteins: application to the purification of the vesicular monoamine transporter. *The Biochemical journal*, 316 (Pt 3, pp.825–831.

- Salaun, C., Greaves, J. & Chamberlain, L.H., 2010. The intracellular dynamic of protein palmitoylation. *The Journal of cell biology*, 191(7), pp.1229–38. Available at: <http://www.pubmedcentral.nih.gov/articlerender.fcgi?artid=3010063&tool=pmcentrez&rendertype=abstract> [Accessed December 29, 2013].
- Salek, R.M. et al., 2011. A metabolomic comparison of mouse models of the Neuronal Ceroid Lipofuscinoses. *Journal of biomolecular NMR*, 49(3–4), pp.175–84. Available at: <http://www.ncbi.nlm.nih.gov/pubmed/21461951> [Accessed May 18, 2011].
- Sander, L.E. et al., 2008. Vesicle associated membrane protein (VAMP)-7 and VAMP-8, but not VAMP-2 or VAMP-3, are required for activation-induced degranulation of mature human mast cells. *European Journal of Immunology*, 38(3), pp.855–863.
- Sanders, S.S. & Hayden, M.R., 2015. Aberrant palmitoylation in Huntington disease. *Biochemical Society Transactions*, 43(2), pp.205–210.
- Schägger, H. & von Jagow, G., 1987. Tricine-sodium dodecyl sulfate-polyacrylamide gel electrophoresis for the separation of proteins in the range from 1 to 100 kDa. *Analytical biochemistry*, 166(2), pp.368–379.
- Scheper, W. & Hoozemans, J.J.M., 2015. The unfolded protein response in neurodegenerative diseases: a neuropathological perspective. *Acta Neuropathologica*, 130(3), pp.315–331.
- Schiavo, G. et al., 1997. Binding of the synaptic vesicle v-SNARE, synaptotagmin, to the plasma membrane t-SNARE, SNAP-25, can explain docked vesicles at neurotoxin-treated synapses. *Proceedings of the National Academy of Sciences of the United States of America*, 94(3), pp.997–1001.

- Schiavo, G., Matteoli, M. & Montecucco, C., 2000. Neurotoxins affecting neuroexocytosis. *Physiological reviews*, 80(2), pp.717–766.
- Schmidt, B.Z. et al., 2009. Cysteine string protein promotes proteasomal degradation of the cystic fibrosis transmembrane conductance regulator (CFTR) by increasing its interaction with the C terminus of Hsp70-interacting protein and promoting CFTR ubiquitylation. *Journal of Biological Chemistry*, 284(7), pp.4168–4178.
- Schmidt, M.F. & Schlesinger, M.J., 1979. Fatty acid binding to vesicular stomatitis virus glycoprotein: a new type of post-translational modification of the viral glycoprotein. *Cell*, 17(4), pp.813–819. Available at: <http://eutils.ncbi.nlm.nih.gov/entrez/eutils/elink.fcgi?dbfrom=pubmed&id=226266&retmode=ref&cmd=prlinks%5Cnpapers3://publication/uuid/43DFB3A5-F83B-42B8-A2B1-9EEBD6BD928B>.
- Schmitz, F. et al., 2006. CSPalpha-deficiency causes massive and rapid photoreceptor degeneration. *PNAS*, 103(8), pp.2926–31. Available at: <http://www.pubmedcentral.nih.gov/articlerender.fcgi?artid=1413794&tool=pmcentrez&rendertype=abstract>.
- Schneider-poetsch, T. et al., 2010. Inhibition of Eukaryotic Translation Elongation by Cycloheximide and Lactimidomycin. *Nature Chemical Biology*, 6(3), pp.209–217.
- Schneider, A. et al., 2008. Flotillin-Dependent Clustering of the Amyloid Precursor Protein Regulates Its Endocytosis and Amyloidogenic Processing in Neurons. *Journal of Neuroscience*, 28(11), pp.2874–2882. Available at: <http://www.jneurosci.org/cgi/doi/10.1523/JNEUROSCI.5345-07.2008>.

- Schoch, S., 2001. SNARE Function Analyzed in Synaptobrevin/VAMP Knockout Mice. *Science*, 294(5544), pp.1117–1122. Available at: <http://www.sciencemag.org/cgi/doi/10.1126/science.1064335>.
- Schulz, A. et al., 2013. NCL diseases - clinical perspectives. *Biochimica et biophysica acta*, 1832(11), pp.1801–6. Available at: <http://www.sciencedirect.com/science/article/pii/S0925443913001324>.
- Shafer, T.J. & Atchison, W.D., 1991. Transmitter, ion channel and receptor properties of pheochromocytoma (PC12) cells: a model for neurotoxicological studies. *Neurotoxicology*, 12(3), pp.473–92.
- Sharma, M., Burré, J., Bronk, P., et al., 2012. CSP α knockout causes neurodegeneration by impairing SNAP-25 function. *The EMBO journal*, 31(4), pp.829–41. Available at: <http://www.pubmedcentral.nih.gov/articlerender.fcgi?artid=3280561&tool=pmcentrez&rendertype=abstract> [Accessed December 18, 2013].
- Sharma, M., Burré, J. & Südhof, T.C., 2011. CSP α promotes SNARE-complex assembly by chaperoning SNAP-25 during synaptic activity. *Nature cell biology*, 13(1), pp.30–9. Available at: <http://www.ncbi.nlm.nih.gov/pubmed/21151134> [Accessed February 21, 2014].
- Sharma, M., Burré, J. & Südhof, T.C., 2012. Proteasome inhibition alleviates SNARE-dependent neurodegeneration. *Science translational medicine*, 4(147), p.147ra113. Available at: <http://www.ncbi.nlm.nih.gov/pubmed/22896677>.
- Sharp, A.H. & Ross, C.A., 1996. Neurobiology of Huntington's disease. *Neurobiology of Disease*, 3, pp.3–15.

- Shen, J. et al., 2007. Selective Activation of Cognate SNAREpins by Sec1 / Munc18 Proteins. *Cell*, 1, pp.183–195.
- Shirley, R.B. et al., 2005. Combination of Proteasomal Inhibitors Lactacystin and MG132 Induced Synergistic Apoptosis in Prostate Cancer Cells. *Neoplasia*, 7(12), pp.1104–1111. Available at: <http://www.ingentaselect.com/rpsv/cgi-bin/cgi?ini=xref&body=linker&reqdoi=10.1593/neo.05520>.
- Siintola, E. et al., 2006. Cathepsin D deficiency underlies congenital human neuronal ceroid-lipofuscinosis. *Brain*, 129(6), pp.1438–1445.
- Singaraja, R.R. et al., 2011. Altered palmitoylation and neuropathological deficits in mice lacking HIP14. *Human molecular genetics*, 20(20), pp.3899–909. Available at: <http://www.pubmedcentral.nih.gov/articlerender.fcgi?artid=3177655&tool=pmcentrez&rendertype=abstract> [Accessed January 5, 2014].
- Singaraja, R.R. et al., 2002. HIP14, a novel ankyrin domain-containing protein, links huntingtin to intracellular trafficking and endocytosis. *Human molecular genetics*, 11(23), pp.2815–28.
- Singleton, a B. et al., 2003. a-Synuclein Locus Triplication Causes Parkinson's Disease. *Science*, 302(October), p.841.
- Siniosoglou, S. & Pelham, H.R.B., 2001. An effector of Ypt6p binds the SNARE Tlg1p and mediates selective fusion of vesicles with late golgi membranes. *EMBO Journal*, 20(21), pp.5991–5998.
- Smith, K.R. et al., 2013. Cathepsin F mutations cause Type B Kufs disease, an adult-onset neuronal ceroid lipofuscinosis. *Human Molecular Genetics*, 22(7), pp.1417–1423.

- Smith, K.R. et al., 2012. Strikingly different clinicopathological phenotypes determined by progranulin-mutation dosage. *American Journal of Human Genetics*, 90(6), pp.1102–1107. Available at: <http://dx.doi.org/10.1016/j.ajhg.2012.04.021>.
- Sollner, Bennett, M.K., et al., 1993. A Protein Assembly-Disassembly Pathway In Vitro That May Correspond to Sequential Steps of Synaptic Vesicle Docking , Activation , and Fusion. *Cell*, 75, pp.409–418.
- Sollner, Whiteheart, S.W., et al., 1993. SNAP receptors implicated in vesicle targeting and fusion. *Nature*, 362, pp.318–324.
- De Souza, R.A.G. & Leavitt, B.R., 2014. Neurobiology of Huntington’s Disease. *Current Topics in Behavioral Neurosciences*, (22), pp.81–100. Available at: http://link.springer.com/chapter/10.1007/7854_2011_176.
- Soyombo, A.A. & Hofmann, S.L., 1997. Molecular cloning and expression of palmitoyl-protein thioesterase 2 (PPT2), a homolog of lysosomal palmitoyl-protein thioesterase with a distinct substrate specificity. *Journal of Biological Chemistry*, 272(43), pp.27456–27463.
- Spillantini, M.G. et al., 1997. Alpha-synuclein in Lewy bodies. *Nature*, 388(6645), pp.839–840.
- Stahl, B., Tobaben, S. & Südhof, T.C., 1999. Two distinct domains in hsc70 are essential for the interaction with the synaptic vesicle cysteine string protein. *European Journal of Cell Biology*, 78(6), pp.375–81. Available at: <http://www.ncbi.nlm.nih.gov/pubmed/10430018>.
- Steegmaier, M. et al., 1999. Vesicle-associated membrane protein 4 is implicated in trans-

Golgi network vesicle trafficking. *Molecular biology of the cell*, 10(6), pp.1957–72.

Available at:

[http://www.pubmedcentral.nih.gov/articlerender.fcgi?artid=25394&tool=pmcentrez
&rendertype=abstract.](http://www.pubmedcentral.nih.gov/articlerender.fcgi?artid=25394&tool=pmcentrez&rendertype=abstract)

Steinfeld, R. et al., 2006. Cathepsin D deficiency is associated with a human neurodegenerative disorder. *American journal of human genetics*, 78(6), pp.988–998.

Available at:

[http://www.pubmedcentral.nih.gov/articlerender.fcgi?artid=1474096&tool=pmcentrez
&rendertype=abstract.](http://www.pubmedcentral.nih.gov/articlerender.fcgi?artid=1474096&tool=pmcentrez&rendertype=abstract)

Stowers, R.S. & Isacoff, E.Y., 2007. Drosophila huntingtin-interacting protein 14 is a presynaptic protein required for photoreceptor synaptic transmission and expression of the palmitoylated proteins synaptosome-associated protein 25 and cysteine string protein. *The Journal of neuroscience: the official journal of the Society for Neuroscience*, 27(47), pp.12874–12883.

Sudhof, T.C. et al., 1989. A Synaptic Vesicle Membrane-Protein Is Conserved from Mammals to Drosophila. *Neuron*, 2(5), pp.1475–1481.

Südhof, T.C., 2013. Neurotransmitter release: The last millisecond in the life of a synaptic vesicle. *Neuron*, 80(3), pp.675–690.

Südhof, T.C., 2004. The Synaptic Vesicle Cycle. *Annual Review of Neuroscience*, 27(1), pp.509–547. Available at:

[http://www.annualreviews.org/doi/10.1146/annurev.neuro.26.041002.131412.](http://www.annualreviews.org/doi/10.1146/annurev.neuro.26.041002.131412)

Suh, Y.H. et al., 2010. A neuronal role for SNAP-23 in postsynaptic glutamate receptor

trafficking. *Nature Neuroscience*, 13(3), pp.338–343.

Sutton, L.M. et al., 2013. Hip14l-deficient mice develop neuropathological and behavioural features of Huntington disease. *Human molecular genetics*, 22(3), pp.452–65. Available at: <http://www.ncbi.nlm.nih.gov/pubmed/23077216> [Accessed January 5, 2014].

Sutton, R.B. et al., 1998. Crystal structure of a SNARE complex involved in synaptic exocytosis at 2.4 Å resolution. *Nature*, 395(6700), pp.347–353. Available at: http://www.ncbi.nlm.nih.gov/entrez/query.fcgi?cmd=Retrieve&db=PubMed&dopt=Citation&list_uids=9759724<http://www.nature.com/nature/journal/v395/n6700/pdf/395347a0.pdf>.

Swarthout, J.T. et al., 2005. DHHC9 and GCP16 constitute a human protein fatty acyltransferase with specificity for H- and N-Ras. *Journal of Biological Chemistry*, 280(35), pp.31141–31148.

Swayne, L.A. et al., 2003. Oligomerization characteristics of cysteine string protein. *Biochemical and Biophysical Research Communications*, 300(4), pp.921–926.

Tait, S.W.G. et al., 2007. Apoptosis induction by Bid requires unconventional ubiquitination and degradation of its N-terminal fragment. *Journal of Cell Biology*, 179(7), pp.1453–1466.

Takada, R. et al., 2006. Monounsaturated Fatty Acid Modification of Wnt Protein : Its Role in Wnt Secretion. , pp.791–801.

Takalo, M. et al., 2013. Protein aggregation and degradation mechanisms in neurodegenerative diseases. *American journal of neurodegenerative disease*, 2(1),

pp.1–14. Available at:
<http://www.pubmedcentral.nih.gov/articlerender.fcgi?artid=3601466&tool=pmcentrez&rendertype=abstract>.

Takamori, S. et al., 2006. Molecular Anatomy of a Trafficking Organelle. *Cell*, 127(4), pp.831–846.

Takeichi, M., 2007. The cadherin superfamily in neuronal connections and interactions. *Nature reviews. Neuroscience*, 8(1), pp.11–20.

Teng, F.Y., Wang, Y. & Tang, B.L., 2001. The syntaxins. *Genome biology*, 2(11), p.3012.1-3012.7.

The International Batten Disease Consortium, 1995. Isolation of a novel gene underlying Batten disease, CLN3. The International Batten Disease Consortium. *Cell*, 82(6), pp.949–957.

Thelen, M. et al., 2012. Disruption of the autophagy-lysosome pathway is involved in neuropathology of the nclf mouse model of neuronal ceroid lipofuscinosis. *PLoS ONE*, 7(4), pp.1–10.

Thomas, G. et al., 2012. Palmitoylation by DHHC5/8 Targets GRIP1 to Dendritic Endosomes to Regulate AMPA-R Trafficking. *Neuron*, 73(3), pp.482–496. Available at:
<http://dx.doi.org/10.1016/j.neuron.2011.11.021>.

Tian, L. et al., 2012. Distinct acyl protein transferases and thioesterases control surface expression of calcium-activated potassium channels. *Journal of Biological Chemistry*, 287(18), pp.14718–14725.

- Tiwari, S.S. et al., 2015. Evidence that the presynaptic vesicle protein CSPalpha is a key player in synaptic degeneration and protection in Alzheimer's disease. *Molecular brain*, 8(1), p.6. Available at: <http://www.molecularbrain.com/content/8/1/6>.
- Tobaben, S. et al., 2001. A trimeric protein complex functions as a synaptic chaperone machine. *Neuron*, 31(6), pp.987–999.
- Togashi, H. et al., 2002. Cadherin regulates dendritic spine morphogenesis. *Neuron*, 35(1), pp.77–89.
- Tomatis, V.M. et al., 2010. Acyl-protein thioesterase 2 catalyzes the deacylation of peripheral membrane-associated GAP-43. *PLoS ONE*, 5(11).
- Topinka, J.R. & Brecht, D.S., 1998. N-terminal palmitoylation of PSD-95 regulates association with cell membranes and interaction with K⁺ channel K(v)1.4. *Neuron*, 20(1), pp.125–134.
- Trimble, W.S., Cowan, D.M. & Scheller, R.H., 1988. VAMP-1: a synaptic vesicle-associated integral membrane protein. *Proceedings of the National Academy of Sciences of the United States of America*, 85(12), pp.4538–42. Available at: <http://www.pubmedcentral.nih.gov/articlerender.fcgi?artid=280466&tool=pmcentrez&rendertype=abstract>.
- Triola, G., Waldmann, H. & Hedberg, C., 2012. Chemical biology of lipidated proteins. *ACS chemical biology*, 7(1), pp.87–99. Available at: <http://www.ncbi.nlm.nih.gov/pubmed/22148864>.
- Ubach, J. et al., 1998. Ca²⁺ binding to synaptotagmin: How many Ca²⁺ ions bind to the tip of a C2-domain? *EMBO Journal*, 17(14), pp.3921–3930.

- Umbach, J.A. et al., 1994. Presynaptic dysfunction in drosophila csp mutants. *Neuron*, 13(4), pp.899–907.
- Valdez-Taubas, J. & Pelham, H., 2005. Swf1-dependent palmitoylation of the SNARE Tlg1 prevents its ubiquitination and degradation. *The EMBO journal*, 24(14), pp.2524–32. Available at: <http://www.pubmedcentral.nih.gov/articlerender.fcgi?artid=1176453&tool=pmcentrez&rendertype=abstract>.
- Valtorta, F. et al., 2004. Synaptophysin: Leading actor or walk-on role in synaptic vesicle exocytosis? *BioEssays*, 26(4), pp.445–453.
- Varshavsky, A., 1997. The ubiquitin system. *Trends in Biochemical Sciences*, 22, pp.383–387.
- Veit, M., Becher, A. & Ahnert-Hilger, G., 2000. Synaptobrevin 2 is palmitoylated in synaptic vesicles prepared from adult, but not from embryonic brain. *Molecular and Cellular Neuroscience*, 15(4), pp.408–416.
- Veit, M., Söllner, T.H. & Rothman, J.E., 1996. Multiple palmitoylation of synaptotagmin and the t-SNARE SNAP-25. *FEBS Letters*, 385(1–2), pp.119–123.
- Velinov, M. et al., 2012. Mutations in the gene DNAJC5 cause autosomal dominant Kufs disease in a proportion of cases: study of the Parry family and 8 other families. *PLoS one*, 7(1), p.e29729. Available at: <http://www.pubmedcentral.nih.gov/articlerender.fcgi?artid=3250487&tool=pmcentrez&rendertype=abstract> [Accessed December 18, 2013].
- Verkruyse, L.A. & Hofmann, S.L., 1996. Lysosomal targeting of palmitoyl-protein thioesterase. *Journal of Biological Chemistry*, 271(26), pp.15831–15836.

- Vesa, J. et al., 1995. Mutations in the palmitoyl protein thioesterase gene causing infantile neuronal ceroid lipofuscinosis. *Nature*, 376, pp.584–587.
- Vicente Miranda, H., El-Agnaf, O.M.A. & Outeiro, T.F., 2016. Glycation in Parkinson's disease and Alzheimer's disease. *Movement Disorders*, 31(6), pp.782–790.
- Voges, D., Zwickl, P. & Baumeister, W., 1999. The 26S Proteasome : a Molecular Machine Designed for Controlled Proteolysis. *Annual review of biochemistry*, 68, pp.1015–1068. Available at: http://apps.webofknowledge.com/full_record.do?product=UA&search_mode=GeneralSearch&qid=2&SID=U1zLqPOC7sAhhkRZ8lz&page=1&doc=2.
- Vosper, J.M.D. et al., 2009. Ubiquitylation on canonical and non-canonical sites targets the transcription factor neurogenin for ubiquitin-mediated proteolysis. *Journal of Biological Chemistry*, 284(23), pp.15458–15468.
- Wang, X. et al., 2014. Dysregulation of protein trafficking in neurodegeneration. *Mol Neurodegener*, 9(1), p.31. Available at: <http://www.ncbi.nlm.nih.gov/pubmed/25152012>.
- Wang, Y., Lin, F. & Qin, Z.H., 2010. The role of post-translational modifications of huntingtin in the pathogenesis of Huntington's disease. *Neuroscience Bulletin*, 26(2), pp.153–162.
- Warrier, V., Vieira, M. & Mole, S.E., 2013. Genetic basis and phenotypic correlations of the neuronal ceroid lipofusinoses. *Biochimica et Biophysica Acta - Molecular Basis of Disease*, 1832, pp.1827–1830.
- Washbourne, P. et al., 2002. Genetic ablation of the t-SNARE SNAP-25 distinguishes mechanisms of neuroexocytosis. *Nature Neuroscience*, 5(1), pp.19–26. Available at:

<http://www.ncbi.nlm.nih.gov/pubmed/11753414>.

- Washbourne, P., Schiavo, G. & Montecucco, C., 1995. Vesicle-associated membrane protein-2 (synaptobrevin-2) forms a complex with synaptophysin. *The Biochemical journal*, 305, pp.721–724.
- Weber, T. et al., 1998. SNAREpins: Minimal machinery for membrane fusion. *Cell*, 92(6), pp.759–772.
- Weimbs, T. et al., 1997. A conserved domain is present in different families of vesicular fusion proteins : A new superfamily. *PNAS*, 94, pp.3046–3051.
- Wiedenmann, B. & Franke, W.W., 1985. Identification and localization of synaptophysin, an integral membrane glycoprotein of Mr 38,000 characteristic of presynaptic vesicles. *Cell*, 41(3), pp.1017–1028.
- Williams, R.E. & Mole, S.E., 2012. New nomenclature and classification scheme for the neuronal ceroid lipofuscinoses. *Neurology*, 79(2), pp.183–191.
- Wong, S.H. et al., 1998. Endobrevin, a novel synaptobrevin/VAMP-like protein preferentially associated with the early endosome. *Molecular biology of the cell*, 9(June), pp.1549–1563.
- Wu, M.N. et al., 1999. Syntaxin 1A interacts with multiple exocytic proteins to regulate neurotransmitter release in vivo. *Neuron*, 23(3), pp.593–605.
- Xu, J., Mashimo, T. & Südhof, T.C., 2007. Synaptotagmin-1, -2, and -9: Ca²⁺ Sensors for Fast Release that Specify Distinct Presynaptic Properties in Subsets of Neurons. *Neuron*, 54(4), pp.567–581.

- Xu, M., St Clair, D. & He, L., 2010. Testing for genetic association between the ZDHHC8 gene locus and susceptibility to schizophrenia: An integrated analysis of multiple datasets. *American Journal of Medical Genetics, Part B: Neuropsychiatric Genetics*, 153(7), pp.1266–1275.
- Xu, Y., Su, L. & Rizo, J., 2010. Binding of Munc18-1 to synaptobrevin and to the SNARE four-helix bundle. *Biochemistry*, 49(8), pp.1568–1576.
- Yamamoto, Y. et al., 2007. Gain of 5p15.33 is associated with progression of bladder cancer. *Oncology*, 72(1–2), pp.132–138.
- Yan, S.-M. et al., 2013. Reduced expression of ZDHHC2 is associated with lymph node metastasis and poor prognosis in gastric adenocarcinoma. *PloS one*, 8(2), p.e56366. Available at: <http://www.pubmedcentral.nih.gov/articlerender.fcgi?artid=3574152&tool=pmcentrez&rendertype=abstract>.
- Yanai, A. et al., 2006. Palmitoylation of huntingtin by HIP14 is essential for its trafficking and function. *Nature neuroscience*, 9(6), pp.824–31. Available at: <http://www.pubmedcentral.nih.gov/articlerender.fcgi?artid=2279235&tool=pmcentrez&rendertype=abstract> [Accessed December 21, 2013].
- Yang, B. et al., 1999. SNARE Interactions Are Not Selective. *The Journal of Biological Chemistry*, 274(9), pp.5649–5653.
- Yang, G. & Cynader, M.S., 2011. Palmitoyl acyltransferase zD17 mediates neuronal responses in acute ischemic brain injury by regulating JNK activation in a signaling module. *Journal of Neuroscience*, 31(33), pp.11980–11991. Available at:

<http://www.jneurosci.org/content/31/33/11980.full.pdf>.

Yang, H. & Hu, H.Y., 2016. Sequestration of cellular interacting partners by protein aggregates: Implication in a loss-of-function pathology. *FEBS Journal*, 283, pp.3705–3717.

Yang, J. et al., 2008. Identification of the Acyltransferase that Octanoylates Ghrelin , an Appetite-Stimulating Peptide Hormone. , pp.387–396.

Yang, Y. et al., 2013. Application and interpretation of current autophagy inhibitors and activators. *Acta pharmacologica Sinica*, 34(5), pp.625–35. Available at: <http://www.ncbi.nlm.nih.gov/pubmed/23524572>.

Yeh, D.C. et al., 1999. Depalmitoylation of endothelial nitric-oxide synthase by acyl-protein thioesterase 1 is potentiated by Ca²⁺ - Calmodulin. *The Journal of*, 274(46), pp.33148–33154.

Yokoi, N. et al., 2016. Identification of PSD-95 Depalmitoylating Enzymes. *The Journal of Neuroscience*, 36(24), pp.6431–44. Available at: <http://www.ncbi.nlm.nih.gov/pubmed/27307232>.

Yoshida, A. et al., 1992. HPC-1 is associated with synaptotagmin and ω -conotoxin receptor. *Journal of Biological Chemistry*, 267(35), pp.24925–24928.

Yoshimori, T. et al., 1991. Bafilomycin-a1, a Specific Inhibitor of Vacuolar-Type H⁺-Atpase, Inhibits Acidification and Protein-Degradation in Lysosomes of Cultured-Cells. *Journal of Biological Chemistry*, 266(26), pp.17707–17712.

Young, F.B. et al., 2012. Putting proteins in their place: palmitoylation in Huntington disease

and other neuropsychiatric diseases. *Progress in neurobiology*, 97(2), pp.220–38. Available at: <http://www.ncbi.nlm.nih.gov/pubmed/22155432> [Accessed January 4, 2014].

Zeidman, R., Jackson, C.S. & Magee, A.I., 2009. Analysis of protein acylation. *Current Protocols in Protein Science*, Chapter 14(Unit 14.2), pp.1–12.

Zhang, F.L. & Casey, P.J., 1996. Protein Prenylation: Molecular Mechanisms and Functional Consequences. *Annual Review of Biochemistry*, 65(1), pp.241–269. Available at: <http://www.annualreviews.org/doi/10.1146/annurev.bi.65.070196.001325>.

Zhang, H. et al., 1999. Mutational analysis of cysteine-string protein function in insulin exocytosis. *Journal of cell science*, 112 (Pt 9, pp.1345–51. Available at: <http://www.ncbi.nlm.nih.gov/pubmed/10194413>.

Zhang, Y. & Chandra, S.S., 2014. Oligomerization of Cysteine String Protein alpha mutants causing adult neuronal ceroid lipofuscinosis. *Biochimica et Biophysica Acta (BBA) - Molecular Basis of Disease*, 1842(11), pp.2136–2146. Available at: <http://linkinghub.elsevier.com/retrieve/pii/S092544391400221X>.

Zhang, Y.Q. et al., 2012. Identification of CSP α Clients Reveals a Role in Dynamin 1 Regulation. *Neuron*, 74(1), pp.136–150. Available at: <http://dx.doi.org/10.1016/j.neuron.2012.01.029>.

Zhu, X.C. et al., 2013. Autophagy modulation for alzheimer's disease therapy. *Molecular Neurobiology*, 48(3), pp.702–714.

Zinsmaier et al., 1990. A Cysteine-String Protein is Expressed in Retina and Brain of *Drosophila*. *Journal of Neurogenetics*, 7(1), pp.15–29.

Zinsmaier, K.E. et al., 1994. Paralysis and early death in cysteine string protein mutants of *Drosophila*. *Science*, 263(January), pp.977–980.

Appendix I

Table I. EGFP-tagged plasmids in Chapter 3. Listed in order of appearance.

NAME	MUTATION/ COMMENTS	TAG	PLASMID	REFERENCE
hWT	none (human CSP)	EGFP	pEGFP_C2	(Greaves et al. 2012)
dL	Δ L116 (human CSP)	EGFP	pEGFP_C2	(Greaves et al. 2012)
LR	L115R (human CSP)	EGFP	pEGFP_C2	(Greaves et al. 2012)
WT 1-136	truncation 1-136 (CSP)	EGFP	pEGFP_C2	(Diez-Ardanuy et al. 2017; Greaves and Chamberlain 2006)
dL 1-136	Δ L116 + truncation 1-136	EGFP	pEGFP_C2	(Diez-Ardanuy et al. 2017)
LR 1-136	L115R + truncation 1-136	EGFP	pEGFP_C2	(Diez-Ardanuy et al. 2017)
WT C(1-3)A	WT (hCSP) + Cys 1 to 3 \rightarrow A	EGFP	pEGFP_C2	(Diez-Ardanuy et al. 2017; Greaves and Chamberlain 2006)
dL C(1-3)A	Δ L116 (hCSP) + Cys 1 to 3 \rightarrow A	EGFP	pEGFP_C2	(Diez-Ardanuy et al. 2017)
LR C(1-3)A	L115R (hCSP) + Cyst 1 to 3 \rightarrow A	EGFP	pEGFP_C2	(Diez-Ardanuy et al. 2017)
WT C(11- 14)A	WT (hCSP) + Cys 11 to 14 \rightarrow A	EGFP	pEGFP_C2	(Diez-Ardanuy et al. 2017)
dL C(11- 14)A	Δ L116 (hCSP) + Cys 11 to 14 \rightarrow A	EGFP	pEGFP_C2	(Diez-Ardanuy et al. 2017)
LR C(11- 14)A	L115R (hCSP) Cys 11 to 14 \rightarrow A	EGFP	pEGFP_C2	(Diez-Ardanuy et al. 2017)
WT C(8- 10)A	WT (hCSP) + Cys 1 to 8 \rightarrow A	EGFP	pEGFP_C2	(Diez-Ardanuy et al. 2017)
dL C(8-10)A	Δ L116 (hCSP) + Cys 1 to 8 \rightarrow A	EGFP	pEGFP_C2	(Diez-Ardanuy et al. 2017)
LR C(8-10)A	L115R (hCSP) + Cys 1 to 8 \rightarrow A	EGFP	pEGFP_C2	(Diez-Ardanuy et al. 2017)
WT C(4-7)A	WT (hCSP) + Cys 4 to 7 \rightarrow A	EGFP	pEGFP_C2	(Diez-Ardanuy et al. 2017; Greaves and Chamberlain 2006)
dL C(4-7)A	Δ L116 (hCSP) + Cys 4 to 7 \rightarrow A	EGFP	pEGFP_C2	(Diez-Ardanuy et al. 2017)
LR C(4-7)A	L115R (hCSP) + Cys 4 to 7 \rightarrow A	EGFP	pEGFP_C2	(Diez-Ardanuy et al. 2017)

Table I (continued)

NAME	MUTATION/ COMMENTS	TAG	PLASMID	REFERENCE
WT C(4-7)L	WT (hCSP) + Cys 4 to 7 → L	EGFP	pEGFP_C2	(Diez-Ardanuy et al. 2017; Greaves and Chamberlain 2006)
dL C(4-7)L	ΔL116 (hCSP) + Cys 4 to 7 → L	EGFP	pEGFP_C2	(Diez-Ardanuy et al. 2017)
LR C(4-7)L	L115R (hCSP) + Cys 4 to 7 → L	EGFP	pEGFP_C2	(Diez-Ardanuy et al. 2017)
WT C(4-5)L	WT (hCSP) + Cys 4 to 5 → L	EGFP	pEGFP_C2	(Diez-Ardanuy et al. 2017)
dL C(4-5)L	ΔL116 (hCSP) + Cys 4 to 5 → L	EGFP	pEGFP_C2	(Diez-Ardanuy et al. 2017)
LR C(4-5)L	L115R (hCSP) + Cys 4 to 5 → L	EGFP	pEGFP_C2	(Diez-Ardanuy et al. 2017)
WT C(6-7)L	WT (hCSP) + Cys 6 to 7 → L	EGFP	pEGFP_C2	(Diez-Ardanuy et al. 2017)
dL C(6-7)L	ΔL116 (hCSP) + Cys 6 to 7 → L	EGFP	pEGFP_C2	(Diez-Ardanuy et al. 2017)
LR C(6-7)L	L115R (hCSP) + Cys 6 to 7 → L	EGFP	pEGFP_C2	(Diez-Ardanuy et al. 2017)

Appendix II

Table II. Untagged and HA-tagged plasmids in Chapter 3. Listed in order of appearance.

NAME	MUTATION/ COMMENTS	TAG	PLASMID	REFERENCE
pDest WT	WT h CSP	untagged	pDest40	(Diez-Ardanuy et al. 2017)
pDest dL	Δ L116 hCSP	untagged	pDest40	(Diez-Ardanuy et al. 2017)
pDest LR	L115R hCS	untagged	pDest40	(Diez-Ardanuy et al. 2017)
WT C(1-3)A	WT (hCSP) + Cys 1 to 3 \rightarrow A	untagged	pDest40	(Diez-Ardanuy et al. 2017)
dL C(1-3)A	Δ L116 (hCSP) + Cys 1 to 3 \rightarrow A	untagged	pDest40	(Diez-Ardanuy et al. 2017)
LR C(1-3)A	L115R (hCSP) + Cyst 1 to 3 \rightarrow A	untagged	pDest40	(Diez-Ardanuy et al. 2017)
WT C(11-14)A	WT (hCSP) + Cys 11 to 14 \rightarrow A	untagged	pDest40	(Diez-Ardanuy et al. 2017)
dL C(11-14)A	Δ L116 (hCSP) + Cys 11 to 14 \rightarrow A	untagged	pDest40	(Diez-Ardanuy et al. 2017)
LR C(11-14)A	L115R (hCSP) + Cys 11 to 14 \rightarrow A	untagged	pDest40	(Diez-Ardanuy et al. 2017)
WT C(8-10)A	WT (hCSP) + Cys 1 to 8 \rightarrow A	untagged	pDest40	(Diez-Ardanuy et al. 2017)
dL C(8-10)A	Δ L116 (hCSP) + Cys 1 to 8 \rightarrow A	untagged	pDest40	(Diez-Ardanuy et al. 2017)
LR C(8-10)A	L115R (hCSP) + Cys 1 to 8 \rightarrow A	untagged	pDest40	(Diez-Ardanuy et al. 2017)
WT C(4-7)A	WT (hCSP) + Cys 4 to 7 \rightarrow A	untagged	pDest40	(Diez-Ardanuy et al. 2017)
dL C(4-7)A	Δ L116 (hCSP) + Cys 4 to 7 \rightarrow A	untagged	pDest40	(Diez-Ardanuy et al. 2017)
LR C(4-7)A	L115R (hCSP) + Cys 4 to 7 \rightarrow A	untagged	pDest40	(Diez-Ardanuy et al. 2017)
WT C(4-7)L	WT (hCSP) + Cys 4 to 7 \rightarrow L	untagged	pDest40	(Diez-Ardanuy et al. 2017)
dL C(4-7)L	Δ L116 (hCSP) + Cys 4 to 7 \rightarrow L	untagged	pDest40	(Diez-Ardanuy et al. 2017)
LR C(4-7)L	L115R (hCSP) + Cys 4 to 7 \rightarrow L	untagged	pDest40	(Diez-Ardanuy et al. 2017)
DHHC3	zDHHC3	HA	pEF-BOS	(Greaves et al. 2008)

Appendix III

Table II. Plasmids used in Chapter 4. New plasmid introduced in Chapter 4.

NAME	MUTATION/ COMMENTS	TAG	PLASMID	REFERENCE
PPT1	none	HA	pHM6	Dr. Christine Salaun (unpublished)

Appendix IV

Table IV. Plasmids used in Chapter 5. Listed in order of appearance.

NAME	MUTATION/ COMMENTS	TAG	PLASMID	REFERENCE
WT 14KR	hCSP + all K → R	EGFP	pEGCP_C2	-
dL 14KR	hCSP + ΔL116 + all K → R	EGFP	pEGFP_C2	-
LR 14KR	hCSP + L115R + all K → R	EGFP	pEGFP_C2	-
pDest WT	WT hCSP	untagged	pDest40	-
pDest dL	ΔL116 hCSP	untagged	pDest40	-
pDest LR	L115R hCS	untagged	pDest40	-
pDest 14KR	hCSP + all K → R	untagged	pDest40	-
CSP(1-136)	C-terminal truncation	EGFP	pEGFP_C2	(Greaves and Chamberlain 2006)
CSP(1-146)	C-terminal truncation	EGFP	pEGFP_C2	(Greaves and Chamberlain 2006)
CSP(1-156)	C-terminal truncation	EGFP	pEGFP_C2	Dr. Jennifer Greaves (unpublished)
CSP(87-198)	C-terminal truncation	EGFP	pEGFP_C2	Dr. Jennifer Greaves (unpublished)
CSP(106-198)	C-terminal truncation	EGFP	pEGFP_C2	Dr. Jennifer Greaves (unpublished)
14-198 utg	N-terminal truncation	untagged	pDest40	-
84-198 utg	N-terminal truncation	untagged	pDest40	-
113-198 utg	N-terminal truncation	untagged	pDest40	-
136-198 utg	N-terminal truncation	untagged	pDest40	-
WT C(8-14)A	Cys 8 to 14 → A	EGFP	pEGFP_C2	-

Table IV (continued)

NAME	MUTANT/ COMMENTS	TAG	PLASMID	REFERENCE
G114	non Cys residues in CSD (WT hCSP)	EGFP	pEGFP_C2	-
T117A	non Cys residues in CSD (WT hCSP)	EGFP	pEGFP_C2	-
Y120A	non Cys residues in CSD (WT hCSP)	EGFP	pEGFP_C2	-
L125A	non Cys residues in CSD (WT hCSP)	EGFP	pEGFP_C2	-
FN129AA	non Cys residues in CSD (WT hCSP)	EGFP	pEGFP_C2	-
G134A	non Cys residues in CSD (WT hCSP)	EGFP	pEGFP_C2	-
CSP(144-148)A	- Name on tube: E144A - PEST seq. mutant: residues 144 to 148 →A	EGFP	pEGFP_C2	-
CSP(179-182)A	- Name on tube: S151A - PEST seq. mutant: 179 to 182 → A	EGFP	pEGFP_C2	-
CSP(179-182)A	- Name on tube: T179A - PEST seq. mutant: 179 to 182 → A	EGFP	pEGFP_C2	-
HAKR wt	WT hCSP	HA no R	GW-HA-pEF-BOS	-
HAKR dL	ΔL116 hCSP	HA no R	GW-HA-pEF-BOS	-
HAKR LR	L115R hCS	HA no R	GW-HA-pEF-BOS	-
HAKR 14KR	WT hCSP without K	HA no R	GW-HA-pEF-BOS	-

Appendix V



S-ACYLATION IN NEURODEGENERATION

Cinta Diez-Ardanuy, Jennifer Greaves, Luke H. Chamberlain
Strathclyde Institute of Pharmacy and Biomedical Sciences, University of Strathclyde
Glasgow, UK



INTRODUCTION

Neuronal Ceroid Lipofuscinoses (NCLs) are a group of neurodegenerative disorders characterized by the accumulation of autofluorescent material in neurons and other cell types. Common characteristics of affected individuals with NCL include generalised seizures, movement disorders, cognitive deterioration and progressive dementia, which leads to a decrease in life expectancy.

Mutations (A1116 and L115R) in the DNAJC5 gene encoding *cysteine-string protein* (CSP) have been identified to cause autosomal-dominant adult-onset NCL (ANCL). CSP is a chaperone that regulates protein folding. These mutations occur within the cysteine-string domain, a region of CSP that is extensively S-acylated.



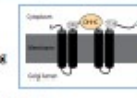
S-acylation is a post-translational modification consisting of the attachment of fatty acids to cysteine residues via thioester bonds.



Regulation of S-acylation status is determined by two types of enzymes: protein acyltransferases (PATs), which catalyse the addition of palmitate and other fatty acids to the substrate; and protein acylthioesterases, responsible for catalysing the removal of the fatty acids.

PATs share a common and defining S1-amino acid DHHC (aspartate-histidine-histidine-cysteine)-cysteine rich (CR) domain, essential for S-acylation activity.

- Reversible
- Regulates
 - Membrane binding
 - Protein sorting
 - Protein-protein interaction



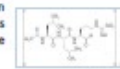
OBJECTIVES

We found that ANCL mutations cause CSP to form SDS-resistant aggregates, which are induced and maintained by S-acylation [1]. The present study aims to further characterise the possible links between aggregation of CSPs mutants and NCL by examining:

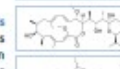
- The mechanisms mediating wild-type and mutant CSP degradation and clearance from cells.
- How ANCL mutations affect the intracellular localisation of CSP.
- The composition of CSP aggregates.
- The potential of specific S-acyltransferase enzymes to serve as drug targets to prevent CSP aggregation.

MATERIALS AND METHODS

Three different inhibitors of protein degradation pathways were used to assess the mechanism of turnover of wild-type and mutant CSPs.



LP – Leupeptin hemisulfate



BF – Belomycin A1



MG-132 – Proteasome inhibitor

Rat pheochromocytoma-12 (PC12) cells were labelled with different concentrations of the inhibitors overnight. The expression of wild-type and mutant proteins was evaluated through SDS and blue native gel electrophoresis.

RESULTS

Effects of proteasomal and lysosomal inhibitors on CSP expression

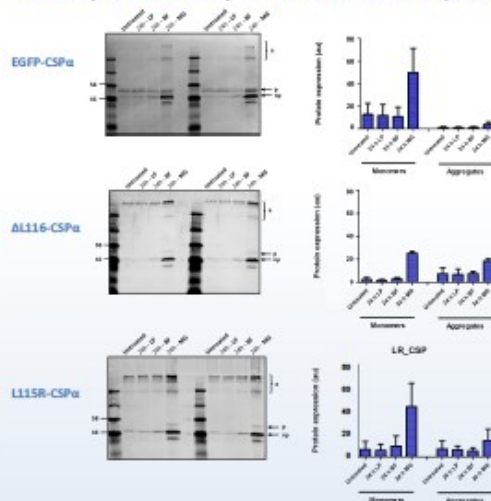


Figure 1. Analysis of the degradation pathway of CSPs mutants and aggregates. Presence of aggregates and monomeric forms of CSPs on SDS gels revealed by immunoblotting with anti-GFP antibody (left) and densitometric quantification (right) of the monomeric and aggregated forms of the protein (right). [monomers; p,palmitoylated; n,pnon palmitoylated].

Analysis of aggregation under native gel conditions

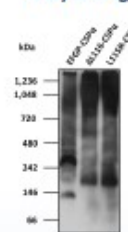


Figure 2. Migration pattern of wild-type and mutant CSPs. PC12 cells expressing the wild-type and mutant forms of CSPs, were transfected for 48 hours and subsequently lysed and resolved on blue native gels, transferred onto PVDF membranes and immunoblotted using an anti-GFP antibody. Position of size markers are shown on the left hand side.

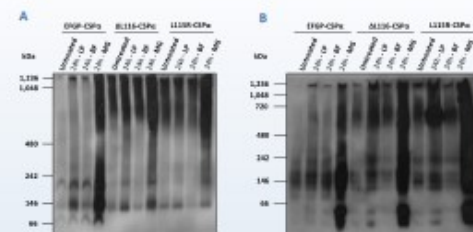


Figure 3. Analysis of degradation pathways of CSPs mutants and aggregates under native gel conditions. PC12 cells expressing the wild-type and mutant forms of the protein were transfected for 48 hours and labelled with different proteasome and lysosome inhibitors, and subsequently resolved on blue native gels after a treatment with digibiotin (A) or SDS (B).

CONCLUSIONS

The proteasome is implicated in the degradation pathway of wild-type and mutant CSPs proteins, as well as in the clearance of aggregates from the cell.

These results confirm the different oligomeric status of wild-type and mutant forms of CSPs.

ACKNOWLEDGEMENTS

This work is supported by The Strathclyde Institute of Pharmaceutical and Biomedical Sciences (SIPS) and the Wellcome Trust.

*For further information contact cinta.diez-ardanuy@strath.ac.uk.

FUTURE WORK

To more precisely determine the degradation pathway of CSP proteins and aggregates and their relative turnover rates.

Analysis of the accumulation of the mutant proteins on lysosomes or alterations in the organelle structure by confocal microscopy.

To validate target DHHC enzymes that S-acylate CSPs as a drug target for ANCL

REFERENCES

[1] Greaves, J. et al., 2012. Palmitoylation-induced aggregation of cysteine-string protein mutants that cause neuronal ceroid lipofuscinoses. *The Journal of biological chemistry*, 287(44), pp.37330-9.

Molecular and cellular analysis of Cysteine-String Protein mutants that cause Neuronal Ceroid Lipofuscinosis



Cinta Diez-Ardanuy, Jennifer Greaves and Luke H. Chamberlain
 Strathclyde Institute of Pharmacy and Biomedical Sciences, University of Strathclyde, Glasgow, UK



INTRODUCTION

Neuronal Ceroid Lipofuscinoses

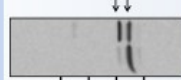
Neuronal Ceroid Lipofuscinoses (NCLs) are a group of neurodegenerative disorders characterized by the accumulation of autofluorescent material in neurons and other cell types. Common characteristics of affected individuals with NCL include generalised seizures, movement disorders, cognitive deterioration and progressive dementia, which leads to a decrease in life expectancy.

Mutations in the DNAJC5 gene encoding cysteine-string protein (CSP) have been identified to cause autosomal-dominant adult-onset NCL (ANCL). These mutations lead to amino acid changes in CSP: L115R or ΔL116.



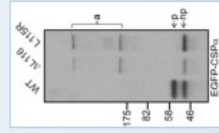
Cysteine-String Protein

CSP is a chaperone that regulates folding of the SNARE protein SNAP25. ANCL mutations occur within the cysteine-string domain, a region of CSP that is extensively palmitoylated. Palmitoylation of CSP leads to a marked band shift on SDS gels (see opposite, np= non-palmitoylated; p=palmitoylated).



Cysteine-String Protein and disease

- ANCL mutations affect the properties of CSP causing the formation of high molecular weight SDS-resistant aggregates and a loss of palmitoylated monomer.
- Co-expression with active zDHC enzymes drives aggregation of the ANCL mutants, suggesting palmitoylation and aggregation are linked.



RESULTS

The role of the cysteine-string domain in aggregation

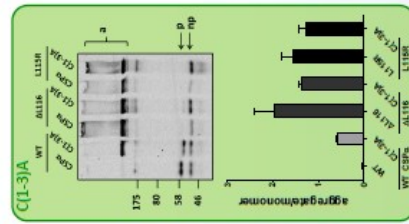
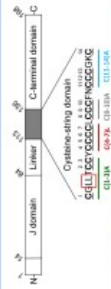


Figure 1. GFP-CSP mutants were expressed in PC12 cells and analysed by immunoblotting and densitometric quantification (n=4). [a=aggregates; p=palmitoylated; np=non palmitoylated].

Palmitoylation of the C(4-7)L mutant does not lead to aggregation

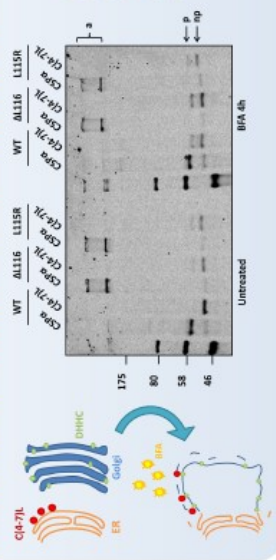


Figure 2. GFP-CSP mutants expressed in PC12 cells, treated with BPA for 4 hours and analysed by immunoblotting.

Analysis of the degradation pathways of CSP

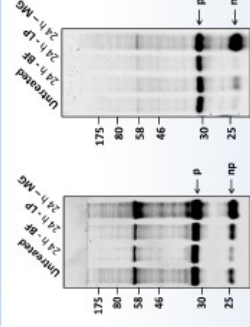


Figure 3. PC12 cells expressing untagged wild-type or 14KR mutant CSP were treated with different proteasome and lysosome inhibitors for 24 hours and analysed by immunoblotting with anti-CSP antibody.

CONCLUSIONS

- Aggregation of ANCL mutants is driven by co-expression of zDHC enzymes.
- There is a link between palmitoylation and aggregation.
- Cysteines 4-7 are critical for aggregation of the L115R and ΔL116 mutants.

FUTURE WORK

- Delineate the existing link between palmitoylation, cysteines 4-7 and aggregation of ANCL mutants.
- More precisely determine the degradation pathway of CSP proteins and aggregates and their relative turnover rates.

REFERENCES

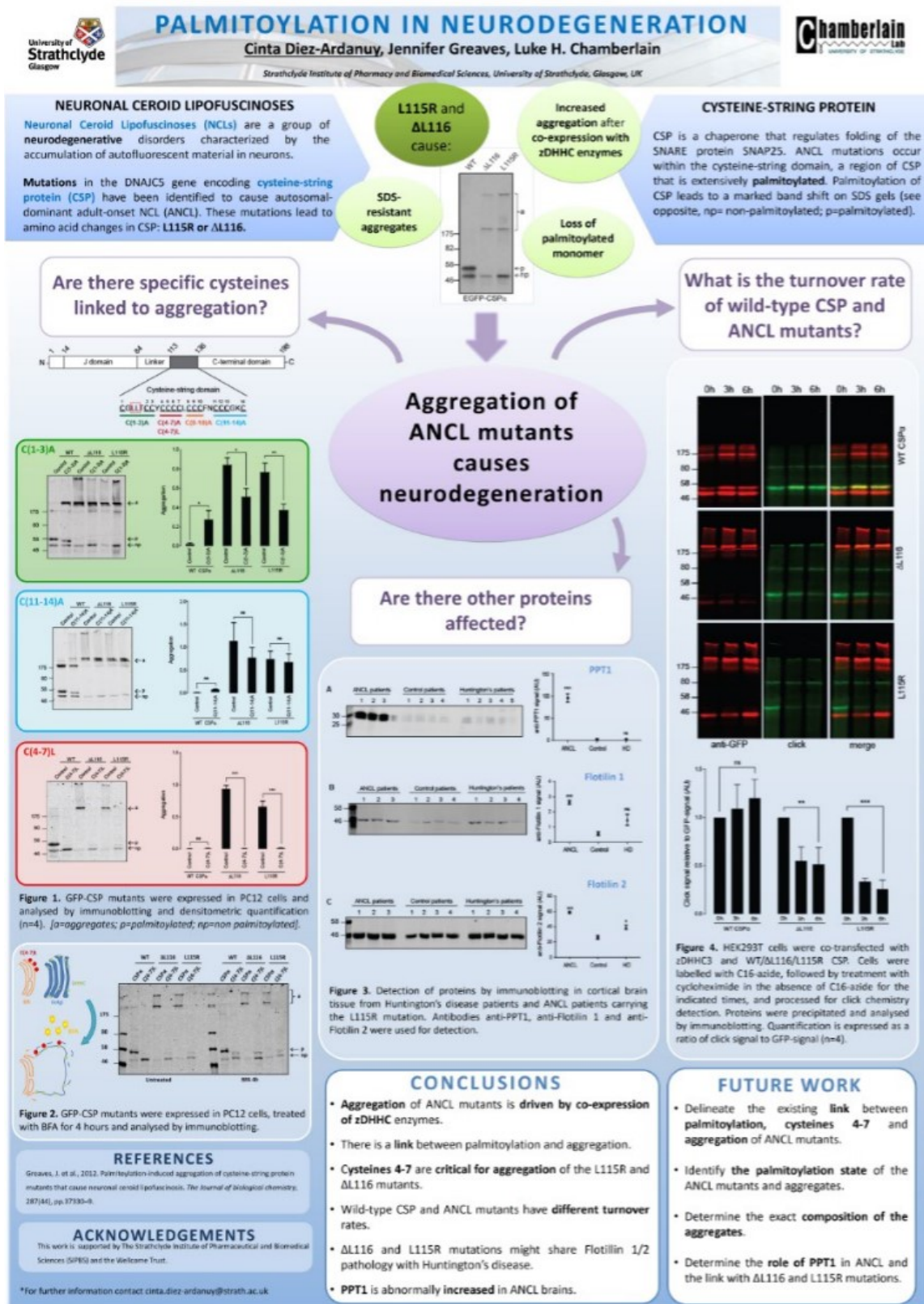
Greaves, J. et al., 2012. Neurodegenerative aggregation of cysteine-string protein mutants that cause neuronal ceroid lipofuscinosis. *The Journal of Biological Chemistry*, 287(44), pp.15339-4.

ACKNOWLEDGEMENTS

This work is supported by the Strathclyde Institute of Pharmaceutical and Biomedical Sciences (SIBS) and the Wellcome Trust.

*For further information contact: cinta.diez-ardanuy@strath.ac.uk

Appendix VII



Appendix VIII

PALMITOYLATION IN NEURODEGENERATION

Cinta Diez-Ardanuy, Jennifer Greaves and Luke H. Chamberlain
Strathclyde Institute of Pharmacy and Biomedical Sciences, University of Strathclyde, Glasgow, UK

Neuronal Ceroid Lipofuscinoses (NCLs) are a group of neurodegenerative disorders characterized by the accumulation of autofluorescent material in neurons and other cell types. Common characteristics of affected individuals with NCL include generalised seizures, movement disorders, cognitive deterioration and progressive dementia, which leads to a decrease in life expectancy.

Mutations in the DNAJC5 gene encoding **cysteine-string protein (CSP)** have been identified to cause autosomal-dominant adult-onset NCL (ANCL). These mutations lead to amino acid changes in CSP: **L115R or ΔL116**.

L115R and ΔL116 CAUSE:

- Loss of palmitoylated monomer
- Increased aggregation after co-expression with zDHHC enzymes
- SDS-resistant aggregates

Are there other proteins affected?

Are there specific cysteines linked to aggregation?

Are there any other proteins affected?

Figure 1. GFP-CSP mutants were expressed in PC12 cells and analysed by immunoblotting and densitometric quantification (n=4). (p=aggregates; p=palmitoylated; np=non palmitoylated).

Figure 2. GFP-CSP mutants were expressed in PC12 cells, treated with Brefeldin A (BFA) for 4 hours and analysed by immunoblotting.

Figure 3. Detection of proteins by immunoblotting in cortical brain tissue from Huntington's disease patients and ANCL patients carrying the L115R mutation. Antibodies anti-PPT1, anti-Flotilin 1, and anti-Flotilin 2 were used for detection.

Figure 4. HEK293T cells were co-transfected with zDHHCs and GFP-CSP. GFP-CSP mutants were labelled in C16s followed by treatment with cycloheximide in the absence of C16s-sside for the indicated times, and processed for click chemistry detection. Proteins were precipitated and analysed by immunoblotting. Quantification is expressed as a ratio of click signal to GFP-signal (n=4).

Figure 5. Palmitoylation-induced aggregation of cysteine-string protein mutants that cause neuronal ceroid lipofuscinoses. The Journal of Biological Chemistry, 287(46), pp. 3730-9.

NEURONAL CEROID LIPOFUSCINOSES

Palmitoylation is a **reversible** post-translational modification consisting of the attachment of fatty acids (palmitate) to cysteine residues via thioester bonds. Regulates **membrane binding, protein sorting and protein-protein interaction**.

Regulation of palmitoylation is determined by protein acyltransferases (PATs), which catalyse the addition of palmitate. PATs are commonly named **zDHHC enzymes**.

What is the turnover rate of wild-type CSP and ANCL mutants?

CONCLUSIONS

- Aggregation of ANCL mutants is **driven by co-expression of zDHHC enzymes**.
- There is a **link between palmitoylation and aggregation**.
- Cysteines 4-7 are critical for aggregation** of the L115R and ΔL116 mutants.
- Wild-type CSP and ANCL mutants have **different turnover rates**.
- ΔL116 and L115R mutations might share **Flotillin 1/2 pathology** with Huntington's disease.
- PPT1 is abnormally increased** in ANCL brains.

Are there any other proteins affected?

Are there specific cysteines linked to aggregation?

Are there any other proteins affected?

Are there any other proteins affected?

Are there specific cysteines linked to aggregation?

Are there any other proteins affected?

Are there any other proteins affected?

Are there specific cysteines linked to aggregation?

Are there any other proteins affected?

PROTEIN

CSP is a chaperone that regulates folding of the SNARE protein SNAP25. ANCL mutations occur within the cysteine-string domain, a region of CSP that is extensively **palmitoylated**. Palmitoylation of CSP leads to a marked band shift on SDS gels (see above, np= non-palmitoylated; p=palmitoylated).

FUTURE WORK

- Delimitate the existing link between **palmitoylation, cysteines 4-7 and aggregation** of ANCL mutants.
- Identify the **palmitoylation state** of the ANCL mutants and aggregates.
- Determine the **exact composition of the aggregates**.
- Determine the **role of PPT1** in ANCL and the link with ΔL116 and L115R mutations.

*For further information contact: cinta.diez-ardanuy@strath.ac.uk

This work is supported by the Strathclyde Institute of Pharmaceutical and Biomedical Sciences (SIPBS) and the Wellcome Trust.